In Vitro and In Vivo Characterization of Novel Small-Molecule Alzheimer's Disease Amyloid-Beta Therapies

---

A Dissertation

Presented to

the faculty of the School of Engineering and Applied Science

University of Virginia

---

in partial fulfillment

of the requirements for the degree

Doctor of Philosophy

by

Jacob A. Irwin

December

2014

APPROVAL SHEET

The dissertation

is submitted in partial fulfillment of the requirements

for the degree of

Doctor of Philosophy

_____

AUTHOR

The dissertation has been read and approved by the examining committee:

Inchan Kwon

_____

Advisor

Kyle Lampe

_____

David Green

_____

Alev Erisir

_____

Roseanne Ford

_____

_____

Accepted for the School of Engineering and Applied Science:

Dean, School of Engineering and Applied Science

December

2014

In Vitro and In Vivo Characterization of Novel Small-Molecule Alzheimer's Disease Amyloid-Beta Therapies

A Dissertation

Presented to

the faculty of the School of Engineering and Applied Science

University of Virginia

In Partial Fulfillment

Of the requirements for the Degree

Doctor of Philosophy (Chemical Engineering)

By

Jacob A. Irwin

August 2014

Acknowledgements

I would like to thank the following people:

My research advisor, Professor Inchan Kwon, for his continued guidance, faith, and insight in helping me navigate and understand the dynamics of graduate school and research.

Professors David Green, Alev Erisir, Roseanne Ford, and Kyle Lampe for serving on my Dissertation Committee. The Erisir Group at the Psychology Department at the University of Virginia for assistance with TEM assays and animal studies. The Bloom Group of the Biology Department at the University of Virginia for providing the transgenic mice and M87 antibody. Professor Jerold Floro, Joseph Kassim, and Jatin Amatya at the Materials Science Department at the University of Virginia for assistance with AFM assays.

My lab mates from the Kwon Group for their support and guidance, including Simpson Gregoire, Shun Zheng, Sung In Lim, and in particular, Edward Wong, for helping to teach me many of the lab techniques needed to get started on my research upon joining the research group.

Finally, my friends and family. Specifically, to my parents, Robert and Cathy, and sister, Madeline, for teaching me to find my passion in life and never stop trying to do my best. And, to my best friend, Becca, for her unwavering kindness and love for me, and for putting up with me during all of the late nights and odd hours I sometimes find myself doing experiments at the lab while in graduate school.

This work was supported by the KSEA Young Investigator Grant, a National Science Foundation Graduate Research Fellowship (DGE-00809128), and Award No. 13-6 from the Commonwealth of Virginia's Alzheimer's and Related Diseases Research Award Fund.

Abstract

In recent years, studies have indicated that the presence of neurotoxic forms of aggregated amyloid-beta peptide have a strong correlation with the pathological progression of Alzheimer's Disease. Therefore, the inhibition, modulation, and/or reduction of targeted amyloid-beta aggregates formation are considered promising therapeutic strategies to treat this disease. In order to search for novel small molecule modulators with good biocompatibility, our research group screened various FDA-approved food dyes and their close structural analogs. We recently reported that Brilliant Blue G and Erythrosin B are novel modulators of amyloid-beta monomer in vitro aggregation and cytotoxicity in a dose-dependent manner.

This dissertation details four additional characterization investigations (three in vitro and one in vivo) to further develop Brilliant Blue G, Erythrosin B, and their structural analogs as potential Alzheimer's Disease therapeutics. First, we performed a structure-activity relationship analysis on Erythrosin B and its analogs and discovered the placement of heavy halogen atoms on the xanthene benzoate backbone structure to be a critical feature for the amyloid-beta monomer binding, aggregation, and cytotoxicity modulating activity observed. Second, having seen the potent effect of halogenation at generating effective amyloid-beta binding ligands, we then sought to explore the specific binding sites of Erythrosin B and its structural analogs on the amyloid-beta monomer target peptide. After creating a novel method for identifying ligand binding sites using dot blotting with a sequence-specific antibody panel, the technique revealed amino acids 10-16 of amyloid-beta as a common strong binding site for Erythrosin B and its analogs. Third, since we had thus far characterized the effects of Brilliant Blue G and Erythrosin B on amyloid-beta aggregation from the monomer state, we wanted to also investigate if these molecules could perturb pre-existing aggregates from a different side of the thermodynamic

spectrum. To this end, we performed comparative structural studies on the different fates of very stable amyloid-beta fibrils remodeled by the two compounds, finding that Brilliant Blue G- and Erythrosin B-treatment generate fragmented amyloid-beta fibrils and protofibrils, respectively. Fourth, we sought to further evaluate these novel modulators in a more therapeutically-relevant Alzheimer's Disease mouse model. Brilliant Blue G was selected to be tested first and administered to mice for three months. The results revealed that administration of Brilliant Blue G to the transgenic Alzheimer's Disease mouse was well-tolerated, crossed the blood-brain barrier, rescued neuronal loss, and reduced intraneuronal amyloid-beta loading.

Table of Contents

List of Figures

List of Tables

Chapter 1: Introduction

Alzheimer's Disease - Scope and Significance

Alzheimer's Disease (AD) is a neurodegenerative illness that impairs memory, thinking, and behavior. It is the most common form of irreversible dementia in the world today, usually affecting persons over the age of 65 (termed late onset AD).[1] The symptoms associated with the pathological progression of AD are as follows: sporadic memory loss during early stages, universal decline in cognitive ability as the disease progresses, and finally, the patient becomes bedridden due to the brain's lack of control of the body and is completely dependent on caregivers. On average, death occurs only 9 years after diagnosis of AD.[2]

In addition to the severe effects AD has on the individual patients, the disease also contributes a very significant monetary and emotional burden to society. Currently, it is estimated that AD affects more than 5.3 million people in the United States alone. In fact, AD is becoming such an issue that it is now the sixth leading cause of death in the United States. With increasing age being the biggest risk factor for the disease, the incidence of AD is expected to increase to an estimated 11–16 million cases in the United States in 2050. Furthermore, the total annual costs of AD in the United States have been estimated at over $148 billion.[2] Despite significant research to discover a therapeutic for this disease, an approved treatment with proven disease-modifying effect does not exist (only symptomatic treatments are available). Thus, there exists a great medical need to further investigate the Alzheimer's Disease therapeutic space.

Causes of Alzheimer's Disease

Two pathological hallmarks of Alzheimer's Disease were discovered in biopsied AD brains more than 100 years ago and have since been the subject of much investigation. These hallmarks are as follows: 1) neurofibrillary tangles inside neuron cells consisting of tau protein filaments and 2) intercellular plaques, which in recent years have been found to be formed by amyloid-beta (Aβ) peptide aggregation.[2, 3] Tau protein exists in the healthy human brain to stabilize axon microtubules. However, aggregation and/or hyperphosphorylation of this protein have been shown to cause toxic effects. The Aβ peptide is formed by successive cleavage of the normally occurring neuronal transmembrane protein, Amyloid Precursor Protein (APP), by gamma and beta-secretase enyzmes. The aggregated form of the Aβ peptide has been shown to confer toxicity to neuronal cells.[2]

Research Scope Selection – Amyloid Pathological Hallmark Therapeutic Approach

Despite a strong correlation found between cognitive dysfunction and the existence of tau tangles in various AD case studies,[4] Aβ aggregates have been shown to commonly exist in the AD brain without the presence of any tau protein. In addition, it has been found that the existence of Aβ plaques can in fact initiate the creation of tau filament tangles.[5] Because of this and the fact that all genetic risk factors and mutations linked with AD are also associated with increased amyloid load,[2] the amyloid-beta peptide aggregate hallmark presents itself as a particularly important therapeutic target on which to focus our research efforts.

Amyloid Cascade Hypothesis and Related Treatment Approaches

The process by which the Aβ peptide is generated, subsequently aggregates/accumulates, and is suspected to confer toxicity upon neuronal cells is termed the Amyloid Cascade Hypothesis. As mentioned previously, the process begins when the Aβ peptide (monomer) is generated by sequential cleavage of the APP parent protein by gamma and beta-secretases. Depending upon where gamma-secretase cleavage occurs, Aβ peptide fragments ranging from 39-43 amino acids in length can be generated, but the 40 and 42 amino acid length peptides (herein designated Aβ40 and Aβ42, respectively) are the alloforms most often found in amyloid aggregates in the AD brain. Although the Aβ42 load in the AD brain is only 10% that of Aβ40, Aβ42 has been shown to be more hydrophobic, more aggregation prone, and more neurotoxic than the Aβ40 isoform.[6] **Aβ40 was chosen as the primary platform and target peptide for this dissertation work** because it 1) is more user friendly in that is it less sensitive to person-to-person handling during sample preparation, 2) is nine times physically more prevalent in the AD brain than Aβ42,[6] and 3) has an aggregation pathway that has been found to generally be modulated in a similar fashion by small molecule inhibitors as the Aβ42 aggregation pathway.[7]

From the Amyloid Cascade Hypothesis, several treatment approaches present themselves for consideration as drug development targets. First, the generation of Aβ monomer could be blocked by developing beta and/or gamma secretase enzyme inhibitors. Indeed, this approach was one of the first strategies attempted, probably due to the familiarity of pharmaceutical companies with developing small molecules to inhibit specific enzymes throughout the body. However, several complicating factors have arisen: 1) the normal biological role of beta-secretase is unknown, and 2) the inhibition of gamma-secretase interferes with its action on other

biologically-important substrates.[2] Both of these factors greatly complicate the drug discovery process. Indeed, after almost 20 years of research in this field, no drug candidate has successfully passed human clinical trials, and many gamma-secretase inhibitors have displayed significant side effects or worsened AD clinical symptoms. The second treatment approach involves the prevention or control of the amyloid aggregation pathway once the monomer is generated.[2] Due to the disadvantages of the enzyme inhibitor approach, the second treatment approach involving the prevention and/or control of the amyloid aggregation pathway presents itself as particularly promising for further investigation in our research.

Aβ Aggregation Pathways

After the Aβ40 peptide monomer is generated, multiple independent and dependent aggregation cascades can occur resulting in the formation of various aggregated states of Aβ40 peptide, known as conformers. In one frequently studied pathway, misfolded disordered Aβ40 monomers first self-assemble in to soluble (commonly termed "on-pathway," since they mature to the fibril state) prefibrillar oligomers prior to forming a stacked β-sheet rich aggregate known as protofibrils. Further aggregation of these protofibrils ultimately results in the more thermodynamically stable insoluble Aβ40 fibril conformer.[8] A schematic of this Aβ40 aggregation pathway with the various species is shown in Figure 1.1. Aside from these on-pathway conformers, unstructured "off-pathway" aggregates have also been found to occur during the Aβ aggregation process employing different in vitro aggregation conditions.[9]

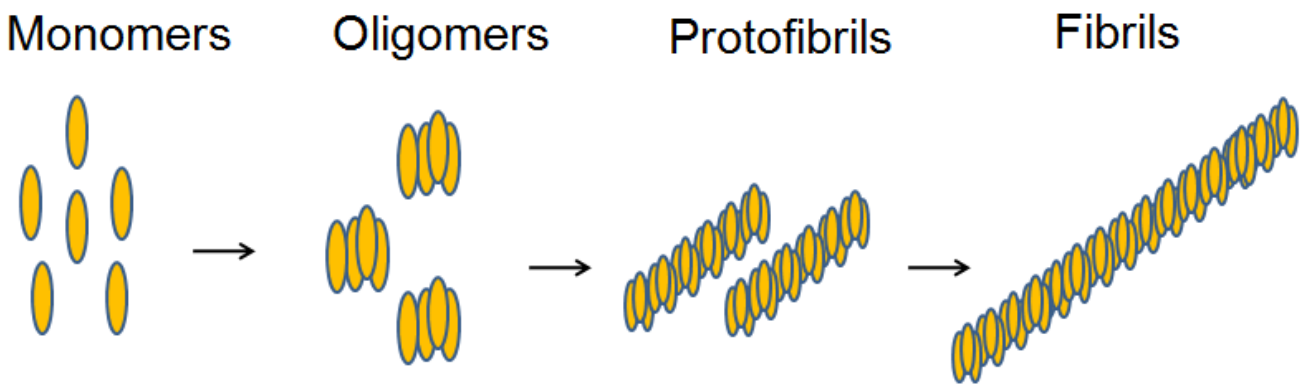

Figure 1.1 - A commonly studied Aβ40 aggregation pathway.

The original version of the Amyloid Cascade Hypothesis cited insoluble fibrils as the principle conformer conferring neurotoxicity in AD.[10] However, recent results have since shown that soluble prefibrillar oligomers and protofibrils are the primary acutely toxic species,[11] and the existence of amyloid fibrils are more responsible for less-acute neuronal toxicity and inflammatory responses.[2] As such, preventing/modulating the creation of or the reduction of pre-existing Aβ oligomers, protofibrils, and fibrils represents a promising strategy for AD disease-modifying treatment and drug development.

Definition of Various Aβ40 Aggregated Conformers

In order to properly interpret Aβ40 aggregation modulatory and structural changes, concrete definitions of the various possible Aβ40 peptide aggregate species are needed. Disordered aggregates, protofibrils, and amyloid fibrils were introduced as three general categories of conformers that can be sampled during the Aβ40 aggregation pathway discussed in the previous section. Therefore, it is important to establish structural criteria (i.e. data endpoints from commonly used techniques) for each of these three conformers.

Listed below are the expected data endpoints from several commonly-used assays (background on assays will be discussed in detail in the Background and Theoretical Development Section) based on reports in the literature for the three conformers:

Disordered Aggregates

- *Thioflavin T (ThT)* – ThT negative.[9, 12] Not applicable if studying samples containing spectrophotometrically active small molecules.[13]
- *Dot Blotting with OC Antibody* – OC negative.[14] Must be careful interpreting results due to possible false negative signals due to small molecule binding.[13]
- *Morphology using Transmission Electron Microscopy (TEM) /Atomic Force Microscopy (AFM)* – Amorphous aggregates with varying sizes/morphologies lacking defined, persistent morphological features.[9, 15-18]
- *Secondary Structure using Circular Dichroism (CD)* – Random coil/disordered secondary structure CD spectra.[19-23]

Protofibrils

- *ThT* – Moderately ThT positive.[20, 24] Not applicable if studying samples containing spectrophotometrically active small molecules.[13]
- *Dot Blotting with OC Antibody* – OC positive.[14] Must be careful interpreting results due to possible false negative signals due to small molecule binding.[13]
- *Morphology using TEM/AFM* – Shorter, filamentous, rod-like aggregate with visible defined and persistent structure. Length < 400 nm.[25] Width ~12 nm.[26]
- *Secondary Structure using CD* – β-sheet secondary structure CD spectra.[19-22]

Fibrils

- *ThT* – Strongly ThT positive.[23, 27-30] Not applicable if studying samples containing spectrophotometrically active small molecules.[13]
- *Dot Blotting with OC Antibody* – OC positive.[14] Must be careful interpreting results due to possible false negative signals due to small molecule binding.[13]
- *Morphology using TEM/AFM* – Long, filamentous, rod-like aggregate with visible defined and persistent structure.[31] Length ~ 1 μm.[31] Width ~ 20 nm.[26, 32]
- *Secondary Structure using CD* – β-sheet secondary structure CD spectra.[19-22]

Aβ Small Molecule Aggregation Modulators

Out of the various therapeutic agents that have been investigated as Aβ aggregation modulators, small molecules have presented themselves as a promising potential treatment for AD. The inherent small physical size of these molecules makes them more likely to be blood-brain barrier permeable than macromolecules (such as trophic factors and other protein therapies).[33] However, because blood-brain barrier permeability is a highly selective and complex phenomenon, each small molecule must be evaluated on a case-by-case basis to ensure that a relevant therapeutic dose of the small molecule can in fact be delivered to the brain. Indeed, in recent years, many small molecule modulators of Aβ aggregation have been identified and characterized in vitro with rather promising results.[23, 34, 35] Some of these small molecules have been found to inhibit the formation of neurotoxic conformers and/or promote the formation of non-toxic species during aggregation from the monomeric state (approach to prevention of

AD). Other small molecules have been investigated to remodel pre-existing toxic aggregates into less toxic (or non-toxic) conformers (approach for AD therapy after acute disease onset has already occurred). A very small subset of these small molecules investigated has advanced through in vivo animal testing and on to clinical trials in humans, but no molecules have yet to demonstrate both safety and efficacy for modifying AD in patients.[2] Because of this, there still remains a great need to identify new small molecule drug candidates and characterize their interaction with the Aβ aggregation pathways.

To this end, the Kwon Research Group at The University of Virginia has been investigating/characterizing two novel small molecules Aβ aggregation modulators and their structural analogs as potential lead drug candidates – **Erythrosin B (ERB) and Brilliant Blue G (BBG).** Multiple characteristics of ERB and BBG make them attractive drug candidates for investigation. BBG and ERB both have been reported to cross the blood-brain barrier (BBB), exhibit low toxicity in vivo, and are biocompatible.[36-38] Furthermore, ERB and a close structural analog of BBG, Brilliant Blue FCF, are FDA-approved for human use as food dyes.[36, 37] All of these factors can potentially help to lessen resistance in the drug approval process as these compounds are developed as therapies. From a chemical structure perspective, these molecules are also attractive because they contain multiple aromatic ring structures and charged groups, features believed to perturb pi-pi stacking in Aβ aggregates and help with binding.[9]

Background and Theoretical Development - Monitoring Protein Aggregation In Vitro[39]

As mentioned previously, AD is closely associated with the aggregation and accumulation of toxic amyloid-beta peptide (Aβ). These aggregates are eventually deposited outside of the cells.[40, 41] Therefore, monitoring Aβ peptide aggregation in vitro is an appropriate and cost-efficient first step to understanding the molecular mechanism of AD and in identifying drug candidates capable of modulating protein aggregation before studying the action in animals or humans. Because of the importance and complexities of in vitro monitoring techniques in the study of protein aggregation/neurodegenerative diseases, it was necessary to have a good fundamental knowledge of the techniques available prior to beginning the dissertation experiments using Aβ40.

Protein aggregates in general have diverse structures, including disordered aggregates, prefibril aggregates, and amyloid fibrils (Figure 1.2). Originally, insoluble fibrils were thought to be the principal conformer conferring neurotoxicity in diseases such as AD.[10] As such, the scientific community committed much time and resources into the development and optimization of many "traditional" in vitro techniques to characterize this particular form of protein aggregate. However, through recent in vivo and in vitro discovery, smaller, prefibril aggregates (Figure 1.2) have now emerged as the primary toxic species in several of these neurodegenerative protein conformation diseases.[42-45] Prefibril aggregates include the following conformers: prefibrillar oligomers (globular aggregates lacking the ordered cross-stacked β-sheet structure) and fibrillar oligomers/protofibrils (aggregates with the cross-stacked β-sheet structure). Because of this paradigm shift, many limitations and potential drawbacks of using "traditional" fibril monitoring techniques to study prefibril aggregates have become apparent. In addition, new techniques (or

new uses of “traditional” techniques) have emerged to better characterize prefibril/oligomeric aggregates and the effectiveness of proposed aggregation modulating therapies. The focus of this section is to review recent trends in the use of several “traditional” techniques (small molecule probes, TEM/AFM, and CD/FTIR) and a new technique (dot-blot assay using conformational-specific antibodies) for routine in vitro monitoring of protein aggregation.

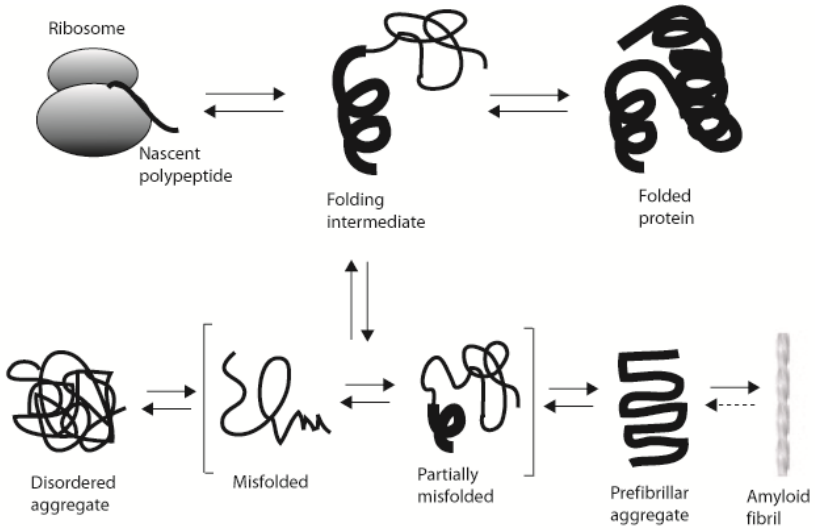

Figure 1.2 - General scheme of protein folding and misfolding/aggregation.

Molecular Probes for Aggregate Characterization

Thioflavin T Binding Assay

The use of a small molecule dye, Thioflavin T (ThT), and its derivatives is arguably the simplest and most widely used method to monitor aggregation of amyloidogenic proteins. ThT displays a fluorescence emission maximum at around the 485 nm wavelength upon binding to

the β-sheet groove structure of fibrillar protein aggregates.[46] The use, binding sites, and binding mechanisms of ThT with protein aggregates have been reviewed extensively.[24, 47-53]

Traditionally, ThT has been used to detect amyloid fibrils only due to the characteristic sigmoidal increase in fluorescence that occurs between the monomer and end fibril state.[13, 23, 27-30] However, ThT has also been found to bind prefibril aggregates that contain the β-sheet groove binding site (fibrillar oligomers and protofibrils). Prefibril aggregates which contain the β-sheet structure have fewer binding sites than fibrils and so their fluorescence is lower, but still observable (1.5 fold increase for prefibril aggregates vs. 100 fold for fibrils).[20, 24] Therefore, ThT signal can prove indicative to the presence of toxic protofibrils and fibrillar oligomers, but not prefibrillar oligomers that lack defined β-sheet structure.[9, 12] Lastly, caution should be taken when using ThT to monitor aggregation in the presence of aggregation inhibitors due to potential spectral interference with ThT fluorescence.[13, 27, 39, 50]

Because small molecule modulators were being studied in this dissertation work, ThT fluorescence was used to monitor aggregation and verify fibril formation in the absence of any small molecule, but could not be used to investigate modulating once the small molecules were applied due to spectral interference issues.

Congo Red Binding Assay

Congo Red (CR) is another small molecule probe which, similar to ThT, has traditionally been used to identify amyloid fibrils, specifically in the form of deposits in the brain tissue or in vitro (reviewed in [24, 47, 49, 54]). CR binds to β-sheet rich structures present in amyloid fibrils[50] and

demonstrates a characteristic shift in the absorbance maximum from 490 to 540 nm and green birefringence with crossed polarized light.[48]

More recent studies have shed light on the use of CR toward examining prefibril aggregates. Walsh et al. observed a change in CR absorbance when applied to protofibrils, albeit the change was less marked than that of amyloid fibrils.[55] Additionally, Maezawa et al. applied surface plasmon resonance to identify the binding affinity/dissociation constant of CR towards prefibrillar oligomers.[49] However, a shift in absorbance maximum upon CR binding was not observed for prefibrillar oligomers. So, as was the case with ThT, recent studies demonstrate that CR could be applicable to characterize protofibrils, fibrils, and fibrillar oligomers, but not prefibrillar oligomers that do not have defined stacked β-sheet structure.

Because CR binding yields similar information as that obtained from ThT fluorescence, it was not needed in the dissertation work to verify fibril formation or monitor aggregation progression.

Antibody Dot Blot Assay

Because of the difficulty in obtaining high resolution crystal structures of protein aggregates (prefibril aggregates, in particular), conformational-specific antibodies have been developed over the past 10 years to help identify and monitor the state of amyloidogenic protein aggregation and screen potential aggregation inhibitors/modulators.

Glabe et al. developed three conformational-specific antibodies that are important to detect physiologically-relevant prefibril aggregates: A11 (recognizing prefibrillar oligomers but

not fibrillar conformers;[42] OC (recognizing the cross-stacked β-sheet structure of fibrillar oligomers, protofibrils, and fibrils;[14] and αAPF (recognizing annular protofibrils[21]). These conformational-specific antibodies have been extensively used and reviewed.[8, 22, 23, 43, 49, 56]

Even though the application of these antibodies has provided important insight into the properties of protein aggregates and the effects of potential therapeutics, recent studies have shown that care must be taken when using and interpreting the results. First, due to the transient nature of prefibril aggregates compared to end-state conformers, preparing a homogeneous sample of exclusively A11, OC, or αAPF reactive (no cross reactivity) aggregates in vitro has proven quite challenging, though preparations of homogeneous prefibril aggregates were reported by a few research groups.[9, 20, 21] Despite their success, non-physiological aggregation conditions (low pH[20]) or incomplete removal of pre-treatment disaggregation agent[9, 20] were employed in order to generate these homogeneous populations. Other groups who have applied the OC and A11 conformational-specific antibodies have observed more non-homogeneous populations, either in the form of fibrillar conformers populations containing significant A11-reactivity[57-59] or prefibrillar oligomer populations possessing significant OC-reactivity.[27, 60] Because of the cross reactivity demonstrated by these populations, it is difficult to discern which species is dominant. Second, in rare but present cases,[61] false positive antibody reactivity has been observed when testing the inhibitory/modulatory activity of extrinsic compounds on protein aggregates. Third, binding of these extrinsic compounds to antibody epitopes on protein aggregates can block subsequent antibody binding,[13] leading the investigator to think that significant and rapid conformational changes have occurred, when in reality, they may not have. Because of these three factors, care must be taken when designing experiments and interpreting the results of these antibodies.

Because of the insight that the three primary conformational-specific antibodies discussed above have given and due to the high degree of polymorphism that exists in prefibril aggregates, additional conformational-dependent antibodies are being developed to further characterize these conformers. Wang et al. developed four single-chain variable fragment antibodies that specifically recognize Aβ oligomers, but not monomers or fibrils.[62] However, the use of this antibody does not appear to have caught on in a widespread manner throughout the community. Furthermore, Kayed et al. developed 6 new monoclonal antibodies that recognize immunologically distinct preparations and sub-variants of prefibrillar oligomers also recognized by the more general polyclonal antibody, A11.[63] Even though the sub-classes of prefibrillar oligomers identified by the monoclonal antibodies showed different molecular weight size distributions through Western blot analysis, it is not yet clear whether or not these variants are more pathologically relevant than A11 antibody.

Because this dissertation work focuses on fibrils, protofibrils, and prefibrillar oligomers, the primary conformationally-specific antibodies used were OC and A11.

Methods for Obtaining Visual Morphological (Quaternary Structure) Information on Protein Aggregate Species

Electron Microscopy & Atomic Force Microscopy

Transmission Electron Microscopy (TEM) and Atomic Force Microscopy (AFM) are the two techniques most commonly used to visualize the morphology of amyloidogenic protein aggregate samples.[20, 23, 27, 29, 30, 49, 50, 58, 60, 64-69] Both TEM and AFM provide information (both

qualitative and quantitative) at the nanometer level of quaternary structure characteristics, including the length, width, curvature, and surface features of protein aggregates (reviewed in [47, 53, 70-74]).

However, there are several significant differences and/or limitations to consider when using these methods to study protein aggregates. Although TEM has the advantage of being a direct method (i.e. crystallization of the sample is not required[70]) and can be performed fairly quickly,[72] the detection limit for smaller aggregates less than ~20 nm is fairly limited compared to higher resolution techniques, such as AFM.[13, 74] Because of this limitation, TEM is generally accepted as being useful in verifying formation, inhibition, and/or disaggregation of larger protofibrils/fibrils and providing an approximate gauge for morphology of smaller aggregates, but not as the sole source for yielding high-resolution, low-error details of small prefibril conformers. However, it is important to note that despite this drawback, TEM has been used to provide a numerical estimation of the length or width of smaller aggregates less than 30 nm.[12, 60, 75]

Conversely, AFM provides sub-nanometer three-dimensional (including height) detection of protein sample characteristics[76] and is thus well-suited for studying smaller prefibril aggregates with low expected error. However, the sample preparation for AFM often takes longer and involves more steps (for example, freezing or adsorption to mica surface) than a simple negative-stain TEM sample preparation[72]. In addition, some convolution of the data is introduced when the radius of curvature of the tip used is close to the dimensions of the aggregates being studied.[13, 77]

Because AFM and TEM are such complimentary techniques (each with their respective strengths and weaknesses), both were used in this dissertation work as required.

Methods for Obtaining Secondary Structure Information on Protein Aggregate Species

Circular Dichroism & Fourier Transform Infrared Spectroscopy

Circular Dichroism (CD) and Fourier Transform Infrared Spectroscopy (FTIR) are two well-established techniques that are used most frequently to assay the secondary structure (β-sheet, α-helix, β-turn, and disordered content) of protein aggregates in vitro.[28, 29, 68, 69] CD measures the differential absorption of right and left polarized light, and FTIR analyzes molecular bond vibration frequencies.[73] Although it has been reported to be theoretically possible to determine antiparallel vs. parallel β-sheet secondary structure using CD,[78, 79] FTIR is used more readily to obtain resolution on secondary structures within the β-sheet group.

Secondary structure content is important for the study of protein aggregates because specific secondary structures are characteristic of different stages in the aggregation pathways. For example, in the Aβ peptide, monomers and small oligomers have been found to consist of mainly unordered/α-helical structures, whereas the intermediate fibrillar oligomers, protofibril, annular protofibril, and ending fibril conformers contain mostly β-sheet secondary structure.[19-22] Unlike the other conformers, there is a considerable amount of disagreement in the literature regarding the secondary structure of soluble prefibrillar oligomers. On one hand, several research groups have reported that Aβ oligomers contain mostly random coil/disordered secondary structure,[9, 12] while others have reported these oligomers possessing prevailing parallel or

antiparallel β-sheet content.[57, 58, 75] Given the transient nature of this aggregate species and the difficulty in preparing a homogeneous conformer sample, it is not surprising that different research labs obtained different results.

Despite extensive general reviews of the techniques[47, 53, 73, 74, 80-82] and the vast amount of primary works employing CD and FTIR to assess protein aggregates, a single, straight-forward protocol does not exist that details how to use these methods to estimate secondary structure content percentages. Instead, researchers employ a milieu of scientifically acceptable approaches to estimate secondary structure content from the raw CD and FTIR data generated. Often, a qualitative-based analysis is used by comparing general features of the CD or FTIR spectra with controls or "expected" results, which are used to correlate secondary structure changes or overall content. For example, the CD or FTIR spectra of an unknown protein aggregate sample could be compared to a predominantly β-sheet fibril control spectra, and deviations could be visualized.[20] Similarly, spectral features of an unknown sample, such as curve minima and maxima between 190-250 nm for CD and 1600-1700 cm^{-1} for FTIR are often compared to established "expected" correlations to obtain a qualitative assessment of the major secondary structure features.[9, 59, 60, 66] Correlations of CD and FTIR curve characteristics to secondary structure have been reviewed.[47, 83] Alternatively, a more complex, but quantitative analysis has been developed and utilized in order to estimate the percentage of secondary structure content of a sample from CD spectral data using one or more single value decomposition, regression, or neural network algorithms available.[84-86] Several examples of these methods/algorithms include CDSSTR, SELCON, CONTIN, and K2D.[87] It is important to note that the majority of these algorithms require that the sample CD spectra is 'matched' to a protein with known secondary structure content within various protein reference sets.[83] Because amyloidogenic proteins (or their parent proteins) and

disordered/random coil proteins are often not included in these reference sets, caution should be taken in interpreting CD spectra of disordered aggregates.[13, 39] Additionally, the numerical results obtained from the analysis should agree (at least directionally) with what is seen upon visual inspection of the sample spectra, and the error value (normalized root mean square deviation) should not be the only criteria used to select the best fit. Lastly, care must be taken to ensure the CD cuvette is sufficiently cleaned and dried prior to reading each sample. Cleaning often needs to be done with a solvent other than water, such as 2% Helmanex Solution or an acid. To ensure the cuvette is sufficiently clean, it is advisable to run a dd H_20 baseline prior to every protein aggregate sample to confirm drift has not occurred.

Due to equipment accessibility and the fact that resolution within the β-sheet secondary structure group was not needed (through FTIR), CD analysis was used in this dissertation work.

Dissertation Research Objectives

The overall goal of the Alzheimer's Disease project in the Kwon Research Group at University of Virginia is to characterize/investigate the capability of Erythrosin B (ERB), Brilliant Blue G (BBG), and their structural analogs to modulate neurotoxic Aβ aggregates in the ultimate pursuit of a novel, effective Alzheimer's Disease-modifying therapy.

This general goal could be approached in several ways, each of which must be investigated in the drug development process due to their inherent therapeutic relevance. First, the small molecules could inhibit the formation of neurotoxic conformers and/or promote the formation of non-toxic species during aggregation from the monomeric state (approach to

prevention of AD). Conversely, the small molecules could remodel pre-existing aggregates in to non-toxic conformers (approach for AD therapy after acute disease onset has already occurred). Regardless of whether the small molecule is acting on preformed conformers or monomers, it is hypothesized that the small molecules will antagonize Aβ aggregation and neurotoxicity through hydrogen bonding, pi-pi stacking between aromatic side-chains, electrostatic, and hydrophobic interaction effects. As such, a long-term goal of this project is to elucidate these specific small-molecule modulator interactions through structure-activity relationship analyses. This investigation could lead to the discovery of a whole group of therapeutic candidates (with the respective critical functional structures identified) that could strengthen the fight against AD.

In order to reach these long-term goals, several intermediate steps have to be performed first in the roadmap. These are listed numerically below:

1. Assess binding and modulating activity of BBG and ERB on overall Aβ monomer-to-fibril aggregation pathway and neurotoxicity.
2. Structure-activity relationship analyses - Assess binding and modulating activity of BBG and ERB structural analogs (with side chain substitutions) on overall Aβ monomer-to-fibril aggregation pathway and toxicity to elucidate important molecular structural features.[88]
3. Assess restructuring activity of BBG and ERB on preformed targeted Aβ aggregate species (fibrils, protofibrils, and oligomers) to test effect from different end of aggregation thermodynamic spectrum.
4. In vivo animal testing of drug candidates' efficacy in a transgenic Alzheimer's Disease mouse model.

Prior to me joining the Kwon Research Group, our lab had performed the following characterization steps: 1) shown that ERB and BBG were effective modulators of Aβ40-associated in vitro aggregation and toxicity from the monomer state[27, 89] and 2) performed a structure-activity relationship analysis of BBG's structural analogs to reveal important structural features for the compounds' modulatory and binding effects on Aβ monomers.[89]

In order to continue the development/characterization progress for these potential small molecule therapeutics, **the following specific dissertation research objectives were set forth.**

1. In vitro structure-activity relationship analysis of ERB and structural analogs to determine important molecular structural features required for molecular binding and subsequent modulatory capacity of Aβ aggregation and neurotoxicity (from monomer starting material).
2. In vitro investigation of ERB and structural analogs ligand binding sites on Aβ target peptide monomers.
3. In vitro comparative studies on the structural fates of mature, thermodynamically very stable Aβ40 amyloid fibrils destabilized by BBG and ERB.
4. In vivo efficacy evaluation of BBG in a transgenic mouse model of Alzheimer's Disease.

Chapter 2: In Vitro Structure-Activity Relationship Analysis of Erythrosin B Analogs Reveals That Halogenation Generates Effective Binders and Modulators of Amyloid-Beta Monomer Aggregation and Neurotoxicity[90]

Abstract

Halogenation of organic compounds plays diverse roles in biochemistry, including selective chemical modification of proteins and improved oral absorption/blood-brain barrier permeability of drug candidates. Moreover, halogenation of aromatic molecules greatly affects aromatic interaction-mediated self-assembly processes, including amyloid fibril formation. Perturbation of the aromatic interaction caused by halogenation of peptide building blocks is known to affect the morphology and other physical properties of the fibrillar structure. Consequently, in this chapter, we performed a structure-activity relationship analysis to investigate the ability of Erythrosin B (ERB) analog halogenated ligands to bind and modulate the self-assembly of the amyloidogenic amyloid-beta peptide (Aβ). Considering that four halogen atoms are attached to the xanthene benzoate group in ERB, we hypothesized that halogenation of the xanthene benzoate plays a critical role in modulating Aβ aggregation and cytotoxicity. Therefore, we evaluated the binding and modulating capacities of four ERB analogs containing different types and numbers of halogen atoms as well as Fluorescein (FLN) as a negative control. We found that FLN is not an effective modulator/binder of Aβ aggregation and cytotoxicity. However, halogenation of either the xanthene or benzoate ring of Fluorescein substantially enhanced the binding and inhibitory capacity on Aβ aggregation. Such Aβ aggregation inhibition by ERB analogs except Rose Bengal correlated well to the inhibition of Aβ cytotoxicity. To our knowledge, this is the first report demonstrating that halogenation of aromatic rings substantially enhance inhibitory capacities of small molecules on Aβ-associated neurotoxicity via Aβ aggregation modulation.

Introduction

Halogenation has been widely used to provide organic compounds, including biomolecules, with new properties. Introduction of aryl halides in to proteins allows chemical modification via versatile palladium catalyzed cross-coupling reactions with terminal alkene or alkyne reaction partners,[91, 92] and facilitates monitoring structural changes of protein.[93, 94] Halogen groups are often inserted during hit-to-lead or lead-to-drug conversions for several reasons, including enhanced antagonistic/agnostic effects due to improved oral absorption/blood-brain barrier permeability.[95] Furthermore, it was reported that halogenation of aromatic molecules greatly affects aromatic interaction-mediated self-assembly processes.[96] Aromatic interaction plays an important role in a broad spectrum of molecular self-assemblies.[93, 97-99] In particular, aromatic interaction is considered one of the critical contributors to forming cross-stacked β-sheet structure, so called, amyloid fibrillar structure.[100, 101] Planar aromatic interaction stabilizes the fibrillar structure and determines the direction and orientation of amyloid fibrils.[102, 103] Therefore, perturbation of the aromatic interaction caused by halogenation of aromatic building blocks affects the morphology and physical properties of the fibrillar structure. [93]

Herein, we have performed a structure-activity relationship analysis to investigate whether halogenation of ligands can also affect binding and self-assembly of amyloid-beta peptide (Aβ), which is implicated in Alzheimer's Disease (AD). A pathological hallmark of AD is the accumulation of insoluble protein aggregates, composed primarily of fibrillar Aβ aggregates. According to the revised amyloid-cascade hypothesis, certain types of soluble Aβ oligomers and protofibrils are more toxic than Aβ fibrils and correlate well with dementia.[9, 11, 75, 104] Therefore, modulation of Aβ aggregation using small molecules is considered a promising way to eliminate Aβ associated toxicity.[16, 23, 35, 46, 59, 88, 93, 105-114] We recently reported that the red

food dye, Erythrosin B (ERB), is a novel modulator of Aβ-aggregation in vitro and Aβ neurotoxicity.[27] The good biocompatibility and possibility of systemic administration make ERB an attractive inhibitor of Aβ neurotoxicity.[115, 116] Considering that ERB has multiple aromatic rings attached to four electronegative halogen atoms (Figure 2.1), we hypothesized that the modulatory capacity of ERB on Aβ aggregation is attributed to halogen atoms. In order to validate our hypothesis that halogen atoms are key chemical structures for Aβ aggregation modulation, we evaluated the modulating and binding capacities of four ERB congeners/analogs, Eosin Y (EOY), Eosin B (EOB), Rose Bengal (ROB), and Phloxine B (PHB) (Figure 2.1), each of which contains different types and numbers of halogen atoms. As a negative control, we also evaluated Fluorescein (FLN), which has the same xanthene benzoate backbone as ERB but lacks a halogen atom. If halogenation of aromatic rings is indeed effective in modulating Aβ aggregation and cytotoxicity, it will enhance our understanding of the molecular mechanism of amyloid formation and facilitate discovery and design of a new series of halogenated small molecule modulators of amyloidogenic peptides/proteins.

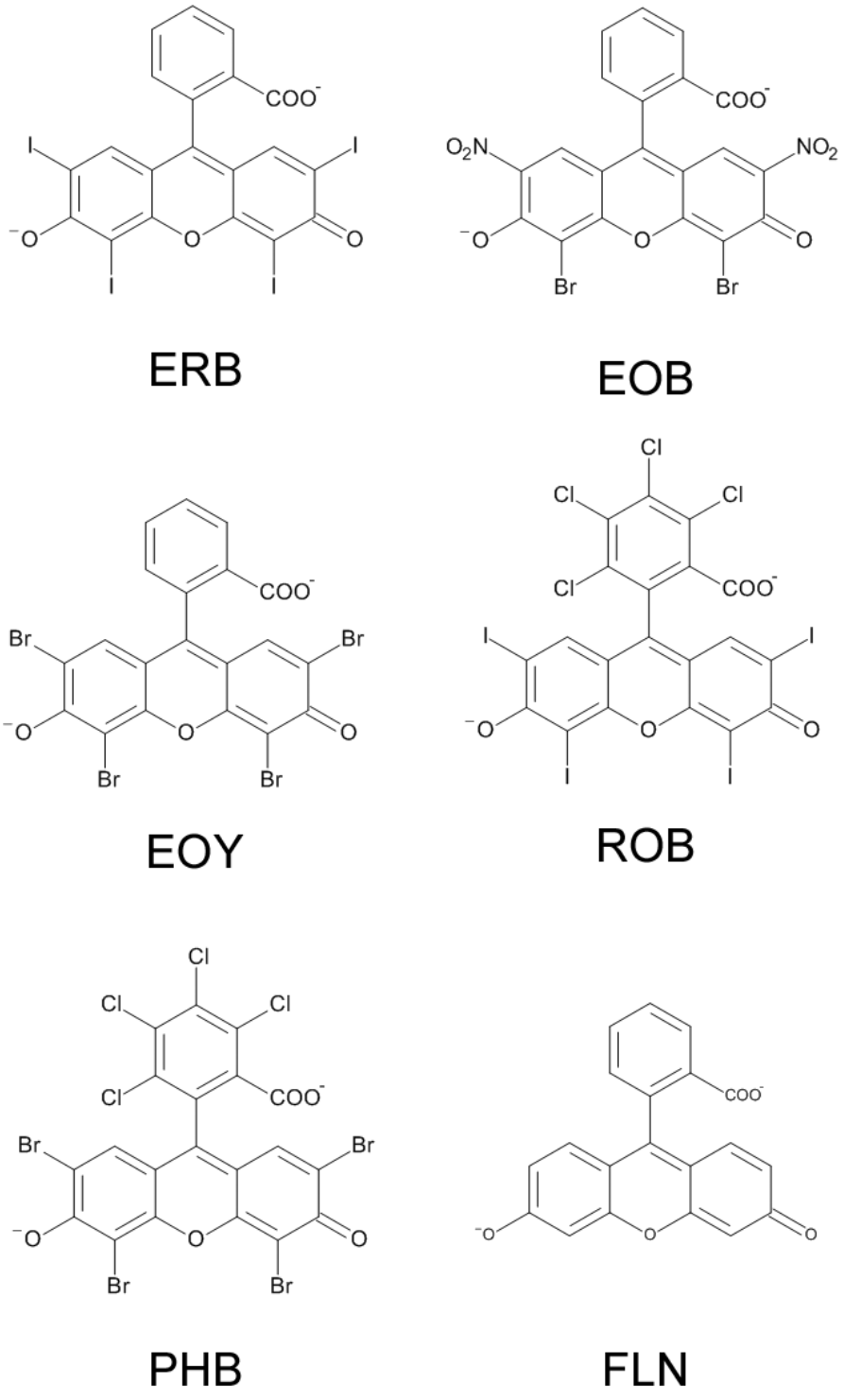

Figure 2.1 - Chemical Structure of Erythrosin B (ERB), Eosin Y (EOY), Eosin B (EOB), Rose Bengal (ROB), Phloxine B (PHB), and Fluorescein (FLN) at neutral pH.

Materials and Methods

Materials

Aβ40 was purchased from Anaspec Inc. (Fremont, CA) and Selleck Chemicals (Houston, TX). Human neuroblastoma SH-SY5Y cells were obtained from the American Type Culture Collection (ATCC; Manassas, VA). Polyclonal A11 anti-oligomer and horseradish peroxidase (HRP)-conjugated anti-rabbit IgG antibodies were obtained from Invitrogen (Carlsbad, CA). 4G8 antibody was obtained from Covance (Dedham, MA). Polyclonal OC antibody and 3-(4,5-dimethylthiazol-2-yl)-2,5-diphenyltetrazolium bromide (MTT) was obtained from Millipore (Billerica, MA). Nitrocellulose membranes and ECL advance chemiluminescence detection kit were obtained from GE Healthcare Life Sciences (Waukesha, WI). Eosin Y was purchased from Acros Organics (Geel, Belgium). All other chemicals were obtained from Sigma-Aldrich (St. Louis, MO) unless otherwise noted.

Aβ Aggregation

Aβ40 stock was prepared as described previously[27, 89] except the pretreatment using hexafluoroisopropanol (HFIP). It has been reported that HFIP increases the α-helix content of a protein and is a strong disaggregating solvent of Aβ.[42, 86] Lyophilized Aβ40 was dissolved in 100 % HFIP (1 mM) and incubated at room temperature for 2 hours. HFIP was evaporated under a constant stream of nitrogen, and the peptide was reconstituted in phosphate buffered saline (PBS) solution (10 mM NaH_2PO_4 and 150 mM NaCl, pH 7.4) to a concentration of 50 μM. If needed, the HFIP treated peptide was dissolved in 100 mM NaOH (2 mM Aβ) prior to dilution in PBS. Erythrosin B, Eosin Y, Eosin B, Rose Bengal, Phloxine B, and Fluorescein were dissolved in

PBS. Concentrated dye stock solutions were added to the peptide solutions. The Aβ40 peptide samples were incubated at 37 ˚C in the absence or in the presence of the dye.

Thioflavin T (ThT) Assay

5 μL of Aβ sample (50 μM) was dissolved in 250 μL of ThT (10 μM). Fluorescence was measured in 96-well microtiter plates (Fisher Scientific, Pittsburgh, PA) using a Synergy 4 UV-Vis/fluorescence multi-mode microplate reader (Biotek, VT) with an excitation and emission wavelength of 438 nm and 485 nm, respectively.

Transmission Electron Microscopy (TEM)

TEM was performed as reported previously.[27, 89] Aβ samples (10 μL of 50 μM Aβ) were placed on 200 mesh formvar coated/copper grids, absorbed for 1 minute, and blotted dry with filter paper. Grids were then negatively stained with 2% uranyl acetate solution, blotted dry, and then inspected with a JEOL 1010 Transmission Electron Microscope operated at 60 kV.

Dot Blotting

Dot blotting was performed as reported previously.[13, 27, 89] 2 μL Aβ samples were spotted onto nitrocellulose membranes and were dried at room temperature. A solution of 0.1 % Tween 20 in Tris-buffered saline (TBS-T) solution (0.1% Tween 20, 20 mM Tris, 150 mM NaCl, pH 7.4) was prepared. Each nitrocellulose membrane was blocked at room temperature for 1 hour (5 % milk TBS-T) and washed with TBS-T. Each membrane was then incubated with antibody (HRP-conjugated 4G8, A11, or OC antibody) in 0.5% milk TBS-T for 1 hour at room temperature and washed with TBS-T. After immunostaining with HRP-conjugated 4G8, the

membranes were coated with ECL advance detection agent (based on manufacturer specifications) and visualized. Alternatively, all other membranes were incubated with HRP-conjugated IgG in 0.5 % milk TBS-T for 1 hour and washed with TBS-T. Signal detection was performed as aforementioned using the ECL Advance Detection kit and was visualized using a Biospectrum imaging system (UVP, Upland, CA). HRP-conjugated 4G8 and OC were applied at a 1:25000 dilution while A11 and HRP-conjugated IgG were applied at a 1:10000 dilution.

MTT Reduction Assay

MTT reduction assay was performed as reported previously.[27, 89] SH-SY5Y cells were cultured in a humidified 5 % CO2/air incubator at 37 ˚C in DMEM/F 12:1:1 containing 10 % fetal bovine serum and 1 % penicillin-streptomycin. 20000 to 25000 cells were seeded into each well of a 96-well microtiter plate (BD, Franklin Lakes, NJ) and allowed to acclimate for 3 days. 10 μL of Aβ sample was added to each well and incubated for 2 days. The cells were washed by replacing the culture media with fresh media and incubating for 1 hour. The wash media was replaced with fresh media. 10 μL of MTT was added to each well and incubated in the dark for 6 hours at 37 ˚C. After incubation, reduced MTT was dissolved with 200 μL of dimethylsulfoxide (DMSO). After reduced MTT dissolution, the absorbance was measured at 506 nm using a Synergy 4 UV-Vis/fluorescence multi-mode microplate reader (Biotek, VT).

Circular Dichroism (CD)

CD analysis of Aβ samples was performed as described previously.[13, 117, 118] Aβ sample was diluted 1:10 using double distilled water. Samples were measured using a Jasco J710 spectropolarimeter with a 1 mm path length. The reported spectrum for each sample was the

average of at least 5 measurements and the background was subtracted using appropriate controls. In case of samples containing any dye, the background spectra were obtained using controls containing only dye at the same concentration.

Aβ Binding Assay

The binding of ERB, EOY, ROB, PHB, and FLN to Aβ40 was assessed using modified assays based on emission fluorescence quenching techniques described in the literature.[119-122] The concentration of each of the dyes was fixed at 20 μM. In order to evaluate fluorescence quenching of the dye upon binding to Aβ40, Aβ40 was mixed with the dye in a final concentration of 0 to 25 μM in citrate buffer at pH 4.5. The excitation wavelengths used are as follows: ERB – 317 nm, EOY – 480 nm, ROB – 510 nm, PHB – 500 nm, and FLN – 432 nm. The emission wavelengths where the data were collected are as follows: ERB – 548 nm, EOY – 536 nm, ROB – 565 nm, PHB – 555 nm, and FLN – 512 nm. With FLN, fluorescence quenching was also investigated due to binding to bovine serum albumin (BSA - New England Biolabs, Ipswich, MA) by mixing with FLN in a final concentration of 0 to 25 μM BSA in citrate buffer at pH 4.5. Where appropriate, the dissociation constant, K_d, was determined using non-linear regression curve fitting to Eq. 1 shown below. In Eq. 1, n is the number of binding sites, and $[D]$ is the molar concentration of free dye.

$$\bar{n} = \frac{n\,[D]}{K_d + [D]} \qquad \textit{Eq. 1}$$

Where, $\bar{n}$ is the average number of dye molecules bound to protein/peptide molecule and thus is calculated as shown in Eq. 2.

$$\bar{n} = \frac{X\,[D_t]}{[P_t]} \qquad \textit{Eq. 2}$$

And, $[D_t]$ and $[P_t]$ are the total molar dye (set at 20 μM) and Aβ40 concentrations, respectively, and X is the fraction of dye bound to Aβ40 at each Aβ40 concentration, calculated as shown in Eq. 3. In Eq. 3, F_{free}, $F_{obs.}$, and F_0 correspond to the free 20 μM dye fluorescence, fluorescence observed at a certain Aβ40 concentration, and the fully quenched fluorescence values, respectively.

$$X = \frac{F_{free} - F_{obs.}}{F_{free} - F_0} \qquad \textit{Eq. 3}$$

We assessed the binding of EOB to Aβ40 and BSA, using an absorbance technique described in the literature based on the observation that upon protein binding,[123] the absorbance maximum of EOB shifts from 514 to 530 ± 5 nm. The concentration of EOB was fixed at 20 μM. Aβ40 and BSA concentrations were varied from 0 to 60 μM and 0 to 25 μM, respectively, and the absorbance was measured at 530 nm. Citrate buffer at pH 4.5 was also used for the EOB binding assay.

Results and Discussion

ERB, EOY, and PHB Substantially Inhibit Aβ-Associated Cytotoxicity

In order to evaluate the modulation capability of ERB and its analogs (EOY, EOB, PHB, and ROB), we employed the widely-used MTT reduction assay.[9, 27, 59, 89, 124, 125] Aβ aggregates were prepared by incubating Aβ monomers with or without 3x ERB analog. In the absence of any ERB analog, Aβ aggregation was monitored by ThT fluorescence assay. The ThT fluorescence of Aβ aggregates started to increase at day 4 and reached the plateau at day 6 (Figure 2.2A), indicating that Aβ protofibrils and fibrils were primarily formed from day 4. In order to evaluate cytotoxicity of Aβ aggregates containing Aβ intermediates, we chose Aβ samples incubated for 5 days in the absence or presence of 3x ERB analog. The preformed Aβ aggregates were then administered to neuroblastoma SH-SY5Y cells, and cell viability was determined by MTT reduction (Figure 2.2B). We determined whether Aβ monomer or ERB analog with no peptide is cytotoxic to neuroblastoma SH-SY5Y cells, and the results are shown in Figure 2.2B. Aβ monomers (5 μM) caused a mild reduction (11%) in the cell viability. All ERB analogs (15 μM) except ROB also caused only mild reduction in the cell viability ranging from 0 to 8%. However, 3x ROB substantially reduced the cell viability (34%). ROB has been tested to ablate certain types of cancer cells including melanoma,[126, 127] and so it is not surprising that ROB is cytotoxic to SH-SY5Y cells.

Next, we determined the cytotoxicity of Aβ monomers incubated with or without ERB analog for 5 days, and the results are shown in Figure 2.2B. 5 μM of Aβ aggregates without any ERB analog (Aβ control) substantially reduced the cell viability to 63%. Co-incubation of Aβ monomers in the presence of 3x EOB (15 μM) resulted in an SH-SY5Y cell viability of 65%, which is not significantly different from that of Aβ control. However, co-incubation of Aβ

monomer with 3x ERB, EOY, or PHB significantly increased the cell viability (around 21%). In the presence of 3x ROB, cell viability was 70%, which is only 7% higher than that of the Aβ control. The MTT reduction assay results clearly indicate that 3x ERB, EOY, and PHB can substantially inhibit Aβ-associated cytotoxicity, but 3x EOB cannot. The Aβ monomers incubated with 3x ROB (15 μM) led to a substantial reduction in the cell viability (30%). However, since 3x ROB alone (no Aβ) was intrinsically toxic and led to a similar reduction in cell viability (34%), it is difficult to gauge the effect 3x ROB co-incubation had on Aβ-induced cytotoxicity. In order to clarify this, we repeated the MTT cell viability assay, this time comparing the results obtained using 2.5 μM and 5 μM Aβ, both with corresponding concentrations of 3x ROB (7.5 μM and 15 μM, respectively – Figure A1; Panels A and B in Appendix A). Since the ThT fluorescence of the Aβ aggregates reach a plateau at day 6, the Aβ aggregates in day 3 were used as Aβ intermediate controls. When 5 μM Aβ and 15 μM ROB were used, we again observed a substantial reduction in cell viability upon the addition of 3x ROB alone ($P < 0.05$) and Aβ intermediate controls compared to Aβ monomer and PBS samples (Figure A1; Panel A). However, when concentrations of 2.5 μM Aβ and 7.5 μM ROB were applied to the cells, the intrinsic cytotoxicity of ROB alone (no Aβ) was greatly reduced to approximately the level of the Aβ monomer control (Figure A1; Panel B). These results allowed us to interpret the true effect ROB had on Aβ-induced toxicity. Similar to EOB, co-incubation of Aβ monomers with 3x ROB for 3 days did not significantly alleviate the Aβ-associated cytotoxicity displayed by the Aβ intermediate control ($P > 0.05$). Next, in order to investigate the effect that dye binding to Aβ had on Aβ-associated toxicity, Aβ intermediates from day 3 of aggregation were mixed with 3x ROB and immediately added to the SH-SY5Y cells. As with the ROB co-incubation, the results showed that ROB binding to Aβ did not alleviate the associated

toxicity ($P > 0.05$) (Figure A1). In addition, since the Aβ intermediates mixed with 3x ROB immediately prior to addition to the cells showed similar cell viability to the Aβ intermediate control, we concluded that the intrinsic toxicity of ROB and Aβ are not additive.

It should be noted that careful execution of the MTT reduction assay and interpretation of the results is required due to several factors. The first potential issue is that of Aβ-induced expedited exocytosis of the reduced MTT. Several reports showed that Aβ aggregates can export the reduced MTT and so promote the crystalline form of the reduced MTT deposit on the cell surface leading to a reduced MTT uptake.[128-130] In our previous studies, there was a good correlation between a MTT reduction and another viability assay based on Alamar blue reduction [89]. Therefore, we considered that the MTT reduction assay is a valid viability assay on the cell line and Aβ preparation method used in this study. The second issue relates to potential interference effects that the dyes investigated in this study might have on the final results obtained from the cell viability MTT assay (itself a color-based test). In order to minimize this potential interference by removing the dyes prior to reading the MTT signal, all viability assays incorporated thorough washing steps, as detailed in the Methods section above. To validate the washing steps conducted, the fraction of each original dye amount remaining in the culture plate wells after thoroughly washing the cells using the MTT protocol was quantified. The results showed that less than 3% of the original dye amounts remained in the wells after washing (Table A1 in Appendix A). Next, we quantified the interference effect these residuals might have on the final MTT absorbance. Our results showed that the interference was less than 5% for all dyes (Table A1 in Appendix A), which is consistent with the intrinsic uncertainty of the MTT assay (4 to 6%) in Figure 2.2B and Figure A1 in Appendix A, indicating that the dyes do not cause significant spectral interference in the MTT assays.

By correlating the chemical structures of ERB analogs and their inhibitory capacities on Aβ cytotoxicity, we deduced the following. First, EOY, which contains four bromine atoms in the same locations as the four iodine atoms in ERB, exhibited similar inhibitory capacities on Aβ cytotoxicity as ERB. However, EOB, which contains two nitro groups in the place of the two bromine atoms in the xanthene group of EOY, did not show any significant inhibitory capacity on Aβ cytotoxicity. Therefore, these findings clearly indicate that either bromine or iodine atoms in the two positions of xanthene group are critical for Aβ cytotoxicity inhibition. Second, PHB, which contains four extra chlorine atoms in the benzoate ring structure present in EOY, exhibits significant inhibitory capacities on Aβ cytotoxicity (similar to EOY). The third conclusion we made was in regards to ROB, which did not eliminate Aβ-associated cytotoxicity. ROB differs from ERB in that it is outfitted with four extra chlorine atoms in the benzoate ring and differs from PHB in that the bromine atoms on the xanthene group are replaced with iodine. The ROB results clearly indicate that not only the presence, but also the specific position of the halogenation, are important in determining the potency in inhibiting Aβ-cytotoxicity.

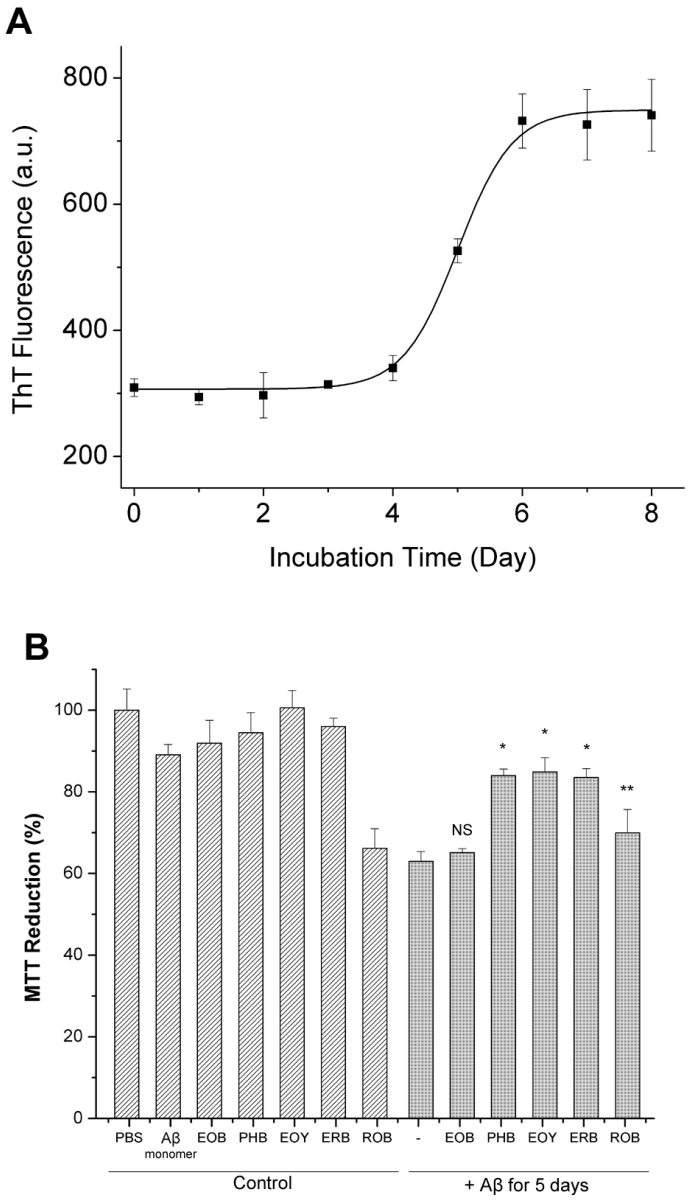

Figure 2.2 - Monitoring Aβ aggregation by ThT fluorescence assay and measuring Aβ-associated cytotoxicity using MTT reduction assay. (A) Time course of ThT fluorescence of Aβ samples. 50 μM of Aβ monomer was incubated at 37 °C. 5 μL of Aβ sample was taken daily for 8 days for ThT fluorescence analysis. ThT fluorescence was measured in arbitrary units (a.u.). Values represent means ± standard deviation (n = 3). (B) Viability of neuroblastoma SH-SY5Y cells incubated with ERB analog controls and preformed Aβ samples in the absence or presence of ERB analog. Preformed Aβ aggregates were prepared by incubating 50 μM of Aβ monomer in the absence or presence of ERB analog (EOB, PHB, EOY, ERB, or ROB) at 37 °C for 5 days. Aggregates were then administered to SH-SY5Y cells at a final concentration of 5 μM. After 48 hours, MTT reducing activity was measured. Values represent means ± standard deviation ($n \geq 3$). Values are normalized to the viability of cells administered with PBS only. Two-sided Student's t-tests were applied to the MTT reduction data of Aβ aggregates in the presence of ERB analog at day 5 compared to that of the Aβ only control. (NS; Not significant, *; $P < 0.001$, **; $P < 0.05$).

Aβ Monomers Aggregate to Form Prefibrillar and Fibrillar Aggregates

In order to determine whether Aβ cytotoxicity inhibition by ERB analogs is associated with Aβ aggregation modulation, we characterized the Aβ aggregates formed in the absence or presence of each ERB analog using CD, TEM, and dot-blot assays. CD analysis has been widely used to monitor secondary structure changes of proteins.[6, 19, 131, 132] The CD spectrum of Aβ monomer did not exhibit any spectral feature of α-helix and β-sheet, but showed typical features of dominantly disordered structure (Figure 2.3A). The CD spectrum of Aβ aggregates at day 5 exhibited the typical signatures of β-sheet structure, including a minimum at 217 nm (Figure 2.3A), which indicate that disordered Aβ monomers aggregated into β-sheet rich fibrillar aggregates. The TEM image of Aβ monomers incubated for 5 days also clearly show the existence of the Aβ aggregates consisting of protofibrils and short fibrils (Figure 2.4; Panel Aβ only). Recently, dot-blotting with Aβ-specific antibodies has been widely used to detect the spectrum of Aβ aggregates with different conformations.[9, 14, 20, 42, 110, 133, 134] OC is a polyclonal antibody that reacts with neurotoxic fibrillar oligomers, protofibrils, and fibrils.[9, 14] It was shown that Aβ-associated toxicity could be eliminated by reducing the OC-reactive species.[9] Dot-blot assay using the OC antibody confirmed the existence of fibrillar structure at day 5 (Figure 2.5; Panel OC). 4G8 is an Aβ-sequence-specific monoclonal antibody[135-138] of which epitope is known to be residues 17 to 24 of Aβ. During transition from monomers to fibrils, β-sheet stacking buries the 4G8 epitope and ultimately limits 4G8 antibody access to the epitope leading to a significant reduction in the 4G8 reactivity.[27, 58, 89] Therefore, the reduction in 4G8 reactivity of Aβ aggregates at days 5 and 6 can be attributed to the formation of fibrils and the lateral fibril stacking (Figure 2.5; Panel 4G8). A11 is a polyclonal antibody that reacts with disordered prefibrillar aggregates.[9] The weak A11-reactivity of the Aβ aggregates at day 5 indicate that

content of disordered prefibrillar Aβ aggregates was low (Figure A2 in Appendix A). Therefore, the CD, TEM, and dot-blot results using Aβ-specific antibodies clearly show that the Aβ aggregates at day 5 mainly consist of fibrillar aggregates including protofibrils and short fibrils.

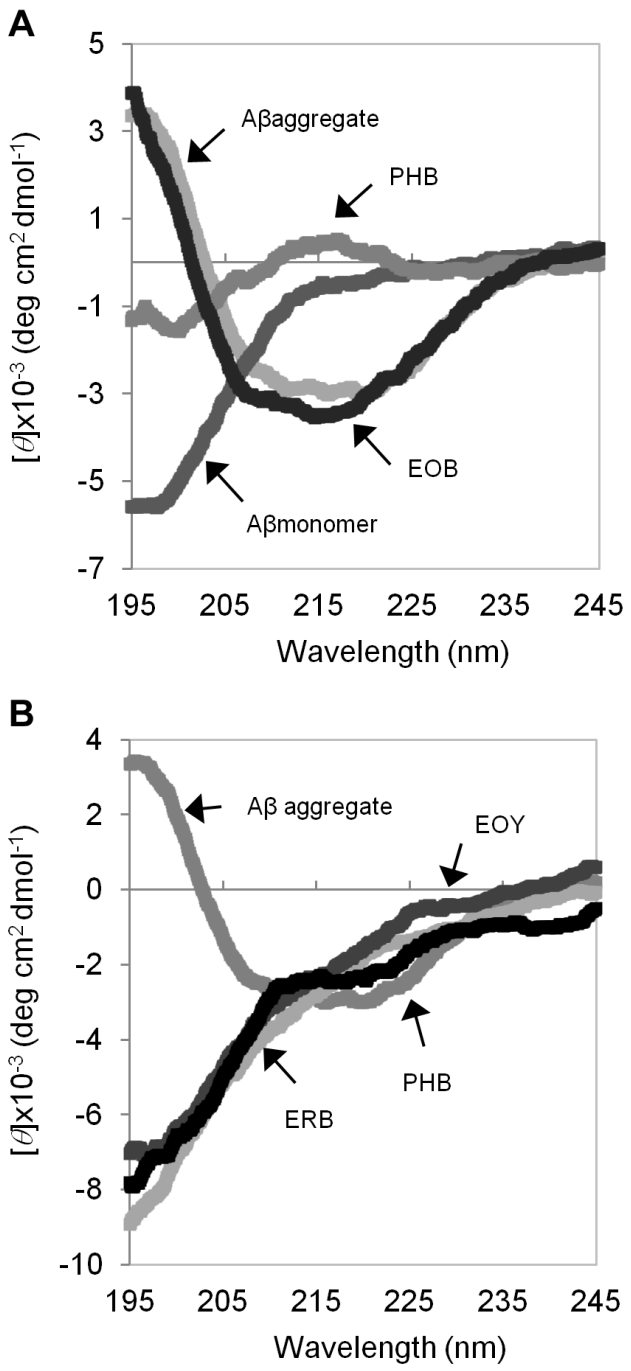

Figure 2.3 - CD spectra of Aβ monomer and preformed Aβ aggregates. (A) CD spectra of Aβ monomer, Aβ aggregates formed in the absence or presence of 10x EOB or PHB for 5 days at 37 °C. (B) CD spectra of Aβ aggregates formed in the absence or presence of 10x EOY, ERB, or ROB for 5 days at 37 °C.

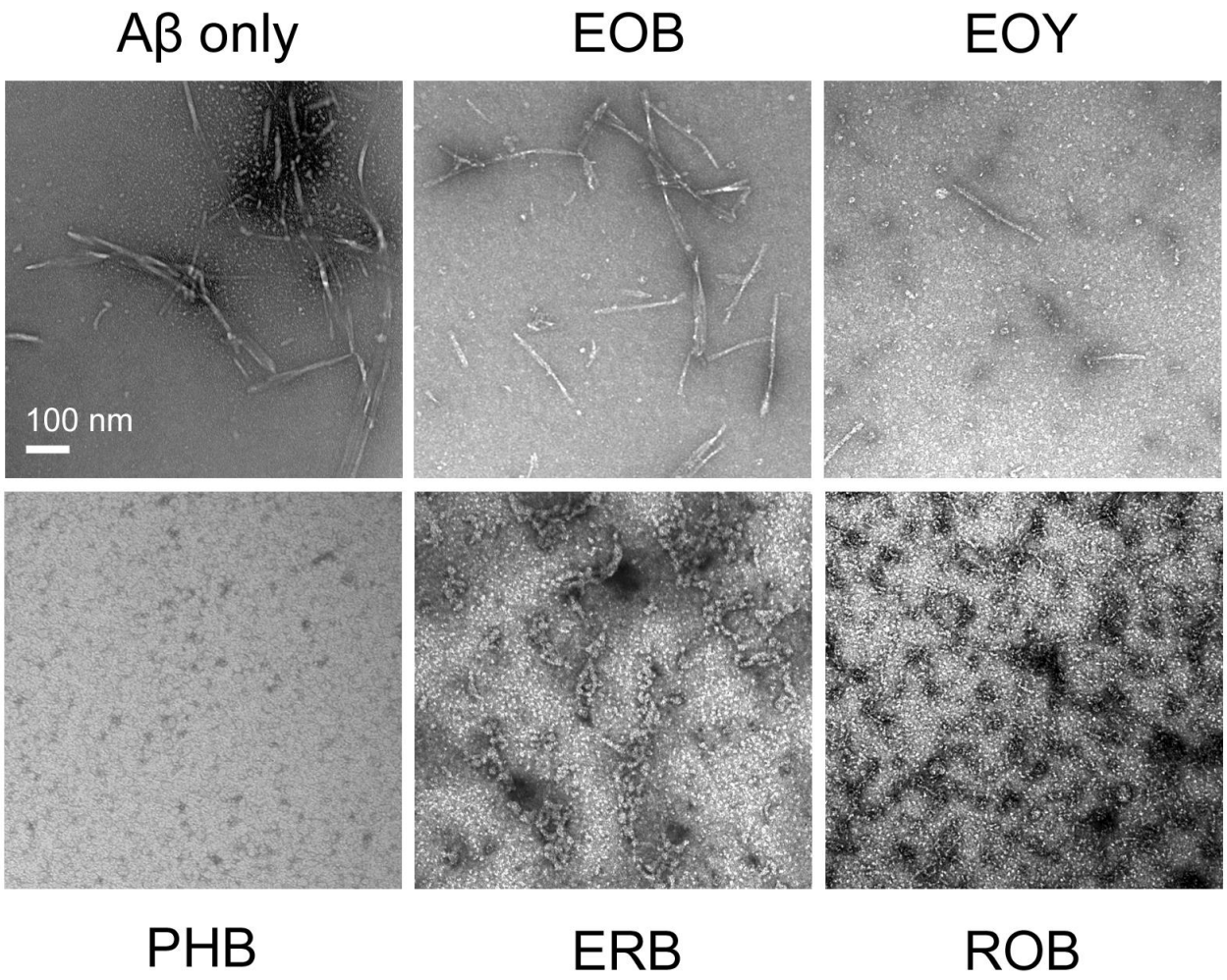

Figure 2.4 - TEM images of 50 µM Aβ incubated for five days at 37 °C in the absence of any dye (Aβ only), or in the presence of 3x EOB, EOY, PHB, ERB, or ROB. Scale bar is 100 nm.

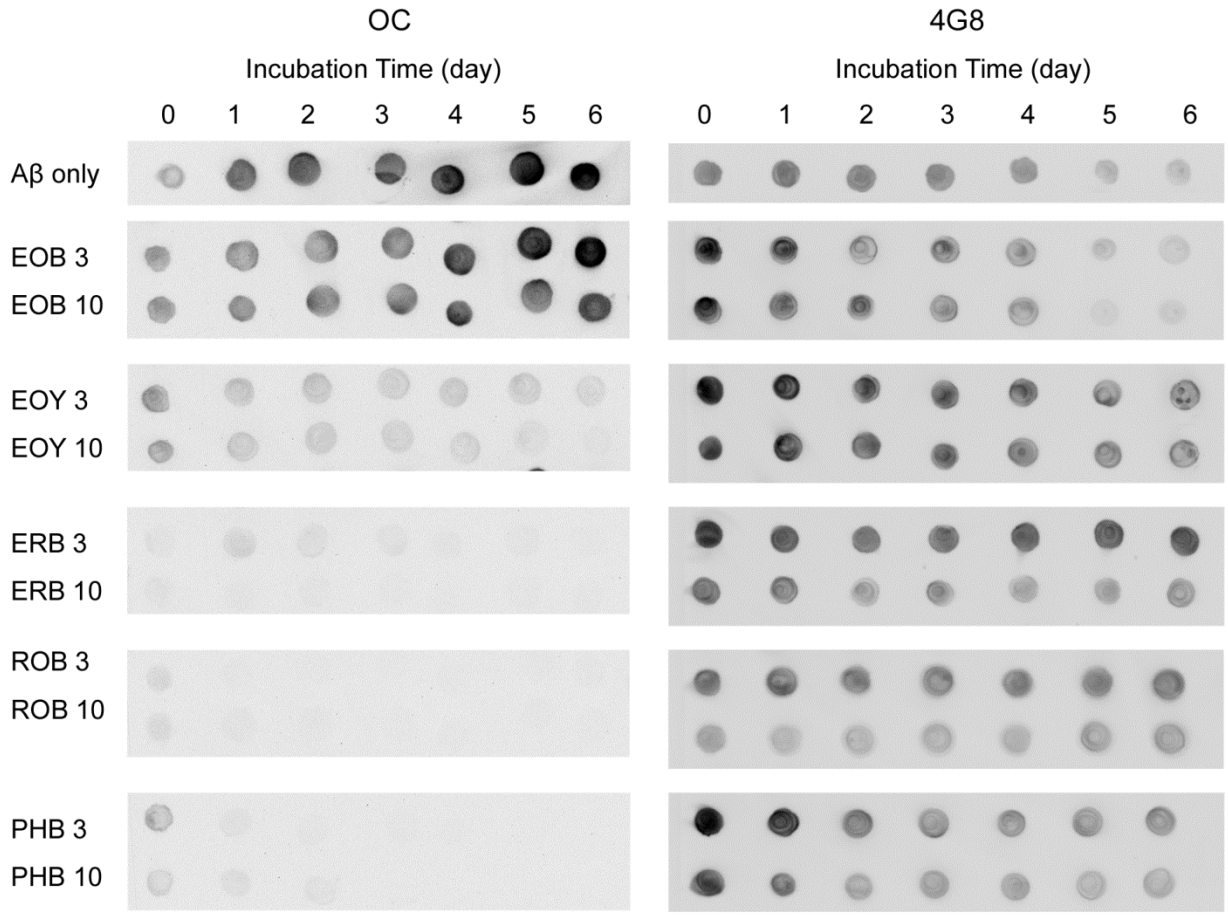

Figure 2.5 - Modulation of Aβ aggregation by ERB and ERB analogs. 50 μM of Aβ monomer was incubated at 37 °C in the absence (Aβ only) or presence of 3x and 10x ERB analogs (EOB, EOY, ERB, ROB, and PHB) for up to 6 days. For each antibody, all samples were spotted onto one nitrocellulose membrane. Each membrane was immunostained with the OC or 4G8 antibody. For clearer presentation of the data, the sections of each membrane were cut and re-arranged.

EOB Does Not Modulate Aβ Aggregation, but PHB Substantially Inhibits Aβ Aggregation

Next, we characterized the Aβ aggregates formed in the presence of 3x or 10x EOB. The CD spectrum of Aβ aggregates formed with EOB exhibits dominant β-sheet structure, possibly fibrillar structures, similar to that of Aβ control (Figure 2.3A). The TEM images also show that the EOB-induced Aβ aggregates have protofibrils and short fibrils similar to the Aβ control (Figure 2.4; Panels EOB and Aβ only). Furthermore, the EOB-induced Aβ aggregates exhibit immuno-reactivity against OC-, 4G8-, and A11-antibodies similar to those of the Aβ control from days 0 to 6 (Figure 2.5; Figure A2 in Appendix A). The CD, TEM, and dot-blot assay results clearly indicate that the co-incubation of EOB with Aβ monomer does not substantially affect Aβ aggregation process, which is consistent with the MTT reduction results showing that the cytotoxicity of the EOB-induced Aβ aggregates was comparable to that of Aβ control (Figure 2.2B). These findings indicate that addition of two nitro groups and two bromine atoms to xanthene benzoate does not enhance modulatory capacity on Aβ aggregation and cytotoxicity. However, considering the possibility of negative effects of two nitro groups on the modulatory capacity of halogenated xanthene benzoates, we also tested the other xanthene benzoate derivatives which contain only halogen atoms.

In case of PHB, the CD, TEM, and dot-blot assay results clearly indicate that co-incubation of Aβ monomer with PHB significantly inhibits the Aβ aggregation process (Figures 2.3A, 2.4, and 2.5). First, the CD spectrum of the Aβ monomers co-incubated with PHB for 5 days do not show any typical features of α-helical and β-sheet structure, strongly indicating that the PHB-induced Aβ species have disordered structure (Figure 2.3A). In the TEM image of the PHB-induced Aβ species, no Aβ aggregates were observed (Figure 2.4; Panel PHB), indicating

no large molecular weight aggregates are present in the Aβ sample. Since no aggregates were detected in the TEM image, the dot-blot assays using fibrillar or disordered oligomer-specific antibodies (OC- or A11-antibodies) were employed to monitor formation of Aβ oligomers. The Aβ monomers co-incubated with either 3x or 10x PHB exhibit neither OC- nor A11-reactivity, indicating that the PHB-induced Aβ species were neither fibrillar nor disordered prefibrillar Aβ oligomers (Figure 2.5 Panel OC; Figure A2 in Appendix A). Therefore, the TEM, CD, and dot-blot assay results strongly support the idea that co-incubation of PHB significant inhibits formation of any Aβ oligomers/higher molecular weight aggregates, but allows maintaining Aβ monomer-like structural features. Considering that Aβ monomer is known to be a non-toxic species,[9, 27, 89] the substantial reduction of Aβ-associated cytotoxicity by co-incubating Aβ monomer with PHB can be attributed to the Aβ monomer-like structure of the PHB-induced Aβ species.

EOY, ERB, and ROB Substantially Inhibit Fibrillar Structure Formation

We then characterized the Aβ aggregates formed in the presence of 3x or 10x EOY, ERB, or ROB. The three CD spectra of the Aβ aggregates formed with one of the three ERB congeners (10x EOY, ERB, and ROB) were almost overlapped (Figure 2.3B), indicating that the secondary structure contents of the Aβ aggregates are similar. The negative ellipticity value over all ranges of wavelength and the strong negative ellipticity values below 200 nm indicate the typical features of denatured proteins[139] or disordered Aβ aggregates induced by small molecules.[9, 16] Therefore, the CD analysis results support the idea that the three Aβ aggregates formed with EOY, ERB, and ROB have an increased disordered structure content but a

decreased β-sheet structure (possibly fibrillar structure) compared to Aβ control. However, the overlapped CD spectra of the Aβ samples with the three 10x dyes make it difficult to determine relative Aβ-aggregation modulating capacities of the three dyes. Therefore, the CD spectrum of the Aβ aggregates formed with a lower concentration (3x) of EOY, ERB, or ROB was also obtained (Figure A3 in Appendix A). The estimated β-sheet content, possibly fibrillar structure, of the Aβ samples with the three dyes based on the ellipticity value around 217 nm is in descending order of EOY, ERB and ROB. The TEM images of the three Aβ aggregates formed with EOY, ERB, and ROB also show that the morphology of the three Aβ aggregates are quite different from that of Aβ control (Figure 2.4). The EOY-induced Aβ aggregates are primarily small protofibrils in the length of 20 to 40 nm and a small portion of ~ 100 nm straight protofibrils (Figure 2.4; Panel EOY), whereas the Aβ control mainly consisted of protofibrils and fibrils in the length of > 300 nm (Figure 2.4; Panel Aβ only). The ERB-induced Aβ aggregates are curvilinear aggregates protofibrils, suggesting that the disordered structure content is higher than that of the Aβ control (Figure 2.4; Panel ERB). The ROB-induced Aβ aggregates also appeared as curvilinear protofibrils, but are thinner than the ERB-induced Aβ aggregates (Figure 2.4; Panel ROB). Dot-blot assays using the OC and A11 antibodies were employed to estimate the relative amount of fibrillar and prefibrillar aggregates in the Aβ samples. At day 5, the EOY-, ERB-, and ROB-induced Aβ aggregates were in descending order of OC-reactivity (Figure 2.5; Panel OC), which is quite consistent with the trend found in the CD analysis (Figure A3 in Appendix A). In contrast, the ROB-, ERB-, and EOY-induced Aβ aggregates were in the descending order of A11-reactivity (Figure A2 in Appendix A). Since the ROB-induced Aβ aggregates exhibit very high A11-reactivity, we investigated whether there was any spectral

interference of all ERB analogs with the dot-blot assay using the A11 antibody. The ERB congeners alone as well as the A11-reactive Aβ aggregates were spotted to a nitrocellulose membrane and then the A11-reactivity of the samples was determined. Only ROB exhibits a significant A11-reactivity comparable to those of Aβ samples (Figure A4 in Appendix A). Therefore, caution should be taken to interpret A11-reactivity of Aβ samples containing ROB. None of the ERB congeners exhibit a significant immuno-reactivity against the OC and 4G8 antibodies (data not shown). The decrease in the OC-reactivity of the ERB analogs can be directly interpreted as a decrease in the fibrillar structure content, but the increase in the A11-reactivity of the ROB-induced should not be interpreted as an increase in the prefibrillar content.

For all three ERB congeners (EOY, ERB and ROB), the CD spectra, TEM images, and dot-blot assay using OC-antibody clearly indicate that there was a substantial of reduction in the fibrillar structure. Combined with the MTT reduction assay results (Figure 2.2B), such a reduction in the fibrillar structure can be attributed to a reduction in the Aβ-associated cytotoxicity for EOY and ERB. Although the A11-reactivity of the ROB-induced Aβ aggregates is greater than that of the Aβ control, the A11-reactivity is most likely overestimated. It is also interesting to note that even though ROB did not reduce Aβ-associated cytotoxicity in the MTT assay, these results show that it is clearly a potent inhibitor of the Aβ-aggregation.

FLN Does Not Effectively Modulate Aβ Aggregation and Cytotoxicity

Investigating the modulatory capacities of ERB congeners on Aβ cytotoxicity and aggregation reveals that even a subtle change in their chemical structure from the ERB structural template can affect their modulatory capacities. In order to further validate our hypothesis that the modulatory capacities of the ERB congeners are related with the presence of halogen atoms,

we also evaluated the modulatory capacities of FLN as a negative control without any halogen atoms (Figure 2.1). The CD spectrum of the FLN-induced Aβ aggregates clearly exhibits the typical features of β-sheet rich structure (Figure 2.6A). The TEM image of the FLN-induced Aβ aggregates also indicates that protofibrils and fibrils are dominant species similar to the Aβ control (Figure 2.6B). Furthermore, the OC-reactivity of the Aβ aggregates formed with FLN at days 5 and 6 are very comparable to those of the Aβ control (Figure 2.6C), indicating that the FLN-induced Aβ aggregates had fibrillar aggregates as much as the Aβ control. The 4G8-reactivity of the FLN-induced Aβ aggregates with FLN remained unchanged up to day 7, whereas the 4G8-reactivity of the Aβ control dropped after day 5. Such a slightly higher 4G8-reactivity of the FLN-induced Aβ aggregates after day 5 is likely because the FLN-induced fibrils are not laterally stacked and so allow the 4G8 binding to its epitope better than the Aβ control. The CD, TEM, and dot-blot assay results conclusively demonstrate that FLN does not modulate the Aβ aggregation as much as EOY, ERB, or ROB.

Next, we investigated whether FLN affects the Aβ-associated cytotoxicity. Similar to the ERB analogs, Aβ monomers were incubated in the absence of or presence of FLN for 5 days, and the resulting aggregates were subjected to the MTT reduction assay. The viability of the SH-SY5Y cells treated with the Aβ control (5 μM) was 66% (Figure 2.6D). Co-incubation of the Aβ monomer with FLN led to a small increase in the cell viability (6%) (Figure 2.6D), but the difference was only marginally significant ($P = 0.013$), while ERB, EOY, and PHB led to a substantial increase in the cell viability ($P < 0.001$). The MTT assay results indicate that FLN did not substantially eliminate Aβ cytotoxicity, which is consistent with the fact that FLN did not modulate Aβ aggregation.

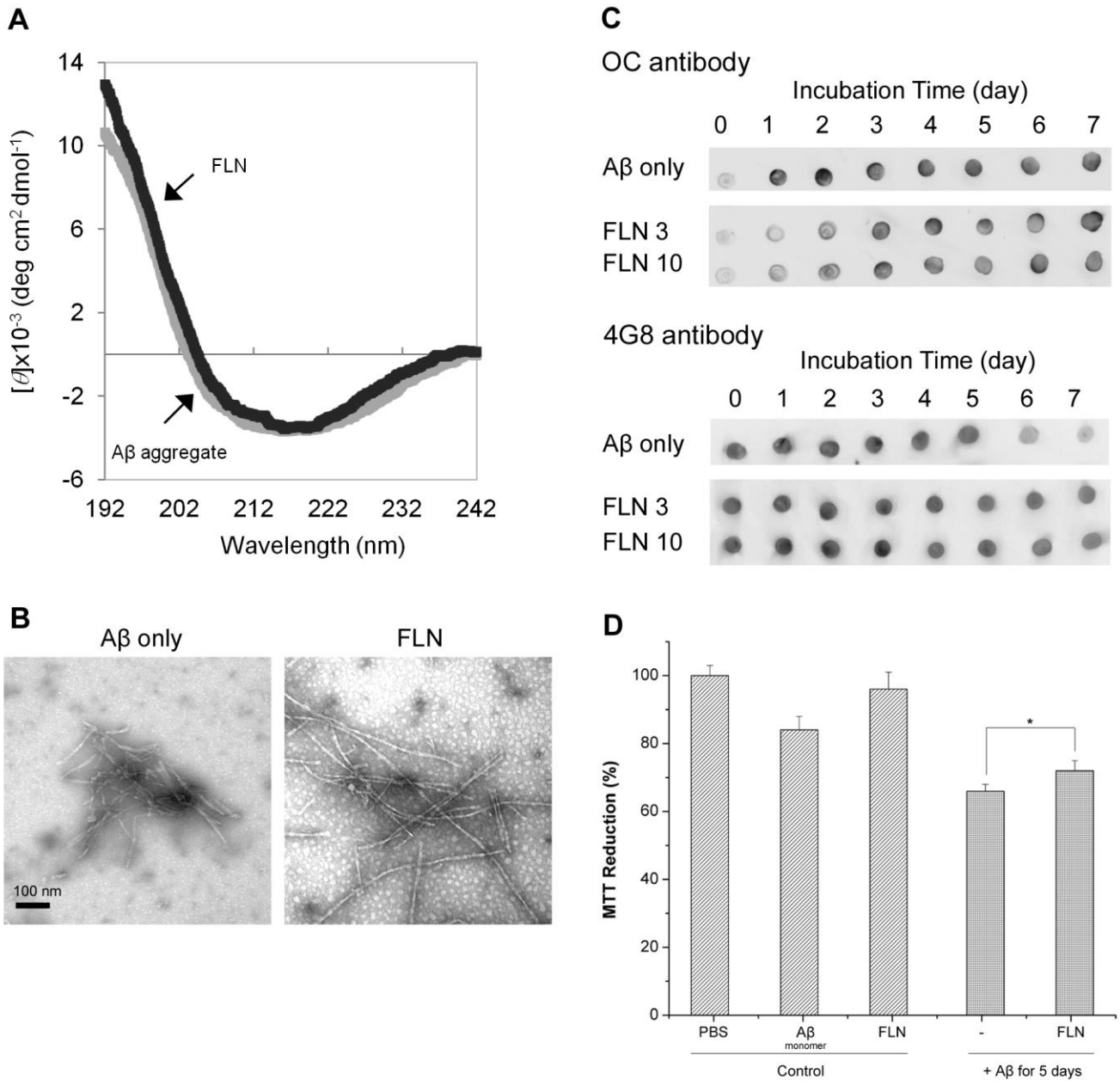

Figure 2.6 - Modulation of Aβ aggregation and cytotoxicity by FLN. (A) CD spectra of Aβ monomer incubated for 7 days at 37 °C in the absence (Aβ aggregate) or presence of 10x FLN (FLN). (B) TEM images of 50 μM Aβ incubated for seven days at 37 °C in the absence of any dye (Aβ only), or in the presence of 3x FLN. Scale bar is 100 nm. (C) Dot blot images of Aβ aggregates formed without (Aβ only) or with 3x and 10x FLN using OC and 4G8 antibodies. For each antibody, all samples were spotted onto one nitrocellulose membrane. Each membrane was immunostained with the OC or 4G8 antibody. For clearer presentation of the data, the sections of each membrane were cut and re-arranged. (D) Viability of neuroblastoma SH-SY5Y cells. Three controls (PBS buffer, Aβ monomer, and FLN) and two Aβ aggregates formed in the absence or presence of 3x FLN at 37 °C for 5 days. Values represent means ± standard deviation ($n \geq 3$). Values are normalized to the viability of cells administered with PBS buffer only. Two-sided Student's t-tests were applied to the MTT reduction data. (*; $P = 0.013$).

Halogenation of Xanthene Benzoate Generates Efficient Binders of Aβ

Having discovered from the CD, TEM, and dot-blotting results that ROB, PHB, ERB, and EOY (but not EOB and FLN) are potent inhibitors of Aβ aggregation, we then investigated possible correlations between these inhibition results and the binding affinity of the dyes to Aβ. Dissociation constant (K_d) values and the number of binding sites were calculated for ROB, PHB, ERB, and EOY using fluorescence quenching of 20 μM concentrations of the dyes upon binding to Aβ (Table 2.1). Intriguingly, the FLN (negative control lacking halogen atoms) quenching results showed that FLN is an exceptionally weak binder of Aβ, with less than 3% of the dye bound even in the presence of an excess molar concentration of 25 μM Aβ (Figure A5; Panel A in Appendix A). In order to maintain consistency with the other five small molecules, our first preference was to employ a similar fluorescence quenching technique to assess the binding of 20 μM EOB (analog of EOY with replacement of the two bromine atoms close to benzoate group in EOY with two nitro groups) to Aβ40. Despite varying reports in the literature about the fluorescence of the EOB molecule[119-122] and trying various solvents and pH conditions (acids, bases, alcohols), in our hands, the EOB fluorescence was too low for use in the quenching assay. Therefore, we employed an assay based on the characteristic shift in the absorbance maximum of EOB upon protein binding. The results showed that like FLN, EOB is a weak binder of Aβ, with less than 3% of the dye bound even in the presence of an excess molar concentration of 25 μM Aβ (Figure A5; Panel B in Appendix A). The number of binding sites on Aβ40 for the four dyes (RRB, EOY, ROB, and PHB) ranges between 1.5 and 2, suggesting that these dyes can interact with multiple sites of Aβ40. The multiple binding sites may explain different properties of the Aβ aggregates induced by the dyes.

Since EOB and FLN displayed very poor binding to Aβ and were also poor inhibitors of Aβ aggregation, it clearly demonstrates that halogenation is very effective in generating molecules that tightly bind and consequently modulate the aggregation of Aβ.

Table 2.1 - Binding properties of ERB analogs to Aβ40 monomers.

Dye (20 μM)	ERB	EOY	PHB	ROB	EOB	FLN
Dissociation constant (μM)	3.35	0.14	0.89	1.36	Poor binding	Poor binding
Number of binding sites	2.1	1.4	1.4	2.0	Poor binding	Poor binding

Poor binding: less than 3% of the dye bound to 25 μM Aβ40

Heavy Halogen Atoms Play a Key Role in Modulating Aβ Aggregation

Taken together, the TEM, CD, dot-blot, dye binding, and MTT reduction assay results indicate that FLN (negative control) without any halogen atom does not bind and modulate the Aβ aggregation and cytotoxicity, whereas ERB congeners (ERB, EOY, PHB) containing multiple halogen atoms substantially modulated the Aβ aggregation and effectively reduced the Aβ cytotoxicity. Considering that FLN has a polyphenol-like structure but is a very poor Aβ aggregation modulator, the molecular mechanism underlying the Aβ aggregation modulation by ERB congeners was different from those of polyphenols. The assay results strongly support the idea that halogen atoms in the ERB congeners play an important role in the modulating Aβ aggregation, and in the case of ERB, PHB, and EOY, ultimately Aβ cytotoxicity. Having established this, the next issue becomes determining which specific features of halogen atoms are critical in modulating the Aβ aggregation.

From the CD, TEM, and dot-blot results of FLN and ERB analogs, several trends were found. First, the electronegativity of the halogen atoms/functional groups attached to xanthene group play an important role in Aβ aggregation modulation. Although the results clearly show that EOY (which has four bromine atoms attached to the xanthene group) and ERB (which has four iodine atoms attached to the xanthene group) are both potent inhibitors of Aβ fibril formation, ERB was slightly more effective than EOY at reducing the formation of fibrillar structures in the dot blotting and TEM assays. Furthermore, when the two bromine atoms close to the benzoate group in the EOY structure are replaced with the two nitro groups in EOB, the inhibitory capacities of the small molecule on Aβ fibril formation are eliminated. Therefore, the order of Aβ fibril formation inhibitory capacity by xanthenes constituent group is I (ERB) > Br

(EOY) > NO_2 (EOB). Because of this, either the electronegativity or size of the functional group attached to xanthene ring can be attributed to the inhibitory capacity of the ERB analogs. The order of the electronegativity and size of three atoms/groups is NO_2 > Br > I or NO_2 > I > Br, respectively. Therefore, we concluded that the inhibitory capacities are inversely proportional to the electronegativity of functional group attached to xanthene group rather than size, which is consistent with the recent findings on organofluorine Aβ aggregation inhibitors.[140] Second, PHB and ROB (both of which contain four chlorine atoms on the benzoate group in addition to xanthenes group structures of EOY and ERB, respectively) led to the potent inhibitory capacities on Aβ aggregation compared to the non-halogenated control molecules, EOB and FLN. This indicates that either polarity change or steric hindrance caused by four chlorine atoms added to the benzoate group resulted in the enhanced inhibitory capacities. However, ROB does not reduce Aβ cytotoxicity, suggesting that both the location and type of halogen atoms on the xanthene benzoate affects the extent of Aβ cytotoxicity inhibition.

Despite the two bromine atoms attached to xanthene benzoate group, EOB is not an effective modulator of Aβ aggregation and cytotoxicity, Alternatively, we speculate that two nitro groups in EOB offset the positive effects of two bromine atoms on the modulatory capacity. Although more studies are required to clearly understand why EOB is not an effective modulator, other halogenated xanthene benzoates without any nitro group clearly exhibited the enhanced modulatory capacity on Aβ aggregation over the xanthene benzoate without any halogen atom (FLN).

Conclusion

In this chapter, our structure-activity relationship investigation has conclusively established that ERB and two ERB analogs (EOY and PHB) effectively reduce Aβ-associated neurotoxicity by modulating Aβ aggregation. In the case of ROB, while modulating capacities of ROB on Aβ aggregation are prominent, it was not capable of alleviating Aβ-associated neurotoxicity. Comparative studies of ERB and ERB analogs on modulation of Aβ aggregation and cytotoxicity revealed that FLN is not an effective modulator, but adding four heavy halogen atoms (either Br or I) to the xanthene group substantially enhanced the modulatory capacities on Aβ aggregation and cytotoxicity. Adding four Cl atoms to the benzoate group also significantly enhanced the Aβ aggregation modulation. In particular, co-incubation of PHB, which contains four bromine atoms in the xanthene group and four chlorine atoms in the benzoate, generates low-molecular-weight Aβ species with disordered structure similar to Aβ monomer, which makes PHB a unique Aβ aggregation modulator. Considering that halogen atoms play an important role in modulating Aβ aggregation and cytotoxicity, ERB analogs are considered a new type of Aβ modulators, halogenated small molecules. To our knowledge, this is the first report demonstrating the heavy halogen atoms added to multiple aromatic rings can confer inhibitory capacities on Aβ-associated cytotoxicity. Our studies can open a door to convert a poor Aβ aggregation modulator into an effective one by adding heavy halogen atoms and serves as guidance to discover or design novel Aβ aggregation modulators. Considering that ERB analogs are effective modulators of α-synuclein aggregation implicated in Parkinson's disease[141] and ERB itself is effective at destabilizing preformed Aβ fibrils (covered in Chapter 4),[13] halogenation of small molecules might be a general way to obtain effective modulators of other amyloidogenic peptides and proteins at multiple stages in aggregation.

Chapter 3: Creation and Use of an In Vitro Ligand Binding Site Identification Method to Characterize Erythrosin B and Structural Analogs Ligand Binding Sites on Aβ Target Peptide Monomer

Abstract

Numerous small molecule modulators of amyloid-beta (Aβ) aggregation and neurotoxicity have been identified with the ultimate goal of Alzheimer's Disease (AD) treatment. Determining binding sites of these modulators on Aβ is an important topic in the mechanistic understanding of AD pathology and drug development. However, Aβ binding sites have been reported for only a very limited number of Aβ modulators, because of highly specialized and expensive equipment/materials or lack of folded structure of Aβ. In this chapter, we developed a convenient method for determining ligand binding sites on Aβ using dot blot immunostaining with a panel of Aβ sequence-specific antibodies. To validate our technique, we first examined one ligand (Congo Red), with known binding sites, which yielded consistent results with previous findings. Then, using the same technique, binding sites on Aβ were investigated for Erythrosin B (ERB) and three other halogenated xanthene benzoate structural analogs, Phloxine B (PHB), Rose Bengal (ROB), and Eosin Y (EOY). This analysis revealed a common locus, amino acids 10-16, as an important strong binding region. The identified ligand binding sites were also confirmed by a separate fluorescence quenching-based binding assay using a panel of overlapping Aβ fragments. The technique described here greatly increases researchers' ability to determine Aβ binding site of ligands and to screen for new ligands that bind specific amino acid regions on Aβ. More broadly, this technique has a great potential for determining ligand binding sites on other target peptides/proteins associated with neurodegenerative disease.

Introduction

The identification of ligand binding sites on a target protein/peptide is a topic of great interest to chemists and biologists alike. The biological function of many proteins is defined by the specific interaction with molecules in the micro-environment.[142] Therefore, knowledge about where and how ligands bind can provide valuable insight in to a target protein's function(s) on a mechanistic level.[143] This is especially important in the post-genomic era where 40% of proteins in the Protein Data Bank (PDB) with a 3D structure lack biological ligand-binding information.[144] Beyond a basic understanding of native function, knowledge of a protein's ligand binding site is crucial for rational, structure-based design of inhibitors or activators to alter the protein's activity.[145] In the realm of pharmaceutical development, many proteins implicated in diseases have known amino acid regions representing active sites, allosteric sites, "druggable" binding pockets, and/or "hot spots" that themselves are the actual targets for drug discovery using high-throughput ligand screening.[145-148] From the opposite point of view where there exists a known drug that works through an unknown mechanism, identification of the drug's binding site(s) on the target protein can provide insight in to 1) potentially negative side effects if the ligand binds multiple and/or unwanted locations[147] and 2) how to design future drugs based on the structure of the interaction site identified.

Alzheimer's Disease (AD) is the most common form of irreversible dementia in the world today.[149] Currently, it is reported that AD affects more than 5.3 million people and is the sixth leading cause of death in the United States.[150] One pathological hallmark of AD is the accumulation of insoluble protein aggregates, composed primarily of neurotoxic Aβ.[150] It is believed that soluble Aβ oligomers and protofibrils are neurotoxic and causative to the onset of AD.[9, 11, 75, 104] Therefore, modulating Aβ aggregation to inhibit toxic Aβ oligomers and

protofibrils formation has been considered as a promising strategy to inhibit Aβ-associated neurotoxicity. Numerous small molecules have been studied for their ability to modulate Aβ aggregation and reduce neurotoxicity.[13, 27, 39, 46, 59, 61, 89, 90, 105-108, 112, 151, 152] Although none have yet to be ultimately FDA-approved for AD-treatment, several of these small molecule modulators, tramiprosate/homotaurine, clioquinol, scyllo-inositol, epigallocatechin-3-gallate, and curcumin,[153, 154] have made significant developmental progress and even reached Phase II / III clinical trials. Most of these modulators are expected to bind to Aβ site-specifically or non-specifically. However, our knowledge on their binding sites on Aβ is quite limited.

Currently, both computational and experimental methods are employed to elucidate ligand-protein/peptide interaction regions. Nuclear Magnetic Resonance (NMR) is considered by many researchers to be the "gold standard" in the field. Indeed, NMR enables solution-based, residue-level ligand-protein interaction site information to be detected, even if the binding is quite weak.[143, 155] However, it is often time consuming, challenging due to complicated spectra assignment procedures, and expensive due to the large amount of labeled isotope material and specialized equipment/personnel required.[143, 156-159] X-ray crystallography has also been employed, but has the distinct disadvantage of not being able to monitor binding in aqueous solution since samples have to be crystallized.[143, 157-159] Several array-based methods have been reported in the literature in recent years, immobilizing either a fragment of the parent peptide[17, 160] or a small molecule ligand[161, 162] on a surface and then detecting the resulting binding that occurs. While innovative, these approaches require the use of shortened amino acid fragments of the full-length target protein, and thus, do not allow for assessment of ligand binding sites using the full 3D protein/peptide structure. A similar limitation exists regarding the method of identifying ligand binding sites using peptide fragment phage display.[163] As computational

technology continues to advance, computer-based methods of predicting ligand binding sites on target proteins evolve as well. Primary categories of these methods include geometric, energy-based, and docking programs.[142, 147, 164-168] However, the majority of these techniques require an established 3D PDB protein/peptide structure, which do not exist for all target proteins (in particular, Aβ monomer), and/or sophisticated molecular dynamic simulations. Furthermore, ligand binding sites predicted by computational methods usually require experimental validation. Many 3D structures are resolved in the presence of a single specific ligand, which makes it difficult to study other ligand molecules.

In order to address the limitations of current methods, we investigated whether binding sites could be identified using a panel of Aβ sequence-specific poly- and monoclonal (mAbs) antibodies. This method is hinted by our previous observations that a reduction in the dot blot immunostaining signal of a sequence-specific antibody upon adding ligand is indicative of potential epitope blocking/binding.[13, 27, 34, 39, 89, 90] Sequence-specific antibodies have been employed in common laboratory techniques throughout the literature for many endpoints, including protein separation, purification, verification of loading/size, and analysis of conformational change.[39, 58, 160, 169] However, to our knowledge, the robust use of sequence-specific antibodies to identify ligand binding sites on a target protein/peptide, including Aβ, was not yet reported.

To validate our hypothesis that dot blot immunostaining with a sequence-specific antibody panel can be used to identify ligand binding sites on Aβ, we employed the 40 amino acid length amyloid-beta peptide (Aβ40 – Figure 3.1, Center Panel), as our target peptide, along with 6 overlapping sequence-specific antibodies (Figure 3.1, Top Panel) to obtain full coverage.

The binding sites of four known ligand binders of Aβ40 (previously reported K_d values of 0.14 – 3.35 μM)[90] with unknown binding sites were evaluated – Erythrosin B (ERB), Eosin Y (EOY), Rose Bengal (ROB), and Phloxine B (PHB) (Figure 3.2C). In order to validate our method, we also used Congo Red (CR), a ligand with previously reported binding sites (K_d value found to be 5 – 300 μM to Aβ40 monomer),[17, 170, 171] Fluorescein (FLN), a poor molecular binder of Aβ (previously reported to have less than 3% of the molecule bound even in the presence of an excess molar concentration of Aβ over FLN)[90] (Figure 3.2A, B), and an Aβ40 peptide sub-fragment panel (Figure 3.1, Bottom Panel) fluorescence quenching assay as controls. If proven effective, the method will greatly facilitate identifying ligand binding sites on Aβ, since only common biochemistry lab equipment is required once antibodies are obtained.

Figure 3.1 - Target Aβ40 peptide, sequence specific antibodies, and peptide fragments. (Top Panel) The six sequence/residue specific antibodies employed to detect ligand amino acid (AA) binding sites on the target peptide, Aβ40. (Center Panel) Primary amino acid sequence of Aβ40 target peptide (at neutral pH, negatively charged AAs – blue, positively charged AAs – red, hydrophobic AAs – green, other types – black). (Bottom Panel) The four Aβ peptide sub-fragments employed in validating the strong ligand binding sites detected by the sequence specific antibodies. Positions of sequence specific antibodies and peptide fragment bars indicate their respective associated regions of the full length target peptide.

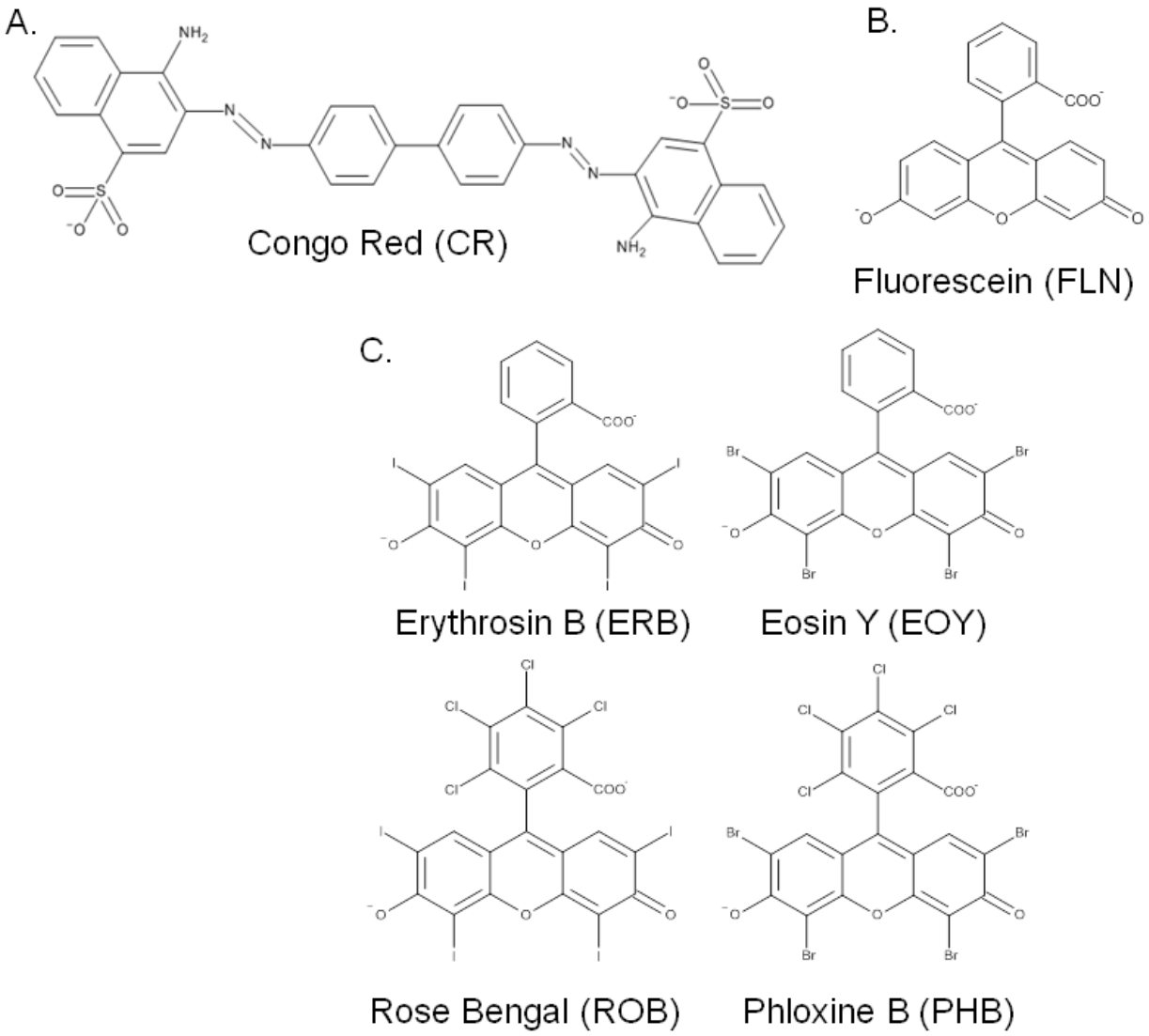

Figure 3.2 - Chemical structures of Aβ40 target peptide ligands. (A) Structure of Congo Red (CR), an Aβ40 ligand with binding sites previously reported in the literature. (B) Structure of Fluorescein (FLN), a molecule previously reported to be a poor binder of Aβ40. (C) Structure of Erythrosin B (ERB), Eosin Y (EOY), Rose Bengal (ROB), and Phloxine B (PHB), known binders and modulators of Aβ40 aggregation, with binding sites unknown.

Materials and Methods

Materials

Full length Aβ40 target peptide was purchased from Anaspec, Inc. and Selleck Chemicals (Purity > 95%). Individual peptide fragments representing amino acids 1-11, 11-22, 17-24, and 33-40 of the full length Aβ40 target peptide were purchased from Genscript. Horseradish peroxidase (HRP)-conjugated goat anti-rabbit and anti-mouse IgG secondary antibodies were obtained from Invitrogen. Primary antibodies were purchased from the following sources: mouse 2H4, HRP-conjugated 4G8, HRP-conjugated 6E10 – Covance, mouse 12C3 – Novus Biologics, rabbit Anti-Aβ22-35 – Sigma, and mouse 11A50-B10 - Abcam. Nitrocellulose membranes and ECL Prime chemiluminescence detection kit were obtained from GE Healthcare Life Sciences. Eosin Y was purchased from Acros Organics, and Tween 20 was purchased from Bio-Rad. All other chemicals were obtained from Sigma-Aldrich unless otherwise noted.

Target Aβ40 Peptide and Sub-Fragment Monomer Preparation

Full length Aβ40 and Aβ peptide sub-fragment monomers were prepared as described previously.[90] Lyophilized Aβ40 or sub-fragment was dissolved in 100 % hexafluoroisopropanol (HFIP) to 1 mM and incubated at room temperature for 2 hours. HFIP was evaporated under a constant stream of nitrogen, and the peptide film dissolved in 100 mM NaOH to a concentration of 2 mM Aβ prior to dilution in phosphate buffered saline (PBS) solution (10 mM NaH_2PO_4 and 150 mM NaCl, pH 7.4) to a concentration of 50 μM Aβ. Separate Erythrosin B (ERB), Eosin Y (EOY), Rose Bengal (ROB), Phloxine B (PHB), Fluorescein (FLN), and Congo Red (CR) ligand stock solutions were dissolved in PBS to a concentration of 10 mM of each small molecule.

Small amounts of these concentrated ligand stock solutions were added to the peptide solutions to yield a final ligand concentration corresponding to 0.3x – 10x (CR) or 0.3x – 3x (ERB, EOY, ROB, PHB, and FLN) molar excess based on the concentration of Aβ.

Dot Blotting / Sequence-Specific Antibody Immunostaining

Dot blotting was performed as reported previously.[13, 27, 89, 90] 2 μL Aβ40 peptide samples were spotted onto nitrocellulose membranes and were dried at room temperature. A solution of 0.1 % Tween 20 in Tris-buffered saline (TBS-T) solution (0.1% (v/v) Tween 20, 20 mM Tris, 150 mM NaCl, pH 7.4) was prepared. Each nitrocellulose membrane was blocked at room temperature for 1 hour (5 % (w/v) milk TBS-T) and washed with TBS-T. Each membrane was then incubated with an Aβ sequence-specific primary antibody (HRP-conjugated 4G8, HRP-conjugated 6E10, 12C3, 2H4, Anti-Aβ-22-35, or 11A50-B10 antibody) in 0.5% (w/v) milk TBS-T for 1 hour at room temperature and washed with TBS-T. After immunostaining with HRP-conjugated 4G8 and 6E10 primary antibodies, the membranes were coated with ECL Prime detection agent (based on manufacturer specifications) and visualized. Alternatively, all other membranes were incubated with the appropriate HRP-conjugated anti-mouse or anti-rabbit IgG secondary antibody in 0.5 % (w/v) milk TBS-T for 1 hour and washed with TBS-T. Signal detection was performed as aforementioned using the ECL Prime Detection kit and was visualized using a Biospectrum imaging system. HRP-conjugated 4G8, 6E10, and IgG secondary antibodies along with the 11A50-B10 antibody were applied at a 1:10000 dilution, while the 2H4, 12C3, and Anti-Aβ-22-35 antibodies were applied at a 1:7000 dilution. The ECL Prime signal detection process, Biospectrum imaging system exposure time, and antibody

concentrations were all carefully optimized to prevent over-exposure and/or over-saturation, artifacts which can skew the dot blotting results.

Quantification of Dot Blotting

The resulting dot blot intensities on the membrane of each sequence-specific antibody were quantified using Image J. Specifically, a circular region of interest (ROI – an equally-sized ROI was used for all dots and background readings on the same membrane) was displayed over each dot, and the integrated density was measured in Image J. After quantifying the integrated densities of all dots on a respective membrane, an average background integrated density value was obtained using the same sized ROI. After carefully subtracting out the background contribution, each 0.3x – 10x ligand-Aβ40 monomer sample's integrated density was normalized to that of the average Aβ40 (no ligand) control signal on the membrane. The resulting normalized intensities were then displayed in the Figures and Tables.

Ligand Fluorescence Quenching Binding Assay

The binding of ERB, EOY, ROB, PHB, and FLN to Aβ peptide sub-fragments was assessed using modified assays based on emission fluorescence quenching techniques described in the literature[119-122] and performed in our previous report.[90] The concentration of each of the ligands was fixed at 20 μM. In order to evaluate fluorescence quenching of the ligand upon peptide binding, the appropriate peptide sub-fragment was mixed with the ligand in a final concentration of 0 to 25 μM in pH 4.5 low salt citrate buffer (25 mM citric acid, 25 mM sodium citrate, pH 4.5). The excitation wavelengths used are as follows: ERB - 486 nm, EOY – 480 nm,

ROB – 510 nm, PHB – 500 nm, and FLN – 432 nm. The maximum emission wavelengths where the data were collected are as follows: ERB – 546 nm, EOY – 536 nm, ROB – 565 nm, PHB – 555 nm, and FLN – 512 nm. After generating binding curves, the % decrease in fluorescence due to ligand-peptide binding was calculated by comparing the fluorescence intensity at 25 μM peptide to the free ligand (no peptide) control.

Results and Discussion

A common interest in the linkage between chemistry and biology is the desire to understand where a ligand containing a certain chemical structure binds on a target protein / peptide of biological interest. However, traditional methods of identifying ligand binding sites, such as NMR and computational simulations, can be cumbersome and are not trivial to use under common biochemistry lab settings. Because of these shortcomings, we have developed a more convenient, user-friendly method employing dot blot immunostaining of sequence-specific dot blotting to identify ligand binding sites on Aβ and then applied it to characterize the binding sites of ERB analogs.

Method Verification - Identification of Congo Red-Aβ40 Binding Sites

As a first step in the development and validation of our proposed method, we wanted to utilize dot blot immunostaining with a sequence-specific antibody panel to identify binding sites of Congo Red (CR – Figure 3.2A), a previously characterized ligand[17, 170, 171] that modulates Aβ aggregation, on the Aβ40 target peptide (Figure 3.1).

Previous reports in the literature have revealed that the interaction of CR and Aβ is a highly complex process that involves multiple steps and possible mechanisms.[171] For example, CR has been reported to 1) interact directly and stabilize Aβ monomers,[172] 2) itself first aggregate in to micelles/vesicles which then interact with Aβ monomers to promote formation of non-amyloid aggregates,[117, 173] and 3) interact with Aβ monomers to form 1:1 and 1:2 Aβ:CR molecular complexes, each containing more than one peptide and one ligand molecule.[171] Specific binding sites of CR on Aβ have also been identified in the literature.[17, 170, 171] Pedersen et al. found using NMR that CR interacts with all 40 amino acid residues, with the most significant binding occurring at the 14-26 and 31-37 amino acid regions.[171] Also using NMR, Abelein et al. identified amino acids 7, 15-25, and 31-37 as the most significant interaction sites of CR on Aβ40 monomers.[170] Finally, using an Aβ peptide fragment spot assay, Grelle et al. found that the strongest CR binding sites were amino acids 12-22 and 24-36.[17]

Having gained an understanding of previously reported Congo Red - Aβ binding sites in the literature, we could then proceed with our new method's validation. Aβ40 target peptide monomers were prepared, mixed in the presence or absence of 0.3, 1, 3, 5, and 10x molar excess concentrations of CR ligand, dotted within a short time (5 minutes – Aβ40 aggregation time scale is much longer at 3-5 days[90]) to prevent any conformation change from occurring,[13] and then the membranes probed with the antibody panel to yield immunostaining results (Figure 3.3). A total of 6 commercially-available sequence-specific antibodies were employed in the analysis to give complete coverage amino acid (AAs) coverage (Figure 3.1, Top Panel): 2H4 (mAb, recognizes AAs 1-8),[174] 6E10 (mAb, recognizes AAs 4-9),[160] 12C3 (mAb, recognizes AAs 10-16), 4G8 (mAb, recognizes AAs 17-24),[90] Anti-Aβ-22-35 (polyclonal antibody, recognizes AAs 22-35),[175] and 11A50-B10 (mAb, recognizes the C-terminus of Aβ40).[176] According to our

hypothesis, in the absence of a conformation change of the target protein/peptide, a reduction in the dot blot immunostaining signal of a sequence-specific antibody upon adding increasing ligand concentrations is indicative of epitope blocking/binding by the ligand.[13, 27, 34, 39, 89, 90] Special care was taken during the optimization of the dot blot assay conditions to prevent over-exposure and/or over-saturation, which can skew interpretation of the results. This optimization ensured that even if the dots were not homogeneous (a phenomenon previously observed in the Aβ dot blotting literature stemming from a weaker signal in one region of the dot versus another[13, 34, 59, 61, 90, 112, 152]), we could still proceed with our analysis without confounding data artifacts.

Potential CR binding sites were assessed by using Image J to normalize the antibody signal intensities of the 0.3 – 10x CR samples (≥ 6 replicates per sample) to the Aβ40- control (no ligand) intensity within each respective antibody (Table 3.1 and Figure B1 in Appendix B for dose-dependency graphical version). From there, a normalized intensity < 20% of the Aβ control signal was selected as the cutoff criteria for identifying the relatively strong binding sites of each ligand (green highlighted cells in Table 3.1).

The resulting normalized dot blot intensities at the 3x – 10x CR concentrations revealed several interesting findings (Table 3.1). First, CR exhibited at least weak non-specific binding to all regions of Aβ40, as evidenced by the relative dot blot intensities being below ~65% for all antibodies at the 3x CR molar excess level. Similarly, at a very large 10x molar excess of CR, binding seems to become fairly non-specific as well, with all dot blot signals being less than 20% of the Aβ control. Broad interaction of CR with all residue regions of Aβ40 (Table 3.1, 3x – 10x CR ligand concentrations and Figure B1 in Appendix B) was also observed in the NMR work by

Pedersen et al. described above.[171] Second, the results revealed that at a 5x CR concentration, ligand binding was strongest at the 6E10 and 12C3 epitopes (AAs 4-9 and 10-16, respectively), with relative intensities less than 20% that of the Aβ control sample without ligand. The amino acid 4-16 region of Aβ40 identified using our antibody panel as a strong relative CR binding location coincides with the Aβ amino acid CR binding sites (AAs 7,[170] 14-26,[171] 15-25[170], and 12-22[17]) previously reported in the literature.

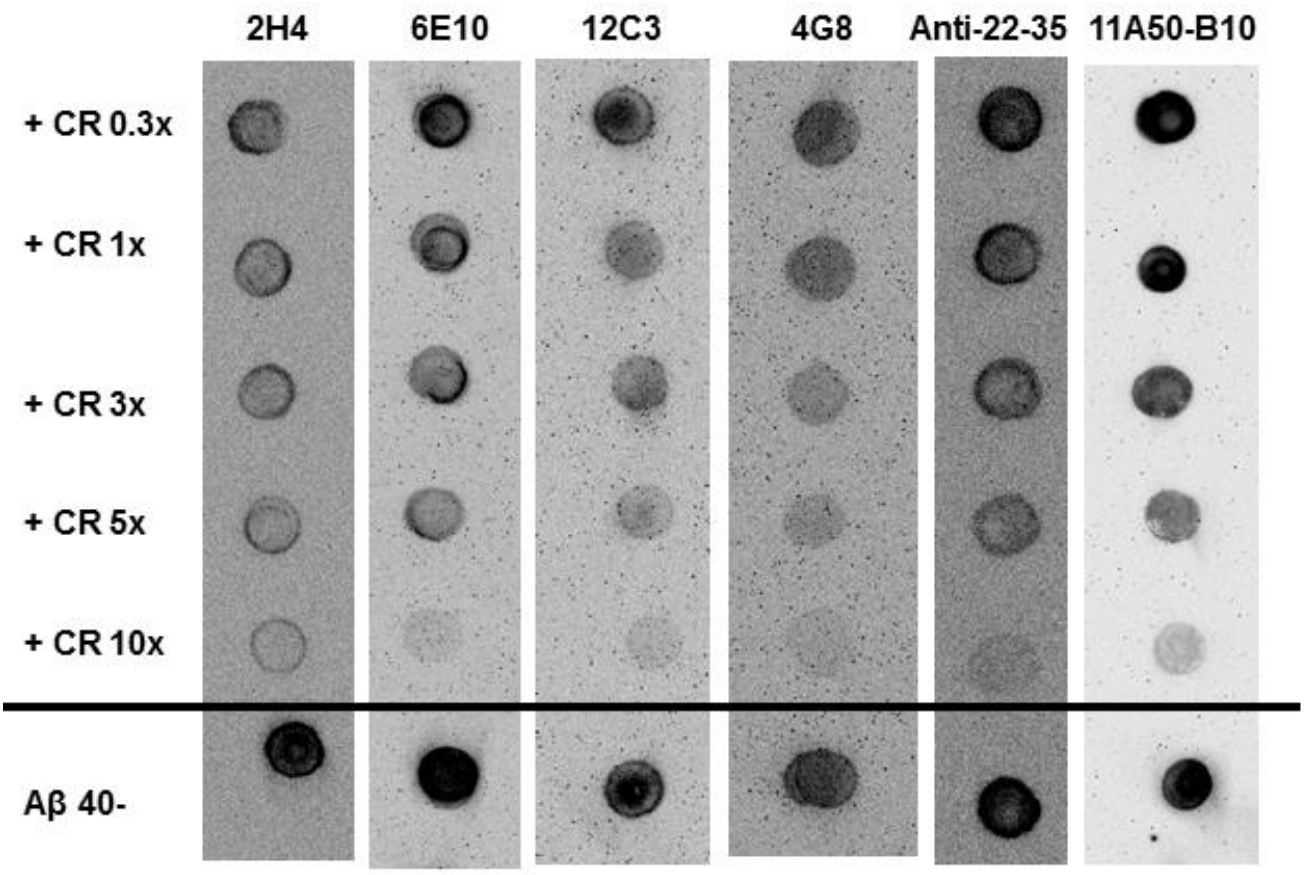

Figure 3.3 - Congo Red (CR) ligand binding site identification using sequence specific antibody panel. Representative dot blotting results of Aβ40 monomers mixed with (+ CR) or without (Aβ40-) 0.3-10x molar excess concentrations of Congo Red (CR) for the six sequence specific antibodies and then dotted within 5 minutes after mixing. For better ease of viewing, each antibody was developed on a separate membrane and then cut and pasted for the compiled results.

Table 3.1 - Normalized dot blot intensities for Congo Red (CR) ligand-Aβ40 binding site identification using sequence specific antibody panel. Dot blot signal intensities for the 0.3-10x Congo Red ligand concentration samples were quantified and normalized to the average Aβ40 control (no ligand) intensity for each respective antibody. Dot blot samples that yielded a normalized signal below 20% of the Aβ control were identified as relatively strong binding sites and highlighted in green. Normalized values are expressed as average ± standard deviation, n ≥ 6 (* indicates a p-value from two-sided Student's T-Test < 0.05 when comparing average of data point to 20% of the Aβ control normalized value, ** indicates a p-value of < 0.005).

	Normalized Dot Blot Signal Intensity					
Congo Red Ligand Concentration	2H4	6E10	12C3	4G8	Anti-Aβ-22-35	11A50-B10
0.3x	0.43 ± 0.11	0.54 ± 0.18	0.46 ± 0.12	0.82 ± 0.18	0.96 ± 0.22	0.87 ± 0.23
1x	0.38 ± 0.13	0.35 ± 0.09	0.39 ± 0.11	0.50 ± 0.18	0.76 ± 0.17	0.69 ± 0.13
3x	0.32 ± 0.07	0.23 ± 0.17	0.23 ± 0.13	0.35 ± 0.14	0.61 ± 0.22	0.63 ± 0.17
5x	0.24 ± 0.04	0.13 ± 0.09	0.05 ± 0.10**	0.29 ± 0.12	0.33 ± 0.10	0.52 ± 0.10
10x	0.18 ± 0.06	0.04 ± 0.08**	0.05 ± 0.10**	0.18 ± 0.07	0.13 ± 0.08*	0.19 ± 0.07

Identification of Erythrosin B Analogs Ligand-Aβ40 Binding Sites

Having used our panel of sequence-specific antibodies to obtain binding site results for Congo Red (a ligand with reported binding sites) consistent with established techniques, we could then apply the method to investigate our ERB analog ligands with unknown binding sites. Recently and in Chapter 2, we reported that halogenation of the xanthene benzoate structural backbone generates binders of the Aβ40 peptide.[90] Halogenated xanthene benzoate structural analogs (Erythrosin B (ERB), Eosin Y (EOY), Rose Bengal (ROB), and Phloxine B (PHB)) (Figure 3.2C) applied at a 3x molar excess concentration were found to effectively bind and modulate Aβ40 aggregation, while a non-halogenated negative control molecule, Fluorescein (FLN – Figure 3.2B), was ineffective.[90]

Aβ40 monomers were again prepared, mixed in the presence or absence of three different concentrations (0.3, 1, and 3x molar excess) of EOY, FLN, ERB, PHB, and ROB ligands, and then dot blotted (EOY and FLN - Figure 3.4, ERB, PHB, and ROB – Figure 3.5). Upon visual inspection of the dot blot results (and unlike CR), the halogenated xanthene benzoate ligands seemed to exhibit localized, specific binding with the N-terminal region epitopes of Aβ40 (Figure 3.4A, 12C3 Panel, Figure 3.5A-C, 2H4, 6E10, and 12C3 Panels), resulting in almost complete blockage / disappearance of several antibody signals at the 1x and 3x ligand concentration levels.

As was done with Congo Red, Image J was used to quantify the integrated density of the halogenated xanthene benzoate ligand-Aβ40 dot blot results. Signal intensities of the ligand samples (≥ 3 replicates per sample) were normalized to the Aβ40- control (no ligand) (Table 3.2 and Figures B2-B6 in Appendix B for dose-dependency graphical versions), and a normalized

intensity < 20% of the Aβ control signal was selected as the cutoff criteria for identifying the strongest relative binding sites of each ligand (green highlighted cells in Table 3.2). As expected, strong binding was not detected for FLN, the non-halogenated, poorly-binding negative control xanthene benzoate structural analog. This was evidenced by 1) the lowest normalized signal of FLN being the 3x FLN 12C3 antibody sample at 49% (Table 3.2, 3x FLN row) and 2) the lack of a dose-dependent decrease in any of the antibody signals between 0.3-3x concentrations of FLN (Figure B3 in Appendix B). This finding provides additional proof that our method is working properly.

Next, the quantified results for ERB were assessed (Table 3.2, ERB rows and Figure B4 in Appendix B). Upon inspection, the results revealed that no significant binding was occurring in the C-terminal amino acid regions (4G8, Anti-Aβ-22-35, and 11A50-B10 epitopes), as evidenced by there being ≤ 10% reduction in the relative intensities compared to the Aβ control. In fact, for the majority of the ERB samples, the average C-terminal antibody signals were greater than that of the Aβ control without any ligand (Table 3.2, ERB panel, 4G8, Anti-Aβ-22-35, and 11A50-B10 columns). However, given the large standard deviation of these samples and that halogenated xanthene benzoate ligands alone (no Aβ) do not artificially promote antibody signals (Figure B7 in Appendix B), the normalized values greater than 1 are most likely due to inherent error in the dot blot assay and not indicative of an actual physical change in Aβ40 monomer epitope exposure. Although the possibility of structural changes of Aβ40 monomer cannot be completely excluded, enhanced signals upon ligand binding, if any, will not prevent the detection of inhibitory effects of ligand on antibody binding to Aβ40, the main objective of this assay. Analyzing the results further, the strongest relative binding site at even the 1x ERB ligand concentration was AAs 10-16 (12C3 epitope), with a relative intensity significantly less

than 20% that of the Aβ control sample without ligand ($p < 0.005$) and a dose-dependent decrease in antibody signal upon addition of higher amounts of ERB ligand. At the higher ligand concentration, strong, dose-dependent binding was also observed for ERB at AAs 1-8 (2H4 epitope). Next, relatively strong binding sites of the three remaining halogenated xanthene benzoate ligands, EOY, PHB, and ROB, were determined (Table 3.2, EOY, PHB, and ROB rows and Figures B2, B5-B6 in Appendix B). As was the case with ERB, the most common and strongest relative binding site between all molecules was again AAs 10-16, the 12C3 antibody epitope. Examination of the 12C3 results in conjunction with the other two N-terminal antibodies', 6E10 and 2H4, signals revealed a significant finding as well (Table 3.2).

One concern may be raised on our interpretation of the reduced signal intensity as the reduced accessibility to epitopes on Aβ, because ligands may block antigen binding sites on antibodies, leading to a similar reduction in the dot blot signal intensity. Although we cannot exclude the possibility of ligand binding to antibodies completely, we speculate that it is not very feasible. The ligand mixed with Aβ was applied to nitrocellulose membranes followed by multiple washing steps prior to addition of antibodies. Therefore, it is very likely that unbound ligand will be almost completely removed before antibodies are applied to the nitrocellulose membrane. Furthermore, in order to confirm our findings, we employed an additional method for determining ligand binding sites based on a different mechanism, fluorescence quenching, as described below.

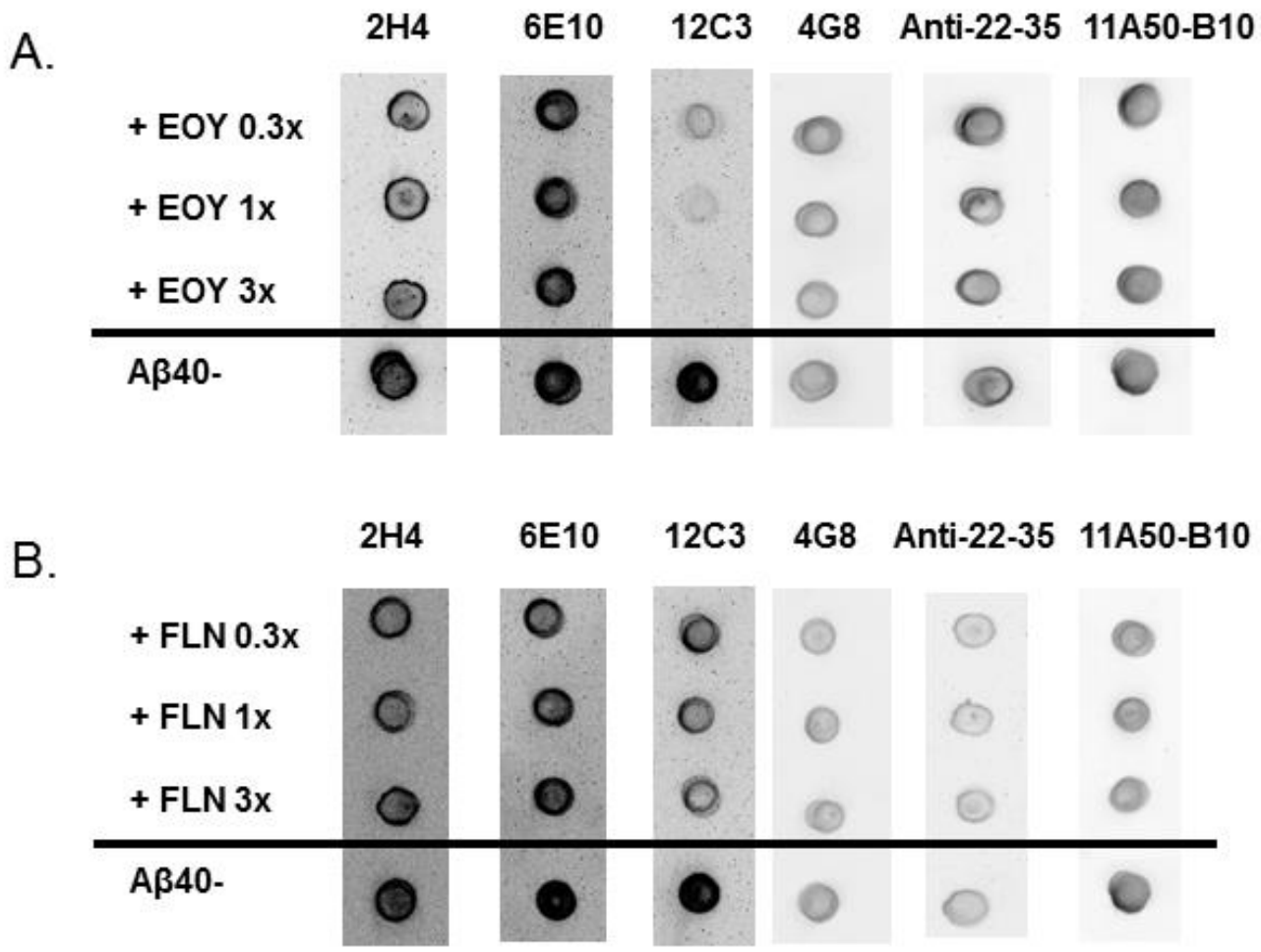

Figure 3.4 - Less halogenated xanthene benzoate ligand binding site identification using sequence specific antibody panel. Representative dot blotting results of Aβ40 monomers mixed with (+ ligand) or without (Aβ40-) 0.3-3x molar excess concentrations of (A) Eosin Y (EOY) or (B) Fluorescein (non-halogenated, poorly-binding negative control – FLN) for the six sequence specific antibodies and then dotted within 5 minutes after mixing. For better ease of viewing, each antibody was developed on a separate membrane and then cut and pasted for the compiled results.

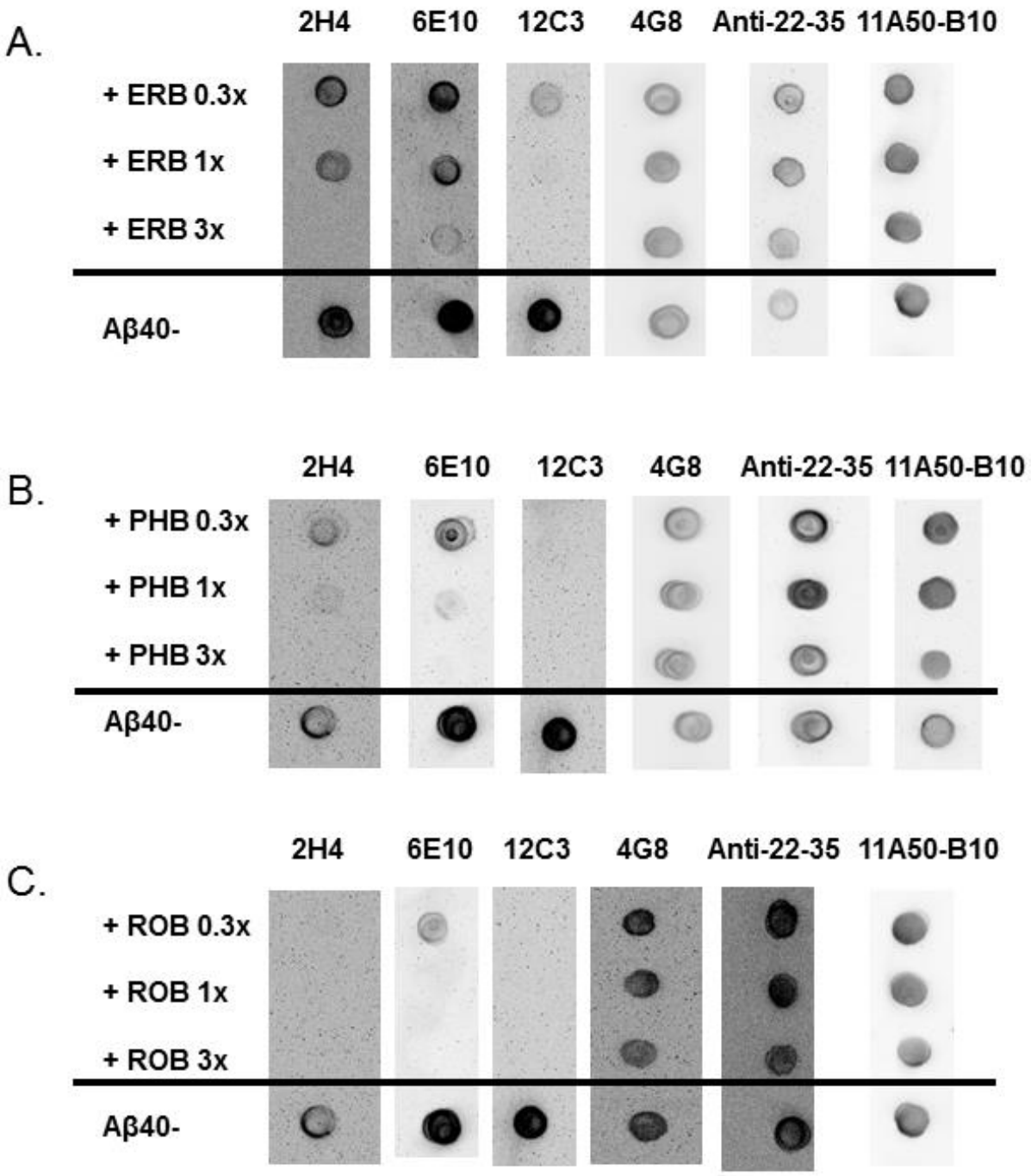

Figure 3.5 - More extensively halogenated xanthene benzoate ligand binding site identification using sequence specific antibody panel. Representative dot blotting results of Aβ40 monomers mixed with (+ ligand) or without (Aβ40-) 0.3-3x molar excess concentrations of (A) Erythrosin B (ERB), (B) Phloxine B (PHB), or (C) Rose Bengal (ROB) for the six sequence specific antibodies and then dotted within 5 minutes after mixing. For better ease of viewing, each antibody was developed on a separate membrane and then cut and pasted for the compiled results.

Table 3.2 - Normalized dot blot intensities for Aβ40 aggregation modulating ligand binding site identification using sequence specific antibody panel. Dot blot signal intensities for the 0.3-3x Eosin Y (EOY), Fluorescein (FLN), Erythrosin B (ERB), Phloxine B (PHB), and Rose Bengal (ROB) ligand concentration samples were quantified and normalized to the average Aβ40 control (no ligand) intensity for each respective antibody. Dot blot samples that yielded a normalized signal below 20% of the Aβ control were identified as relatively strong binding sites and highlighted in green. Normalized values are expressed as average ± standard deviation, n ≥ 3 (* indicates a p-value from two-sided Student's T-Test < 0.05 when comparing average of data point to 20% of the Aβ control normalized value, ** indicates a p-value of < 0.005).

		Normalized Dot Blot Signal Intensity					
Ligand	Ligand Conc.	2H4	6E10	12C3	4G8	Anti-Aβ-22-35	11A50-B10
EOY	0.3x	0.50 ± 0.10	0.65 ± 0.41	0.42 ± 0.22	0.92 ± 0.29	1.20 ± 0.24	0.95 ± 0.07
	1x	0.50 ± 0.13	0.85 ± 0.57	0.25 ± 0.11	1.12 ± 0.38	1.42 ± 0.38	1.07 ± 0.21
	3x	0.59 ± 0.05	0.80 ± 0.45	0.05 ± 0.05**	1.05 ± 0.31	1.53 ± 0.44	1.11 ± 0.20
FLN	0.3x	0.61 ± 0.17	0.68 ± 0.17	0.50 ± 0.18	0.73 ± 0.31	0.70 ± 0.28	0.70 ± 0.09
	1x	0.61 ± 0.24	0.72 ± 0.22	0.57 ± 0.27	0.83 ± 0.31	0.62 ± 0.08	0.71 ± 0.09
	3x	0.77 ± 0.22	0.85 ± 0.31	0.49 ± 0.15	0.94 ± 0.30	0.75 ± 0.29	0.71 ± 0.11
ERB	0.3x	0.64 ± 0.13	1.07 ± 0.20	0.24 ± 0.08	1.46 ± 0.44	1.34 ± 0.28	1.17 ± 0.20
	1x	0.45 ± 0.11	0.59 ± 0.21	0.05 ± 0.05**	1.52 ± 0.52	1.35 ± 0.35	1.13 ± 0.12
	3x	0.14 ± 0.13	0.22 ± 0.18	0.03 ± 0.06**	1.06 ± 0.17	1.49 ± 0.47	0.90 ± 0.19
PHB	0.3x	0.45 ± 0.21	0.70 ± 0.18	0.03 ± 0.05**	1.40 ± 0.38	1.50 ± 0.25	1.23 ± 0.28
	1x	0.12 ± 0.10	0.06 ± 0.09*	0.00 ± 0.00**	1.24 ± 0.21	1.77 ± 0.44	1.12 ± 0.35
	3x	0.06 ± 0.07*	0.03 ± 0.04**	0.00 ± 0.00**	1.41 ± 0.30	1.39 ± 0.58	0.69 ± 0.38
ROB	0.3x	0.09 ± 0.03**	0.21 ± 0.15	0.00 ± 0.01**	1.35 ± 0.29	1.59 ± 0.40	1.17 ± 0.35
	1x	0.01 ± 0.01**	0.06 ± 0.07*	0.02 ± 0.06**	1.38 ± 0.41	1.19 ± 0.42	0.75 ± 0.27
	3x	0.01 ± 0.01**	0.05 ± 0.06**	0.01 ± 0.02**	0.84 ± 0.25	0.93 ± 0.23	0.63 ± 0.26

A graphical summary of the strongest ligand binding sites discovered using our panel of sequence-specific antibodies can be seen in Figure 3.6. One central finding was that the 12C3 antibody epitope, or AAs 10-16, emerged as the only common strong relative binding site for all of the halogenated xanthene benzoate-Aβ40 ligands/aggregation modulators, though ERB, PHB, and ROB bind to other regions of the N-terminus of Aβ at 3x concentration. Next, we sought to confirm this finding using Aβ40 peptide sub-fragments (Figure 3.1, Bottom Panel). Our first choice was to perform dot blot immunostaining with the fragments, as we did with the full length Aβ40 target peptide previously. However, in our hands, the peptide fragments were too small to bind effectively to the nitrocellulose dot blot membrane. In surveying the literature, we found evidence of similar problems experienced in the past with very small peptides.[177] Thus, dot blotting with peptide fragments was not possible, and another method was required. Since the xanthene benzoate ligands employed here are all self-fluorescent, we used fluorescent quenching of 20 μM ligand concentrations upon binding to the panel of Aβ40 peptide sub-fragments. The results clearly showed that the fragment displaying the relatively strongest binding to the ligands, Aβ11-22, contained the AA 10-16 region (Table B1, Aβ11-22 row in Appendix B), which was in line with our dot blot findings. In addition, FLN fluorescence quenching/binding was not detected with any of the peptide sub-fragments (Table B1, FLN column in Appendix B), further supporting our dot blot findings for FLN.

In terms of amino acid composition, the 10-16 AA region of Aβ40 consists of 2 – hydrophobic, 1 - negatively charged, 1 – polar uncharged, and depending on the pH, 3 – positively charged AAs (1 - lysine and 2 – histidines). The positively charged amino acids have been reported to be particularly important for Aβ40 aggregation and toxicity mechanisms, with the histidines (positions 13-14) playing a role in Aβ membrane pore formation and binding of

metal ions implicated in Alzheimer's Disease[178-180] and the lysine at position 16 being involved in salt bridge formation, interaction with other monomers/cell membranes, and required for Aβ40 aggregation and toxicity.[146, 178, 181] In addition, intermonomer contacts centered at positions histidine13 and glutamine15 were found to be required for fibril formation.[12] Indeed, several recent reports of other Aβ-ligand aggregation modulators have revealed binding to these residues contained in the 10-16 AA epitope.[178, 182-187] Because of the mechanistic importance of the 10-16 AA region of Aβ40, it is logical that the ligands we investigated, which are very potent Aβ40 aggregation modulators,[90] also bind strongly to this epitope.

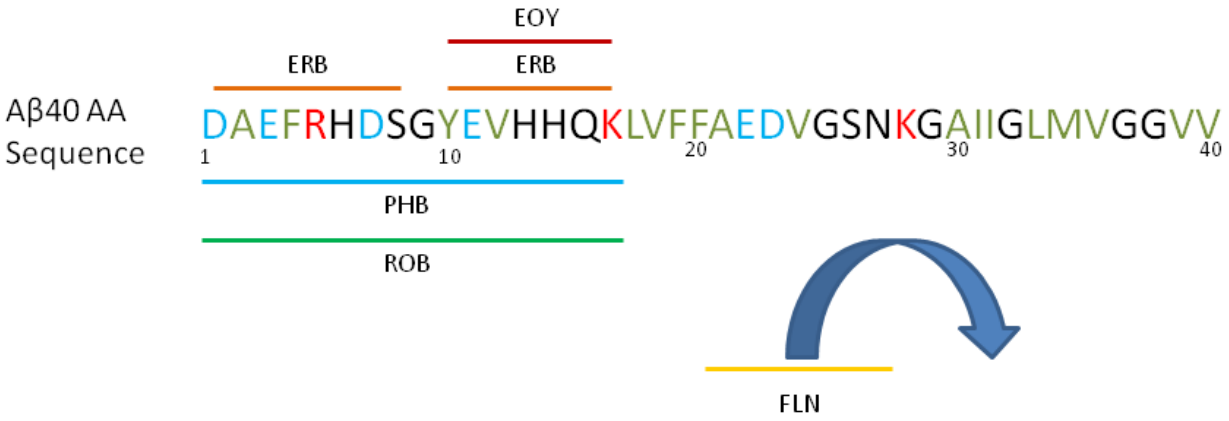

Figure 3.6 - Summary of strong binding sites for Aβ40 aggregation modulating ligands. Fluorescein (FLN) poorly-binding, non-aggregation-modulating negative control does not significantly bind. Erythrosin B (ERB), Eosin Y (EOY), Phloxine B (PHB), and Rose Bengal (ROB) all bind to the common loci of amino acids (AAs) 10-16 on Aβ40. ERB, PHB, and ROB also bind strongly to other sites on the N-terminus.

It is noteworthy that the relatively weak binding site of ERB, PHB, and ROB (the 1-8 AA region of Aβ40) identified by the dot blot using sequence-specific antibodies was not detected by the fluorescence quenching method. We speculate that this discrepancy results from the limitation of fluorescence quenching method in identifying secondary binding sites generated by structural changes of a target protein upon ligand binding to the primary binding site. It is obvious that the 10-16 AA region of Aβ40 is the primary binding site of ERB, PHB, and ROB. Therefore, we speculate that the 1-8 AA region of Aβ40 becomes in contact with ERB, PHB, and ROB only after these dyes bind to the primary binding site.

Conclusion

In this chapter, we have introduced and validated a method for identifying ligand binding sites on Aβ that employs dot blot immunostaining with sequence-specific antibodies. Unlike other current binding site identification methods requiring very specialized equipment and training, this technique can be carried out using apparatuses readily available in the biochemistry laboratory. As a result, this method greatly increases researchers' ability to both screen for new ligands that bind specific amino acid regions on Aβ and gain valuable insight to how existing ligands work. We then proceeded to successfully apply the method to characterize the binding sites of Erythrosin B and its structural analogs to the Aβ40 target peptide, discovering the 10-16 amino acid region is very important for strong molecular binding. More broadly, this method has a great potential to be applied to other target peptides/proteins associated with human diseases. For example, alpha-synuclein, a 140 amino acid protein targeted in Parkinson's disease, has a panel of 10 sequence-specific antibodies, each representing 10-15 amino acid segments,

allowing for full coverage of the protein sequence.[169] In addition, ubiquitin, a common 76 amino acid regulatory protein, and superoxide dismutase 1, a 154 amino acid protein implicated in Lou Gehrig's disease, have panels of 8 and 11 sequence-specific antibodies, respectively, allowing complete sequence coverage.

Chapter 4: Different Fates of Alzheimer's Disease Amyloid-Beta (Aβ) Fibrils Remodeled by Biocompatible Small Molecules[13]

Abstract

Amyloid fibril protein aggregates implicated in numerous human diseases are thermodynamically very stable. Stringent conditions that would not be possible in a physiological environment are often required to disrupt the stable fibrils. Recently, there is increasing evidence that small molecules can destabilize and remodel amyloid fibrils in a physiologically relevant manner. In order to investigate potential mechanisms and whether this approach would be effective for the biocompatible amyloid-beta (Aβ) aggregation modulators our group has been developing, we performed studies on the structural features of the different Aβ aggregates remodeled from Aβ fibrils by Brilliant Blue G (BBG) and Erythrosin B (ERB). For comparison purposes, we also analyzed the effects of a third Aβ small molecule modulator, Methylene Blue (MB). Combined with circular dichroism (CD), immuno-blotting, transmission electron microscopy (TEM), and atomic force microscopy (AFM) results, it was found that Brilliant Blue G- and Erythrosin B-treatment generate fragmented Aβ fibrils and protofibrils, respectively. In contrast, incubation of the Aβ fibrils with Methylene Blue perturbs fibrillar structure leading to amorphous Aβ aggregates. These findings provide insights on the molecular mechanism of amyloid fibril formation and remodeling and also illustrate the possibility of controlled changes in biomolecule nanostructures.

Introduction

The amyloid fibril is one of the most biologically important protein structures due to its implication in numerous neurodegenerative diseases, such as Alzheimer's Disease (AD), Parkinson's disease (PD), and prion disease.[10, 13, 188-190] Intrinsically disordered monomeric peptide and protein, such as amyloid-beta (Aβ) peptide and α-synuclein, aggregate to form prefibrillar or fibrillar oligomers, leading to amyloid fibrils with cross-stacked β-sheet structure.[39]

Since amyloid fibrils are thermodynamically very stable,[13, 191] it has been generally accepted that reversing the preformed amyloid fibrils into smaller intermediates does not occur spontaneously. Therefore, several strategies employing physiological and non-physiological conditions have been investigated to break, disrupt, and/or destabilize amyloid fibrils.[192] As a non-physiological condition, physical energy has been applied to break down mature fibrils. Ultrasonication has been found to fragment preformed amyloid fibrils into shorter fibril fragments that can be used to template further fibril formation.[193] Additionally, high temperatures (above 100◦C) have been found to disrupt the strength of hydrogen-bond networks which are crucial for the rigid fibril structure, leading ultimately to destruction of fibril structure.[192, 194] Because charge is a very important factor in fibril structure stability, drastic changes in pH or salt levels can lead to fibril destruction. Specifically, pH levels above 8 have been shown to lead to complete loss of β-sheet interactions.[195] Similarly, the addition of strong ionic liquids can block the electrostatic repulsion forces needed to hold together neighboring protofibrils during the fibril twisting process.[196] Finally, the introduction of denaturants (such as guanidine hydrochloride) or co-solvents (such as hexafluoroisopropanol (HFIP) and dimethylsufoxide) have also been shown to strongly destabilize preformed amyloid fibrils.[197, 198]

Water-ethanol solutions have been found to have a lesser effect over shorter time periods (< 1 day), but still converted mature fibrils into shorter, worm-like fibrils over a period of several weeks.[199]

Besides these non-physiological conditions, recent findings demonstrate that preformed amyloid fibrils can be destabilized by endogenous or exogenous compounds in physiological conditions.[13] L-dihydroxy-phenylalanine (L-DOPA), an endogenous precursor of dopamine, disaggregated the amyloid fibrils formed in the mouse brain generating toxic smaller aggregates,[200] illustrating the possibility that insoluble amyloid fibrils are a source of toxic soluble oligomers/protofibrils[201] by interacting with destabilizing chemical compounds. Surfactants (such as Triton X-100 and sodium dodecyl sulfate) have been used to destabilize fibrils through the promotion of molecular orientations with unfavorable energy. An interesting example of the interaction of surfactants with mature amyloid fibrils is the work by Ruhs, et al., employing sulfonic-acid-terminated PEG.[202] The strong electrostatic interactions between the PEG and fibrils reduced the entropy of the native amyloid fibril structure, resulting in its conversion to an amorphous, globular ending structure. It was also reported that several small molecules often introduced into human body (exogenous small molecules), such as doxycycline, epigallocatechin gallate, rifampicin, and dequalinium, destabilize preformed amyloid fibrils.[15, 203, 204] Despite the increasing number of cases demonstrating that amyloid fibrils can be destabilized by small molecules, the underlying molecular mechanisms still remain largely unclear.[192] In particular, different fates of the destabilized amyloid fibrils have not yet been extensively investigated. Considering that endogenous and exogenous compounds can directly destabilize amyloid fibrils present in the human body, investigating the different fates of the destabilized amyloid fibrils by small molecules will provide insights on the molecular-level

pathological mechanism of amyloid fibrils as well as small molecule-induced structural conversion of biomacromolecules.[13]

To this end, the scope of this chapter's work was to perform comparative in vitro studies on the structural features of the different Aβ aggregates converted from Aβ40 amyloid fibrils destabilized by three exogenous biocompatible small molecules, Methylene Blue (MB), Brilliant Blue G (BBG), and Erythrosin B (ERB) (Figure 4.1).[13] These three molecules are effective modulators of Aβ aggregation and cytotoxicity and possess several attractive features. Our research group recently reported that red food dye (ERB) and the blue food dye analog (BBG) are novel small-molecule modulators of Aβ40 monomer aggregation and effectively eliminate Aβ-associated cytotoxicity by promoting non-toxic Aβ aggregate formation but reducing toxic Aβ aggregate formation.[27, 89] MB has also been shown to modulate Aβ42 aggregation and cytotoxicity by promoting less toxic amyloid fibril formation but preventing the formation of very toxic prefibrillar oligomers.[23, 34] Therefore, it was expected that these three molecules will interact with Aβ40 fibrils despite the lack of previous evidence. In addition, MB, BBG, and ERB are structurally quite distinct, representing phenothiazine, triphenylmethane, and xanthene benzoate groups, respectively. Therefore, these three molecules most likely have different interaction modes on Aβ40 fibrils. These three molecules also have good potential for therapeutic application since they are safe, biocompatible, and potentially blood-brain barrier permeable.[36-38, 115, 141, 205-212] MB has already been shown to have a wide variety of medicinal applications, including treatment of malaria and cancer.[213-215] Furthermore, the Phase II clinical trials of MB on AD demonstrated promising results.[216] BBG expedited the recovery after spinal cord injury and conferred neuroprotection to the brain by mitigating AD and multiple sclerosis symptoms.[208, 211, 212] ERB is a Food and Drug Administration-approved red food coloring dye. A

daily dose up to 60 mg/kg of ERB is non-toxic to humans.[207] These three compounds are either being taken or might be taken in the future by humans. Since testing small molecules in vivo is not trivial, in vitro studies on the effects of these three molecules on amyloid fibrils will serve a good reference to gauge their destabilizing capacity on the amyloid fibrils in the human brain, thus possibly facilitating clearance.

The following steps were taken in order to investigate and classify these changes.

1. **Assess morphology of the remodeled Aβ aggregates using TEM and AFM.**
    a. If aggregates have a persistent, defined structure, assess average length and thickness.
    b. Compare morphological characteristics to untreated Aβ fibril control.
2. **Assess secondary structure of remodeled aggregates using CD spectra analysis.**
    a. Quantify secondary structure content using numerical deconvolution software platform.
    b. Compare secondary structure content to untreated Aβ fibril control.
3. **Assess morphological changes and/or binding sites of the three small molecules using conformational and sequence-specific antibody dot blot analysis.**
    a. Propose mechanisms by which the small molecules trigger structural changes in the fibrils.
4. **Classify remodeled Aβ aggregates using the criteria for various Aβ40 conformers discussed in Chapter 1's "Definition of Various Aβ40 Aggregated Conformers" Section.**

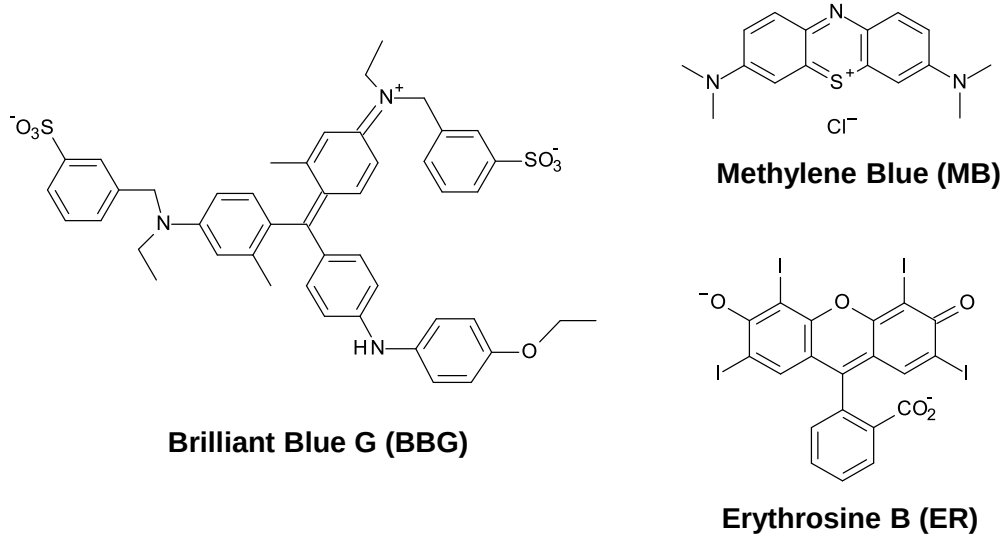

Figure 4.1 - Chemical structure of Brilliant Blue G (BBG), Methylene Blue (MB), and Erythrosin B (ERB) at neutral pH.

Materials and Methods

Materials

Aβ40 lyophilized powder was purchased from Selleck Chemicals (Houston, TX). Horseradish peroxidase (HRP)-conjugated goat anti-rabbit IgG antibody was obtained from Invitrogen (Carlsbad, CA). 4G8 antibody was obtained from Covance (Dedham, MA). Polyclonal OC and monoclonal 6E10 antibodies were obtained from Millipore (Billerica, MA). Nitrocellulose membranes and ECL Advance chemiluminescence detection kit was obtained from GE Healthcare Life Sciences (Waukesha, WI). Thioflavin T was purchased from Acros Organics (Geel, Belgium). All other chemicals were obtained from Sigma-Aldrich (St. Louis, MO) unless otherwise noted.

Methods

Aβ Fibril Formation and Remodeling

Aβ40 fibrils were prepared by dissolving lyophilized Aβ40 peptide powder from Selleck in 100% HFIP at room temperature at a concentration of 1 mM Aβ40. After a 2 hour incubation period at room temperature, the HFIP was evaporated to dryness in a gentle stream of nitrogen gas. Then, the peptide was diluted to 50 μM Aβ40 in phosphate buffered saline (1X PBS) solution (10 mM NaH_2PO_4 and 150 mM NaCl at pH 7.4) and incubated for 10-13 days at 37°C without stirring. To examine the remodeling effect of Brilliant Blue G (BBG), Methylene Blue (MB), and Erythrosin B (ERB), concentrated stock solutions of each small molecule dissolved in

1X PBS were added to the preformed Aβ40 fibrils. The samples were then incubated for an additional 1 day at 37°C without stirring.

Thioflavin T (ThT) Assay

ThT fluorescence assay was performed as reported previously.[27, 89] Aβ40 fibril formation was monitored by diluting 5 μL of 50 μM Aβ sample solution in 250 μL of 10 μM ThT in black 96-well plates (Fisher Scientific, Pittsburgh, PA). The resulting ThT fluorescence of the Aβ sample was measured at an emission wavelength of 485 nm using an excitation wavelength of 438 nm in a Synergy 4 UV-Vis/fluorescence multi-mode microplate reader (Biotek, VT).

Transmission Electron Microscopy (TEM)

Aggregate morphology was assessed using TEM and was performed as reported previously.[27, 89] Aβ samples (10 μL of 50 μM Aβ) were placed on 200 mesh formvar coated/copper grids (Electron Microscopy Sciences, Hatfield, PA), adsorbed for 1 minute, and blotted dry with filter paper. Grids were then negatively stained for 45 seconds with 2% uranyl acetate solution (Electron Microscopy Sciences, Hatfield, PA) in doubly distilled water (ddH_20), blotted dry, and then inspected with a JEOL 1010 Transmission Electron Microscope operated at 60 kV. Aggregate length and width was then quantified where appropriate using Image J software (NIH).

Atomic Force Microscopy (AFM)

10 μL of Aβ samples (diluted to 25 μM Aβ in molecular grade ddH_20) were spotted on freshly cleaved V1 grade muscovite mica (Electron Microscopy Sciences, Hatfield, PA) and allowed to adsorb for 10 minutes. After adsorption, the samples were washed four times with 30 μL molecular grade ddH_20 to remove residual salts, dried with a gentle stream of pure nitrogen gas, and placed in a covered petri dish to dry completely overnight. Dry AFM images were taken using an NT-MDT Solver Pro M system with NSG01 silicon cantilevers (NT-MDT, Santa Clara, CA, guaranteed < 10 nm radius of curvature, 5.1 N/m force constant) in semi-contact mode. Aggregate length and width was then quantified where appropriate using the Gwyddion SPM analysis software package.[217]

Circular Dichroism (CD) and Numerical Spectra Deconvolution

The secondary structure of Aβ aggregates was evaluated using a Jasco 710 spectropolarimeter (1-mm path length quartz cuvette) at room temperature by diluting 30 μL of 50 μM Aβ sample in 270 μL of ddH_20 (1:10 dilution). The background contribution of the 1X PBS solvent and an appropriate small molecule (BBG, MB, or ERB) was then carefully subtracted to obtain the spectra plots displayed. Each background-subtracted sample spectra is the average of at least 10 readings. The background-subtracted sample spectra was then deconvoluted to obtain numerical estimations of secondary structure content using the

DichroWeb online circular dichroism analysis software server,[79] employing the CONTINLL analysis program[218, 219] along with 'Set #6'[139, 220] or the SP175[221] reference sets in DichroWeb.

Antibody Dot-Blot Assay

Dot-blot assays were performed as reported previously.[27, 89] 2 μL of 50 μM Aβ samples were loaded on nitrocellulose membranes at the desired time points during fibril destabilization, allowed to air dry, and then were stored at 4 ^{o}C until immunostaining. For immunostaining, nitrocellulose membranes were first blocked for 1 hour in 5% skim milk dissolved in Tris-buffered saline solution with 0.1% Tween 20 (Bio-Rad, Hercules, CA) (1X TBS-T – 0.05 M Tris base, 0.15 M NaCl, pH 7.44). Membranes were then exposed to three, 5 minute washes with 1X TBS-T. Next, the membranes were incubated for 1 hour with OC (1:14,000 dilution), 6E10 (1:14,000 dilution), or 4G8 (1:7,000 dilution) primary antibody diluted to the specified factor in 0.5% milk 1X TBS-T solution. After the incubation, membranes were then again exposed to three, 5 minute washes with 1X TBS-T. The dot blot intensity of the membrane immunostained with 4G8 antibody (already has horseradish peroxidase conjugated) was visualized by exposing the membrane to the ECL substrate (ECL Advance Detection Kit – GE Healthcare) and then imaged in a BioSpectrum imaging system (UVP, Upland, CA). The membranes immunostained with OC and 6E10 antibodies were incubated for 1 hour with HRP-conjugated goat-anti-rabbit IgG secondary antibody at a 1:10,000 dilution in 0.5% milk 1X TBS-T and then visualized using the ECL substrate as described for the 4G8 membrane.

Results and Discussion

BBG Fragments Preformed Aβ Fibrils

Aβ fibrils were prepared by incubating Aβ40 monomers for 10 to 13 days. Thioflavin T (ThT) fluorescence, transmission electron microscopy (TEM), and circular dichroism (CD) assays were employed to verify the formation Aβ fibrils. ThT binding and its resulting fluorescence is widely used to monitor fibril formation.[39] The initiation of fibril assembly is characterized by a sharp increase in ThT fluorescence, while mature fibrils are predominantly present when the emission signal reaches a maximum and plateaus. Consequently, Aβ fibril assembly as measured by ThT fluorescence can be modeled by sigmoidal regression. The ThT fluorescence curve in Figure C1 exhibits this behavior. Fibril formation commences on day 5 and ThT fluorescence reaches a maximum by day 10 (Figure C1 in Appendix C). Furthermore, from day 9 to day 10, there is no significant increase in ThT fluorescence. Next, TEM was utilized to visually verify the presence of fibrils (Figure 4.2A; Panel Aβ only and Figure C2 Panel Aβ only for wider frame in Appendix C). Consequently, both ThT fluorescence and TEM results verify that fibrils are present. Next, CD was employed to characterize the secondary structure of the fibrils. The CD spectrum of the Aβ fibrils exhibited the typical features of β-sheet structures (Figure 4.2C) supporting the fibrillar structure formation.[39]

Next, we investigated whether BBG can destabilize preformed fibrils and generate different forms of aggregates using transmission electron microscopy (TEM), atomic force microscopy (AFM), circular dichroism (CD), and dot-blot assays with Aβ-specific antibodies. Although measuring ThT fluorescence intensity has also been used to monitor a loss of Aβ fibrils, we could not employ this method in our studies due to the reported spectral interference

of small molecules, including curcumin, BBG, and ERB on ThT fluorescence measurement.[27, 39, 50, 89] The preformed Aβ fibrils were then incubated in the absence or presence of BBG for 1 day. First, both the Aβ fibrils and the BBG-treated Aβ fibrils were subjected to negative-stain TEM analysis. The Aβ fibrils exhibited the typical morphological features of amyloid fibrils (Figure 4.2A; Panel Aβ only and Figure C2; Panel Aβ only for wider frame in Appendix C) – long, filamentous, and rod-like with defined and persistent structure. The length of the Aβ fibril population was measured and found to have an average length of 1,026 ± 621 nm, consistent with the fibril criteria established in Chapter 1's "Definition of Various Aβ40 Aggregated Conformers" Section. The population of the fibrils with a length greater than 1,100 nm is 35% (Table 4.1A). In contrast, BBG treatment generated much shorter, rod-like (with defined structure) aggregates of average length 133 ± 65 nm (Figure 4.2A; Panel BBG and Figure C2: Panel BBG for wider frame in Appendix C; Table 4.1A). Although only 6% of the untreated Aβ fibrils have a length less than 300 nm, 97% of the BBG-treated Aβ aggregates have a length less than 300 nm (Table 4.1A), indicating that the BBG-treated Aβ aggregates were strikingly shorter than the untreated Aβ fibrils. Next, we investigated the morphological trends of the remodeled fibrils observed using AFM. As was the case with the TEM results, most of the untreated Aβ fibrils are intermingled (Figure 4.2B; Panel Aβ only), while treatment with 10X BBG resulted in much shorter, dispersed aggregates (Figure 4.2B: Panel BBG). The lengths and widths of the two Aβ samples were measured using the AFM image analysis software Gwyddion[217] (Table C1A and C1B in the Appendix C). When we first began the AFM analysis of our samples, we expected to be able to directly compare the lengths and widths found with AFM to our TEM results. However, since the intrinsic resolution limit of AFM set by cantilever tip radius affects the absolute values of both lateral and height measurements[77, 222, 223] and the detection limit of

AFM is smaller than that of TEM,[74, 76] a direct comparison between TEM and AFM values was not possible. Therefore, we focused on comparing the length and width distribution trends between samples obtained using the two different microscopic assays. The average length of the 10X BBG-treated fibrils measured using AFM was 96 ± 40 nm, while the average length of the untreated Aβ fibrils was much longer at 329 ± 161 nm, consistent with the remodeling trend observed in the TEM images. In fact, 88% of the BBG-treated sample had a length less than 150 nm, while only 17% of the amyloid fibril sample had a length less than 150 nm (Table C1A in Appendix C). A decrease in the average lengths of both the untreated and the BBG-treated Aβ fibrils in AFM compared to TEM is likely due to the lower detection limit of AFM than that of TEM. In the TEM results, the percentages of the Aβ aggregates of a length less than 200 nm are 2% and 88% for the untreated and the BBG-treated Aβ fibrils, respectively (Table 4.1A). However, in AFM results, these values are 30% and 98% (Table C1A in Appendix C), indicating that small Aβ aggregates were better detected by AFM than TEM resulting in the decrease in the average length in AFM compared to TEM. Despite the differences in absolute average lengths, both the TEM and AFM results strongly support the idea that the BBG-treatment substantially reduces the average length of Aβ fibrils. Therefore, the smaller, rod-like BBG-treated Aβ aggregates could be protofibrils or fibril fragments.

In order to determine whether the BBG-treated aggregates are protofibrils or fibril fragments, their thicknesses/widths were measured and compared to those of untreated Aβ fibrils. According to the Aβ fibril structural model proposed by Schmidt et. al through cryo-EM and mass-per-length analysis of Aβ40 fibrils and protofibrils,[26] the thicknesses of the individual Aβ fibril and protofibril are around 20 nm and 12 nm, respectively. Despite concern over the intrinsic resolution of the technique, negative-stain TEM has been used numerous times in the

literature by different research groups to provide numerical estimation of the length or width of aggregates less than 30 nm.[12, 39, 60, 75] More specifically, Fandrich, et al. employed TEM to measure the widths of Aβ40 fibrils and found the average width to be 20.6 ± 2.8 nm,[32] which is in good agreement with the cryo-EM findings.[26] The untreated Aβ fibrils in this study exhibited an average width of 19 ± 4 nm upon examination of the magnified TEM image (Figure 4.2A; Panel Aβ only_M), with 98% of the fibrils measured having a width greater than 12 nm (Table 4.1B). Upon examination of the magnified TEM image, thickness of the BBG-treated Aβ aggregates seems similar to that of the untreated Aβ fibrils (Figure 4.2A; Panel BBG_M). The average width of the BBG-treated Aβ aggregates is 26 ± 7 nm (Table 4.1B). In particular, none of the aggregates measured have a width of 12 nm or less, clearly indicating that the BBG-treated Aβ aggregates are not protofibrils. Considering that the average width of the BBG-treated Aβ aggregates is comparable to that of the untreated Aβ fibrils, the BBG-treated Aβ aggregates are considered shorter Aβ fibrils compared to the untreated Aβ fibrils. The AFM results also show similar trends in the width of the Aβ aggregates (Table C1B in Appendix C). The average width of the BBG-treated sample was 58 ± 14 nm, and the untreated Aβ fibril sample had an average width of 73 ± 23 nm. In comparing the width distributions of these two samples measured using AFM, it was found that 86% of the BBG-treated sample's aggregate widths fall within one standard deviation of the Aβ fibril average width, indicating that these samples possess similar widths and confirming the trend found in the TEM analysis. An increase in the average width of the Aβ aggregates obtained using AFM assay compared to those of TEM assay can be attributed to the intrinsic resolution limit set by cantilever tip radius leading to over-estimation (convolution) of nanostructure widths.[77, 222] Because BBG-treatment resulted in shorter, rod-like aggregates but of similar thickness as Aβ fibrils, it was hypothesized that the

BBG-induced Aβ aggregates are likely fragmented fibrils but not protofibrils, according to the structural criteria set forth in Chapter 1's "Definition of Various Aβ40 Aggregated Conformers" Section.

In order to confirm this hypothesis, we also performed CD analysis. CD analysis is widely used to analyze secondary structure content of proteins.[6, 19, 39, 131, 132] The CD spectra of both the Aβ fibrils and the BBG-treated Aβ fibrils are shown in Figure 4.2C along with that of Aβ monomers for comparison. In the CD spectrum of Aβ monomers, neither α-helix nor β-sheet structural features were observed, strongly suggesting that Aβ monomers have disordered structure (Figure 4.2C). However, the CD spectrum of the Aβ fibrils exhibited the typical features of β-sheet-rich structure,[39] including a minimum at 217 nm (Figure 4.2C). The BBG-treated Aβ fibrils maintained the typical features of β-sheet structure. The minimum ellipticity value of the BBG-treated Aβ fibrils was observed at 217 nm. The ellipticity of the BBG-treated Aβ fibrils was positive below 200 nm. In order to quantitatively investigate secondary structural changes caused by BBG treatment, we used the web-based server, DichroWeb,[79] and calculated the secondary structure contents from the CD spectra using the CONTIN analysis program[218, 219] and SP175 reference protein set.[79, 221] The α-helix, β-sheet, β-turn, and disordered structure content of the Aβ fibrils are 12.2%, 36.4%, 12.1%, and 39.3% (Table 4.2), respectively, which is consistent with the Aβ fibril structural information that the N-terminus 17 residues (residues 1 – 17) are usually disordered and the 6 residues (residues 23-28) in the middle of Aβ sequence form β-turn structure.[12] Upon one day incubation of the Aβ fibrils with BBG, the secondary structural content was only slightly changed, with the β-sheet content increasing by 8% but the disordered structure content decreasing by around 7%. The β-sheet content of the BBG-treated Aβ fibrils is comparable to that of the Aβ fibril control, suggesting that the BBG-treated Aβ fibrils also have

fibrillar structures similar to the Aβ fibril control. Considering that the BBG-treated Aβ fibrils have persistent fibrillar structures in the TEM image, these results support the idea that the BBG-treated Aβ aggregates are shorter Aβ fibrils than the untreated Aβ fibril control, likely Aβ fibril fragments.

Dot-blot assays of the Aβ samples were also performed using three Aβ-specific antibodies (OC, 4G8, and 6E10). Recently, dot-blotting with Aβ-specific antibodies has been widely used to detect Aβ aggregates with different conformations.[9, 14, 20, 39, 42, 110, 133, 134] OC is a polyclonal antibody that recognizes fibrillar oligomers, protofibrils, and fibrils but not monomer, prefibrillar oligomers, and disordered aggregates.[9, 14] 4G8 is an Aβ sequence-specific monoclonal antibody[135-138] which binds to amino acids 17 to 24 of Aβ. Lastly, 6E10 is a monoclonal antibody that recognizes N-terminus residues of Aβ.[14, 58] Although both 4G8 and 6E10 were originally used to ensure the conservation of Aβ moieties, recent findings demonstrated that immuno-reactivities of these two antibodies can be affected by Aβ conformational changes and small-molecule binding to their epitopes.[27, 58, 89] In order to distinguish the immuno-reactivity changes caused by the small molecules binding to antibody epitopes (fast processes) from those made by Aβ conformation changes (slow processes), we incubated the Aβ fibrils with the small molecules for a very short time (less than 5 min) and for a longer time (one day). Incubation of the Aβ fibrils with 1x BBG (molar concentration equal to that of Aβ peptide) did not alter the immuno-reactivities of Aβ fibrils for all three antibodies (OC, 6E10, and 4G8), strongly indicating that there is no change in the content of fibrillar structure (Figure 4.3). The 6E10 and 4G8 immuno-reactivities of the BBG-treated fibril samples at both 5 minutes and 1 day were maintained when compared to the fibril sample, indicating that

BBG did not significantly bind to the N-terminus and 17-24 residues of Aβ fibrils. It is noteworthy that 10x BBG (10 times the molar concentration of Aβ peptide) resulted in a significant reduction of the OC-reactivity after 1-day incubation (Figure 4.3; Panel 1-day incubation). However, such a reduction in the OC-reactivity of the 10x BBG-treated Aβ fibrils can be explained by BBG binding to the OC epitope rather than a loss of fibrillar structure. The short incubation of Aβ fibrils with 10x BBG is not long enough to cause Aβ conformational changes resulting in a significant reduction in the OC-reactivity (Figure 4.3; Panel < 5 min), indicating that BBG binds to the epitope thus restricting the access of the OC antibody. It was also reported that BBG binds to Aβ peptide in multiple sites.[89] Therefore, we speculate that direct binding of BBG to Aβ fibrils leads to Aβ fibril fragmentation.[13] Unlike Aβ sequence-specific antibodies, the OC antibody recognizes a generic epitope of the protein backbone present in fibrillar conformations, independent of protein sequence.[14] Because of this, it is difficult to conclude the specific location of interaction between BBG and Aβ fibrils that would facilitate the decrease in OC signal due to binding without additional studies. However, structural models of Aβ40 protofibrils have proposed that the hydrophobic C-terminus of the Aβ peptide comprises the core of the cross-stacked β-sheet axis/backbone.[26, 224] Therefore, it is possible that the hydrophobic interactions between the six aromatic rings in each BBG molecule contribute to interaction with the hydrophobic C-terminus, thus destabilizing the fibrils.

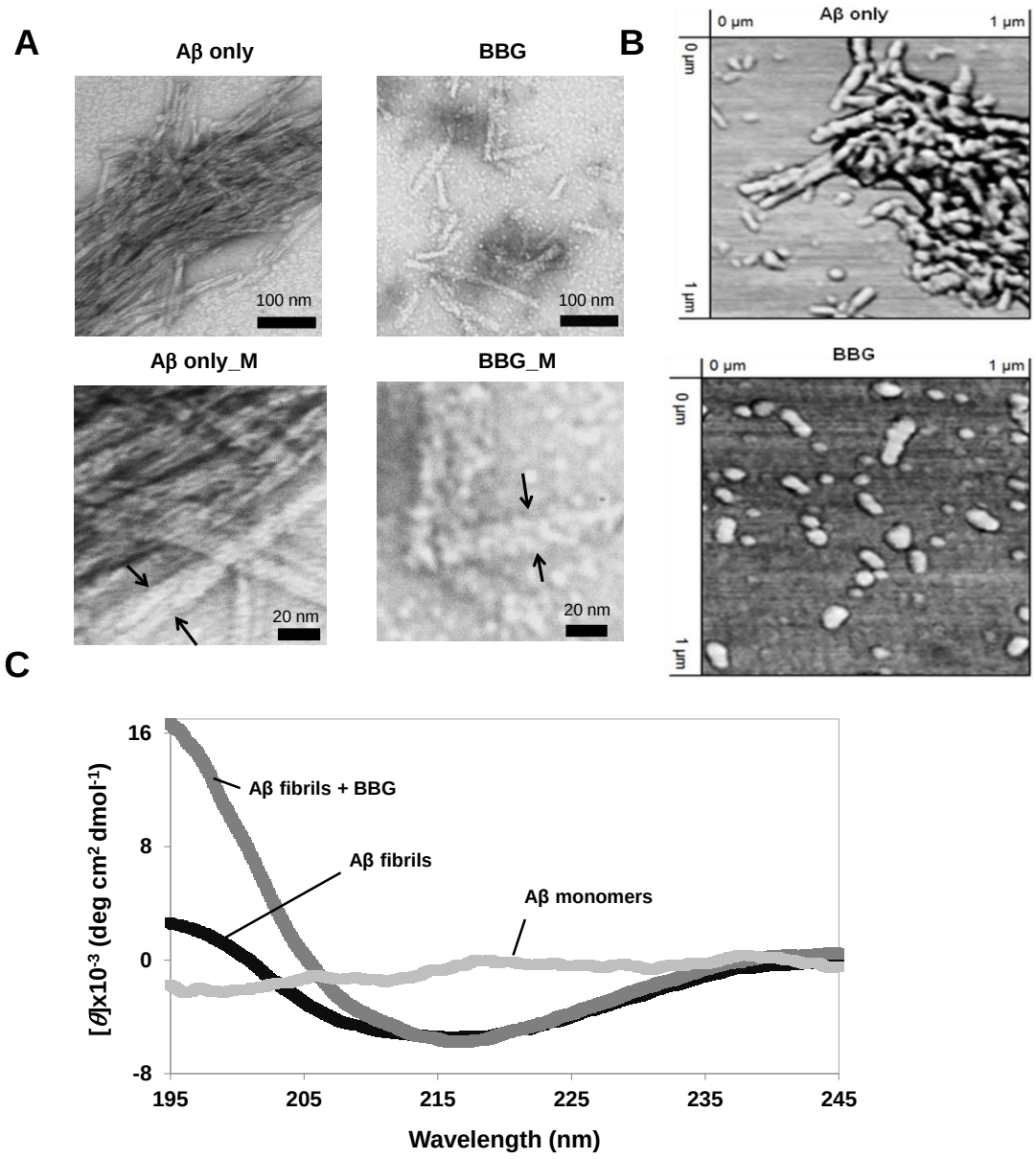

Figure 4.2 - Properties of the Aβ fibrils incubated in the absence or presence of BBG. TEM (A) and AFM images (B, 1x1 µm) of the Aβ fibrils incubated for one day in the absence of any dye (Panel Aβ only) or presence of 10x BBG (Panel BBG). The sections of the two TEM images were magnified (Panels Aβ only_M and BBG_M). Each pair of arrows illustrates the width of the Aβ aggregates. TEM scale bar is 100 nm (Top Panels) or 20 nm (Bottom Panels). (C) CD spectra of Aβ monomers, Aβ fibrils incubated in the absence (Aβ fibrils) or presence of 10x BBG (Aβ fibrils + BBG) for one day.

Table 4.1 - Measured[a] TEM length (A) and width (B) distribution[b] of Aβ fibrils incubated in the presence or absence of 10X BBG and 10X ERB for one day at 37°C.

A.

	Length of Aβ Aggregates (μm)												
	0.1	0.2	0.3	0.4	0.5	0.6	0.7	0.8	0.9	1	1.1	>1.1	Average (nm)
Fibrils Only	ND	2%	4%	8%	10%	10%	6%	10%	4%	2%	10%	35%	1026 ± 621
10X BBG	34%	54%	9%	3%	ND	ND	ND	ND	ND	ND	ND	ND	133 ± 65
10X ERB	3%	18%	32%	32%	9%	3%	2%	1%	ND	ND	ND	ND	303 ± 129

B.

	Width of Aβ Aggregates (nm)													
	6	8	10	12	14	16	18	20	22	24	26	28	>28	Average (nm)
Fibrils Only	ND	ND	ND	2%	10%	10%	25%	13%	21%	10%	4%	4%	1%	19 ± 4
10X BBG	ND	ND	ND	ND	ND	1%	10%	4%	10%	11%	19%	8%	37%	26 ± 7
10X ERB	1%	7%	48%	25%	17%	2%	ND	ND	ND	ND	ND	ND	ND	10 ± 2

[a]Measured using Image J software.
[b]The aggregate length or width bin labels represent the maximum length or width of aggregates in each respective bin. Shown on the table are the proportions of each sample population measured possessing the respective maximum bin length or width. Minimum one hundred aggregates except fifty one fibrils only aggregates for length distribution were used to obtain the distribution.
ND: Not Detected

Table 4.2 - Secondary structure content[a] of Aβ fibrils incubated[b] in the absence or presence of BBG or ERB.

Dye added[c]	α-helix	β-sheet	β-turn	Disordered
-	12.2%	36.4%	12.1%	39.3%
BBG	12.8%	44.4%	9.9%	32.9%
ERB	12.7%	36.8%	11.8%	38.6%

[a] Determined by DichroWeb using CONTIN method and SP175 reference proteins

[b] Incubated at 37 °C without shaking for one day.

[c] Aβ:small molecule (BBG or ERB) = 1:10 molar ratio

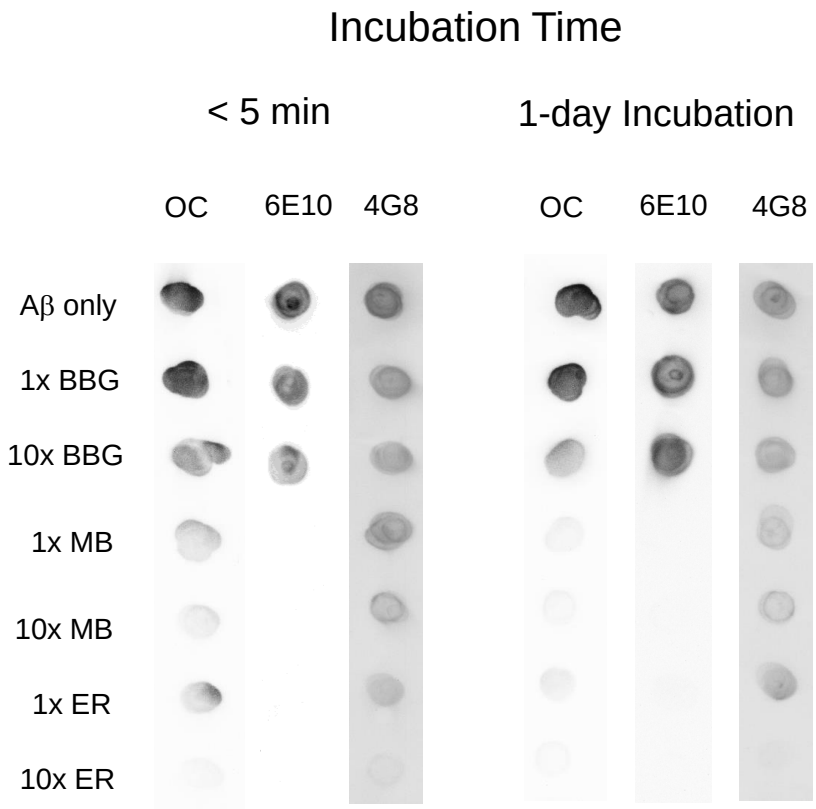

Figure 4.3 - Dot-blot images of the Aβ fibrils incubated in the absence (Aβ only) or presence of 1x and 10x BBG, MB, or ERB for less than 5 minutes (Panel < 5 min) or one day (Panel 1-day incubation). For each antibody, all samples were spotted onto the same nitrocellulose membrane. Each membrane was immunostained with the OC, 6E10, or 4G8 antibody. For clearer presentation of the data, the sections of each membrane were cut and re-arranged.

MB Converts Preformed Aβ fibrils into Amorphous Aggregates

Next, Aβ fibrils were treated with 1x or 10x MB for one day. The TEM and AFM images of the MB-treated Aβ fibrils showed that no structural features of fibrils were observed (lacking a persistent defined structure), and neither the size nor the shape of the MB-treated Aβ aggregates were homogenous (Figure 4.4A), indicating the possibility of structural changes from fibrils to amorphous aggregates. The CD spectrum of the MB-treated Aβ fibrils showed three changes from that of Aβ fibrils – a shift in the wavelength of a minimum ellipticity, negative ellipticity below 200 nm, and an upward shift of ellipticity above 200 nm toward zero (Figure 4.4B). Furthermore, the CD spectrum of the MB-treated Aβ fibrils shifted toward that of the Aβ monomers (Figure 4.4B). Because Aβ monomers have been shown to possess predominantly disordered/random-coil secondary structure[19, 39] and low ellipticity above 210 nm and negative banding at 195 nm are general characteristics of disordered proteins,[87] the changes observed with MB-treated fibrils strongly indicate a substantial loss of the β-sheet content but an increase in the disordered structural content. Similar to the BBG-treated Aβ fibrils, the CD spectrum of the MB-treated Aβ fibrils was used to estimate the secondary structure content numerically using DichroWeb. Because the SP175 reference set contains the greatest range of protein structures/conformations among the total eight reference sets explicitly described in DichroWeb, our first choice was to employ this reference set for the CD analysis with all three small molecules (BBG, MB, and ERB). However, when we used the SP175 reference protein set to analyze the MB-treated fibril CD spectrum, no significant change in the secondary structure content was observed despite the obvious changes in the spectrum described previously (Table C2 in Appendix C). After searching through the literature for a possible explanation to this disparity, we found that the accuracy of the secondary structure content deconvolution estimation

greatly relies on the choice of a reference protein set containing proteins with similar structure to the one being studied.[79, 139] Since many of the intrinsically disordered amyloidogenic proteins do not fold into only one stable conformation that can be used to construct a reference set, finding an appropriate reference set for intrinsically disordered Aβ is particularly challenging. To our knowledge, there are no existing reference sets containing intrinsically disordered monomeric peptides/proteins, such as Aβ monomer. After thoroughly examining the SP175 reference protein set,[221] we found that α-helix-, β-sheet, and β-turn –rich reference proteins are well represented in the SP175 reference set, allowing successful estimation of the secondary structure contents of numerous folded proteins. However, we also found that the SP175 set includes only 1-2 disordered reference proteins among a total of 72 reference proteins. Since the proteins used to construct the SP175 reference set were prepared by folding recombinant proteins produced from bacteria, denatured or unfolded proteins were rarely included. Such a relatively low frequency of the disordered reference proteins is most likely attributed to the underestimated disordered structure content. In fact, the developers of the SP175 reference set also acknowledged that the validity of the reference set is limited to α-helical and β-rich proteins, not disordered proteins.[221] This further underlines the importance of performing an in-depth review of the reference set being used before beginning the analysis.

In order to address the issue of finding an appropriate reference set for the spectrum of the MB-treated Aβ fibrils, different reference protein sets contained within the DichroWeb server were evaluated. Among the reference protein sets embedded in DichroWeb, Set No. 6 has the highest frequency of disordered reference proteins (11 out of 42 total reference proteins). Therefore, the secondary structure contents of both the Aβ fibrils and the MB-treated Aβ fibrils were re-evaluated using the Set No. 6 and the estimated values are presented in Table 4.3.

Compared to the Aβ fibrils, the MB-treated Aβ fibrils exhibited a significant reduction in the β-sheet and β-turn content, but a substantial increase in the unordered structure content, which is quite consistent with the observation of the amorphous aggregates in the TEM monograph, AFM scan (Figure 4.4A), and qualitative visual analysis of the CD spectra. To our knowledge, conversion of Aβ fibrils into disordered-structured aggregates has not been shown previously through numerical deconvolution analysis of corresponding CD spectra.

The interaction between MB and preformed Aβ40 fibrils was further explored using dot-blotting with 6E10, OC, and 4G8 antibodies. Incubation of Aβ fibrils with either 1x or 10x MB for a very short time (less than 5 min) led to a substantial loss of the OC-reactivity (Figure 4.3; Panel < 5 min), clearly indicating that MB binds to the OC antibody epitope. Because of this strong binding affinity of MB to the OC antibody epitope, it is difficult to discern whether the weak OC signals observed in the MB-treated fibrils for 1 day (Figure 4.3, Panel 1 day) can be attributed to the direct MB binding to the OC epitope or the structural changes induced by MB (resulting in loss of the cross-stacked β-sheet epitope). The Aβ fibrils treated with MB for a short time also led to a complete loss of the 6E10 reactivity, indicating that MB binds to the 6E10 antibody epitope (N-terminus of Aβ). According to the structural model of Aβ fibrils, the N-terminus of Aβ is involved in the assembly of two protofibrils into one fibril.[26] Therefore, we speculate that MB destabilizes fibrils into amorphous aggregates at least in part via MB binding to a joint region between the two protofibrillar components of an Aβ fibril.[13] MB carries a positive charge at neutral pH, and therefore, has the potential to interact with negatively charged amino acids in the N-terminus of Aβ (Aspartic and/or Glutamic Acid) through electrostatic interactions.

Table 4.3 - Secondary structure content[a] of Aβ fibrils incubated[b] in the absence or presence of MB.

Small molecule added[c]	α-helix	β-sheet	β-turn	Disordered
-	10.1%	32.2%	27.4%	30.3%
MB	8.4%	18.3%	4.3%	69.0%

[a] Determined by DichroWeb using CONTIN method and Set 6 reference proteins

[b] Incubated at 37 °C without shaking for one day.

[c] Aβ:MB = 1:10 molar ratio

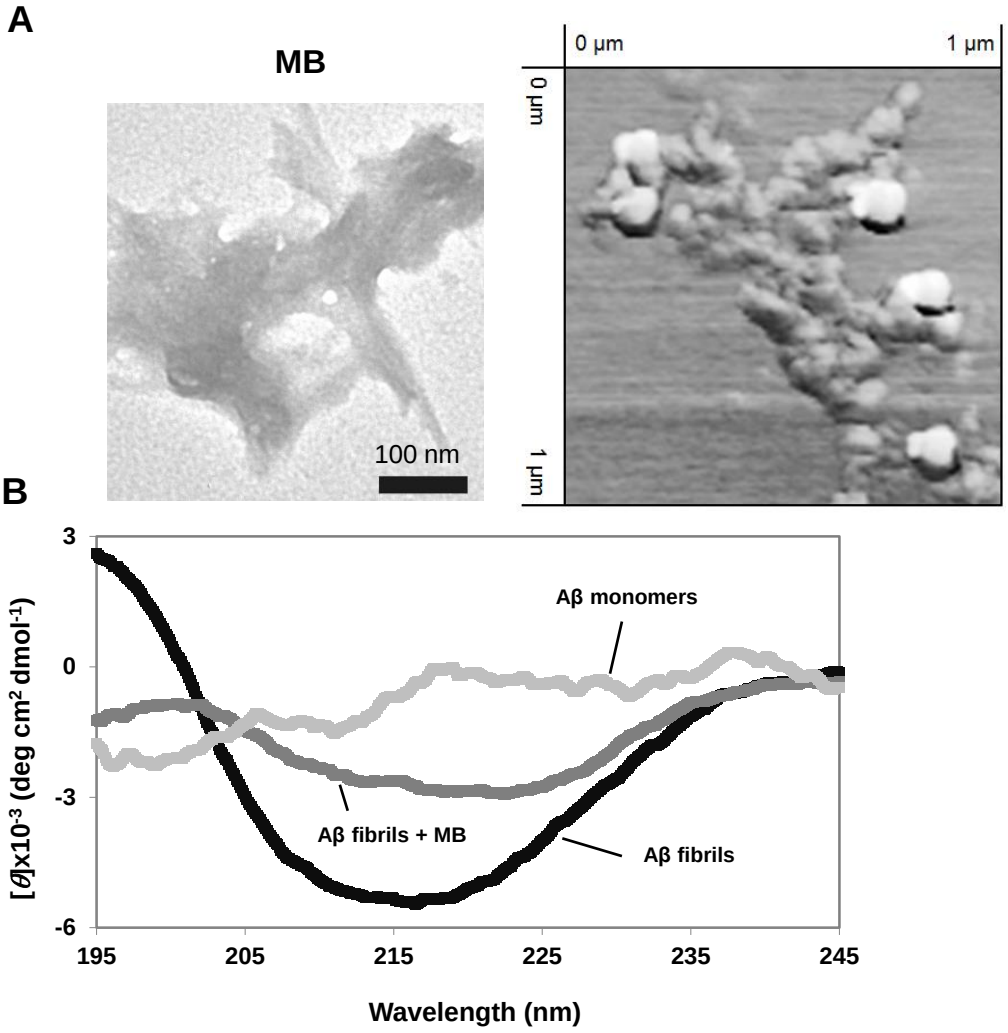

Figure 4.4 - Properties of the Aβ fibrils incubated in the absence or presence of MB. (A) TEM (left panel) and AFM (right panel, 1x1 µm) images of the Aβ fibrils incubated for one day in the presence of 10x MB. TEM scale bar is 100 nm. (B) CD spectra of Aβ monomers, Aβ fibrils incubated in the absence (Aβ fibrils) or presence of 10x MB (Aβ fibrils + MB) for one day.

ERB Disrupts Preformed Aβ fibrils into Protofibrils

In order to investigate the action of the third small molecule modulator, 1x or 10x ERB was incubated with the Aβ fibrils for one day. The TEM image of the ERB-treated Aβ fibrils showed many filamentous, persistent fibrillar structures (Figure 4.5A and Figure C2; ERB panel for wider frame in Appendix C) that seemed to be less tightly bundled/stacked than the untreated fibril sample (Figure 4.2A-B; Aβ only panels and Figure C2; Aβ only panel in Appendix C). The average length of the ERB-treated fibrils measured using TEM was 303 ± 129 nm, less than the average length of the untreated fibrils mentioned previously, but longer than the fibrils treated with 10X BBG (Table 4.1A). The majority (73%) of the ERB-treated aggregates measured had a length between 200 and 500 nm. Next, the morphological fate trends of Aβ fibrils remodeled with ERB were investigated using AFM and compared to the TEM findings. Similar to TEM, the AFM scan of the ERB-treated Aβ fibrils (Figure 4.5B) showed many fibrillar structures, still in close proximity to each other, but less stacked than with the untreated fibril sample (Figure 4.2B; Aβ only panel). From the AFM scan, the average length of the ERB-treated sample was found to be 162 ± 60 nm (Table C1 in Appendix C). This length data matched the trend seen in the TEM data that the ERB-treated fibrils were shorter than the untreated Aβ fibrils, but longer than the BBG-treated sample's aggregate population. As was the case for the untreated- and the BBG-treated Aβ samples, the average length of the ERB-treated sample measured by AFM is shorter than that by TEM, likely because AFM detects shorter Aβ aggregates better than TEM. The ERB-treated Aβ aggregates (with persistent filamentous structure) that are shorter than the untreated Aβ fibrils could be protofibrils or Aβ fibril fragments.

In order to determine whether the ERB-treated aggregates are protofibrils or fibril fragments, their widths were measured and compared to those of untreated Aβ fibrils. From the

TEM images (Figure 4.5A: ER_M Panel and Figure C2 in Appendix C), the average width of the ERB-induced aggregates is significantly smaller than that of both the untreated Aβ fibrils and the 10X BBG-treated Aβ fibrils (Table 4.1B). The average measured width of the ERB-treated Aβ fibrils was 10 ± 2 nm, which matches well with the width of an individual protofibril according to the Aβ protofibrils and fibrils structural model discussed previously.[26] Furthermore, none of the ERB-treated Aβ fibrils measured displayed widths greater than 16 nm, whereas 78% and 99%, respectively, of the untreated Aβ fibrils and the BBG-treated fibrils samples measured contained widths greater than the 16 nm cutoff. It is also noteworthy to mention that co-incubation of Aβ monomer with ERB also led to formation of dominant protofibrils with the width of 12 nm.[27] Furthermore, the ERB-treated samples did not exhibit the twisted structure, a typical feature of Aβ fibrils in general and also observed in our untreated Aβ fibril samples, in the TEM images (Figure 4.5A for ERB-treated sample and Figure 4.2A for Aβ only sample). Moreover, the widths of the ERB-treated aggregates (35 ± 6 nm) analyzed using AFM were much thinner than the Aβ fibril (73 ± 23 nm) and BBG-treated samples (58 ± 14 nm) (Table C1B in Appendix C), reinforcing the trend found in the TEM analysis. In fact, the width distribution data show that only 6% of the ERB-treated sample's aggregate population displayed widths within one standard deviation from the 73 nm mean width for the untreated fibril sample. Because of these morphological changes/findings, the ERB-treated Aβ fibrils are most likely protofibrils. As was the case for the untreated Aβ fibrils and the BBG-treated Aβ fibrils, the width of the ERB-treated Aβ fibrils determined by AFM is considered over-estimated compared to the width determined of TEM due to the lateral convolution caused by cantilever tip radius.[77, 222]

The CD spectrum of the ERB-treated Aβ fibrils clearly shows typical features of β-sheet-rich structure (Figure 4.5C). The estimates of the secondary structure content of the ERB-treated Aβ fibrils are essentially the same as those of Aβ fibrils (Table 4.2), indicating that the ERB-treated Aβ fibrils are β-sheet –rich, and most likely fibrillar structures.

In the dot-blot assays, the short time incubation (less than 5 minutes) of the Aβ fibrils with 1x or 10x ERB led to a significant reduction of the OC-reactivity (Figure 4.3), clearly indicating that ERB binds to the OC antibody epitope (as was the case with MB). Further, both 1x and 10x ERB led to a complete loss of the 6E10 reactivity indicating that an ERB binding site on Aβ is located at the 6E10 antibody epitope (Aβ N-terminus), which is consistent with the results reported previously.[27] As mentioned previously in the structural model of Aβ fibrils, the N-terminus of Aβ is involved in the assembly of two protofibrils into one fibril. Therefore, we conclude that ERB separates fibrils in to the ERB-induced protofibrils by binding to the N-terminus of the two protofibrillar components of Aβ fibrils, thus destabilizing the fibril complex.[13] Although both MB and ERB were shown to bind to the N-terminus of Aβ sequence, they most likely interact with different residues in Aβ. MB has a positive charge, but ERB has negative charges at neutral pH. Therefore, we speculate that ERB interacts with positively charged residues in the N-terminus of Aβ (one Lysine, one Arginine, and/or the three Histidines present in the N-terminus of Aβ), which led to a different fate of the destabilized Aβ fibrils compared to the action of MB.

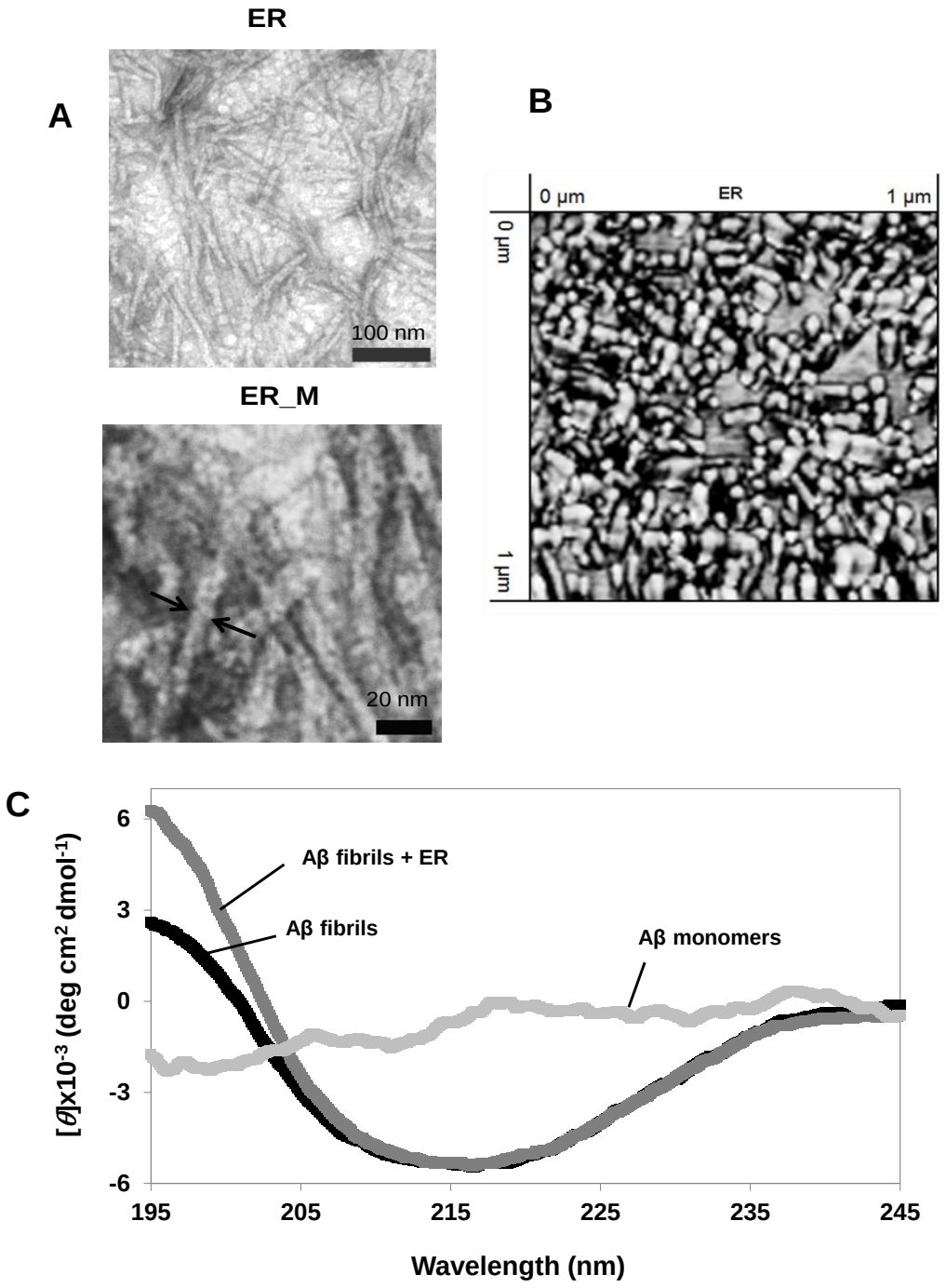

Figure 4.5 - Properties of the Aβ fibrils incubated in the absence or presence of ERB. TEM (A) and AFM (B, 1x1 µm) images of the Aβ fibrils incubated for one day in the presence of 10x ERB (Panel ER) and the magnified section (Panel ER_M). The pair of arrows illustrates the width of the Aβ aggregates. TEM scale bar is 100 nm (Panel ER) or 20 nm (Panel ER_M). (C) CD spectra of Aβ monomers, Aβ fibrils incubated in the absence (Aβ fibrils) or presence of 10x ERB (Aβ fibrils + ER) for one day.

Conclusion

In this chapter's work, we evaluated three biocompatible small molecule Aβ aggregation modulators (BBG, MB, and ERB) for their capacities to trigger structural changes of the Aβ fibrils in a physiologically-relevant manner and then characterized the structural features of the restructured Aβ fibrils and the mechanisms by which the changes occur. This investigation has conclusively established that thermodynamically stable preformed Aβ fibrils can be destabilized or remodeled by three small molecules (BBG, MB, and ERB). The results also successfully illustrate the possibility of controlling changes in biomolecule-based nanostructures using chemical compounds.

Combined with TEM, AFM, and dot-blot assays, conversion of Aβ fibrils into different types of aggregates was quantitatively analyzed through numerical deconvolution analysis of corresponding CD spectra with appropriate choices of reference protein sets. Incubation of the preformed Aβ fibrils with these molecules (BBG, MB, and ERB) effectively destabilized the preformed Aβ fibrils but led to three distinct fates. BBG fragmented the Aβ fibrils into shorter fibrils. MB restructured the Aβ fibrils into amorphous aggregates. Finally, ERB separated the Aβ fibrils into protofibrils. We found that BBG binds to the OC antibody epitope. Previously, it was shown that BBG binds to Aβ peptide in multiple sites.[89] Therefore, it is likely that direct binding of BBG to Aβ fibrils causes the Aβ fibril fragmentation. We also found that both MB and ERB bind to the N-terminus of Aβ, a joining region between two protofibrils in the formation of one Aβ fibril. Therefore, we speculate that MB or ERB binding to the joint between two protofibrils is a key step that triggers drastic structural changes of the Aβ fibrils into amorphous aggregates or separate protofibrils, respectively.

Chapter 5: Triphenylmethane Food Dye Analog Crosses Blood-Brain Barrier and Rescues Neuronal Loss and Amyloid-Beta Pathologies In A Transgenic Mouse Model of Alzheimer's Disease

Abstract

Reducing amyloid-beta (Aβ) accumulation represents a promising strategy for developing Alzheimer's Disease (AD) therapeutics. We recently reported that Brilliant Blue G (BBG), Erythrosin B, and their structural analogs are novel modulators of in vitro amyloid-beta aggregation and cytotoxicity in cell-based assays in a dose-dependent manner. Following up on this recent work, we sought to further evaluate these novel modulators in a more therapeutically-relevant AD mouse model. The triphenylmethane food dye analog, BBG, was selected to be tested first due to its superior biocompatibility consensus and use in existing investigations to treat neurological diseases. Brilliant Blue G was administered to APPSwDI/NOS2-/- mice for three months in order to assess biocompatibility, ability of the small molecule to cross the blood-brain barrier, and efficacy at rescuing key AD pathologies. The results showed that BBG was well-tolerated, showed no gross toxicity, and was able to significantly cross the AD blood-brain barrier. Immunohistochemical analysis of the brain sections revealed that BBG was able to significantly rescue neuronal loss and reduce intraneuronal Aβ loading in the hippocampus. To our knowledge, this is the first report of the effect of Brilliant Blue G on neuronal loss in a transgenic animal model of AD as well as the first report of oral (not injected) animal administration of BBG affecting a protein conformation/aggregation disease.

Introduction

Alzheimer's Disease (AD), the most common form of senile dementia today, is characterized and diagnosed by three key pathological hallmarks: neurofibrillary tau protein tangles, loss of neurons, and the accumulation of insoluble protein aggregates, composed primarily of neurotoxic amyloid-beta (Aβ).[225] Among the various isoforms of Aβ, Aβ40 and Aβ42 are the most physiologically relevant, with Aβ42 being more aggregation-prone.[6] Aβ is formed by sequential cleavage of the Amyloid Precursor Protein (APP) by beta- followed by gamma-secretase. The amyloid-cascade hypothesis states that Aβ accumulation is toxic to the brain and causative to the tau / neuronal death pathologies and cognitive deficits seen in AD patients.[11, 225] Therefore, reducing Aβ accumulation and aggregation represents a promising strategy for developing AD therapeutics.

Numerous small molecules have been studied for their ability to modulate Aβ aggregation and reduce neurotoxicity.[35, 106] In particular, several lipid-based modulators and polyphenols have been reported to modulate Aβ aggregation and reduce Aβ-associated toxicity.[16, 59, 88, 105, 107, 108, 111, 112] Although the results from these studies are encouraging and validate Aβ aggregation modulation as a promising strategy, a practical and effective therapeutic has yet to be identified. Not all Aβ aggregation small molecule modulators identified are suitable for AD therapeutic leads because they may not possess good biocompatibility and/or blood-brain barrier (BBB) permeability. Crossing the BBB is a big challenge in AD drug development; 98% of small molecule drugs and almost 100% of large molecule drugs cannot cross the BBB.[226] For example, therapeutic application of Congo Red has been hindered by poor BBB-permeability and carcinogenicity.[227] Although polyphenol tannic acid is also very effective in reducing Aβ neurotoxicity in cell-based assays,[23] tannic acid does not cross the animal BBB.[228] As a result,

there remains a strong driving force to identify new small molecule AD therapeutic candidates with desirable features.

In order to search for novel small molecule modulators with good biocompatibility, our research group screened various FDA-approved food dyes and their close analogs. We recently reported that the triphenylmethane dye, Brilliant Blue G (BBG), and its structural analog are novel modulators of in vitro Aβ40-aggregation and Aβ cytotoxicity in cell-based assays in a dose-dependent manner.[13, 27, 89, 90] Therefore, with good biocompatibility, BBG is an attractive potential therapeutic inhibitor of Aβ cytotoxicity in the treatment of AD. Following up on our recent work, we sought to further evaluate this novel modulator's efficacy in a more therapeutically-relevant AD mouse model.

Being a well-documented P2X7 receptor antagonist, BBG has been tested numerous times in animal models and as a potential therapy for neurodegenerative diseases.[229] Young et. al. gave intraperitoneal (i.p.) injections of 125 mg/kg/day BBG to mice and reported no adverse effects.[230] Peng et. al. administered BBG intravenously (i.v.) to a rat model of an acute spinal cord injury and found that it effectively reduced damage/inflammation and improved motor function recovery.[208] In one of the few reports of administering BBG orally, Kimbler et. al. gave ~3000 mg/kg/day BBG in drinking water to a mouse model of traumatic brain injury and also found that it improved injury recovery.[231] In a mouse model of prion protein disease, Iwamuru et. al. administered injections of BBG, finding that the dye prevented prion protein accumulation in mouse brains and cells.[232] Although detailed metabolic loss studies have not been conducted with BBG, Brilliant Blue FCF (BBF – FDA approved food dye, FD&C blue No. 1), a close structural analog of BBG, has been found to be absorbed 5% by the gastro-intestinal tract following oral consumption and absorbed 10% by the plasma when given intravenously.[210]

Brilliant Blue G (BBG) has been investigated twice in animal models of Alzheimer's Disease. In both of these reports, the primary goal was to explore antagonism of the P2X7 receptor as a viable therapeutic mechanism for future AD therapies, rather than the in vivo advancement of BBG as a lead AD therapeutic molecule. Ryu et. al. administered i.p. injections of BBG to rats that had been injected in the hippocampus with Aβ42 protofibrils (a model used to simulate the inflammation state of the AD brain) and found that BBG treatment resulted in a 38% increase in viable neurons, reduced gliosis/inflammatory response, and decreased leakage of the BBB.[211] The effect of BBG on Aβ loading was not assessed in this study. In addition, although insightful from a mechanistic exploration perspective, blunt injection of toxic Aβ42 protofibrils in to the brain of healthy animals may not recapitulate the complex Alzheimer's Disease brain chemistry as well as a transgenic mouse model that develops AD-pathology over its life-span. More recently, Diaz-Hernandez et. al. performed a very important first assessment of BBG in a transgenic mouse model of familial Alzheimer's Disease.[233] Specifically, they administered 45.5 mg/kg BBG via i.p. injections to J20 hAPP mice for 4 months (starting at age 3-4 months), discovering that BBG effectively penetrated the BBB (brain tissue concentration found to be 200-220 nM) and reduced the number and size of hippocampal Aβ plaques. The mechanism reported to cause the ultimate reduction in Aβ plaques was that BBG inhibits/antagonizes the P2X7 receptor, subsequently inhibiting GSK-3 (glycogen synthase kinase 3), which then promotes non-amyloidogenic processing of the Amyloid Precursor Protein (APP) by alpha-secretase, and a decrease in the amyloidogenic/Aβ progressing of APP by beta-secretase. Unfortunately, even though the J20 hAPP mouse model they employed does exhibit neuronal loss at age 3 months,[234] the authors did not investigate if BBG administration was able to rescue the neuronal loss pathological hallmark,[233] an important characterization step in the

development of BBG as a lead AD therapeutic candidate targeted at the amyloid-cascade hypothesis.

In order to complete the in vivo characterization of BBG's effect on Aβ-related Alzheimer's pathologies and advance the compound as a potential lead drug for AD-therapy, we investigated the effect of oral administration of the compound on intraneuronal / extracellular Aβ loading and neuronal loss in the APPSwDI/NOS2-/- mouse, a well-established transgenic model of AD. The APPSwDI/NOS2-/- strain is an optimized bigenic mouse AD model created to more accurately simulate the interactions between the three essential pathological features for diagnosis of AD. Since macrophages in the mouse brain display more activity in producing nitric oxide that provides protection during an immune response than human macrophages,[235] knocking out the nitric oxide synthase 2 encoding gene (NOS2-/-) allows for a better representation of human brain chemistry in a mouse model.[225] The mouse strain was validated as displaying severe amyloid deposition, tau pathology, 30-40% hippocampal neuron loss, and significant memory deficits as measured by radial-arm water maze testing at 12-14 months of age.[225,236, 237,238-240] Since the initial validation, these transgenic mice have been employed several times in the literature to assess how various potential therapeutic options affect AD pathology/behavior[236, 237] and also to study AD brain chemistry.[238-240] Because of these considerations, these transgenic mice are well-suited for studying the efficacy of small molecules in eliminating AD pathological features, neuronal loss in particular. To our knowledge, this is the first report of the effect of Brilliant Blue G on neuronal loss in a transgenic animal model of Alzheimer's Disease as well as the first report of oral (not i.v. / i.p injected) animal administration of BBG affecting a protein conformation/aggregation disease.

Materials and Methods

Mice

Female 6-7 month old wild type C57BL/6 (Jackson Laboratories) and APPSwDI/NOS2-/- familial Alzhiemer's Disease transgenic mice (generously provided by Professor George Bloom of the Biology Department at the University of Virginia) were randomly divided up in to untreated control and drug experimental groups. The APPSwDI/NOS2 -/- transgenic strain was originally generated by crossing the widely accepted cerebral amyloidosis angiopathic model APPSwDI (Amyloid Precursor Protein with Swedish K670N/M671L, Dutch E693Q, and Iowa D694N mutations) transgenic mice with NOS2-/- (nitric oxide synthase 2 knockout) mice. All experiments involving vertebrate mice were performed according to University of Virginia's Institutional Animal Care and Use Committee (IACUC) regulations, which operate under approval by the Association for Assessment and Accreditation of Laboratory Animal Care (AALAC).

Brilliant Blue G (BBG) Preparation, Administration, and Monitoring

Mice received either i.p. injections of 100 mg/kg BBG (Sigma Aldrich) dissolved in 0.2 µm filtered 0.9% NaCl every 48 hours (3 times total per week) for 3 months or 2,000 mg/kg/day BBG for 3 months total ad libitum blended in to the standard mice chow food and provided in cages. Mice in the untreated control groups were fed standard basal mouse chow diet (no sham/saline injections).

Observations of coloring of body parts/urine/feces, unusual behavior, body condition, appearance of skin, haircoat, eyes, nose, posture, survival, and if applicable, palatability of the BBG-food mixture were recorded 1-2 times per week throughout the 3 month administration period to assess gross biocompatibility, biodistribution, and any potential gross toxicological effects. In addition, the weight of each mouse was measured once weekly and recorded. Average weights of each experimental or control group's weekly readings were then calculated.

Tissue Processing for Immunohistochemistry and Biochemical Analysis

After completing the 3 month BBG-administration regimen, mice were euthanized with Euthasol solution administered i.p., with death being confirmed by cardiac puncture / desanguination during transcardial perfusion. For immunohistochemistry, mice were perfused transcardially with Tyrode's buffer followed by 4% paraformaldehyde, 0.1% glutaraldehyde prior to extraction of the brain. Extracted brains were post-fixed overnight at 4^{o}C in 4% paraformaldehyde, 0.1% glutaraldehyde, cut in to 60 µm thick sections on a vibratome (Leica VT1000S), collected serially in a 12-well plate, and then preserved with 1% $NaBH_4$ to deactive fixative. For biochemical BBG tissue concentration analysis, mice were perfused transcardially with PBS only. Following extraction from the skull and bisection, the hemibrains for BBG concentration analysis were flash-frozen in liquid nitrogen and subsequently stored at -80 C.[208]

Quantification of Brilliant Blue G (BBG) in Brain Tissue

A gauge of blood-brain barrier (BBB)-permeability of BBG was assessed based on the concentration of the blue BBG dye detected in the snap-frozen mouse brain hemispheres using a spectroscopic/absorbance method reported in the literature.[208] After the brain tissue was thawed, the wet weight and volume of each hemisphere was measured. Next, 5 mL of 1X PBS (10 mM NaH_2PO_4 and 150 mM NaCl, pH 7.4) was added to each brain in a 15 mL centrifuge tube, the tube placed on ice, and the tissue was homogenized with an ultrasonic converter (Branson Sonifier model 102C CE equipped with a Fisher Scientific Sonic Dismembrator Model 500 Control System, 30 minutes, 10% amplitude, 15 seconds on pulse, 5 seconds off pulse). Samples of the brain homogenate (100 µL replicates) were aliquoted in to 96-well plate. Next, the absorbance spectra were scanned from 200-800 nm with a Synergy 4 UV-Vis/fluorescence multi-mode microplate reader (Biotek), reading the maximal absorbance of BBG at 576 nm, and using 800 nm as a reference point to correct for tissue sample differences. Reference subtracted absorbance values were then normalized to untreated controls. The BBG concentration in the tissue of experimental groups was quantified via correlation to calibration curves constructed by adding known amounts of BBG to homogenized brain tissue from untreated control mice that did not receive the dye compound.

Free-Floating Immunohistochemistry

Brain sections for histological analysis were first blocked for 30 minutes at room temperature with 1% BSA, 0.01M PBS solution. Representative section series were then incubated with one of the following primary antibodies and dilutions overnight at room

temperature in a scint vial: 1:200 6E10 (Covance), 1:200 M87 (generously provided by Professor George Bloom at the Biology Department at University of Virginia), and 1:200 NeuN (Millipore). Antibody solutions were always prepared fresh and were not re-used to prevent skewing of the quantified results. The next day, brain sections underwent a 2 hour room temperature incubation with the appropriate biotinylated secondary antibody (Vector Labs – 1:1000 dilution of anti-rabbit secondary antibody for M87, 1:1000 dilution of anti-mouse secondary antibody for 6E10, and 1:100 dilution of anti-mouse secondary antibody for NeuN). Each primary antibody's immunoreactivity was then visualized with the use of the Vectastain ABC Elite Kit (Vector Labs) and 3,3'-diaminobenzidine, tetrahydrochloride (DAB). DAB stain reaction times were optimized for each specific antibody and standardized across brain sections from different animals. Finally, the sections were mounted on subbed slides, air-dried, dehydrated with ethanol, de-fatted with xylene, and cover-slipped using DPX mountant.

Light Microscopy Imaging

After the DPX-mounted slides had dried overnight, light microscopy images of the immunohistochemical stain were collected using optimized conditions for each primary antibody. In addition, for each antibody, all camera and microscope settings (exposure time, light illumination voltage, filters, aperture, condenser) were standardized across different sections and animals, and anatomical landmarks were employed to ensure that similar brain sections were analyzed for each animal. For M87, black and white images of the whole hippocampus and cerebral cortex regions were captured for each brain section (3-4 sections per animal, 12-16 images per section on average) using the 5x objective lens on a Zeiss Axio Imager M2 light

microscope equipped with a Zeiss AxioCam Ice3 digital camera (total magnification between objective and digital camera = 50x). For 6E10, black and white images from the CA1 – CA2 hippocampus and cerebral cortex regions were captured for each brain section (2 sections per animal, 22 images per section on average) using the 20x objective lens on a Zeiss Axio Imager M2 light microscope with motorized z-scan equipped with a Zeiss AxioCam Ice3 digital camera (total magnification between objective and digital camera = 200x). For NeuN, color images from the CA1, CA2, and subiculum hippocampal regions were captured for each brain section (3 sections per animal, 8 images per section on average) using the 10x objective lens on a Leica DMLB light microscope equipped with a Leica MC170 HD digital camera.

Image Processing - Quantification of Neuronal Loss and Aβ Loading

Hippocampal neuronal loss was quantified through manual counts and width measurements of the DAB-positive NeuN antibody stain on the light microscopy images using Image J analysis software (NIH). Neuronal density was assessed by projecting 5000 μm^2 sub-grids on the subiculum region, manually counting the number of neurons in each grid box (Grid and Cell Counter plugins in Image J, respectively), and then taking an overall average. Thickness of the CA1-CA2 pyramidal neuron cell layer was analyzed by projecting 1000 μm^2 sub-grids on the CA region, and then manually measuring the width of the contiguous neuronal cell layer at each grid increment.

Aβ loading was quantified as the percentage of positively stained area of 6E10 and M87 antibody DAB-immunohistochemical products per total area analyzed/measured. For the 6E10 hippocampal CA1-CA2 pyramidal cell layer and M87 analyses in the cerebral cortex, dentate

gyrus and CA / lacunosum moleculare, this was performed in Image Pro Plus 7.0 by applying a threshold pixel intensity value to distinguish between positive stain and background signal. In order to maintain consistency across different brain sections and animals for each antibody, an average background pixel signal intensity for each section analyzed was calculated and then used to correct the consensus threshold value for analyzing the percent area occupied by stain in the section. When applicable to obtain a larger sample size, multiple measurements of percent staining were taken within each light microscopy image by analyzing small incremental regions of interest (ROIs) across the respective image. Loading of diffuse, extracellular Aβ plaque deposits was assessed in the cerebral cortex by manually tracing the area (in Image J) occupied by diffuse plaques stained by 6E10 antibody.

Once all staining was quantified, the average results (displayed as ± SEM) were compared between transgenic, wild-type, and untreated control animal groups using standard two-sided Student T-tests ($p < 0.05$ required for significancy) to gauge whether BBG was effective at alleviating the various AD-associated pathologies.

Results

Administration of Brilliant Blue G (BBG) is Well-Tolerated, Results in No Apparent Gross Toxicity, and Achieves Peripheral Biodistribution

Considering the need to evaluate the efficacy of Brilliant Blue G (BBG), which our research group previously found to effectively inhibit Aβ aggregation-associated cytotoxicity in

an in vitro cell culture assay,[89] in a more physiologically relevant setting, we extended our characterization investigation to the APPSwDI/NOS2-/- transgenic AD mouse model. Wild Type (WT) and APPSwDI/NOS2-/- (APP) transgenic mice aged 6-7 months were administered 2,000 mg/kg/day BBG ad libitum in food for 3 months. This oral dosage level was determined based on safe dosage levels previously reported in the literature.[230, 231] The administration period of 3 months was chosen based on previous reports of Aβ efficacy testing of drug candidates in mouse AD-models using administration periods ranging from 2 weeks to 6 months[216, 241-245] and then choosing an approximate mid-point. We initiated BBG administration at an earlier age than the 12-14 months previously used in strain validation[225] in order to assess the small molecule's potential to prevent the formation of AD pathology.

Overall, the administration of BBG was very well-tolerated. Observations of unusual behavior/activity, body condition, posture, and survival were recorded 1-2 times per week throughout the 3 month drug administration period, revealing no signs of gross toxicity or death. In addition, no palatability issues of blending the BBG in to standard mouse chow were recorded. Mice were also weighed once per week, with no overall weight loss being observed (Table 5.1). Intriguingly, the weight tracking results showed that untreated control wild type mice (WT Cont.) gained significantly more weight than the untreated control APPSwDI/NOS2-/- (APP Cont.) group ($p < 0.05$, two-sided Student's t-test), suggesting strain differences play a role in body weight change and eating habits. The oral administration of BBG was not found to significantly affect overall average weight change in either mouse strain (BBG-Food compared to Cont. groups, Table 5.1, $p > 0.1$), although it did cause a modest increase in week-to-week fluctuation of the weights of individual APPSwDI/NOS2-/- mice ($p < 0.001$ in comparing SEMs of APP Cont. and APP BBG-Food groups). Lastly, in order to assess the

biodistribution/bioavailability of BBG (a blue-colored dye) upon administration, observations of blue coloring of body parts, urine, and feces were recorded 1-2 times per week. Starting approximately 4 days after beginning the BBG administration period, mice in both the wild type and APPSwDI/NOS2-/- groups displayed a light bluish-green hue on the extremities (nose, ears, skin) as well as a darker blue color in the urine and fecal matter, suggesting that some of the compound achieved peripheral distribution.

Table 5.1 – Weekly weight monitoring during 3 month oral Brilliant Blue G (BBG) administration period. Percent weight change of APPSwDI/NOS2-/- (APP) and wild type (WT) untreated (Cont.) and orally-administered BBG (BBG-Food) mice. Data expressed as the overall change in each group's average weight in a respective week during 3 month BBG administration period compared to starting weight, +/- SEM (n = 4-5 mice per group).

	% Weight Change During 3 Month BBG Administration Period													
Group	**1**	**2**	**3**	**4**	**5**	**6**	**7**	**8**	**9**	**10**	**11**	**12**	**13**	**14**
APP BBG-Food	2.3 ± 3.4%	3.4 ± 3.0%	4.6 ± 2.9%	2.3 ± 2.9%	-1.1 ± 1.3%	1.1 ± 1.9%	4.6 ± 2.2%	3.4 ± 3.0%	3.4 ± 3.0%	4.6 ± 2.2%	4.6 ± 3.4%	4.6 ± 3.4%	8.0 ± 3.0%	4.6 ± 2.2%
APP Cont.	1.0 ± 1.5%	1.0 ± 2.2%	1.9 ± 1.0%	1.0 ± 0.0%	3.4 ± 1.4%	2.2 ± 1.2%	2.2 ± 1.2%	1.0 ± 2.0%	4.6 ± 2.3%	7.0 ± 2.3%	4.6 ± 1.2%	4.6 ± 1.2%	3.4 ± 1.4%	3.4 ± 1.4%
WT BBG-Food	5.3 ± 1.7%	0.9 ± 1.7%	1.8 ± 1.4%	3.5 ± 2.3%	1.8 ± 1.4%	3.5 ± 1.1%	5.3 ± 1.7%	7.1 ± 1.7%	8.8 ± 3.0%	7.1 ± 1.7%	6.2 ± 1.4%	9.7 ± 2.2%	13.3 ± 3.0%	11.5 ± 2.2%
WT Cont.	0.9 ± 1.1%	2.7 ± 2.0%	0.9 ± 1.1%	1.8 ± 0.9%	5.4 ± 1.1%	4.5 ± 1.8%	4.5 ± 2.3%	5.4 ± 1.1%	6.3 ± 1.7%	7.1 ± 2.4%	6.3 ± 1.7%	7.1 ± 2.4%	8.0 ± 2.2%	9.8 ± 2.3%

Brilliant Blue G (BBG) Effectively Penetrates the Alzheimer's Disease (AD) Blood-Brain Barrier (BBB)

After mice had successfully finished the 3 month oral BBG administration period, the concentration of the blue dye in homogenized brain tissue was quantified by reading the maximum absorbance located at 576 nm, as previously performed in the literature.[208] Intriguingly, reference-subtracted absorbance results (Figure 5.1) revealed that in wild type mice, the compound was not able to significantly pass through the BBB, as evidenced by no significant difference in absorbance being detected between WT Cont. and WT BBG-Food groups. However, in the transgenic APPSwDI/NOS2-/- familial AD mice fed with BBG (APP BBG-Food group), a significant increase in the absorbance at 576 nm was detected compared to the untreated APPSwDI/NOS2-/- (APP Cont.) group, corresponding to a BBG brain tissue concentration of 3.91 ± 0.13 μM.

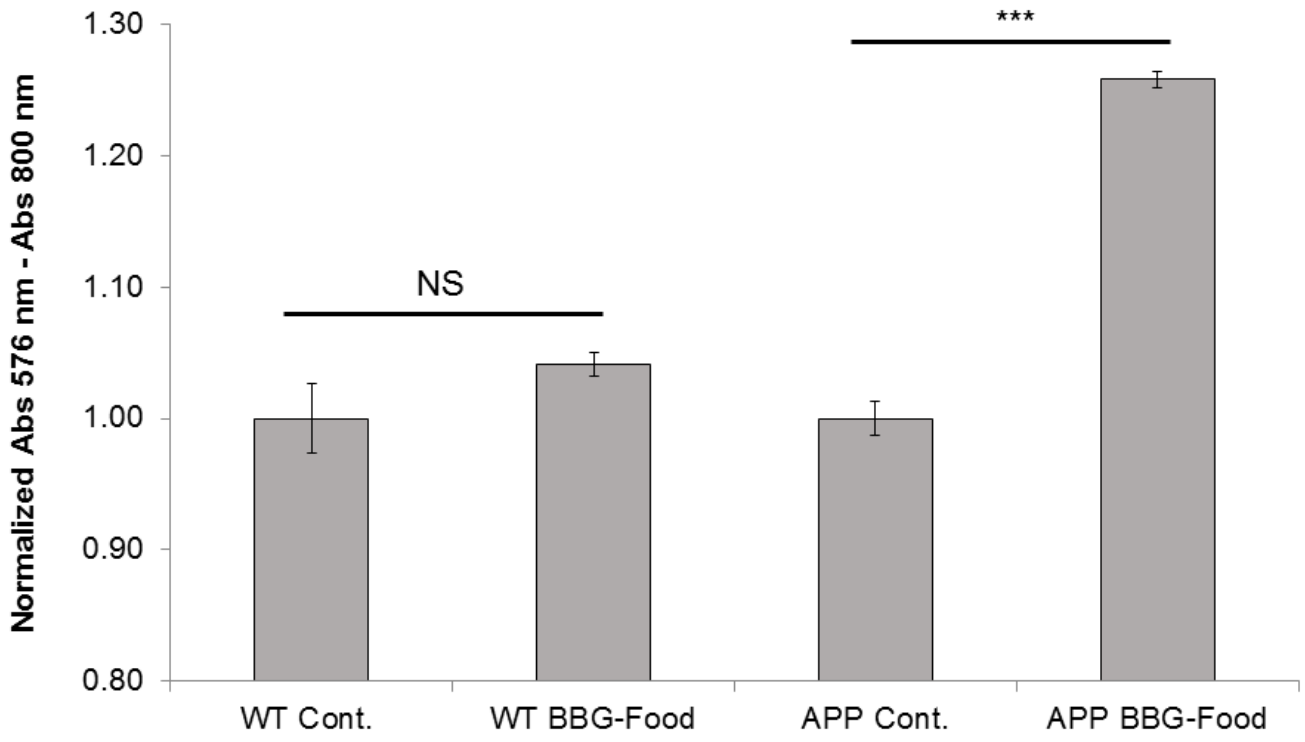

Figure 5.1 – Spectroscopic analysis of orally administered Brilliant Blue G (BBG) in mouse brain tissue. Average reference subtracted normalized absorbance values of homogenized brain tissue from wild type (WT) and APPSwDI/NOS2-/- transgenic AD (APP) mice either untreated (Cont.) or orally administered BBG for 3 months (BBG-Food). Error bars indicate ± SEM ($n \geq 20$ replicates, 1-2 mice per group). NS indicates no statistically significant difference detected ($p > 0.05$ from two-sided Student's t-test). *** indicates significant difference ($p < 0.001$).

Brilliant Blue G (BBG) Rescues Hippocampal Neuronal Loss Alzheimer's Disease Pathology

Given that it is an important AD-associated pathological feature and there have been no prior reports characterizing the effect, we next investigated whether oral administration of Brilliant Blue G (BBG) could alleviate the loss of neurons that occurs in transgenic familial Alzheimer's Disease mouse model progression. To do this, we performed DAB chromagen-based immunohistochemistry with the NeuN primary antibody, a widely characterized and accepted antibody that recognizes a neuronal-specifc nucelar protein[211, 225, 236, 237, 246, 247] In a survey of the animal model literature, there is a very strong positive correlation between therapeutics (peptides, small molecules, and antibodies) rescuing AD-related neuronal loss using NeuN immunohistochemical methods and cognitive/behavioral enhancement.[236, 237, 248-251] The comprehensive validation by Wilcock et. al. of the APPSwDI/NOS2-/- transgenic AD mouse model (using mice aged 12-14 months) revealed that the greatest neuronal loss occurred in the subiculum and CA regions of the hippocampus, displaying a 35% and 40% loss, respectively.[225] Therefore, we assessed neuronal loss / neuronal levels in these areas as well, calculating neuronal count density in the subiculum and width of the pyramidal neuron layer in the CA1-CA2 fields (Figure 5.2A, C for subiculum, Figure 5.2B, D for CA1-2). As expected given the favorable biocompatibility profile of the compound, no significant difference in neuronal levels was observed upon inspection of the results for wild type untreated versus wild type animals fed BBG (WT Cont. and WT BBG-Food groups, Figure 5.2A-D). A comparison of untreated wild type and untreated APPSwDI/NOS2-/- animal groups revealed substantial neuronal loss of 20-22% for transgenic animals in the subiculum and CA1-CA2 regions (WT Cont. and APP Cont. groups, Figure 5.2A-D). Intriguingly however, 3 months oral administration of Brilliant Blue G

was able to completely rescue the APPSwDI/NOS2-/- neuronal loss back to the levels seen with wild type animals in both regions of the hippocampus (APP Cont. and APP BBG-Food groups, Figure 5.2A-D).

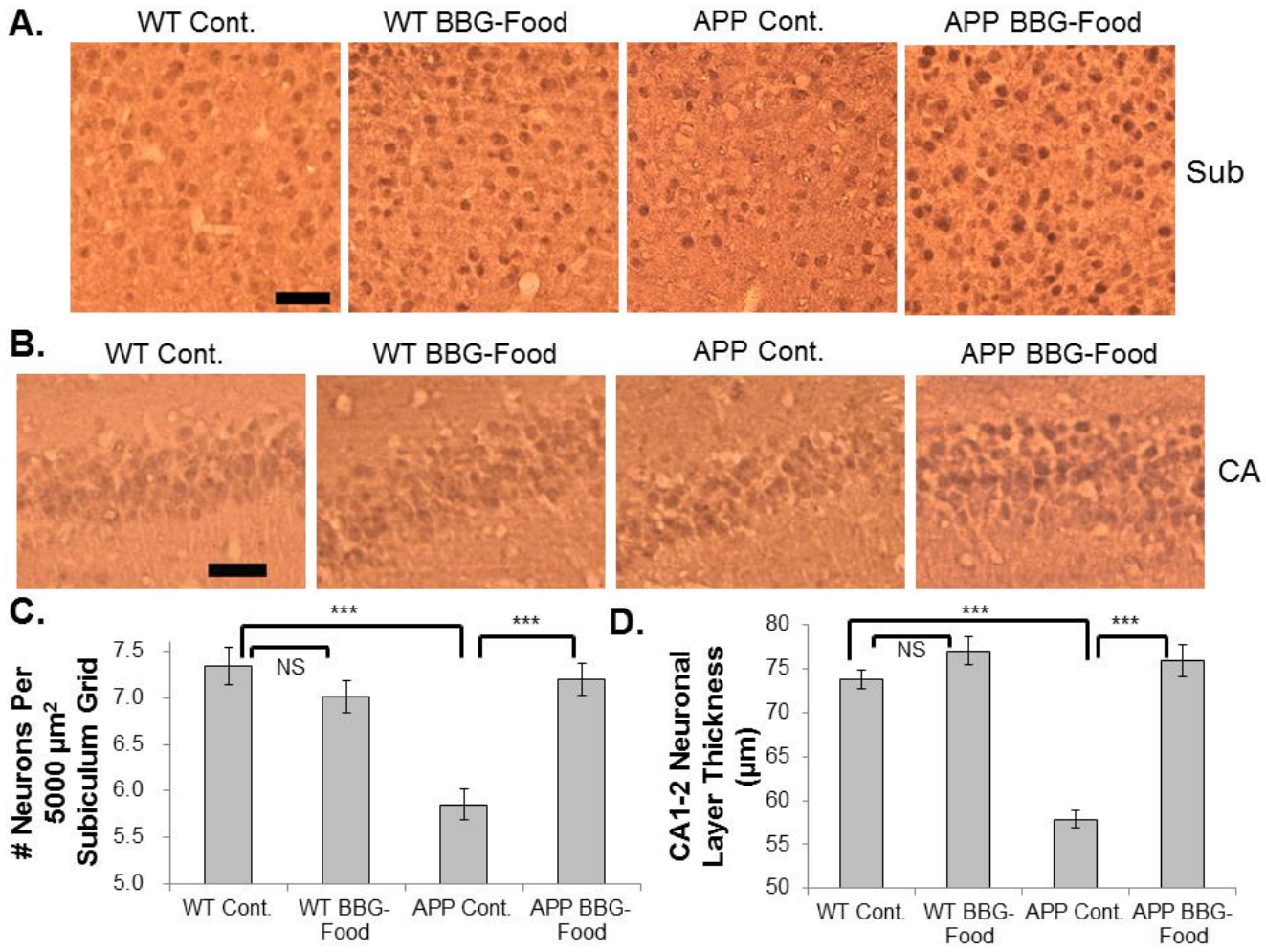

Figure 5.2 – NeuN immunohistochemical assessment of neuronal loss in hippocampus with oral Brilliant Blue G (BBG) administration. Representative light microscopy images of NeuN staining in the subiculum (A) and CA1-CA2 cell layer (B) of the hippocampus for wild type (WT) and APPSwDI/NOS2-/- (APP) mice either untreated (Cont.) or orally administered BBG for 3 months (BBG-Food). Scale bar displayed = 50 µm for the subiculum images (A) and 40 µm for the CA1-2 images (B). Neuronal loss was quantified by counting neuron density in the subiculum (C) and measuring width/thickness of the CA1-2 neuron layer (D). Data expressed as average ± SEM ($n \geq 350$ replicates, 3 animals per group). *** indicates significant difference ($p < 0.001$ from two-sided Student's t-test). NS indicates no significant difference detected ($p > 0.05$).

Brilliant Blue G (BBG) Reduces Intraneuronal Aβ Loading in the CA1-CA2 Pyramidal Neuron Cell Layer of the Hippocampus, But Does Not Affect Extracellular Aβ in the Cerebral Cortex

Given Aβ loading/accumulation's implication as a key pathological hallmark of AD[9, 11, 75, 104] and that our research group had previously investigated the Brilliant Blue G (BBG) small molecule to alleviate Aβ-associated cytotoxicity in vitro, we next explored if our 3 month oral BBG administration affected Aβ deposition in the hippocampus and cortex of APPSwDI/NOS2-/- mice.

To do this, we performed immunohistochemistry using the 6E10 primary antibody, which recognizes the N-terminal amino acid 4-9 sequence of Aβ,[216,160] to analyze Aβ loading in the CA1-CA2 pyramidal neuron cell layer of the hippocampus. It is worthwhile to note that this location is also where neuronal loss was assessed in the previous section. The results showed that the majority of 6E10 staining in CA pyramidal cell layer was localized on neuronal bodies (Figure 5.3A, APP Cont. and APP BBG-Food groups), closely resembling the intraneuronal/intracellular Aβ loading previously reported using the 6E10 antibody.[252-256] The CA pyramidal cell layer is a very densely packed layer of neurons in the hippocampus, and therefore, the area analyzed here was almost completely composed of these cells. Because of these factors, it was concluded that the Aβ loading quantified in the CA1-CA2 cell layer was mainly intraneuronal Aβ. As expected, the results showed negligible Aβ loading for both wild type mice groups, with only ~ 0.1% of the CA neuron layer occupied by positive stain (Figure 5.3B, WT Cont. and WT BBG-Food groups). The wild type loading results gave us assurance that our assay was working correctly and was not resulting in false positive staining. Further, the

wild type percent area occupied by 6E10 stain was 100 times less than the APPSwDI/NOS2-/- untreated control group, which had ~ 10% Aβ loading (Figure 5.3A-B, APP Cont. group). Importantly, when BBG was blended in with the mouse chow and fed to the APPSwDI/NOS2-/- strain, it caused a striking decrease in Aβ loading, resulting in only ~ 5% of the area analyzed being occupied by 6E10 positive stain (Figure 5.3A-B, APP BBG-Food group). Thus, there was a strong positive correlation between neurotoxicity (neuronal loss) and intraneuronal Aβ loading.

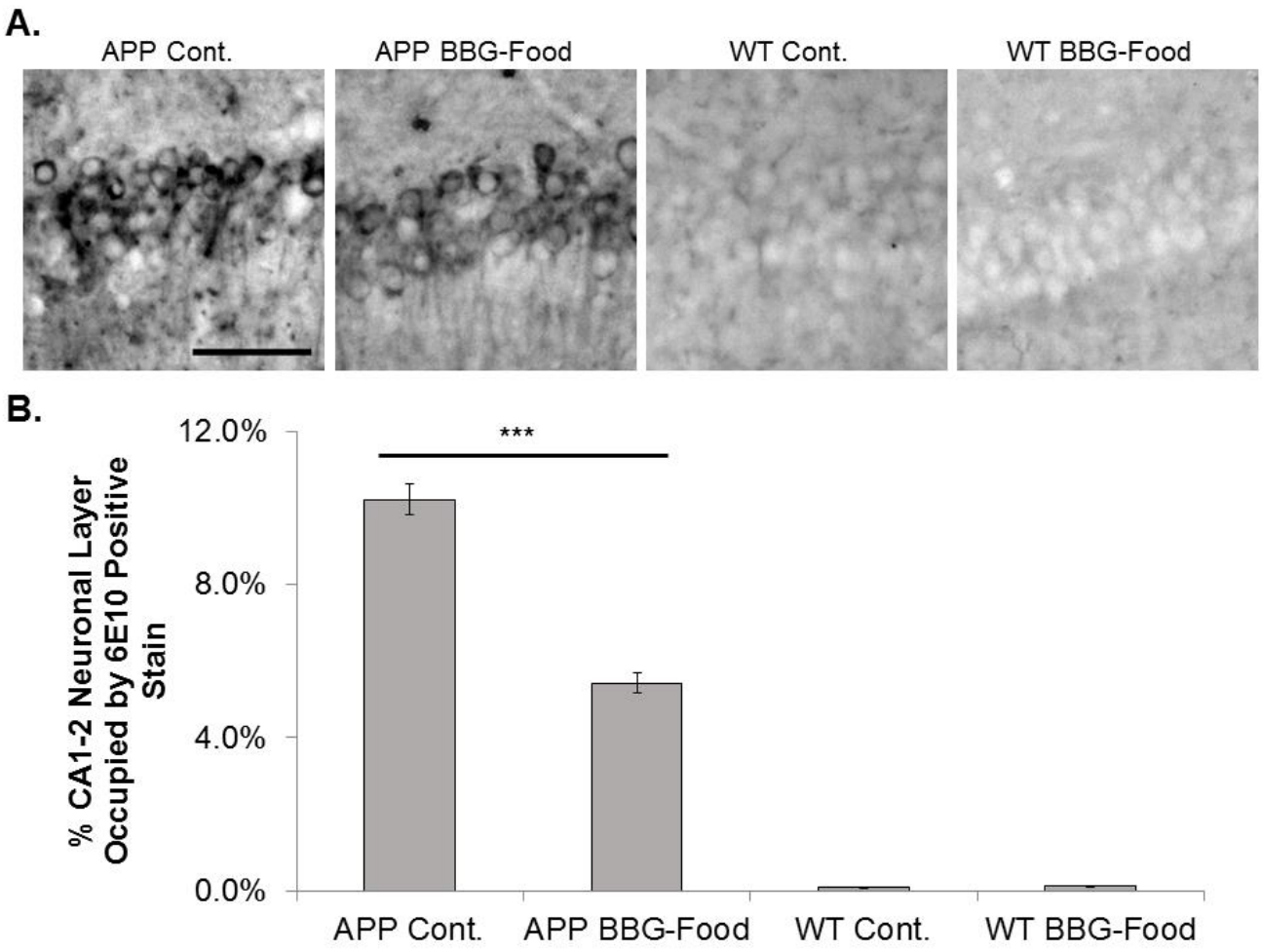

Figure 5.3 – 6E10 immunohistochemical assessment of intraneuronal / intracellular Aβ loading with oral Brilliant Blue G (BBG) administration. (A) Representative light microscopy images of 6E10 antibody staining in the CA1-CA2 neuronal cell layer of the hippocampus for wild type (WT) and APPSwDI/NOS2-/- (APP) mice either untreated (Cont.) or orally administered BBG for 3 months (BBG-Food). Scale bar displayed = 50 µm. (B) Quantification of intraneuronal Aβ loading expressed as the average percentage of area occupied by 6E10-positive stain per total area analyzed ± SEM ($n \geq 450$ replicates, 2-3 animals per transgenic group). *** indicates significant difference ($p < 0.001$ from two-sided Student's t-test).

Next, 6E10-positive Aβ loading was assessed in the cerebral cortex (Figure 5.4A). Close inspection of the APPSwDI/NOS2-/- cortex brain sections revealed that along with recognizing Aβ localized to neurons, the 6E10 antibody also stained diffuse Aβ deposits that appeared extracellular in nature (Figure 5.4A, APP Cont. and APP BBG-Food groups). Since intraneuronal Aβ was already assessed in the hippocampus, we focused the cortex 6E10 analysis on the diffuse plaques, quantifying each plaque by tracing its area using Image J. The results revealed that BBG fed to APPSwDI/NOS2-/- mice did not significantly affect the percentage of area occupied by the plaques (Figure 5.4A, Right Panel, APP Cont. and APP BBG-Food groups). In addition, oral administration of BBG did not significantly affect the average area of individual plaques traced, with both untreated and BBG-fed APPSwDI/NOS2-/- mice presenting an average plaque size of ~ 650 μm^2.

As a supplementary element for the Aβ loading characterization with the 6E10 antibody, we also employed immunohistochemistry with the M87 primary antibody in the relatively large areas of the cerebral cortex and hippocampus (Figure 5.4B-C and Figure D2 in Appendix D). Compared to 6E10, M87 is newer, investigational antibody reported to recognize lower order aggregation intermediates of Aβ.[238] Being a newer antibody, we first wanted to gauge the type (conformer) and location of Aβ stained by M87 in our specific APPSwDI/NOS2-/- transgenic mouse model. To do this, we qualitatively examined close-up, 20x zoom images taken of the M87 staining in the cortex and hippocampus of an APPSwDI/NOS2-/- control animal (Figure D1 in Appendix D). Although some Aβ aggregation intermediate staining was localized to neuronal bodies in the CA pyramidal neuron layer (Figure D1B in Appendix D), the vast majority of the staining seemed to be extracellular, in the general parenchyma and cerebrovasculature (Figure D1A-F in Appendix D). Because of this identified pattern and that the CA neuronal layer

represents only a small portion of the total area analyzed in the hippocampus and cortex, it was assumed that M87 represented mostly extracellular Aβ species. We then proceeded to quantify the percent area occupied by these M87-positive extracellular Aβ aggregates in the retrosplenial, motor, and visual cortex (Figure 5.4B, Right Panel) and the CA - lacunosum moleculare (Figure 5.4C, Right Panel) and dentate gyrus (Figure D2B in Appendix D) regions of the hippocampus. The results revealed that < 0.1 % of the area analyzed was occupied by M87-positive stain for any of the wild type mice (WT Cont. and WT BBG-Food groups), indicating that the M87 antibody was acting specifically and not generating false positive signals. Conversely, M87 staining for the APPSwDI/NOS2-/- untreated control groups (APP Cont.) was much more intense, at ~ 6% of the area occupied in the hippocampus and ~ 16% in the cerebral cortex regions. In all areas analyzed (cerebral cortex, CA - lacunosum moleculare, and the dentate gyrus), 3 months of oral administration of BBG to APPSwDI/NOS2-/- mice in food did not have any significant effect on M87 extracellular staining loading (APP Cont. and APP BBG-Food groups). Taken together, the combined 6E10 and M87 Aβ loading analysis indicates that oral BBG administration was able to significantly ameliorate intraneuronal Aβ in the CA1 and CA2 region in hippocampus, but not extracellular Aβ deposition in the cortex in our transgenic mouse model of AD.

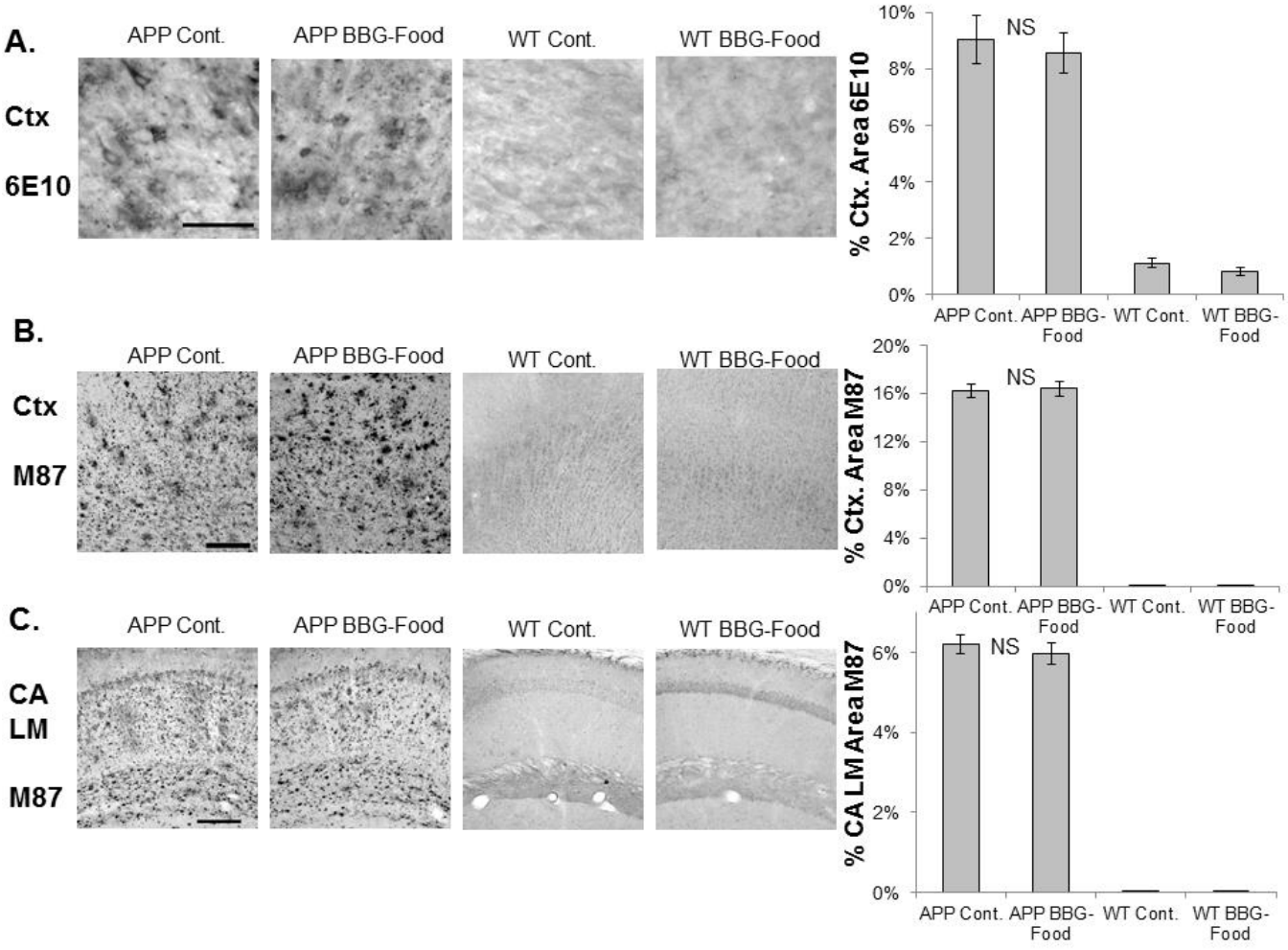

Figure 5.4 – Immunohistochemical assessment of extracellular Aβ loading with oral Brilliant Blue G (BBG) administration. Left panels display representative light microscopy images of 6E10 staining of diffuse extracellular deposits in the cerebral cortex (Ctx. - A) and M87 Aβ aggregation intermediate staining in the cerebral cortex (B) and CA / lacunosum moleculare (CA LM - C) regions of the hippocampus. Images are shown for untreated control (Cont.) and orally administered BBG (BBG-Food) groups of both wild type (WT) and transgenic APPSwDI/NOS2-/- (APP) mice. Scale bar displayed = 50 µm for the cortex 6E10 images (A) and 150 µm for the cortex and hippocampus M87 images (B and C). Right panels display quantification of extracellular Aβ loading expressed as the average percentage of area occupied by 6E10-positive manually traced diffuse plaques (A) or M87-positive stain (B and C) per total area analyzed ± SEM ($n \geq 270$ replicates for M87, $n \geq 50$ for 6E10, 2-3 animals per transgenic group). NS indicates no statistically significant difference detected compared to APPSwDI/NOS2-/- untreated control group ($p > 0.1$ from two-sided Student's t-test).

Brilliant Blue G (BBG) Injection Efficacy Evaluation

In addition to administering BBG orally (in food), we also gave i.p. injections of 100 mg/kg BBG every 48 hours for 3 months. This injection dosage levels was determined based on safe dosage levels previously reported in the literature,[230, 231] and the administration frequency of 48 hours between doses was employed because at least ~ 40 hours is required for the mice to eliminate non-absorbed BBG.[233, 257] Again, the weight of each mouse was measured and recorded once per week (Table D1 in Appendix D). Similar to the oral administration of BBG, injecting BBG three times per week caused an increase in the week-to-week fluctuation of individual mouse weights, this time for both the wild type and APPSwDI/NOS2-/- strain groups ($p < 0.01$ from two-sided Student's t-test when comparing SEMs for respective Cont. Non-Inj. and BBG-Inj. groups within each strain). Neither abnormal weight loss nor any other sign of gross toxicity were observed in the BBG-injected groups. However, i.p. administration of BBG caused the APPSwDI/NOS2-/- mice to experience less overall weight *gain* ($p < 0.05$ when comparing APP Cont. Non-Inj. and APP BBG-Inj. groups). To gauge potential BBB-permeability of Brilliant Blue G, the absorbance at 576 nm was again read for the homogenized brain tissue of BBG-injected animals. Similar to oral administration, a significant amount of BBG was detected in the APPSwDI/NOS2-/-, but not wild type brain tissue (Figure D3 in Appendix D), with the concentration of blue dye in the BBG-injected APPSwDI/NOS2-/- brain calculated to be 3.35 ± 0.06 μM. Next, neuronal loss in the subiculum (Figure 5.5A, Left Panel) and CA1-CA2 (Figure D4A in Appendix D) fields of the hippocampus was assessed using NeuN antibody immunohistochemistry. Surprisingly (and different from oral administration), quantitative comparison of the wild type untreated control and wild type BBG-injected results revealed a significant neuronal loss of 12-16% (WT Cont. Non-Inj. and WT BBG Inj. groups in

Figure 5.5A, Right Panel and Figure D4B in Appendix D), indicating that either the injection handling procedure or indeed the BBG compound itself was inducing a degree of neurotoxicity. Nevertheless, injection of BBG to APPSwDI/NOS2-/- mice was still able to significant improve (reduce) neuronal loss by 9-13% compared to the untreated transgenic control group (comparison of APP Cont. Non-Inj. and APP BBG Inj. groups). In order to see how this reduction in neuronal loss correlated Aβ loading, intraneuronal Aβ was assessed using 6E10 immunohistochemistry in the CA1-CA2 neuronal layer of the hippocampus (Figure 5.5B). Similar to food administration, BBG injection resulted in a significant ~ 50% decrease in intraneuronal Aβ loading, as measured by area occupied by positive 6E10 staining in the APPSwDI/NOS2-/- untreated control (APP Cont. Non-Inj.) versus the APPSwDI/NOS2-/- BBG-injected (APP BBG-Inj.) groups. In the 6E10 extracellular diffuse Aβ plaque analysis (Figure 5.5C, Left Panel), BBG injection was found to significantly increase the average area of each individual deposit to ~ 800 μm^2. However, the overall percent area occupied by diffuse plaques was not significantly affected (Figure 5.5C, Right Panel, APP Cont. Non-Inj. and APP BBG Inj. groups), indicating that there were fewer numbers of individual plaques. Extracellular Aβ loading was also investigated using M87 antibody immunohistochemistry as a supplement (Figure D5A-C, Left Panels in Appendix D). Although there was no significant change in the cerebral cortex between APPSwDI/NOS2-/- untreated control and APPSwDI/NOS2-/- BBG-injected groups, there was a significant increase in extracellular Aβ aggregate loading in the hippocampus upon injection of the blue dye (APP Cont. Non-Inj. and APP BBG-Inj. groups, Right Panels of Figure D5A, B, and C, for cortex, CA – lacunosum moleculare, and dentate gyrus, respectively in Appendix D).

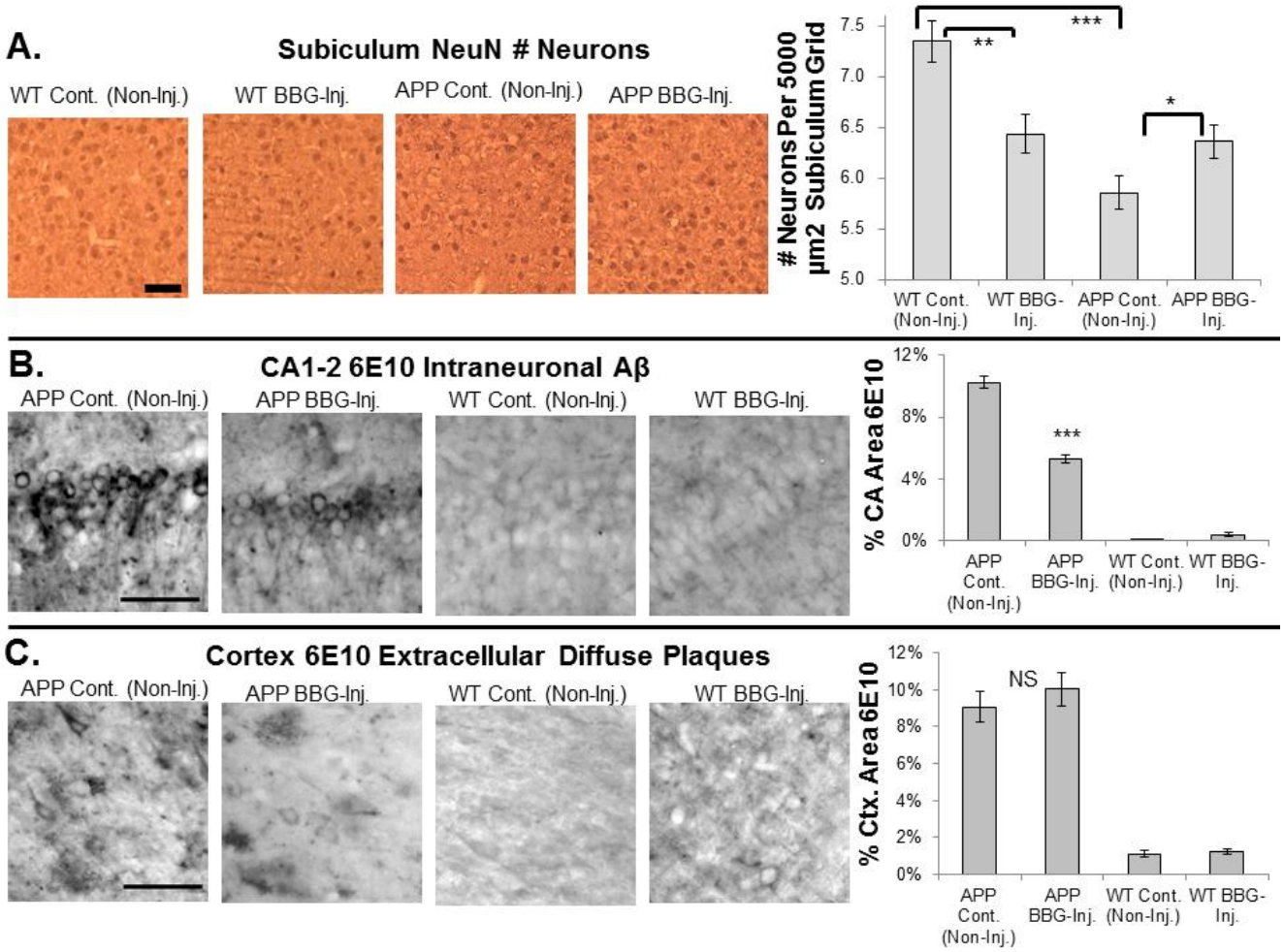

Figure 5.5 –Immunohistochemical assessment of efficacy of 3 month Brilliant Blue G (BBG) injection administration on neuronal loss and Aβ loading. Left Panels show representative light microscopy images of NeuN staining in the subiculum (A) and 6E10 staining in the CA1-CA2 cell layer (B) of the hippocampus and cerebral cortex (C) and for wild type (WT) and APPSwDI/NOS2-/- (APP) mice either untreated (Cont. Non-inj.) or administered i.p. injections of BBG for 3 months (BBG-Inj.). Scale bar displayed = 50 µm for NeuN subiculum images (A) and 50 µm for 6E10 cortex and CA1-2 images (B and C). (A, Right Panel) Neuronal loss quantified by counting neuron density in the subiculum ($n \geq 350$ replicates). (B, Right Panel) Quantification of intraneuronal Aβ loading by calculating percentage of area occupied by 6E10-positive stain per total area analyzed in the CA1-CA2 pyramidal neuron layer of the hippocampus ($n \geq 450$ replicates). (C, Right Panel) Quantification of extracellular Aβ diffuse plaques by calculating percentage of area occupied by 6E10-positive manually traced diffuse plaques per total area analyzed ($n \geq 50$ replicates). Data expressed as average ± SEM (number of replicates, n, mentioned above, 2-3 animals per transgenic group). NS indicates no statistically significant difference detected compared to APPSwDI/NOS2-/- untreated control group ($p > 0.1$ from two-sided Student's t-test). *, **, and *** indicate significant differences detected ($p < 0.05$, $p < 0.01$, and $p < 0.001$, respectively).

Discussion – Brilliant Blue G (BBG) Food Administration

In this chapter, we found that 3 month oral administration of the triphenylmethane food dye analog, Brilliant Blue G (BBG), to the APPSwDI/NOS2-/- transgenic mouse was well-tolerated, crossed the blood-brain barrier, rescued neuronal loss, and reduced intraneuronal Aβ loading.

Although the weekly weight monitoring data showed BBG did not significantly affect overall average weight change, it did reveal that the weights of individual mice in the group fed BBG fluctuated more week-to-week compared to the group fed normal mouse chow. We postulate that this difference could be due to short-term accessibility differences between the BBG-containing food and the normal mouse chow. In the untreated control group cages, hard-packed mouse food pellet-bricks are presented from an open-wire basket on the top of the cage in such a way that food is accessible to many individual mice at one time. This is different from the cages where the mice were fed BBG-blended food ad libitum in a single 3-inch diameter ceramic tray, generally accessible to only 1-2 mice at once.

The BBG brain-tissue concentration quantification revealed the intriguing finding that the triphenylmethane dye could cross the animal blood-brain barrier (BBB) in familial AD-transgenic mice, but not significantly for wild type control mice. Since BBG is water-soluble (to 50 mM) with a molecular weight over 800 Da,[258] the compound would not be expected to readily pass through the BBB from a theoretical perspective. This is given that most drugs that passively cross the BBB through endothelial transcellular diffusion are lipophilic and less than 450 Da in size.[259, 260] Furthermore, Brilliant Blue G is unlikely to be transported across the BBB via carrier-mediated influx transporters for endogenous polar molecules / analogs or receptor-mediated

transcytosis for proteins, given the nature of the compound.[259, 260] Because of this, the most likely BBB-permeation mechanism for Brilliant Blue G is the paracellular pathway between endothelial cells through extremely robust tight junctions sealed with protein complexes.[261] Therefore, the passage of BBG through the healthy, intact blood-brain barrier of a mouse is unlikely, as evidenced by our wild type control mice results. However, it is now well-established that the BBB experiences disruption and dysfunction in Alzheimer's and other neurodegenerative diseases, resulting from damage occurring to pericytes, microglia, astrocytes, and neurons that collectively make up the neurovascular unit.[262-264] For example, Brilliant Blue G was peripherally (i.v.) administered to rodent models of traumatic brain injury[231] and spinal cord injury,[208] with the dye being found to significantly accumulate at the contusion site (at up to ~44 μM concentrations). These findings implicated that the compound was able to cross in to the central nervous system (CNS) tissue through the disrupted BBB. In Alzheimer's Disease specifically, evidence for leakage of the blood-brain barrier is increased CNS infiltration (from the periphery) of inflammatory cells/immunoglobulins[259, 263, 264] and blood proteins, such as albumin,[211, 262, 263] hemoglobin,[263] prothrombin,[263] and fibrinogen.[264] Although these reports of BBB leakage resulting from Alzheimer's Disease present a potentially promising opportunity for small molecules therapeutics to enter the CNS, it is not a guarantee, given the different mechanisms required to transport larger proteins vs. smaller water-soluble molecules, the nature of the individual small molecule, and the extent to which the brain (human or transgenic model) has been damaged.[259, 262]

Perhaps the most important and novel finding from this study was the efficacy of BBG at ameliorating AD-related neuronal loss in the hippocampus. Because many of the AD-mouse models do not develop significant neuronal loss,[225] this pathological endpoint is often excluded

from efficacy studies of new therapeutics. The hippocampus is a critical region of the brain for learning, consolidating information from short to long term memory, and spatial navigation.[265, 266] Input signals are received from the entorhinal cortex, pass sequentially through the dentate gyrus, CA3, CA2, and CA1 subfields, and then information is output from the hippocampus through the subiculum.[266] The dentate gyrus is also one of the few regions of the brain which continue undergoing neurogenesis during adulthood.[266] Unfortunately, the hippocampus is one of the most vulnerable areas of the brain to physiological changes, and in AD, is one of the earliest areas to be affected.[265] Because of the importance of the hippocampus and the positive correlation between therapeutics rescuing AD-related neuronal loss cognitive/behavioral enhancement,[236, 237, 248-251] our findings about BBG being able to improve this pathological feature in the subiculum and CA1-CA2 regions makes it very promising to proceed as a AD-therapeutic.

Since we had previously demonstrated in vitro that Brilliant Blue G modulated AD-associated cytotoxicity through the mechanism of modulating Aβ aggregation, we were also interested in testing what effect BBG had on Aβ loading/accumulation. In reviewing the literature, ELISA investigations of 6-10 month old transgenic AD mice reported an approximate total Aβ brain tissue concentration in the range of 0.02 – 2.7 μM (depending on the mouse strain employed), with only one reported concentration being above 0.25 μM.[267-270] In our results, we found that the total brain tissue concentration of BBG was 3.91 μM. It is important to note that this concentration represents both bound and unbound BBG, and that the concentration of free/unbound dye would likely be less due to the high binding affinity of BBG for proteins, but additional investigation would be required to determine the exact mechanics.[208, 259] Nevertheless, using these numbers yields an approximate in vivo molar ratio of BBG:Aβ of 15:1, which falls

well within our previously reported in vitro aggregation-modulating IC_{50} and cytotoxicity-alleviating BBG:Aβ molar concentration ratios of 0.72:1 and 3:1, respectively.[89] Therefore, it was reasonable to assume that the BBG concentrations achieved in the brain tissue would be sufficient to affect Aβ loading.

The Aβ immunohistochemistry results showed that oral BBG administration was able to significantly reduce intraneuronal/intracellular, but not extracellular Aβ loading. Traditionally, extracellular aggregated species of secreted Aβ were believed to initiate the cascade of events in the toxicity of Alzheimer's Disease.[271] However, there is now increasing evidence that the neurodegenerative cascade may actually be triggered first by Aβ accumulating inside neurons (intraneuronal Aβ).[272] Indeed, recent studies have demonstrated that neuronal loss, cognitive decline, and synapse degradation can occur prior (i.e. at an earlier age) to the appearance of extracellular plaques in the Alzheimer's Disease brain, and that intraneuronal Aβ loading coincides better with these pathological events.[255, 256, 271, 273-286] In fact, it was reported that the formation of Aβ oligomers and fibrils actually begins by Aβ monomer being sorted to multivesicular bodies inside of cells, where aggregation then proceeds. The aggregates are then only released to the extracellular space once the cells undergo cell death.[253, 287, 288] Furthermore, intraneuronal Aβ has been found to be many times more toxic than extracellular Aβ.[289] Due to these factors and that very few small molecules have been reported targeting intracellular Aβ,[289-298] our current result that BBG can reduce intraneuronal Aβ loading is of interest from a therapeutic and novelty perspective. Given this, two questions present themselves for our specific results – 1) what type of conformer species does the intraneuronal Aβ represent, and 2) was BBG able to reduce intraneuronal Aβ loading through inhibition of Aβ aggregation or inhibition of Aβ monomer generation from the APP parent protein? Unfortunately, further

investigation is needed to definitively answer these questions, since with the current data, the 6E10 antibody is cross reactive to all APP proteins/fragments that contain the N-terminal amino acid sequence of Aβ (both cleaved and uncleaved products) and the quantitative M87 antibody analysis was not designed to target areas containing only neurons. In the literature, some discord exists between research groups regarding the exact APP-cleavage product and aggregation-state of intraneuronal amyloid staining seen in transgenic mice models and human AD patients when using sequence-specific antibody (such as 6E10) immunohistochemistry.[272, 274, 282, 299] However, there is a substantial body of literature indicating that intraneuronal amyloid staining by these sequence-specific antibodies does indeed represent Aβ (the majority being aggregation prone Aβ42 and not the APP parent protein or other cleavage product)[256, 273, 300] and often, aggregated Aβ species identified using oligomer-specific antibodies or Thioflavin S.[271, 275-278, 281, 301, 302] In the context of our results, we postulate that at least part of the intraneuronal Aβ staining in the CA1-CA2 regions of the hippocampus is an aggregated form. This is because in our results, the M87 antibody did stain several neuronal bodies in the CA1-CA2 region, substantial neuronal loss was observed in that area in untreated transgenic animals, and non-aggregated forms of Aβ are considered to have negligible toxicity.[90, 277] Regarding mechanisms, Diaz-Hernandez et. al. reported that BBG reduced Aβ plaques by promoting non-amyloidogenic processing of APP by alpha-secretase through the P2X7 receptor.[233] The dissociation constant between Aβ monomer and BBG was reported to be 92 μM.[89] Conversely, the dissociation constant for BBG and P2X7 human receptor was much lower at 185 nM,[303] with the IC_{50} value for P2X7 antagonism was reported to be 10 – 200 nM.[233] Because of these factors and our previously reported in vitro aggregation modulating data,[89] the exact mechanism by which BBG reduces intraneuronal Aβ loading in conjunction with the brain's existing Aβ clearance pathways (Supporting Information

D1 in Appendix D) will require additional investigation. Indeed, epigallocatechin-3-gallate (EGCG), a well-known Aβ aggregation modulating compound,[15, 17, 152] has also been reported to reduce cerebral amyloidosis by promoting non-amyloidogenic APP processing by alpha-secretase.[304]

Regarding the discrepancy of BBG being able to reduce intraneuronal but not extracellular Aβ loading, we hypothesis two possible causes under the assumption that BBG does indeed modulate Aβ aggregation in vivo. First, it is possible that BBG is more efficacious at inhibiting the formation of new aggregates, leaving existing aggregates unaffected. Accumulating evidence shows that Aβ monomer aggregates inside of cells,[287] implying that BBG may be internalized (either along with Aβ or separately), and then modulate aggregation inside the cell. Second, it is also possible that the transgenic mice used in our study were analyzed at a young enough age prior to having accumulated significant enough extracellular Aβ pathology to detect differences upon application of the BBG compound. For example, the initial validation of the APPSwDI/NOS2-/- strain using 12-14 month mice revealed extensive extracellular Aβ deposits, but a lack of intraneuronal Aβ staining.[225] Since the mice used in our study were 9-10 months at the time of analysis and it has been reported that intraneuronal Aβ appears first in the aging process followed by decline and an inversely proportional increase in extracellular Aβ,[254] it is quite possible that extracellular Aβ pathology was not developed enough in our studies.

Discussion -- Brilliant Blue G (BBG) Injection Administration

The 3 month BBG i.p. injection administration regimen produced some truly unexpected results from both the biochemical and immunohistochemical assays in this study. The most unexpected finding was the significant amount of neuronal loss that occurred between the untreated, non-injected control and the BBG-injected wild type mice. Since wild mice do not normally develop neuronal loss AD-associated pathology, BBG has a very favorable safety profile with no neuronal loss being observed between wild type rats injected with saline vs. BBG only,[211] and no gross toxicity was observed throughout our 3 month administration period, we were expecting neuronal levels to be fairly equivalent between these wild type groups (as was the case with BBG administered orally). In an effort to explain this finding, a literature search was performed on potential effects of handling (i.p. injection, in particular) on rodent brain physiochemistry. The search revealed that light, predictable handling of rodents (such as restraining a rat in a plastic square right side up or socializing with human contact) or providing an enriched environment is beneficial for neurogenesis and cognitive performance.[305-309] Conversely, it was found that chronic unpredictable stress, such as picking rodents up by their tails and IP injection of saline, causes increases in corticotropin, corticosterone, and glucocorticoid stress chemicals, anxious behavior, nullification of the action of anti-anxiety drugs, and decreased neuronal levels.[309-316] These reports highlight the importance of having rigorous control groups in an in vivo drug testing investigation. In relation to our current study, it signifies that having one untreated control group for both oral (food) and injection (i.p.) administration routes was insufficient to draw robust efficacy conclusions for both administration types. Since the untreated control group was fed normal mouse diet and not injected, it is an appropriate control for the oral administration of BBG experimental groups, but

not for the injected ones. Instead, the studies should have been designed to include 0.9% saline/sham-injected controls. Unfortunately, due to limited resources and number of mice, this was not employed in the current work. Therefore, it is not possible to conclusively determine whether the neuronal loss that occurred between the untreated, non-injected control and the BBG-injected wild type mice was due to neurotoxicity of the BBG compound or an artifact of injection handling. However, we postulate that it was likely an animal handling artifact, given that BBG-injection was still able to significant reduce neuronal loss in the APPSwDI/NOS2-/- transgenic mice. A similar question can also be raised regarding the unexpected increase in extracellular Aβ loading in the hippocampus as identified by the M87 antibody staining, a result that again was not observed in our studies of orally-administered BBG. Again, since we did not employ sham-injected controls, it is not possible to conclude if this effect was due to the BBG compound or a by-product of injection handling itself. As mentioned previously, injection handling has been shown to release stress chemicals/hormones, which in recent years have been linked to increasing Aβ-associated pathology.[252, 314, 317, 318] Lastly, it is worthwhile to note that the M87 is a relatively new conformationally-specific Aβ antibody reported once in the literature.[238] The initial use/validation study of the antibody revealed that it recognized lower order aggregation intermediates / low 'n' oligomers of Aβ42 (but not monomers or fibrils) and whose epitope is amino acids 3-7 of Aβ peptide spotted sub-fragment monomers.[238] Generally, aggregation intermediates, such as the ones identified by the A11 and OC conformationally-specific antibodies, are thought to be cytotoxic.[89, 90] However, cell viability assays revealed that the low 'n' oligomers recognized by the M87 were not cytotoxic.[238] Therefore, additional investigation may be needed to elucidate the exact meaning/toxicity of the species identified by the M87 antibody in the pathology of Alzheimer's Disease.

Also intriguing is the comparison of the Brilliant Blue G brain tissue concentrations resulting from the compound administered in food (3.91 ± 0.13 μM) or injected (3.35 ± 0.06 μM) in this investigation and the value previously reported by Diaz-Hernandez et. al (200 – 220 nM).[233] As mentioned previously, detailed metabolic fate analyses have been conducted for Brilliant Blue FCF (BBF), a close structural analog of Brilliant Blue G (BBG). When BBF was injected to animal models, it was found to enter the blood stream and quickly be cleared through the liver in to the bile fluid. The blood plasma half-life elimination time was found to be 2.8 minutes, with 20% remaining after 25 minutes, and only 10% remaining in the blood after 4 hours.[210, 319, 320] Once in the bile, the compound can enter the gastrointestinal tract via the gallbladder, where it is either reabsorbed in to the blood or excreted in feces. When BBF is administered orally, the compound proceeds to the gastrointestinal tract, where it was reported that over a 36 hour period, 95% is excreted in feces and ~5% is absorbed to the bloodstream, through the liver, and in to bile fluid.[210] Virtually no BBF was excreted through the bloodstream, to the kidneys, and out through the urine.[210] Importantly, in mice, only ~50% of the total BBF administered was found to be excreted in feces in the 0-24 hour period following oral dosing.[321] Because of these metabolic considerations, the slightly increased brain tissue concentration in our studies of orally vs. i.p. administered BBG could be due to the compound being presented at more consistent levels to the blood brain barrier with the mice consuming BBG-containing food consistently each day, instead of receiving a large spike from BBG injection, which is then cleared within a few hours. Alternatively, there have also been reports that stress-related hormones/chemicals, which can be produced by i.p. injections as discussed previously, can decrease blood-brain barrier permeability of small molecules therapeutics.[322, 323] Regarding the difference in BBG brain tissue concentration between the values reported here and those

obtained previously by Diaz-Hernandez et. al.,[233] it is most likely due to the different dosages and transgenic mice utilized in the two studies. For example, the investigation by Diaz-Hernandez et. al. employed an i.p. BBG dosage of 45.5 mg/kg in the J20 hAPP mouse model of Alzheimer's Disease. This was less than one-half of the i.p. employed in our investigation with APPSwDI/NOS2-/- mice. In addition, it is also plausible that the APPSwDI/NOS2-/- mouse model displays more blood-brain barrier disruption than the J20 hAPP strain.[324] A literature search did not reveal any investigations in to potential blood-brain barrier disruptions of the J20 hAPP mouse. However, the nitric oxide synthase 2 knockout in the APPSwDI/NOS2-/- mouse decreases protection against the immune response, allowing for increased inflammation.[235] And, inflammation has been linked to leakage of the blood-brain barrier in the Alzheimer's Disease brain.[264] In addition, the APPSwDI/NOS2-/- mouse exhibits decreased aquaporin 4 and glial fibrillary acid protein astrocytic end feet, both features which are required for the integrity of the blood-brain barrier.[240, 325, 326]

Conclusion

In this chapter, we administered the triphenylmethane food dye analog, BBG, to APPSwDI/NOS2-/- familial AD mice for 3 months in order to evaluate its efficacy at improving Aβ and neuronal loss AD-pathologies. The results showed that BBG administered both orally and through i.p. injection was well-tolerated, showed no gross toxicity, and was able to cross the AD blood-brain barrier. In addition, immunohistochemical analysis of the brain sections revealed that BBG was able to significantly rescue neuronal loss and reduce intraneuronal Aβ loading. To

our knowledge, this is the first report of the effect of BBG on neuronal loss in a transgenic animal model of AD as well as the first report of oral animal administration of BBG affecting a protein conformation/aggregation disease. Given that these successful results were obtained regarding the compound's ability to improve key biochemical AD pathologies, BBG is a strong candidate to proceed with behavioral studies with AD transgenic mice to determine if it can also improve AD-associated cognitive decline/function. Lastly, the positive results obtained in this chapter enhance our understanding of the general potential of food dye analog-based small molecules Aβ modulators to be effective therapeutics in a more physiologically relevant in vivo system and what specific AD-related pathologies they can alleviate. For example, since the red food dye, Erythrosin B (ERB), was found to be an effective modulator of Aβ-aggregation and Aβ neurotoxicity in vitro[27] and has a favorable biocompatibility profile (Supporting Information D2 in Appendix D), it presents itself as a promising therapy to explore further in an AD animal model.

Chapter 6: Project Objectives, Summary, and Avenues for Future Work

Project Objectives and Summary

In order to continue the developmental progress of Brilliant Blue G (BBG), Erythrosin B (ERB), and their structural analogs as potential small molecule Alzheimer's Disease therapeutics, four (three in vitro and one in vivo) additional characterization investigations were undertaken in this dissertation research.

All research objectives were completed:

1. In vitro structure-activity relationship analysis of ERB and structural analogs to determine important molecular structural features required for molecular binding and subsequent modulatory capacity of Aβ aggregation and neurotoxicity (from monomer starting material).

We evaluated the binding and modulating capacities of ERB and three analogs containing different types and numbers of halogen atoms as well as Fluorescein as a non-halogenated negative control. We found that Fluorescein is not an effective modulator/binder of Aβ aggregation and cytotoxicity. However, halogenation of either the xanthenes or benzoate ring of Fluorescein substantially enhanced the binding and inhibitory capacity on Aβ aggregation. Such Aβ aggregation inhibition by ERB analogs except Rose Bengal correlated well to the inhibition of Aβ cytotoxicity. To our knowledge, this is the first report demonstrating that halogenation of aromatic rings substantially enhance inhibitory capacities of small molecules on Aβ-associated neurotoxicity via Aβ aggregation modulation.

2. In vitro investigation of ERB and structural analogs ligand binding sites on Aβ target peptide monomers.

In order to address and improve upon the limitations of current methods, we developed a technique for identifying binding sites on a ligand-exposed target protein using dot-blot immunostaining with a panel of sequence-specific antibodies. The method was then employed to characterize the Aβ binding sites of Erythrosin B and three other halogenated xanthene benzoate structural analog binders, Phloxine B, Rose Bengal, and Eosin Y. This analysis revealed a common locus, amino acids 10-16, as an important strong binding region.

3. In vitro comparative studies on the structural fates of mature, thermodynamically very stable Aβ40 amyloid fibrils destabilized by BBG and ERB.

We performed studies on the structural features of the different Aβ aggregates remodeled from Aβ fibrils by BBG, ERB, and a third exogeneous small molecule modulator, Methylene Blue (MB), for mechanistic comparative purposes. Combined with circular dichroism (CD), immuno-blotting, transmission electron microscopy (TEM), and atomic force microscopy (AFM) results, it was found that Brilliant Blue G- and Erythrosin B-treatment generate fragmented Aβ fibrils and protofibrils, respectively. In contrast, incubation of the Aβ fibrils with Methylene Blue perturbs fibrillar structure leading to amorphous Aβ aggregates.

4. In vivo efficacy evaluation of BBG in a transgenic mouse model of Alzheimer's Disease.

We administered BBG to APPSwDI/NOS2-/- AD mice for 3 months in order to evaluate its efficacy at improving Aβ and neuronal loss AD-pathologies. The results showed that BBG administered both orally and through i.p. injection was well-tolerated, showed no gross toxicity, and was able to cross the AD blood-brain barrier. In addition, immunohistochemical analysis of the brain sections revealed that BBG was able to significantly rescue neuronal loss and reduce intraneuronal Aβ loading. To our knowledge, this is the first report of the effect of BBG on neuronal loss in a transgenic animal model of AD as well as the first report of oral animal administration of BBG affecting a protein conformation/aggregation disease.

Future Work and Suggestions

In this dissertation work, we were very fortunate to gain hands-on experience with both the in vitro and in vivo development of Brilliant Blue G, Erythrosin B, and their structural analogs as potential small molecule Alzheimer's Disease therapeutics. This was possible due to the talented array of collaborators and robust equipment/facilities accessible at the University of Virginia. As we have seen, there are both advantages and disadvantages of using in vitro and in vivo models in drug development. In vitro investigation allows more specific mechanistic testing of neurodegenerative therapies since the test tube or cell culture environment can be more rigorously controlled compared to the complex composition of the animal nervous system. Conversely, in vivo testing is required and beneficial since it allows for testing conditions more physiologically-relevant to the human body. As such, it is logical to break down suggestions for future work in to these two categories (in vitro and in vivo investigations) as well.

Suggestions for Future In Vitro Investigations

The structure-activity relationship analysis of Erythrosin B (Chapter 2) revealed that halogenation of either the xanthene or benzoate backbone substantially enhanced the binding and inhibitory capacity on Aβ aggregation. Following up on this finding, there are several intriguing investigations that could be performed. First, it would be interesting to further explore the molecular mechanism(s) by which halogenation modulates Aβ aggregation and toxicity, specifically looking at the orientation of the functional groups of the halogenated xanthene benzoate molecules during the process. The investigation in Chapter 2 of this dissertation revealed the halogenation aggregation modulating capacity/mechanism as being quite complex, finding that it was inversely proportional to the electronegativity of functional group attached to xanthene group and regulated by polarity change or steric hindrance (size) caused by halogenation of the benzoate group. Computational modeling would likely be best-suited to investigate deeper in to the molecular interactions. Of course, obtaining this kind of molecular mechanistic level understanding is quite challenging with Aβ, given that it does not have the crystal structure required traditionally for computational models. However, in recent years, there have been models developed to serve as a starting point for Aβ molecular simulations, most of which utilize key solvation or force-field assumptions to overcome the lack of a crystal structure.[327] Second, it would be illuminating to further explore the generalizability of the concept that halogenation of other small molecules (not just xanthene benzoate analogs) can result in effective modulation of Aβ aggregation and toxicity. This could be accomplished by testing the Aβ modulating capacity of existing biocompatible halogenated small molecules, such as the ones that have been investigated as plaque detection probes.[328-333] Or, newly synthesized

halogenated derivatives of previously ineffective molecules (such as melatonin, fenofibrate, and dimethyl yellow[61]) could be investigated as to their efficacy at modulating Aβ aggregation with the added halogen functionality.

The key finding from Chapter 3's investigation of ERB analog ligand binding sites on Aβ revealed amino acids 10-16 as an important binding region for the four aggregation modulating small molecules tested. Given this, it would be both logical and illuminating to investigate (using our method of dot blot immunostaining with the sequence-specific antibody panel) if the 10-16 amino acid sequence is also a strong binding site of other small molecules that were previously reported to effectively modulate Aβ aggregation.

The investigation in Chapter 4 established that thermodynamically stable preformed Aβ fibrils can be destabilized or remodeled by three small molecules (BBG, MB, and ERB). In addition to the experiments performed, there are several logical continuations of studying the effect of these three small molecules on preformed Aβ40 fibrils in vitro that could provide fascinating insights. First, an investigation of the binding/dissociation constant of the small molecules to Aβ fibrils would yield interesting information on both the binding affinity and number of binding sites for each molecule. This information could then be compared to the existing data our research group obtained for Aβ monomers. Second, monomer seeding experiments could be performed to determine if the remodeled Aβ fibrils can be considered "on" or "off-pathway" ("on-pathway" if the restructured aggregates can seed/accelerate fibril formation from the monomer state). Third, it would be interesting to test whether or not the restructured aggregates are non-covalently associated by exposing them to high temperatures and observe if dissociation occurs. Fourth, in this dissertation work, high concentrations of small

molecules (10X molar excess over Aβ) and a one-day restructuring period were used in order to observe overall/ending structure change. However, it would provide interesting insight to perform a similar set of analyses using lower concentrations of small molecules and/or shorter restructuring time to characterize the progression of the change. Lastly, it would be interesting to remove the small molecules from the restructured aggregates by desalting and determine if the structural changes are reversible or not.

Suggestions for Future In Vivo Investigations

The in vivo efficacy evaluation of Brilliant Blue G in Chapter 5 revealed that both oral or injection administration of the compound allowed it to cross the blood-brain barrier and rescue neuronal loss and intraneuronal Aβ pathologies in a transgenic mouse model of AD. Regarding future work, the highest priority from the perspective of advancing BBG as an AD therapy is to test whether administration of the compound can ameliorate cognitive/behavioral impairments in an AD mouse model. Unfortunately, we were not able to perform behavioral studies in this dissertation work due to resource limitations. However, there is great need to obtain that information through the use of Y- or Morris Water Mazes, since it has not been performed previously in the literature. Once this preclinical work is completed, commercialization of the drug could potentially proceed through the FDA's IND stage and in to Phase I clinical trials.

In addition, there are several worthwhile extensions of the dissertation's current in vivo work relating to AD-pathologies. Since it prevented clear interpretation of some of the injection results, the most obvious improvement/extension for future studies would be to include sham/saline-injected control groups if it is desired to study injection administration of BBG.

Further, ELISA-based biochemical analysis could be performed on the brain tissue to determine the effect that BBG administration had on total, soluble, and insoluble Aβ0 and Aβ42 species, since this discrimination can be important from a therapeutic mechanism perspective. Second, as a supplement to the light level microscopy analysis that was performed to assess neuronal loss, a much closer examination (inside the cell) of neuronal state/health could be obtained by applying electron microscopy to the pyramidal neurons in the hippocampus. In addition to the Aβ loading and neuronal loss that we explored, other important factors often investigated in the characterization of new AD therapies in animal models include neurofibrillary tau tangles and inflammation/gliosis. Ryu et. al. demonstrated that BBG could reduce inflammatory factors associated with Aβ peptide being injected in to the brain.[211] However, the effect of the drug on tau levels has not yet been investigated. As such, immunohistochemistry for hyperphosphorylated tau protein with the AT8 antibody would be valuable to perform. Lastly, an important unanswered question from the in vivo studies in this dissertation relates to the mechanism by which BBG administration rescues neuronal loss and reduced intraneuronal Aβ loading in the hippocampus. Specifically, does BBG bind Aβ and then modulate its aggregation (as our research group reported previously from in vitro studies[89])? Or, does BBG signal through the inhibition of the P2X7 receptor (which then inhibits GSK-3) to affect processing of the APP parent protein (as Diaz-Hernandez et. al. previously reported)?[233] Since creating new transgenic AD mice strains (with P2X7 knocked out or GSK-3 hyperactivated, for example) is not trivial, a potential method to elucidate the implication of the P2X7 receptor mechanism would be co-administer BBG to mice along with activators of P2X7 or GSK-3. The species/aggregation state of intraneuronal Aβ could be identified through the addition of Thioflavin staining of brain sections (which recognizes only aggregated fibrillar species) and immunohistochemistry with

antibodies that are not cross reactive like 6E10 (Aβ40/Aβ42 specific antibodies, or antibodies specific to the secretase-processed fragments of APP parent protein). To leverage the antibodies we already applied in this dissertation, a closer analysis with the M87 antibody (which recognizes aggregation intermediates) could also be performed on areas containing only neurons, such as CA1-CA2 neuron layer of the hippocampus.

References

1. Brookmeyer, R., Gray, S., and Kawas, C. (1998) Projections of Alzheimer's disease in the United States and the public health impact of delaying disease onset, *American Journal of Public Health 88*, 1337-1342.
2. Citron, M. (2010) Alzheimer's disease: strategies for disease modification, *Nature Reviews Drug Discovery 9*, 387-398.
3. Alzheimer, A. (1907) Über eine eigenartige Erkrankung der Hirnrinde, *Centralblatt fur Nervenheilkunde Psychiatrie 30*, 177-179.
4. Thal, D. R., Holzer, M., Rüb, U., Waldmann, G., Günzel, S., Zedlick, D., and Schober, R. (2000) Alzheimer-related tau-pathology in the perforant path target zone and in the hippocampal stratum oriens and radiatum correlates with onset and degree of dementia, *Experimental neurology 163*, 98-110.
5. Selkoe, D. J. (2001) Alzheimer's Disease: Genes, Proteins, and Therapy, *Physiological Reviews 81*, 741-767.
6. Bitan, G., Kirkitadze, M. D., Lomakin, A., Vollers, S. S., Benedek, G. B., and Teplow, D. B. (2003) Amyloid Beta-protein assembly: Aβ40 and Aβ42 oligomerize through distinct pathways, *Proc. Natl. Acad. Sci. U. S. A. 100*, 330-335.
7. Ono, K., Hasegawa, K., Naiki, H., and Yamada, M. (2004) Anti-amyloidogenic activity of tannic acid and its activity to destabilize Alzheimer's beta-amyloid fibrils in vitro, *Biochimica et biophysica acta 1690*, 193-202.
8. Glabe, C. C. (2005) Amyloid Accumulation and Pathogensis of Alzheimer's Disease: Significance of Monomeric, Oligomeric, and Fibrillar Amyloid-Beta, *Subcellular Biochemistry 38*, 167-177.
9. Ladiwala, A. R. A., Lin, J. C., Bale, S. S., Marcelino-Cruz, A. M., Bhattacharya, M., Dordick, J. S., and Tessier, P. M. (2010) Resveratrol selectively remodels soluble oligomers and fibrils of amyloid Abeta into off-pathway conformers, *J. Biol. Chem. 285*, 24228-24237.
10. Hardy, J., and Higgins, G. (1992) Alzheimer's Disease: The Amyloid Cascade Hypothesis, *Science 256*, 184-185.
11. Hardy, J., and Selkoe, D. J. (2002) The amyloid hypothesis of Alzheimer's disease: progress and problems on the road to therapeutics, *Science (New York, N.Y.) 297*, 353-356.
12. Ahmed, M., Davis, J., Aucoin, D., Sato, T., Ahuja, S., Aimoto, S., Elliott, J. I., Van Nostrand, W. E., and Smith, S. O. (2010) Structural conversion of neurotoxic amyloid-beta(1-42) oligomers to fibrils, *Nat. Struct. Mol. Biol. 17*, 561-567.
13. Irwin, J. A., Wong, H. E., and Kwon, I. (2013) Different Fates of Alzheimer's Disease Amyloid-β Fibrils Remodeled by Biocompatible Small Molecules, *Biomacromolecules 14*, 264-274.
14. Kayed, R., Head, E., Sarsoza, F., Saing, T., Cotman, C. W., Necula, M., Margol, L., Wu, J., Breydo, L., Thompson, J. L., Rasool, S., Gurlo, T., Butler, P., and Glabe, C. G. (2007) Fibril specific, conformation dependent antibodies recognize a generic epitope common to amyloid fibrils and fibrillar oligomers that is absent in prefibrillar oligomers, *Mol. Neurodegener. 2*, 18.

15. Bieschke, J., Russ, J., Friedrich, R. P., Ehrnhoefer, D. E., Wobst, H., Neugebauer, K., and Wanker, E. E. (2010) EGCG remodels mature alpha-synuclein and amyloid-beta fibrils and reduces cellular toxicity, *Proc. Natl. Acad. Sci. U. S. A. 107*, 7710-7715.
16. Ehrnhoefer, D. E., Bieschke, J., Boeddrich, A., Herbst, M., Masino, L., Lurz, R., Engemann, S., Pastore, A., and Wanker, E. E. (2008) EGCG redirects amyloidogenic polypeptides into unstructured, off-pathway oligomers, *Nat Struct Mol Biol 15*, 558-566.
17. Grelle, G., Otto, A., Lorenz, M., Frank, R. F., Wanker, E. E., and Bieschke, J. (2011) Black Tea Theaflavins Inhibit Formation of Toxic Amyloid-β and α-Synuclein Fibrils, *Biochemistry 50*, 10624-10636.
18. Wood, S. J., Maleeff, B., Hart, T., and Wetzel, R. (1996) Physical, Morphological and Functional Differences between pH 5.8 and 7.4 Aggregates of the Alzheimer's Amyloid Peptide A β, *Journal of Molecular Biology 256*, 870-877.
19. Bartolini, M., Bertucci, C., Bolognesi, M. L., Cavalli, A., Melchiorre, C., and Andrisano, V. (2007) Insight into the kinetic of amyloid beta (1-42) peptide self-aggregation: elucidation of inhibitors' mechanism of action, *ChemBioChem 8*, 2152-2161.
20. Wu, J. W., Breydo, L., Isas, J. M., Lee, J., Kuznetsov, Y. G., Langen, R., and Glabe, C. (2010) Fibrillar oligomers nucleate the oligomerization of monomeric amyloid beta but do not seed fibril formation, *J. Biol. Chem. 285*, 6071-6079.
21. Kayed, R., Pensalfini, A., Margol, L., Sokolov, Y., Sarsoza, F., Head, E., Hall, J., and Glabe, C. (2009) Annular Protofibrils Are a Structurally and Functionally Distinct Type of Amyloid Oligomer, *Journal of Biological Chemistry 284*, 4230-4237.
22. Fändrich, M. (2012) Oligomeric Intermediates in Amyloid Formation: Structure Determination and Mechanisms of Toxicity, *Journal of Molecular Biology 421*, 427-440.
23. Ladiwala, A. R. A., Dordick, J. S., and Tessier, P. M. (2011) Aromatic Small Molecules Remodel Toxic Soluble Oligomers of Amyloid-beta through Three Independent Pathways, *J. Biol. Chem. 286*, 3209-3218.
24. Reinke, A. a., and Gestwicki, J. E. (2011) Insight into amyloid structure using chemical probes, *Chem. Biol. Drug Des. 77*, 399-411.
25. Koo, E. H., Lansbury, P. T., and Kelly, J. W. (1999) Amyloid diseases: Abnormal protein aggregation in neurodegeneration, *Proceedings of the National Academy of Sciences 96*, 9989-9990.
26. Schmidt, M., Sachse, C., Richter, W., Xu, C., Fändrich, M., and Grigorieff, N. (2009) Comparison of Alzheimer Aβ(1–40) and Aβ(1–42) amyloid fibrils reveals similar protofilament structures, *Proc. Natl. Acad. Sci. U. S. A. 106*, 19813-19818.
27. Wong, H. E., and Kwon, I. (2011) Xanthene Food Dye, as a Modulator of Alzheimer's Disease Amyloid-beta Peptide Aggregation and the Associated Impaired Neuronal Cell Function, *PLoS ONE 6*, e25752.
28. Bhak, G., Lee, J.-H., Hahn, J.-S., and Paik, S. R. (2009) Granular Assembly of α-Synuclein Leading to the Accelerated Amyloid Fibril Formation with Shear Stress, *PLoS ONE 4*, e4177.
29. Lee, J.-H., Bhak, G., Lee, S.-G., and Paik, S. R. (2008) Instantaneous Amyloid Fibril Formation of α-Synuclein from the Oligomeric Granular Structures in the Presence of Hexane, *Biophysical Journal 95*, L16-L18.
30. Ryu, J., Kanapathipillai, M., Lentzen, G., and Park, C. B. (2008) Inhibition of β-amyloid peptide aggregation and neurotoxicity by α-d-mannosylglycerate, a natural extremolyte, *Peptides 29*, 578-584.

31. Fändrich, M., Schmidt, M., and Grigorieff, N. (2011) Recent progress in understanding Alzheimer's β-amyloid structures, *Trends in Biochemical Sciences 36*, 338-345.
32. Klement, K., Wieligmann, K., Meinhardt, J., Hortschansky, P., Richter, W., and Fändrich, M. (2007) Effect of Different Salt Ions on the Propensity of Aggregation and on the Structure of Alzheimer's Aβ(1-40) Amyloid Fibrils, *J. Mol. Biol. 373*, 1321-1333.
33. Re, F., Airoldi, C., Zona, C., Masserini, M., Ferla, B. L., Quattrocchi, N., and Nicotra, F. (2010) Beta Amyloid Aggregation Inhibitors : Small Molecules as Candidate Drugs for Therapy of Alzheimer ' s Disease, *Current*, 2990-3006.
34. Necula, M., Breydo, L., Milton, S., Kayed, R., van der Veer, W. E., Tone, P., and Glabe, C. G. (2007) Methylene blue inhibits amyloid Abeta oligomerization by promoting fibrillization, *Biochemistry 46*, 8850-8860.
35. Necula, M., Kayed, R., Milton, S., and Glabe, C. G. (2007) Small molecule inhibitors of aggregation indicate that amyloid beta oligomerization and fibrillization pathways are independent and distinct, *The Journal of biological chemistry 282*, 10311-10324.
36. Remy, M., Thaler, S., Schumann, R. G., May, C. a., Fiedorowicz, M., Schuettauf, F., Grüterich, M., Priglinger, S. G., Nentwich, M. M., Kampik, a., and Haritoglou, C. (2008) An in vivo evaluation of Brilliant Blue G in animals and humans, *Br. J. Ophthalmol. 92*, 1142-1147.
37. Borzelleca, J. F., and Hallagan, J. B. (1990) Multigeneration study of FD & C Red No. 3 (erythrosine) in Sprague-Dawley rats, *Food Chem. Toxicol. 28*, 813-819.
38. Levitan, H., Ziylan, Z., Smith, Q. R., Takasato, Y., and Rapoport, S. I. (1984) Brain uptake of a food dye, erythrosin B, prevented by plasma protein binding, *Brain Res. 322*, 131-134.
39. Gregoire, S., Irwin, J., and Kwon, I. (2012) Techniques for monitoring protein misfolding and aggregation in vitro and in living cells, *Korean J. Chem. Eng. 29*, 693-702.
40. Kabuta, T., Suzuki, Y., and Wada, K. (2006) Degradation of amyotrophic lateral sclerosis-linked mutant Cu,Zn-superoxide dismutase proteins by macroautophagy and the proteasome, *J. Biol. Chem. 281*, 30524-30533.
41. Niwa, J., Yamada, S., Ishigaki, S., Sone, J., Takahashi, M., Katsuno, M., Tanaka, F., Doyu, M., and Sobue, G. (2007) Disulfide bond mediates aggregation, toxicity, and ubiquitylation of familial amyotrophic lateral sclerosis-linked mutant SOD1, *J. Biol. Chem. 282*, 28087-28095.
42. Kayed, R., Head, E., Thompson, J. L., McIntire, T. M., Milton, S. C., Cotman, C. W., and Glabe, C. G. (2003) Common structure of soluble amyloid oligomers implies common mechanism of pathogenesis, *Science 300*, 486-489.
43. Glabe, C. G. (2008) Structural classification of toxic amyloid oligomers, *The Journal of biological chemistry 283*, 29639-29643.
44. Bucciantini, M., Giannoni, E., Chiti, F., Baroni, F., Formigli, L., Zurdo, J., Taddei, N., Ramponi, G., Dobson, C. M., and Stefani, M. (2002) Inherent toxicity of aggregates implies a common mechanism for protein misfolding diseases, *Nature 416*, 507-511.
45. Cleary, J. P., Walsh, D. M., Hofmeister, J. J., Shankar, G. M., Kuskowski, M. a., Selkoe, D. J., and Ashe, K. H. (2005) Natural oligomers of the amyloid-beta protein specifically disrupt cognitive function, *Nature neuroscience 8*, 79-84.
46. Reinke, A. a., and Gestwicki, J. E. (2007) Structure-activity relationships of amyloid beta-aggregation inhibitors based on curcumin: influence of linker length and flexibility, *Chem. Biol. Drug Des. 70*, 206-215.

47. Nilsson, M. R. (2004) Techniques to study amyloid fibril formation in vitro, *Methods 34*, 151-160.
48. Groenning, M. (2010) Binding mode of Thioflavin T and other molecular probes in the context of amyloid fibrils—current status, *Journal of Chemical Biology 3*, 1-18.
49. Maezawa, I., Hong, H.-S., Liu, R., Wu, C.-Y., Cheng, R. H., Kung, M.-P., Kung, H. F., Lam, K. S., Oddo, S., Laferla, F. M., and Jin, L.-W. (2008) Congo red and thioflavin-T analogs detect Abeta oligomers, *Journal of neurochemistry 104*, 457-468.
50. Hudson, S. a., Ecroyd, H., Kee, T. W., and Carver, J. a. (2009) The thioflavin T fluorescence assay for amyloid fibril detection can be biased by the presence of exogenous compounds, *FEBS J. 276*, 5960-5972.
51. Biancalana, M., and Koide, S. (2010) Molecular Mechanism of Thioflavin-T binding to amyloid fibrils, *Biochimica et biophysica acta 1804*, 1405-1412.
52. Hatters, D. M., and Griffin, M. D. W. (2011) Protein Folding, Misfolding, and Disease, ch. 8, *Amyloid International Journal Of Experimental And Clinical Investigation 752*, 121-136.
53. Lindgren, M., and Hammarström, P. (2010) Amyloid oligomers: spectroscopic characterization of amyloidogenic protein states, *The FEBS journal 277*, 1380-1388.
54. Klunk, W. E., Jacob, R. F., and Mason, R. P. (1999) Quantifying Amyloid by Congo Red Spectra Shift Assay, *Methods in enzymology 309*, 6879-6879.
55. Walsh, D. M., Hartley, D. M., Kusumoto, Y., Fezoui, Y., Condron, M. M., Lomakin, A., Benedek, G. B., Selkoe, D. J., Teplow, D. B., and Biol, D. B. J. (1999) Amyloid Beta Protein Fibrillogenesis, *Journal of Biological Chemistry 274*, 25945-25952.
56. LeVine, H., III, and Walker, L. C. (2010) Molecular polymorphism of amyloid-beta in Alzheimer's disease, *Neurobiology of aging 31*, 542-548.
57. Cerf, E., Sarroukh, R., Tamamizu-Kato, S., Breydo, L., Derclaye, S., Dufrêne, Y. F., Narayanaswami, V., Goormaghtigh, E., Ruysschaert, J.-M., and Raussens, V. (2009) Antiparallel B-sheet: a signature structure of the oligomeric amyloid B-peptide, *Biochemical Journal 421*, 415-423.
58. Sarroukh, R., Cerf, E., Derclaye, S., Dufrêne, Y., Goormaghtigh, E., Ruysschaert, J.-M., and Raussens, V. (2011) Transformation of amyloid β(1–40) oligomers into fibrils is characterized by a major change in secondary structure, *Cell. Mol. Life Sci. 68*, 1429-1438.
59. Feng, Y., Wang, X.-p., Yang, S.-g., Wang, Y.-j., Zhang, X., Du, X.-t., Sun, X.-x., Zhao, M., Huang, L., and Liu, R.-t. (2009) Resveratrol inhibits beta-amyloid oligomeric cytotoxicity but does not prevent oligomer formation, *Neurotoxicology 30*, 986-995.
60. Woods, L. a., Platt, G. W., Hellewell, A. L., Hewitt, E. W., Homans, S. W., Ashcroft, A. E., and Radford, S. E. (2011) Ligand binding to distinct states diverts aggregation of an amyloid-forming protein, *Nat. Chem. Biol. 7*, 730-739.
61. Necula, M., Kayed, R., Milton, S., and Glabe, C. G. (2007) Small molecule inhibitors of aggregation indicate that amyloid beta oligomerization and fibrillization pathways are independent and distinct, *J. Biol. Chem. 282*, 10311-10324.
62. Wang, X.-p., Zhang, J.-h., Wang, Y.-j., Feng, Y., Zhang, X., Sun, X.-x., Li, J.-l., Du, X.-t., Lambert, M. P., Yang, S.-g., Zhao, M., Klein, W. L., and Liu, R.-t. (2009) Conformation-dependent single-chain variable fragment antibodies specifically recognize beta-amyloid oligomers, *FEBS letters 583*, 579-584.

63. Kayed, R., Canto, I., Breydo, L., Rasool, S., Lukacsovich, T., Wu, J., Albay, R., Pensalfini, A., Yeung, S., Head, E., Marsh, J. L., and Glabe, C. (2010) Conformation dependent monoclonal antibodies distinguish different replicating strains or conformers of prefibrillar Aβ oligomers, *Mol. Neurodegener. 5*, 57-57.
64. Bolognesi, B., Kumita, J. R., Barros, T. P., Esbjorner, E. K., Luheshi, L. M., Crowther, D. C., Wilson, M. R., Dobson, C. M., Favrin, G., and Yerbury, J. J. (2010) ANS binding reveals common features of cytotoxic amyloid species, *ACS chemical biology 5*, 735-740.
65. Ladiwala, A. R. A., Perchiacca, J. M., Fishman, Z. S., Bhattacharya, M., Hickey, A. M., Domigan, B. G., Dordick, J. S., and Tessier, P. M. (2012) Polyphenolic disaccharides endow proteins with unusual resistance to aggregation, *Biotechnology and Bioengineering 109*, 1869-1874.
66. Sood, A., Abid, M., Sauer, C., Hailemichael, S., Foster, M., Török, B., and Török, M. (2011) Disassembly of preformed amyloid beta fibrils by small organofluorine molecules, *Bioorganic & medicinal chemistry letters 21*, 2044-2047.
67. Lee, D., Lee, E.-K., Lee, J.-H., Chang, C.-S., and Paik, S. R. (2001) Self-oligomerization and protein aggregation of α-synuclein in the presence of Coomassie Brilliant Blue, *European Journal of Biochemistry 268*, 295-301.
68. Ha, C., and Park, C. B. (2005) Template-directed self-assembly and growth of insulin amyloid fibrils, *Biotechnology and Bioengineering 90*, 848-855.
69. Ku, S. H., and Park, C. B. (2008) Highly Accelerated Self-Assembly and Fibrillation of Prion Peptides on Solid Surfaces, *Langmuir 24*, 13822-13827.
70. Friedman, R. (2011) Aggregation of amyloids in a cellular context: modelling and experiment, *The Biochemical journal 438*, 415-426.
71. Dasilva, K. a., Shaw, J. E., and McLaurin, J. (2010) Amyloid-beta fibrillogenesis: structural insight and therapeutic intervention, *Experimental neurology 223*, 311-321.
72. Gras, S. L., Waddington, L. J., and Goldie, K. N. (2011) Protein Folding, Misfolding, and Disease, *Notes 752*, 197-214.
73. Toyama, B. H., and Weissman, J. S. (2011) Amyloid structure: conformational diversity and consequences, *Annual review of biochemistry 80*, 557-585.
74. Langkilde, A. E., and Vestergaard, B. (2009) Methods for structural characterization of prefibrillar intermediates and amyloid fibrils, *FEBS Lett. 583*, 2600-2609.
75. Chimon, S., Shaibat, M. a., Jones, C. R., Calero, D. C., Aizezi, B., and Ishii, Y. (2007) Evidence of fibril-like beta-sheet structures in a neurotoxic amyloid intermediate of Alzheimer's beta-amyloid, *Nat. Struct. Mol. Biol. 14*, 1157-1164.
76. Stine, W. B., Dahlgren, K. N., Krafft, G. a., and LaDu, M. J. (2003) In vitro characterization of conditions for amyloid-beta peptide oligomerization and fibrillogenesis, *J. Biol. Chem. 278*, 11612-11622.
77. Santos, S., Barcons, V., Christenson, H. K., Font, J., and Thomson, N. H. (2011) The Intrinsic Resolution Limit in the Atomic Force Microscope: Implications for Heights of Nano-Scale Features, *PLoS ONE 6*, e23821.
78. Perczel, A., Park, K., and Fasman, G. D. (1992) Deconvolution of the circular dichroism spectra of proteins: The circular dichroism spectra of the antiparallel β-sheet in proteins, *Proteins: Structure, Function, and Bioinformatics 13*, 57-69.
79. Whitmore, L., and Wallace, B. A. (2008) Protein secondary structure analyses from circular dichroism spectroscopy: Methods and reference databases, *Biopolymers 89*, 392-400.

80. Greenfield, N. J. (1999) Applications of circular dichroism in protein and peptide analysis, *Trends in analytical chemistry 18*, 236-244.
81. Pelton, J. T., and McLean, L. R. (2000) Spectroscopic methods for analysis of protein secondary structure, *Analytical biochemistry 277*, 167-176.
82. Surewicz, W. K., Mantsch, J. H. H., and Chapman, D. (1993) Determination of Protein Secondary Structure by Fourier Transform Infrared Spectroscopy : A Critical Assessment, *Biochemistry 32*, 389-394.
83. Corrêa, D. H. A., and Ramos, C. H. I. (2009) The use of circular dichroism spectroscopy to study protein folding , form and function, *Journal of Biochemistry 3*, 164-173.
84. Soto, C., and Castan, E. M. (1996) The conformation of Alzheimer's Beta peptide determines the rate of amyloid formation and its resistance to proteolysis, *Journal of Biochemistry 314*, 701-707.
85. Vieira, E. P., Hermel, H., and Möhwald, H. (2003) Change and stabilization of the amyloid-beta(1-40) secondary structure by fluorocompounds, *Biochimica et biophysica acta 1645*, 6-14.
86. Tomaselli, S., Esposito, V., Vangone, P., van Nuland, N. a. J., Bonvin, A. M. J. J., Guerrini, R., Tancredi, T., Temussi, P. a., and Picone, D. (2006) The alpha-to-beta conformational transition of Alzheimer's Abeta-(1-42) peptide in aqueous media is reversible: a step by step conformational analysis suggests the location of beta conformation seeding, *Chembiochem : a European journal of chemical biology 7*, 257-267.
87. Greenfield, N. J. (2006) Using circular dichroism spectra to estimate protein secondary structure, *Nat. Protoc. 1*, 2876-2890.
88. Reinke, A. a., and Gestwicki, J. E. (2007) Structure-activity relationships of amyloid beta-aggregation inhibitors based on curcumin: influence of linker length and flexibility, *Chemical biology & drug design 70*, 206-215.
89. Wong, H. E., Qi, W., Choi, H.-M., Fernandez, E. J., and Kwon, I. (2011) A Safe, Blood-Brain Barrier Permeable Triphenylmethane Dye Inhibits Amyloid-β Neurotoxicity by Generating Nontoxic Aggregates, *ACS Chem. Neurosci. 2*, 645-657.
90. Wong, H. E., Irwin, J. A., and Kwon, I. (2013) Halogenation Generates Effective Modulators of Amyloid-Beta Aggregation and Neurotoxicity, *PLoS ONE 8*, e57288.
91. Chalker, J. M., Wood, C. S. C., and Davis, B. G. (2009) A Convenient Catalyst for Aqueous and Protein Suzuki−Miyaura Cross-Coupling, *J. Am. Chem. Soc. 131*, 16346-16347.
92. Ojida, A., Tsutsumi, H., Kasagi, N., and Hamachi, I. (2005) Suzuki coupling for protein modification, *Tetrahedron Lett. 46*, 3301-3305.
93. Nowak, M. W., Gallivan, J. P., Silverman, S. K., Labarca, C. G., Dougherty, D. A., and Lester, H. A. (1998) In vivo incorporation of unnatural amino acids into ion channels in Xenopus oocyte expression system, In *Ion Channels, Pt B*, pp 504-529.
94. Kitevski-LeBlanc, J. L., and Prosser, R. S. (2012) Current applications of F-19 NMR to studies of protein structure and dynamics, *Prog. Nucl. Magn. Reson. Spectrosc. 62*, 1-33.
95. Hernandes, M. Z., Cavalcanti, S. M. T., Moreira, D. R. M., de Azevedo Junior, W. F., and Leite, A. C. L. (2010) Halogen Atoms in the Modern Medicinal Chemistry: Hints for the Drug Design, *Curr. Drug Targets 11*, 303-314.

96. Ryan, D. M., Anderson, S. B., and Nilsson, B. L. (2010) The influence of side-chain halogenation on the self-assembly and hydrogelation of Fmoc-phenylalanine derivatives, *Soft Matter 6*, 3220-3231.
97. Burley, S. K., and Petsko, G. A. (1985) Aromatic-aromatic interaction - a mechanism of protein-structure stabilization, *Science 229*, 23-28.
98. Claessens, C. G., and Stoddart, J. F. (1997) pi-pi interactions in self-assembly, *J. Phys. Org. Chem. 10*, 254-272.
99. Tartaglia, G. G., Cavalli, A., Pellarin, R., and Caflisch, A. (2004) The role of aromaticity, exposed surface, and dipole moment in determining protein aggregation rates, *Protein Science 13*, 1939-1941.
100. Gazit, E. (2002) A possible role for pi-stacking in the self-assembly of amyloid fibrils, *FASEB J. 16*, 77-83.
101. Porat, Y., Abramowitz, A., and Gazit, E. (2006) Inhibition of amyloid fibril formation by polyphenols: Structural similarity and aromatic interactions as a common inhibition mechanism, *Chemical Biology & Drug Design 67*, 27-37.
102. Azriel, R., and Gazit, E. (2001) Analysis of the structural and functional elements of the minimal active fragment of islet amyloid polypeptide (IAPP) - An experimental support for the key role of the phenylalanine residue in amyloid formation, *J. Biol. Chem. 276*, 34156-34161.
103. Gazit, E. (2002) Global analysis of tandem aromatic octapeptide repeats: The significance of the aromatic-glycine motif, *Bioinformatics 18*, 880-883.
104. McLean, C. A., Cherny, R. A., Fraser, F. W., Fuller, S. J., Smith, M. J., Konrad, V., Bush, A. I., and Masters, C. L. (1999) Soluble pool of Aβ amyloid as a determinant of severity of neurodegeneration in Alzheimer's disease, *Ann. Neurol. 46*, 860-866.
105. Hawkes, C. A., Ng, V., and McLaurin, J. (2009) Small molecule inhibitors of Aβ-aggregation and neurotoxicity, *Drug Dev. Res. 70*, 111-124.
106. Hamaguchi, T., Ono, K., and Yamada, M. (2006) Anti-amyloidogenic therapies: strategies for prevention and treatment of Alzheimer's disease, *Cell. Mol. Life Sci. 63*, 1538-1552.
107. McLaurin, J., Golomb, R., Jurewicz, A., Antel, J. P., and Fraser, P. E. (2000) Inositol Stereoisomers Stabilize an Oligomeric Aggregate of Alzheimer Amyloid β Peptide and Inhibit Aβ-induced Toxicity, *J. Biol. Chem. 275*, 18495-18502.
108. Moss, M. A., Varvel, N. H., Nichols, M. R., Reed, D. K., and Rosenberry, T. L. (2004) Nordihydroguaiaretic Acid Does Not Disaggregate β-Amyloid(1–40) Protofibrils but Does Inhibit Growth Arising from Direct Protofibril Association, *Mol. Pharmacol. 66*, 592-600.
109. Park, J.-W., Ahn, J. S., Lee, J.-H., Bhak, G., Jung, S., and Paik, S. R. (2008) Amyloid Fibrillar Meshwork Formation of Iron-Induced Oligomeric Species of Aβ40 with Phthalocyanine Tetrasulfonate and Its Toxic Consequences, *ChemBioChem 9*, 2602-2605.
110. Williams, A. D., Sega, M., Chen, M., Kheterpal, I., Geva, M., Berthelier, V., Kaleta, D. T., Cook, K. D., and Wetzel, R. (2005) Structural properties of Aβ protofibrils stabilized by a small molecule, *Proc. Natl. Acad. Sci. U. S. A. 102*, 7115-7120.
111. McLaurin, J., Kierstead, M. E., Brown, M. E., Hawkes, C. A., Lambermon, M. H. L., Phinney, A. L., Darabie, A. A., Cousins, J. E., French, J. E., Lan, M. F., Chen, F., Wong, S. S. N., Mount, H. T. J., Fraser, P. E., Westaway, D., and George-Hyslop, P. S. (2006)

Cyclohexanehexol inhibitors of A[beta] aggregation prevent and reverse Alzheimer phenotype in a mouse model, *Nat Med 12*, 801-808.
112. Yang, F., Lim, G. P., Begum, A. N., Ubeda, O. J., Simmons, M. R., Ambegaokar, S. S., Chen, P. P., Kayed, R., Glabe, C. G., Frautschy, S. A., and Cole, G. M. (2005) Curcumin Inhibits Formation of Amyloid β Oligomers and Fibrils, Binds Plaques, and Reduces Amyloid in Vivo, *J. Biol. Chem. 280*, 5892-5901.
113. Thapa, A., Woo, E. R., Chi, E. Y., Sharoar, M. G., Jin, H. G., Shin, S. Y., and Park, I. S. (2011) Biflavonoids Are Superior to Monoflavonoids in Inhibiting Amyloid-beta Toxicity and Fibrillogenesis via Accumulation of Nontoxic Oligomer-like Structures, *Biochemistry 50*, 2445-2455.
114. Wahlström, A., Cukalevski, R., Danielsson, J., Jarvet, J., Onagi, H., Rebek, J., Linse, S., and Gräslund, A. (2012) Specific Binding of a β-Cyclodextrin Dimer to the Amyloid β Peptide Modulates the Peptide Aggregation Process, *Biochemistry 51*, 4280-4289.
115. Hirohashi, T., Terasaki, T., Shigetoshi, M., and Sugiyama, Y. (1997) In Vivo and In Vitro Evidence for Nonrestricted Transport of 2′,7′-Bis(2-Carboxyethyl)-5(6)-Carboxyfluorescein Tetraacetoxymethyl Ester at the Blood-Brain Barrier, *J. Pharmacol. Exp. Ther. 280*, 813-819.
116. Terasaki, T., and Hosoya, K.-i. (1999) The blood–brain barrier efflux transporters as a detoxifying system for the brain, *Advanced Drug Delivery Reviews 36*, 195-209.
117. Pratim Bose, P., Chatterjee, U., Xie, L., Johansson, J., Göthelid, E., and Arvidsson, P. I. (2010) Effects of Congo Red on Aβ1−40 Fibril Formation Process and Morphology, *ACS Chem. Neurosci. 1*, 315-324.
118. Ono, K., Condron, M. M., Ho, L., Wang, J., Zhao, W., Pasinetti, G. M., and Teplow, D. B. (2008) Effects of grape seed-derived polyphenols on amyloid beta-protein self-assembly and cytotoxicity, *The Journal of biological chemistry 283*, 32176-32187.
119. Jones, G. R., Cundall, R. B., Murray, D., and Duddell, D. A. (1984) Eosin Y-macromolecule complexes. Part 2.-Interactions between eosin Y and polycations, a cationic surfactant and proteins, *J. Chem. Soc., Faraday Trans. 2 80*, 1201-1213.
120. Ma, C. Q., Li, K. A., and Tong, S. Y. (1996) Determination of proteins by fluorescence quenching of erythrosin B, *Anal. Chim. Acta 333*, 83-88.
121. Pérez, M., Ribe, E., Rubio, A., Lim, F., Morán, M. A., Ramos, P. G., Ferrer, I., Isla, M. T. G., and Avila, J. (2005) Characterization of a double (amyloid precursor protein-tau) transgenic: Tau phosphorylation and aggregation, *Neuroscience 130*, 339-347.
122. Vlasova, I. M., and Saletskii, A. M. (2010) Dependence of the constants of binding for nanomarkers of the fluorescein family with human serum albumin on Ph, *Russ. J. Phys. Chem. A 84*, 1065-1070.
123. Waheed, A. A., Rao, K. S., and Gupta, P. D. (2000) Mechanism of Dye Binding in the Protein Assay Using Eosin Dyes, *Analytical Biochemistry 287*, 73-79.
124. Feng, Y., Yang, S. G., Du, X. T., Zhang, X., Sun, X. X., Zhao, M., Sun, G. Y., and Liu, R. T. (2009) Ellagic acid promotes A beta 42 fibrillization and inhibits A beta 42-induced neurotoxicity, *Biochem. Biophys. Res. Commun. 390*, 1250-1254.
125. Pollack, S. J., Sadler, I. I. J., Hawtin, S. R., Tailor, V. J., and Shearman, M. S. (1995) Sulfonated dyes attenuate the toxic effects of beta-amyloid in a structure-specific fashion, *Neuroscience Letters 197*, 211-214.

126. Agarwala, S. S., Thompson, J., Smithers, M., Ross, M., Coventry, B., Minor, D., Scoggins, C., Hersey, P., and Wachter, E. (2009) Chemoablation of melanoma with intralesional rose bengal (PV-10), *J. Clin. Oncol. 27*.
127. Thompson, J. F., Hersey, P., and Wachter, E. (2008) Chemoablation of metastatic melanoma using intralesional Rose Bengal, *Melanoma Res. 18*, 405-411.
128. Liu, Y., and Schubert, D. (1997) Cytotoxic Amyloid Peptides Inhibit Cellular 3-(4,5-Dimethylthiazol-2-yl)-2,5-Diphenyltetrazolium Bromide (MTT) Reduction by Enhancing MTT Formazan Exocytosis, *J. Neurochem. 69*, 2285-2293.
129. Abe, K., and Saito, H. (1998) Amyloid [beta] protein inhibits cellular MTT reduction not by suppression of mitochondrial succinate dehydrogenase but by acceleration of MTT formazan exocytosis in cultured rat cortical astrocytes, *Neurosci. Res. 31*, 295-305.
130. Hertel, C., Hauser, N., Schubenel, R., Seilheimer, B., and Kemp, J. A. (1996) β-Amyloid-Induced Cell Toxicity: Enhancement of 3-(4,5-Dimethylthiazol-2-yl)-2,5-Diphenyltetrazolium Bromide-Dependent Cell Death, *J. Neurochem. 67*, 272-276.
131. Harada, T., and Kuroda, R. (2011) CD measurements of β-amyloid (1-40) and (1-42) in the condensed phase, *Biopolymers 95*, 127-134.
132. Soto, C., Castaño, E. M., Frangione, B., and Inestrosa, N. C. (1995) The -Helical to -Strand Transition in the Amino-terminal Fragment of the Amyloid -Peptide Modulates Amyloid Formation, *J. Biol. Chem. 270*, 3063-3067.
133. Chen, Y.-R., and Glabe, C. G. (2006) Distinct Early Folding and Aggregation Properties of Alzheimer Amyloid-β Peptides Aβ40 and Aβ42, *J. Biol. Chem. 281*, 24414-24422.
134. Hu, Y., Su, B., Kim, C.-S., Hernandez, M., Rostagno, A., Ghiso, J., and Kim, J. R. (2010) A strategy for designing a peptide probe for detection of β-amyloid oligomers, *ChemBioChem 11*, 2409-2418.
135. Iijima, K., Liu, H. P., Chiang, A. S., Hearn, S. A., Konsolaki, M., and Zhong, Y. (2004) Dissecting the pathological effects of human A beta 40 and A beta 42 in Drosophila: A potential model for Alzheimer's disease, *Proc. Natl. Acad. Sci. U. S. A. 101*, 6623-6628.
136. Kimura, N., Yanagisawa, K., Terao, K., Ono, F., Sakakibara, I., Ishii, Y., Kyuwa, S., and Yoshikawa, Y. (2005) Age-related changes of intracellular A beta in cynomolgus monkey brains, *Neuropathol. Appl. Neurobiol. 31*, 170-180.
137. Klyubin, I., Walsh, D. M., Lemere, C. A., Cullen, W. K., Shankar, G. M., Betts, V., Spooner, E. T., Jiang, L. Y., Anwyl, R., Selkoe, D. J., and Rowan, M. J. (2005) Amyloid beta protein immunotherapy neutralizes A beta oligomers that disrupt synaptic plasticity in vivo, *Nat. Med. (N. Y., NY, U. S.) 11*, 556-561.
138. Thakker, D. R., Weatherspoon, M. R., Harrison, J., Keene, T. E., Lane, D. S., Kaemmerer, W. F., Stewart, G. R., and Shafer, L. L. (2009) Intracerebroventricular amyloid-beta antibodies reduce cerebral amyloid angiopathy and associated micro-hemorrhages in aged Tg2576 mice, *Proc. Natl. Acad. Sci. U. S. A. 106*, 4501-4506.
139. Sreerama, N., Venyaminov, S. Y., and Woody, R. W. (2000) Estimation of Protein Secondary Structure from Circular Dichroism Spectra: Inclusion of Denatured Proteins with Native Proteins in the Analysis, *Anal. Biochem. 287*, 243-251.
140. Török, B., Sood, A., Bag, S., Kulkarni, A., Borkin, D., Lawler, E., Dasgupta, S., Landge, S., Abid, M., Zhou, W., Foster, M., LeVine, H., and Török, M. (2012) Structure–Activity Relationships of Organofluorine Inhibitors of β-Amyloid Self-Assembly, *ChemMedChem 7*, 910-919.

141. Shin, H.-J., Lee, E.-K., Lee, J.-H., Lee, D., Chang, C.-S., Kim, Y.-S., and Paik, S. R. (2000) Eosin interaction of α-synuclein leading to protein self-oligomerization, *Biochim. Biophys. Acta, Protein Struct. Mol. Enzymol. 1481*, 139-146.
142. Yang, J., Roy, A., and Zhang, Y. (2013) Protein–ligand binding site recognition using complementary binding-specific substructure comparison and sequence profile alignment, *Bioinformatics 29*, 2588-2595.
143. Holdgate, G. A., Anderson, M., Edfeldt, F., and Geschwindner, S. (2010) Affinity-based, biophysical methods to detect and analyze ligand binding to recombinant proteins: Matching high information content with high throughput, *J. Struct. Biol. 172*, 142-157.
144. Yang, J., Roy, A., and Zhang, Y. (2013) BioLiP: a semi-manually curated database for biologically relevant ligand–protein interactions, *Nucleic Acids Res. 41*, D1096-D1103.
145. Ciulli, A., Williams, G., Smith, A. G., Blundell, T. L., and Abell, C. (2006) Probing Hot Spots at Protein−Ligand Binding Sites: A Fragment-Based Approach Using Biophysical Methods, *J. Med. Chem. 49*, 4992-5000.
146. Sinha, S., Lopes, D. H. J., and Bitan, G. (2012) A Key Role for Lysine Residues in Amyloid β-Protein Folding, Assembly, and Toxicity, *ACS Chem. Neurosci. 3*, 473-481.
147. Pérot, S., Sperandio, O., Miteva, M. A., Camproux, A.-C., and Villoutreix, B. O. (2010) Druggable pockets and binding site centric chemical space: a paradigm shift in drug discovery, *Drug Discovery Today 15*, 656-667.
148. Murray, C. W., and Blundell, T. L. (2010) Structural biology in fragment-based drug design, *Curr. Opin. Struct. Biol. 20*, 497-507.
149. Brookmeyer, R., Gray, S., and Kawas, C. (1998) Projections of Alzheimer's disease in the United States and the public health impact of delaying disease onset, *Am. J. Public Health 88*, 1337-1342.
150. Citron, M. (2010) Alzheimer's disease: strategies for disease modification, *Nat. Rev. Drug Discovery 9*, 387-398.
151. McLaurin, J., Kierstead, M. E., Brown, M. E., Hawkes, C. A., Lambermon, M. H. L., Phinney, A. L., Darabie, A. A., Cousins, J. E., French, J. E., Lan, M. F., Chen, F., Wong, S. S. N., Mount, H. T. J., Fraser, P. E., Westaway, D., and George-Hyslop, P. S. (2006) Cyclohexanehexol inhibitors of Abeta aggregation prevent and reverse Alzheimer phenotype in a mouse model, *Nat. Med. (N. Y., NY, U. S.) 12*, 801-808.
152. Ehrnhoefer, D. E., Bieschke, J., Boeddrich, A., Herbst, M., Masino, L., Lurz, R., Engemann, S., Pastore, A., and Wanker, E. E. (2008) EGCG redirects amyloidogenic polypeptides into unstructured, off-pathway oligomers, *Nat. Struct. Mol. Biol. 15*, 558-566.
153. Mangialasche, F., Solomon, A., Winblad, B., Mecocci, P., and Kivipelto, M. (2010) Alzheimer's disease: clinical trials and drug development, *Lancet Neurol. 9*, 702-716.
154. Baum, L., Lam, C. W., Cheung, S. K., Kwok, T., Lui, V., Tsoh, J., Lam, L., Leung, V., Hui, E., Ng, C., Woo, J., Chiu, H. F., Goggins, W. B., Zee, B. C., Cheng, K. F., Fong, C. Y., Wong, A., Mok, H., Chow, M. S., Ho, P. C., Ip, S. P., Ho, C. S., Yu, X. W., Lai, C. Y., Chan, M. H., Szeto, S., Chan, I. H., and Mok, V. (2008) Six-month randomized, placebo-controlled, double-blind, pilot clinical trial of curcumin in patients with Alzheimer disease, *J. Clin. Psychopharmacol. 28*, 110-113.
155. Meyer, B., and Peters, T. (2003) NMR Spectroscopy Techniques for Screening and Identifying Ligand Binding to Protein Receptors, *Angew. Chem., Int. Ed. 42*, 864-890.

156. Kodama, Y., Takeuchi, K., Shimba, N., Ishikawa, K., Suzuki, E.-i., Shimada, I., and Takahashi, H. (2013) Rapid Identification of Ligand-Binding Sites by Using an Assignment-Free NMR Approach, *J. Med. Chem. 56*, 9342-9350.
157. Vajda, S., and Guarnieri, F. (2006) Characterization of protein-ligand interaction sites using experimental and computational methods, *Curr. Opin. Drug Discovery Dev. 9*, 354 - 362.
158. Brünger, A. T. (1997) X-ray crystallography and NMR reveal complementary views of structure and dynamics, *Nat. Struct. Biol. 4*, 862 - 865.
159. Ambrus, A., and Fesus, L. (1997) Comparison of NMR and X-Ray Crystallography as Methods of the Protein Structure Determination, http://www.cryst.bbk.ac.uk/pps97/assignments/projects/ambrus/html.htm#ref. Accessed 14-July-2014.
160. Bieschke, J., Herbst, M., Wiglenda, T., Friedrich, R. P., Boeddrich, A., Schiele, F., Kleckers, D., Lopez del Amo, J. M., Grüning, B. A., Wang, Q., Schmidt, M. R., Lurz, R., Anwyl, R., Schnoegl, S., Fändrich, M., Frank, R. F., Reif, B., Günther, S., Walsh, D. M., and Wanker, E. E. (2012) Small-molecule conversion of toxic oligomers to nontoxic β-sheet–rich amyloid fibrils, *Nat. Chem. Biol. 8*, 93-101.
161. Vegas, A. J., Fuller, J. H., and Koehler, A. N. (2008) Small-molecule microarrays as tools in ligand discovery, *Chem. Soc. Rev. 37*, 1385-1394.
162. Chen, J., Armstrong, A. H., Koehler, A. N., and Hecht, M. H. (2010) Small Molecule Microarrays Enable the Discovery of Compounds That Bind the Alzheimer's Aβ Peptide and Reduce its Cytotoxicity, *J. Am. Chem. Soc. 132*, 17015-17022.
163. Cwirla, S. E., Peters, E. A., Barrett, R. W., and Dower, W. J. (1990) Peptides on phage: a vast library of peptides for identifying ligands, *Proc. Natl. Acad. Sci. U. S. A. 87*, 6378-6382.
164. Kitchen, D. B., Decornez, H., Furr, J. R., and Bajorath, J. (2004) Docking and scoring in virtual screening for drug discovery: methods and applications, *Nat. Rev. Drug Discovery 3*, 935-949.
165. Glaser, F., Morris, R. J., Najmanovich, R. J., Laskowski, R. A., and Thornton, J. M. (2006) A method for localizing ligand binding pockets in protein structures, *Proteins: Struct., Funct., Bioinf. 62*, 479-488.
166. Kinoshita, K., and Nakamura, H. (2005) Identification of the ligand binding sites on the molecular surface of proteins, *Protein Sci. 14*, 711-718.
167. Henrich, S., Salo-Ahen, O. M. H., Huang, B., Rippmann, F. F., Cruciani, G., and Wade, R. C. (2010) Computational approaches to identifying and characterizing protein binding sites for ligand design, *J. Mol. Recognit. 23*, 209-219.
168. Di Scala, C., Yahi, N., Lelièvre, C., Garmy, N., Chahinian, H., and Fantini, J. (2012) Biochemical Identification of a Linear Cholesterol-Binding Domain within Alzheimer's β Amyloid Peptide, *ACS Chem. Neurosci. 4*, 509-517.
169. Masuda, M., Hasegawa, M., Nonaka, T., Oikawa, T., Yonetani, M., Yamaguchi, Y., Kato, K., Hisanaga, S.-i., and Goedert, M. (2009) Inhibition of α-synuclein fibril assembly by small molecules: Analysis using epitope-specific antibodies, *FEBS Lett. 583*, 787-791.
170. Abelein, A., Lang, L., Lendel, C., Gräslund, A., and Danielsson, J. (2012) Transient small molecule interactions kinetically modulate amyloid β peptide self-assembly, *FEBS Lett. 586*, 3991-3995.

171. Pedersen, M. Ø., Mikkelsen, K., Behrens, M. A., Pedersen, J. S., Enghild, J. J., Skrydstrup, T., Malmendal, A., and Nielsen, N. C. (2010) NMR Reveals Two-Step Association of Congo Red to Amyloid β in Low-Molecular-Weight Aggregates, *J. Phys. Chem. B 114*, 16003-16010.
172. Podlisny, M. B., Walsh, D. M., Amarante, P., Ostaszewski, B. L., Stimson, E. R., Maggio, J. E., Teplow, D. B., and Selkoe, D. J. (1998) Oligomerization of endogenous and synthetic amyloid beta-protein at nanomolar levels in cell culture and stabilization of monomer by Congo red, *Biochemistry 37*, 3602-3611.
173. Feng, B. Y., Toyama, B. H., Wille, H., Colby, D. W., Collins, S. R., May, B. C. H., Prusiner, S. B., Weissman, J., and Shoichet, B. K. (2008) Small-molecule aggregates inhibit amyloid polymerization, *Nat. Chem. Biol. 4*, 197-199.
174. Chauhan, N. B., and Siegel, G. J. (2005) Efficacy of anti-Aβ antibody isotypes used for intracerebroventricular immunization in TgCRND8, *Neurosci. Lett. 375*, 143-147.
175. Lichtenthaler, S. F., Beher, D., Grimm, H. S., Wang, R., Shearman, M. S., Masters, C. L., and Beyreuther, K. (2002) The intramembrane cleavage site of the amyloid precursor protein depends on the length of its transmembrane domain, *Proc. Natl. Acad. Sci. U. S. A. 99*, 1365-1370.
176. Parvathy, S. S., Davies, P., Haroutunian, V., and et al. (2001) Correlation between aβx-40–, aβx-42–, and aβx-43–containing amyloid plaques and cognitive decline, *Arch. Neurol. (Chicago) 58*, 2025-2031.
177. Tovey, E. R., and Baldo, B. A. (1989) Protein binding to nitrocellulose, nylon and PVDF membranes in immunoassays and electroblotting, *J. Biochem. Biophys. Methods 19*, 169-183.
178. Keshet, B., Gray, J. J., and Good, T. A. (2010) Structurally distinct toxicity inhibitors bind at common loci on β-amyloid fibril, *Protein Sci. 19*, 2291-2304.
179. Chen, W.-T., Hong, C.-J., Lin, Y.-T., Chang, W.-H., Huang, H.-T., Liao, J.-Y., Chang, Y.-J., Hsieh, Y.-F., Cheng, C.-Y., Liu, H.-C., Chen, Y.-R., and Cheng, I. H. (2012) Amyloid-Beta (Aβ) D7H Mutation Increases Oligomeric Aβ42 and Alters Properties of Aβ-Zinc/Copper Assemblies, *PLoS ONE 7*, e35807.
180. Parthasarathy, S., Long, F., Miller, Y., Xiao, Y., McElheny, D., Thurber, K., Ma, B., Nussinov, R., and Ishii, Y. (2011) Molecular-Level Examination of Cu2+ Binding Structure for Amyloid Fibrils of 40-Residue Alzheimer's β by Solid-State NMR Spectroscopy, *J. Am. Chem. Soc. 133*, 3390-3400.
181. Sato, M., Murakami, K., Uno, M., Nakagawa, Y., Katayama, S., Akagi, K.-i., Masuda, Y., Takegoshi, K., and Irie, K. (2013) Site-Specific Inhibitory Mechanism for Amyloid-β42 Aggregation by Catechol-Type Flavonoids Targeting the Lys Residues, *J. Biol. Chem. 288*, 23212-23224.
182. Kroth, H., Ansaloni, A., Varisco, Y., Jan, A., Sreenivasachary, N., Rezaei-Ghaleh, N., Giriens, V., Lohmann, S., López-Deber, M. P., Adolfsson, O., Pihlgren, M., Paganetti, P., Froestl, W., Nagel-Steger, L., Willbold, D., Schrader, T., Zweckstetter, M., Pfeifer, A., Lashuel, H. A., and Muhs, A. (2012) Discovery and Structure Activity Relationship of Small Molecule Inhibitors of Toxic β-Amyloid-42 Fibril Formation, *J. Biol. Chem. 287*, 34786-34800.
183. Convertino, M., Vitalis, A., and Caflisch, A. (2011) Disordered Binding of Small Molecules to Aβ(12–28), *J. Biol. Chem. 286*, 41578-41588.

184. Geng, J., Li, M., Ren, J., Wang, E., and Qu, X. (2011) Polyoxometalates as Inhibitors of the Aggregation of Amyloid β Peptides Associated with Alzheimer's Disease, *Angew. Chem. 123*, 4270-4274.
185. Sinha, S., Lopes, D. H. J., Du, Z., Pang, E. S., Shanmugam, A., Lomakin, A., Talbiersky, P., Tennstaedt, A., McDaniel, K., Bakshi, R., Kuo, P.-Y., Ehrmann, M., Benedek, G. B., Loo, J. A., Klärner, F.-G., Schrader, T., Wang, C., and Bitan, G. (2011) Lysine-Specific Molecular Tweezers Are Broad-Spectrum Inhibitors of Assembly and Toxicity of Amyloid Proteins, *J. Am. Chem. Soc. 133*, 16958-16969.
186. Sinha, S., Du, Z., Maiti, P., Klärner, F.-G., Schrader, T., Wang, C., and Bitan, G. (2012) Comparison of Three Amyloid Assembly Inhibitors: The Sugar scyllo-Inositol, the Polyphenol Epigallocatechin Gallate, and the Molecular Tweezer CLR01, *ACS Chem. Neurosci. 3*, 451-458.
187. Ono, K., Li, L., Takamura, Y., Yoshiike, Y., Zhu, L., Han, F., Mao, X., Ikeda, T., Takasaki, J.-i., Nishijo, H., Takashima, A., Teplow, D. B., Zagorski, M. G., and Yamada, M. (2012) Phenolic Compounds Prevent Amyloid β-Protein Oligomerization and Synaptic Dysfunction by Site-specific Binding, *J. Biol. Chem. 287*, 14631-14643.
188. Li, J., Uversky, V. N., and Fink, A. L. (2001) Effect of familial Parkinson's disease point mutations A30P and A53T on the structural properties, aggregation, and fibrillation of human alpha-synuclein, *Biochemistry 40*, 11604-11613.
189. Li, J., Zhu, M., Rajamani, S., Uversky, V. N., and Fink, A. L. (2004) Rifampicin Inhibits α-Synuclein Fibrillation and Disaggregates Fibrils, *Chem. Biol. (Cambridge, MA, U. S.) 11*, 1513-1521.
190. Spillantini, M. G., Crowther, R. A., Jakes, R., Cairns, N. J., Lantos, P. L., and Goedert, M. (1998) Filamentous alpha-synuclein inclusions link multiple system atrophy with Parkinson's disease and dementia with Lewy bodies, *Neurosci. Lett. 251*, 205-208.
191. Jahn, T. R., and Radford, S. E. (2005) The Yin and Yang of protein folding, *FEBS J. 272*, 5962-5970.
192. Jones, O. G., and Mezzenga, R. (2012) Inhibiting, promoting, and preserving stability of functional protein fibrils, *Soft Matter 8*, 876-895.
193. Chatani, E., Lee, Y.-H., Yagi, H., Yoshimura, Y., Naiki, H., and Goto, Y. (2009) Ultrasonication-dependent production and breakdown lead to minimum-sized amyloid fibrils, *Proc. Natl. Acad. Sci. U. S. A. 106*, 11119-11124.
194. Arora, A., Ha, C., and Park, C. B. (2004) Insulin amyloid fibrillation at above 100°C: New insights into protein folding under extreme temperatures, *Protein Sci. 13*, 2429-2436.
195. Dubois, J., Ismail, Chan, and Ali, K. (1999) Fourier Transform Infrared Spectroscopic Investigation of Temperature- and Pressure-Induced Disaggregation of Amyloid A, *Scand. J. Immunol. 49*, 376-380.
196. Adamcik, J., and Mezzenga, R. (2011) Adjustable twisting periodic pitch of amyloid fibrils, *Soft Matter 7*, 5437-5443.
197. Narimoto, T., Sakurai, K., Okamoto, A., Chatani, E., Hoshino, M., Hasegawa, K., Naiki, H., and Goto, Y. (2004) Conformational stability of amyloid fibrils of β2-microglobulin probed by guanidine-hydrochloride-induced unfolding, *FEBS Lett. 576*, 313-319.
198. Hirota-Nakaoka, N., Hasegawa, K., Naiki, H., and Goto, Y. (2003) Dissolution of β2-Microglobulin Amyloid Fibrils by Dimethylsulfoxide, *J. Biochem. 134*, 159-164.

199. Jordens, S., Adamcik, J., Amar-Yuli, I., and Mezzenga, R. (2010) Disassembly and Reassembly of Amyloid Fibrils in Water−Ethanol Mixtures, *Biomacromolecules 12*, 187-193.
200. Li, J., Zhu, M., Manning-Bog, A. B., Di Monte, D. A., and Fink, A. L. (2004) Dopamine and L-dopa disaggregate amyloid fibrils: implications for Parkinson's and Alzheimer's disease, *FASEB J. 18*, 962-964.
201. Benilova, I., Karran, E., and De Strooper, B. (2012) The toxic A[beta] oligomer and Alzheimer's disease: an emperor in need of clothes, *Nat. Neurosci. 15*, 349-357.
202. Ruhs, P. A., Adamcik, J., Bolisetty, S., Sanchez-Ferrer, A., and Mezzenga, R. (2011) A supramolecular bottle-brush approach to disassemble amyloid fibrils, *Soft Matter 7*, 3571-3579.
203. Park, J.-W., Lee, I.-H., Hahn, J.-S., Kim, J., Chung, K. C., and Paik, S. R. (2008) Disintegration of amyloid fibrils of α-synuclein by dequalinium, *Biochim. Biophys. Acta, Gen. Subj. 1780*, 1156-1161.
204. Giorgetti, S., Raimondi, S., Pagano, K., Relini, A., Bucciantini, M., Corazza, A., Fogolari, F., Codutti, L., Salmona, M., Mangione, P., Colombo, L., De Luigi, A., Porcari, R., Gliozzi, A., Stefani, M., Esposito, G., Bellotti, V., and Stoppini, M. (2011) Effect of Tetracyclines on the Dynamics of Formation and Destructuration of β2-Microglobulin Amyloid Fibrils, *J. Biol. Chem. 286*, 2121-2131.
205. Callaway, N. L., Riha, P. D., Wrubel, K. M., McCollum, D., and Gonzalez-Lima, F. (2002) Methylene blue restores spatial memory retention impaired by an inhibitor of cytochrome oxidase in rats, *Neurosci. Lett. 332*, 83-86.
206. Korth, C., May, B. C., Cohen, F. E., and Prusiner, S. B. (2001) Acridine and phenothiazine derivatives as pharmacotherapeutics for prion disease, *Proc. Natl. Acad. Sci. U. S. A. 98*, 9836-9841.
207. Gardner, D. F., Utiger, R. D., Schwartz, S. L., Witorsch, P., Meyers, B., Braverman, L. E., and Witorsch, R. J. (1987) Effects of oral erythrosine (2′,4′,5′,7′-tetraiodofluorescein) on thyroid function in normal men, *Toxicol. Appl. Pharmacol. 91*, 299-304.
208. Peng, W., Cotrina, M. L., Han, X., Yu, H., Bekar, L., Blum, L., Takano, T., Tian, G.-F., Goldman, S. A., and Nedergaard, M. (2009) Systemic administration of an antagonist of the ATP-sensitive receptor P2X7 improves recovery after spinal cord injury, *Proc. Natl. Acad. Sci. U. S. A. 106*, 12489-12493.
209. Borzelleca Joseph, F., and Hallagan John, B. (1992) Safety and Regulatory Status of Food, Drug, and Cosmetic Color Additives, In *Food Safety Assessment*, pp 377-390, American Chemical Society.
210. Borzelleca, J. F., Depukat, K., and Hallagan, J. B. (1990) Lifetime toxicity/carcinogenicity studies of FD & C blue No. 1 (Brilliant blue FCF) in rats and mice, *Food Chem. Toxicol. 28*, 221-234.
211. Ryu, J. K., and McLarnon, J. G. (2008) Block of purinergic P2X7 receptor is neuroprotective in an animal model of Alzheimer's disease, *NeuroReport 19*, 1715-1719.
212. Matute, C., Torre, I., Pérez-Cerdá, F., Pérez-Samartín, A., Alberdi, E., Etxebarria, E., Arranz, A. M., Ravid, R., Rodríguez-Antigüedad, A., Sánchez-Gómez, M., and Domercq, M. (2007) P2X7 Receptor Blockade Prevents ATP Excitotoxicity in Oligodendrocytes and Ameliorates Experimental Autoimmune Encephalomyelitis, *J. Neurosci. 27*, 9525-9533.

213. Simmons, R., Thevarajah, S., Brennan, M., Christos, P., and Osborne, M. (2003) Methylene Blue Dye as an Alternative to Isosulfan Blue Dye for Sentinel Lymph Node Localization, *Ann. Surg. Onc. 10*, 242-247.
214. Thevarajah, S., Huston, T. L., and Simmons, R. M. (2005) A comparison of the adverse reactions associated with isosulfan blue versus methylene blue dye in sentinel lymph node biopsy for breast cancer, *Am. J. Surg. 189*, 236-239.
215. Zoungrana, A., Coulibaly, B., Sié, A., Walter-Sack, I., Mockenhaupt, F. P., Kouyaté, B., Schirmer, R. H., Klose, C., Mansmann, U., Meissner, P., and Müller, O. (2008) Safety and Efficacy of Methylene Blue Combined with Artesunate or Amodiaquine for Uncomplicated Falciparum Malaria: A Randomized Controlled Trial from Burkina Faso, *PLoS ONE 3*, e1630.
216. Medina, D. X., Caccamo, A., and Oddo, S. (2011) Methylene Blue Reduces Aβ Levels and Rescues Early Cognitive Deficit by Increasing Proteasome Activity, *Brain Pathol. 21*, 140-149.
217. http://gwyddion.net/. Accessed August 27th, 2012.
218. Provencher, S. W., and Gloeckner, J. (1981) Estimation of globular protein secondary structure from circular dichroism, *Biochemistry 20*, 33-37.
219. Vanstokkum, I. (1990) Estimation of protein secondary structure and error analysis from circular dichroism spectra, *Anal. Biochem. 191*, 110-118.
220. Sreerama, N., and Woody, R. W. (2000) Estimation of Protein Secondary Structure from Circular Dichroism Spectra: Comparison of CONTIN, SELCON, and CDSSTR Methods with an Expanded Reference Set, *Anal. Biochem. 287*, 252-260.
221. Lees, J. G., Miles, A. J., Wien, F., and Wallace, B. A. (2006) A reference database for circular dichroism spectroscopy covering fold and secondary structure space, *Bioinformatics 22*, 1955-1962.
222. Del Mercato, L. L., Maruccio, G., Pompa, P. P., Bochicchio, B., Tamburro, A. M., Cingolani, R., and Rinaldi, R. (2008) Amyloid-like Fibrils in Elastin-Related Polypeptides: Structural Characterization and Elastic Properties, *Biomacromolecules 9*, 796-803.
223. Pires, R. H., Saraiva, M. J., Damas, A. M., and Kellermayer, M. S. Z. (2011) Structure and assembly–disassembly properties of wild-type transthyretin amyloid protofibrils observed with atomic force microscopy, *J. Mol. Recognit. 24*, 467-476.
224. Tycko, R. (2004) Progress towards a molecular-level structural understanding of amyloid fibrils, *Current Opinion in Structural Biology 14*, 96-103.
225. Wilcock, D. M., Lewis, M. R., Van Nostrand, W. E., Davis, J., Previti, M. L., Gharkholonarehe, N., Vitek, M. P., and Colton, C. A. (2008) Progression of Amyloid Pathology to Alzheimer's Disease Pathology in an Amyloid Precursor Protein Transgenic Mouse Model by Removal of Nitric Oxide Synthase 2, *The Journal of Neuroscience 28*, 1537-1545.
226. Pardridge, W. A. (2009) Alzheimer's disease drug development and the problem of the blood-brain barrier, *Alzheimers. Dement. 5*, 427-432.
227. Frid, P., Anisimov, S. V., and Popovic, N. (2007) Congo red and protein aggregation in neurodegenerative diseases, *Brain Res. Rev. 53*, 135-160.
228. Yazawa, K., Kihara, T., Shen, H. L., Shimmyo, Y., Niidome, T., and Sugimoto, H. (2006) Distinct mechanisms underlie distinct polyphenol-induced neuroprotection, *Febs Letters 580*, 6623-6628.

229. Takenouchi, T., Sekiyama, K., Sekigawa, A., Fujita, M., Waragai, M., Sugama, S., Iwamaru, Y., Kitani, H., and Hashimoto, M. (2010) P2X7 Receptor Signaling Pathway as a Therapeutic Target for Neurodegenerative Diseases, *Archivum Immunologiae et Therapiae Experimentalis 58*, 91-96.
230. Young, C. N. J., Brutkowski, W., Lien, C.-F., Arkle, S., Lochmüller, H., Zabłocki, K., and Górecki, D. C. (2012) P2X7 purinoceptor alterations in dystrophic mdx mouse muscles: relationship to pathology and potential target for treatment, *Journal of Cellular and Molecular Medicine 16*, 1026-1037.
231. Kimbler, D. E., Shields, J., Yanasak, N., Vender, J. R., and Dhandapani, K. M. (2012) Activation of P2X7 Promotes Cerebral Edema and Neurological Injury after Traumatic Brain Injury in Mice, *PLoS ONE 7*, e41229.
232. Iwamaru, Y., Takenouchi, T., Murayama, Y., Okada, H., Imamura, M., Shimizu, Y., Hashimoto, M., Mohri, S., Yokoyama, T., and Kitani, H. (2012) Anti-Prion Activity of Brilliant Blue G, *PLoS ONE 7*, e37896.
233. Diaz-Hernandez, J. I., Gomez-Villafuertes, R., León-Otegui, M., Hontecillas-Prieto, L., del Puerto, A., Trejo, J. L., Lucas, J. J., Garrido, J. J., Gualix, J., Miras-Portugal, M. T., and Diaz-Hernandez, M. (2012) In vivo P2X7 inhibition reduces amyloid plaques in Alzheimer's disease through GSK3β and secretases, *Neurobiology of Aging 33*, 1816-1828.
234. Wright, A. L., Zinn, R., Hohensinn, B., Konen, L. M., Beynon, S. B., Tan, R. P., Clark, I. A., Abdipranoto, A., and Vissel, B. (2013) Neuroinflammation and Neuronal Loss Precede Aβ Plaque Deposition in the hAPP-J20 Mouse Model of Alzheimer's Disease, *PLoS ONE 8*, e59586.
235. Mestas, J., and Hughes, C. C. W. (2004) Of Mice and Not Men: Differences between Mouse and Human Immunology, *The Journal of Immunology 172*, 2731-2738.
236. Sudduth, T. L., Wilson, J. G., Everhart, A., Colton, C. A., and Wilcock, D. M. (2012) Lithium Treatment of APPSwDI/NOS2−/− Mice Leads to Reduced Hyperphosphorylated Tau, Increased Amyloid Deposition and Altered Inflammatory Phenotype, *PLoS ONE 7*, e31993.
237. Wilcock, D. M., Gharkholonarehe, N., Van Nostrand, W. E., Davis, J., Vitek, M. P., and Colton, C. A. (2009) Amyloid Reduction by Amyloid-β Vaccination Also Reduces Mouse Tau Pathology and Protects from Neuron Loss in Two Mouse Models of Alzheimer's Disease, *The Journal of Neuroscience 29*, 7957-7965.
238. Nussbaum, J. M., Schilling, S., Cynis, H., Silva, A., Swanson, E., Wangsanut, T., Tayler, K., Wiltgen, B., Hatami, A., Ronicke, R., Reymann, K., Hutter-Paier, B., Alexandru, A., Jagla, W., Graubner, S., Glabe, C. G., Demuth, H.-U., and Bloom, G. S. (2012) Prion-like behaviour and tau-dependent cytotoxicity of pyroglutamylated amyloid-[bgr], *Nature 485*, 651-655.
239. Ridnour, L. A., Dhanapal, S., Hoos, M., Wilson, J., Lee, J., Cheng, R. Y. S., Brueggemann, E. E., Hines, H. B., Wilcock, D. M., Vitek, M. P., Wink, D. A., and Colton, C. A. (2012) Nitric oxide-mediated regulation of β-amyloid clearance via alterations of MMP-9/TIMP-1, *Journal of Neurochemistry 123*, 736-749.
240. Wilcock, D. M., Vitek, M. P., and Colton, C. A. (2009) Vascular amyloid alters astrocytic water and potassium channels in mouse models and humans with Alzheimer's disease, *Neuroscience 159*, 1055-1069.

241. Kukar, T., Prescott, S., Eriksen, J., Holloway, V., Murphy, M. P., Koo, E., Golde, T., and Nicolle, M. (2007) Chronic administration of R-flurbiprofen attenuates learning impairments in transgenic amyloid precursor protein mice, *BMC neuroscience 8*, 54.
242. Hawkes, C. A., Deng, L.-H., Shaw, J. E., Nitz, M., and McLaurin, J. (2010) Small molecule β-amyloid inhibitors that stabilize protofibrillar structures in vitro improve cognition and pathology in a mouse model of Alzheimer's disease, *European Journal of Neuroscience 31*, 203-213.
243. Zhang, J., Zhen, Y.-f., Pu Bu Ci, R., Song, L.-g., Kong, W.-n., Shao, T.-m., Li, X., and Chai, X.-q. (2013) Salidroside attenuates beta amyloid-induced cognitive deficits via modulating oxidative stress and inflammatory mediators in rat hippocampus, *Behavioural Brain Research 244*, 70-81.
244. Parthsarathy, V., McClean, P. L., Hölscher, C., Taylor, M., Tinker, C., Jones, G., Kolosov, O., Salvati, E., Gregori, M., Masserini, M., and Allsop, D. (2013) A Novel Retro-Inverso Peptide Inhibitor Reduces Amyloid Deposition, Oxidation and Inflammation and Stimulates Neurogenesis in the APPswe/PS1ΔE9 Mouse Model of Alzheimer's Disease, *PLoS ONE 8*, e54769.
245. Murata, N., Murakami, K., Ozawa, Y., Kinoshita, N., Irie, K., Shirasawa, T., and Shimizu, T. (2010) Silymarin Attenuated the Amyloid β Plaque Burden and Improved Behavioral Abnormalities in an Alzheimer’s Disease Mouse Model, *Bioscience, Biotechnology, and Biochemistry 74*, 2299-2306.
246. Ryu, J. K., Franciosi, S., Sattayaprasert, P., Kim, S. U., and McLarnon, J. G. (2004) Minocycline inhibits neuronal death and glial activation induced by β-amyloid peptide in rat hippocampus, *Glia 48*, 85-90.
247. Calon, F., Lim, G. P., Yang, F., Morihara, T., Teter, B., Ubeda, O., Rostaing, P., Triller, A., Salem Jr, N., Ashe, K. H., Frautschy, S. A., and Cole, G. M. (2004) Docosahexaenoic Acid Protects from Dendritic Pathology in an Alzheimer's Disease Mouse Model, *Neuron 43*, 633-645.
248. Serenó, L., Coma, M., Rodríguez, M., Sánchez-Ferrer, P., Sánchez, M. B., Gich, I., Agulló, J. M., Pérez, M., Avila, J., Guardia-Laguarta, C., Clarimón, J., Lleó, A., and Gómez-Isla, T. (2009) A novel GSK-3β inhibitor reduces Alzheimer's pathology and rescues neuronal loss in vivo, *Neurobiology of Disease 35*, 359-367.
249. Nunes, A., Amaral, J., Lo, A., Fonseca, M., Viana, R. S., Callaerts-Vegh, Z., D'Hooge, R., and Rodrigues, C. P. (2012) TUDCA, a Bile Acid, Attenuates Amyloid Precursor Protein Processing and Amyloid-β Deposition in APP/PS1 Mice, *Molecular Neurobiology 45*, 440-454.
250. Butovsky, O., Koronyo-Hamaoui, M., Kunis, G., Ophir, E., Landa, G., Cohen, H., and Schwartz, M. (2006) Glatiramer acetate fights against Alzheimer's disease by inducing dendritic-like microglia expressing insulin-like growth factor 1, *Proceedings of the National Academy of Sciences 103*, 11784-11789.
251. Dong, H., Goico, B., Martin, M., Csernansky, C. A., Bertchume, A., and Csernansky, J. G. (2004) Modulation of hippocampal cell proliferation, memory, and amyloid plaque deposition in APPsw (Tg2576) mutant mice by isolation stress, *Neuroscience 127*, 601-609.
252. Green, K. N., Billings, L. M., Roozendaal, B., McGaugh, J. L., and LaFerla, F. M. (2006) Glucocorticoids increase amyloid-beta and tau pathology in a mouse model of Alzheimer's disease, *J Neurosci 26*, 9047-9056.

253. Oddo, S., Caccamo, A., Tran, L., Lambert, M. P., Glabe, C. G., Klein, W. L., and LaFerla, F. M. (2006) Temporal Profile of Amyloid-β (Aβ) Oligomerization in an in Vivo Model of Alzheimer Disease: A LINK BETWEEN Aβ AND TAU PATHOLOGY, *Journal of Biological Chemistry 281*, 1599-1604.
254. Oddo, S., Caccamo, A., Smith, I. F., Green, K. N., and LaFerla, F. M. (2006) A dynamic relationship between intracellular and extracellular pools of Abeta, *Am J Pathol 168*, 184-194.
255. Mastrangelo, M. A., and Bowers, W. J. (2008) Detailed immunohistochemical characterization of temporal and spatial progression of Alzheimer's disease-related pathologies in male triple-transgenic mice, *BMC Neurosci 9*, 81.
256. Billings, L. M., Oddo, S., Green, K. N., McGaugh, J. L., and LaFerla, F. M. (2005) Intraneuronal Aβ Causes the Onset of Early Alzheimer's Disease-Related Cognitive Deficits in Transgenic Mice, *Neuron 45*, 675-688.
257. WHO. (1970) Specifications for the identity and purity of food additives and their toxicological evaluation: some food colours, emulsifiers, stabilizers, anticaking agents, and certain other substances: Thirteenth Report of the Joint FAO-WHO Expert Committee on Food Additives, Rome, 27 May-4 June 1969, *World Health Organ Tech Rep Ser 445*, 1-36.
258. Green, F. J., ed (1990) *Sigma-Aldrich Handbook of Stains, Dyes and Indicators*.
259. Cheng, Z., Zhang, J., Liu, H., Li, Y., Zhao, Y., and Yang, E. (2010) Central nervous system penetration for small molecule therapeutic agents does not increase in multiple sclerosis- and Alzheimer's disease-related animal models despite reported blood-brain barrier disruption, *Drug Metab Dispos 38*, 1355-1361.
260. Pardridge, W. M. (2012) Drug transport across the blood-brain barrier, *J Cereb Blood Flow Metab 32*, 1959-1972.
261. Bell, R. D., and Ehlers, M. D. (2014) Breaching the blood-brain barrier for drug delivery, *Neuron 81*, 1-3.
262. Banks, W. A. (2012) Drug delivery to the brain in Alzheimer's disease: consideration of the blood-brain barrier, *Adv Drug Deliv Rev 64*, 629-639.
263. Erickson, M. A., and Banks, W. A. (2013) Blood-brain barrier dysfunction as a cause and consequence of Alzheimer's disease, *J Cereb Blood Flow Metab 33*, 1500-1513.
264. Ryu, J. K., and McLarnon, J. G. (2009) A leaky blood–brain barrier, fibrinogen infiltration and microglial reactivity in inflamed Alzheimer's disease brain, *Journal of Cellular and Molecular Medicine 13*, 2911-2925.
265. Mu, Y., and Gage, F. H. (2011) Adult hippocampal neurogenesis and its role in Alzheimer's disease, *Mol Neurodegener 6*, 85.
266. Intlekofer, K. A., and Cotman, C. W. (2013) Exercise counteracts declining hippocampal function in aging and Alzheimer's disease, *Neurobiol Dis 57*, 47-55.
267. Deane, R., Du Yan, S., Submamaryan, R. K., LaRue, B., Jovanovic, S., Hogg, E., Welch, D., Manness, L., Lin, C., Yu, J., Zhu, H., Ghiso, J., Frangione, B., Stern, A., Schmidt, A. M., Armstrong, D. L., Arnold, B., Liliensiek, B., Nawroth, P., Hofman, F., Kindy, M., Stern, D., and Zlokovic, B. (2003) RAGE mediates amyloid-beta peptide transport across the blood-brain barrier and accumulation in brain, *Nat Med 9*, 907-913.
268. Kawarabayashi, T., Younkin, L. H., Saido, T. C., Shoji, M., Ashe, K. H., and Younkin, S. G. (2001) Age-dependent changes in brain, CSF, and plasma amyloid (beta) protein in the Tg2576 transgenic mouse model of Alzheimer's disease, *J Neurosci 21*, 372-381.

269. Johnson-Wood, K., Lee, M., Motter, R., Hu, K., Gordon, G., Barbour, R., Khan, K., Gordon, M., Tan, H., Games, D., Lieberburg, I., Schenk, D., Seubert, P., and McConlogue, L. (1997) Amyloid precursor protein processing and A beta42 deposition in a transgenic mouse model of Alzheimer disease, *Proc Natl Acad Sci U S A 94*, 1550-1555.
270. Leissring, M. A., Farris, W., Chang, A. Y., Walsh, D. M., Wu, X., Sun, X., Frosch, M. P., and Selkoe, D. J. (2003) Enhanced proteolysis of beta-amyloid in APP transgenic mice prevents plaque formation, secondary pathology, and premature death, *Neuron 40*, 1087-1093.
271. Bayer, T. A., and Wirths, O. (2010) Intracellular accumulation of amyloid-Beta - a predictor for synaptic dysfunction and neuron loss in Alzheimer's disease, *Front Aging Neurosci 2*, 8.
272. Gouras, G. K., Tampellini, D., Takahashi, R. H., and Capetillo-Zarate, E. (2010) Intraneuronal beta-amyloid accumulation and synapse pathology in Alzheimer's disease, *Acta Neuropathol 119*, 523-541.
273. Philipson, O., Lannfelt, L., and Nilsson, L. N. (2009) Genetic and pharmacological evidence of intraneuronal Abeta accumulation in APP transgenic mice, *FEBS Lett 583*, 3021-3026.
274. Wirths, O., and Bayer, T. A. (2012) Intraneuronal Abeta accumulation and neurodegeneration: lessons from transgenic models, *Life Sci 91*, 1148-1152.
275. Umeda, T., Tomiyama, T., Sakama, N., Tanaka, S., Lambert, M. P., Klein, W. L., and Mori, H. (2011) Intraneuronal amyloid beta oligomers cause cell death via endoplasmic reticulum stress, endosomal/lysosomal leakage, and mitochondrial dysfunction in vivo, *J Neurosci Res 89*, 1031-1042.
276. Oakley, H., Cole, S. L., Logan, S., Maus, E., Shao, P., Craft, J., Guillozet-Bongaarts, A., Ohno, M., Disterhoft, J., Van Eldik, L., Berry, R., and Vassar, R. (2006) Intraneuronal beta-amyloid aggregates, neurodegeneration, and neuron loss in transgenic mice with five familial Alzheimer's disease mutations: potential factors in amyloid plaque formation, *J Neurosci 26*, 10129-10140.
277. Crowther, D. C., Kinghorn, K. J., Miranda, E., Page, R., Curry, J. A., Duthie, F. A., Gubb, D. C., and Lomas, D. A. (2005) Intraneuronal Abeta, non-amyloid aggregates and neurodegeneration in a Drosophila model of Alzheimer's disease, *Neuroscience 132*, 123-135.
278. LaFerla, F. M., Green, K. N., and Oddo, S. (2007) Intracellular amyloid-beta in Alzheimer's disease, *Nat Rev Neurosci 8*, 499-509.
279. Tampellini, D., Rahman, N., Gallo, E. F., Huang, Z., Dumont, M., Capetillo-Zarate, E., Ma, T., Zheng, R., Lu, B., Nanus, D. M., Lin, M. T., and Gouras, G. K. (2009) Synaptic activity reduces intraneuronal Abeta, promotes APP transport to synapses, and protects against Abeta-related synaptic alterations, *J Neurosci 29*, 9704-9713.
280. Knobloch, M., Konietzko, U., Krebs, D. C., and Nitsch, R. M. (2007) Intracellular Abeta and cognitive deficits precede beta-amyloid deposition in transgenic arcAbeta mice, *Neurobiol Aging 28*, 1297-1306.
281. Wirths, O., Multhaup, G., and Bayer, T. A. (2004) A modified beta-amyloid hypothesis: intraneuronal accumulation of the beta-amyloid peptide--the first step of a fatal cascade, *J Neurochem 91*, 513-520.

282. Gouras, G. K., Willen, K., and Tampellini, D. (2012) Critical role of intraneuronal Abeta in Alzheimer's disease: technical challenges in studying intracellular Abeta, *Life Sci 91*, 1153-1158.
283. Gouras, G. K., Almeida, C. G., and Takahashi, R. H. (2005) Intraneuronal Abeta accumulation and origin of plaques in Alzheimer's disease, *Neurobiol Aging 26*, 1235-1244.
284. Casas, C., Sergeant, N., Itier, J. M., Blanchard, V., Wirths, O., van der Kolk, N., Vingtdeux, V., van de Steeg, E., Ret, G., Canton, T., Drobecq, H., Clark, A., Bonici, B., Delacourte, A., Benavides, J., Schmitz, C., Tremp, G., Bayer, T. A., Benoit, P., and Pradier, L. (2004) Massive CA1/2 neuronal loss with intraneuronal and N-terminal truncated Abeta42 accumulation in a novel Alzheimer transgenic model, *Am J Pathol 165*, 1289-1300.
285. Kienlen-Campard, P., Miolet, S., Tasiaux, B., and Octave, J. N. (2002) Intracellular amyloid-beta 1-42, but not extracellular soluble amyloid-beta peptides, induces neuronal apoptosis, *J Biol Chem 277*, 15666-15670.
286. Gouras, G. K., Tsai, J., Naslund, J., Vincent, B., Edgar, M., Checler, F., Greenfield, J. P., Haroutunian, V., Buxbaum, J. D., Xu, H., Greengard, P., and Relkin, N. R. (2000) Intraneuronal Abeta42 accumulation in human brain, *Am J Pathol 156*, 15-20.
287. Friedrich, R. P., Tepper, K., Ronicke, R., Soom, M., Westermann, M., Reymann, K., Kaether, C., and Fandrich, M. (2010) Mechanism of amyloid plaque formation suggests an intracellular basis of Abeta pathogenicity, *Proc Natl Acad Sci U S A 107*, 1942-1947.
288. Takahashi, R. H., Milner, T. A., Li, F., Nam, E. E., Edgar, M. A., Yamaguchi, H., Beal, M. F., Xu, H., Greengard, P., and Gouras, G. K. (2002) Intraneuronal Alzheimer abeta42 accumulates in multivesicular bodies and is associated with synaptic pathology, *Am J Pathol 161*, 1869-1879.
289. Maezawa, I., Hong, H. S., Wu, H. C., Battina, S. K., Rana, S., Iwamoto, T., Radke, G. A., Pettersson, E., Martin, G. M., Hua, D. H., and Jin, L. W. (2006) A novel tricyclic pyrone compound ameliorates cell death associated with intracellular amyloid-beta oligomeric complexes, *J Neurochem 98*, 57-67.
290. Jarvis, C. I., Goncalves, M. B., Clarke, E., Dogruel, M., Kalindjian, S. B., Thomas, S. A., Maden, M., and Corcoran, J. P. (2010) Retinoic acid receptor-alpha signalling antagonizes both intracellular and extracellular amyloid-beta production and prevents neuronal cell death caused by amyloid-beta, *Eur J Neurosci 32*, 1246-1255.
291. Cole, S. L., Grudzien, A., Manhart, I. O., Kelly, B. L., Oakley, H., and Vassar, R. (2005) Statins cause intracellular accumulation of amyloid precursor protein, beta-secretase-cleaved fragments, and amyloid beta-peptide via an isoprenoid-dependent mechanism, *J Biol Chem 280*, 18755-18770.
292. D'Andrea, M. R., Lee, D. H. S., Wang, H.-Y., and Nagele, R. G. (2002) Targeting intracellular Aβ42 for Alzheimer's disease drug discovery, *Drug Development Research 56*, 194-200.
293. Fuller, S. J., Storey, E., Li, Q. X., Smith, A. I., Beyreuther, K., and Masters, C. L. (1995) Intracellular production of beta A4 amyloid of Alzheimer's disease: modulation by phosphoramidon and lack of coupling to the secretion of the amyloid precursor protein, *Biochemistry 34*, 8091-8098.
294. Green, K. N., Martinez-Coria, H., Khashwji, H., Hall, E. B., Yurko-Mauro, K. A., Ellis, L., and LaFerla, F. M. (2007) Dietary docosahexaenoic acid and docosapentaenoic acid

ameliorate amyloid-beta and tau pathology via a mechanism involving presenilin 1 levels, *J Neurosci 27*, 4385-4395.
295. Lee, L. L., Ha, H., Chang, Y.-T., and DeLisa, M. P. (2009) Discovery of amyloid-beta aggregation inhibitors using an engineered assay for intracellular protein folding and solubility, *Protein Sci. 18*, 277-286.
296. Vingtdeux, V., Chandakkar, P., Zhao, H., d'Abramo, C., Davies, P., and Marambaud, P. (2011) Novel synthetic small-molecule activators of AMPK as enhancers of autophagy and amyloid-beta peptide degradation, *Faseb J 25*, 219-231.
297. Qin, X. Y., Cheng, Y., and Yu, L. C. (2012) Potential protection of green tea polyphenols against intracellular amyloid beta-induced toxicity on primary cultured prefrontal cortical neurons of rats, *Neurosci Lett 513*, 170-173.
298. Lin, C. L., Chen, T. F., Chiu, M. J., Way, T. D., and Lin, J. K. (2009) Epigallocatechin gallate (EGCG) suppresses beta-amyloid-induced neurotoxicity through inhibiting c-Abl/FE65 nuclear translocation and GSK3 beta activation, *Neurobiol Aging 30*, 81-92.
299. Hirata-Fukae, C., Li, H. F., Hoe, H. S., Gray, A. J., Minami, S. S., Hamada, K., Niikura, T., Hua, F., Tsukagoshi-Nagai, H., Horikoshi-Sakuraba, Y., Mughal, M., Rebeck, G. W., LaFerla, F. M., Mattson, M. P., Iwata, N., Saido, T. C., Klein, W. L., Duff, K. E., Aisen, P. S., and Matsuoka, Y. (2008) Females exhibit more extensive amyloid, but not tau, pathology in an Alzheimer transgenic model, *Brain Res 1216*, 92-103.
300. Lord, A., Kalimo, H., Eckman, C., Zhang, X. Q., Lannfelt, L., and Nilsson, L. N. (2006) The Arctic Alzheimer mutation facilitates early intraneuronal Abeta aggregation and senile plaque formation in transgenic mice, *Neurobiol Aging 27*, 67-77.
301. Tomiyama, T., Matsuyama, S., Iso, H., Umeda, T., Takuma, H., Ohnishi, K., Ishibashi, K., Teraoka, R., Sakama, N., Yamashita, T., Nishitsuji, K., Ito, K., Shimada, H., Lambert, M. P., Klein, W. L., and Mori, H. (2010) A mouse model of amyloid beta oligomers: their contribution to synaptic alteration, abnormal tau phosphorylation, glial activation, and neuronal loss in vivo, *J Neurosci 30*, 4845-4856.
302. Martins, I. C., Kuperstein, I., Wilkinson, H., Maes, E., Vanbrabant, M., Jonckheere, W., Van Gelder, P., Hartmann, D., D'Hooge, R., De Strooper, B., Schymkowitz, J., and Rousseau, F. (2008) Lipids revert inert Abeta amyloid fibrils to neurotoxic protofibrils that affect learning in mice, *Embo J 27*, 224-233.
303. Jiang, L. H., Mackenzie, A. B., North, R. A., and Surprenant, A. (2000) Brilliant blue G selectively blocks ATP-gated rat P2X(7) receptors, *Mol Pharmacol 58*, 82-88.
304. Rezai-Zadeh, K., Shytle, D., Sun, N., Mori, T., Hou, H., Jeanniton, D., Ehrhart, J., Townsend, K., Zeng, J., Morgan, D., Hardy, J., Town, T., and Tan, J. (2005) Green tea epigallocatechin-3-gallate (EGCG) modulates amyloid precursor protein cleavage and reduces cerebral amyloidosis in Alzheimer transgenic mice, *J Neurosci 25*, 8807-8814.
305. Schmitt, U., and Hiemke, C. (1998) Strain differences in open-field and elevated plus-maze behavior of rats without and with pretest handling, *Pharmacol Biochem Behav 59*, 807-811.
306. Hilakivi-Clarke, L. A. (1992) Injection of vehicle is not a stressor in Porsolt's swim test, *Pharmacol Biochem Behav 42*, 193-196.
307. Gariepy, J. L., Rodriguiz, R. M., and Jones, B. C. (2002) Handling, genetic and housing effects on the mouse stress system, dopamine function, and behavior, *Pharmacol Biochem Behav 73*, 7-17.

308. Kempermann, G., Kuhn, H. G., and Gage, F. H. (1997) More hippocampal neurons in adult mice living in an enriched environment, *Nature 386*, 493-495.
309. Parihar, V. K., Hattiangady, B., Kuruba, R., Shuai, B., and Shetty, A. K. (2011) Predictable chronic mild stress improves mood, hippocampal neurogenesis and memory, *Mol Psychiatry 16*, 171-183.
310. Joels, M., Karst, H., Krugers, H. J., and Lucassen, P. J. (2007) Chronic stress: implications for neuronal morphology, function and neurogenesis, *Front Neuroendocrinol 28*, 72-96.
311. Misslin, R., Herzog, F., Koch, B., and Ropartz, P. (1982) Effects of isolation, handling and novelty on the pituitary--adrenal response in the mouse, *Psychoneuroendocrinology 7*, 217-221.
312. Lapin, I. P. (1995) Only controls: effect of handling, sham injection, and intraperitoneal injection of saline on behavior of mice in an elevated plus-maze, *J Pharmacol Toxicol Methods 34*, 73-77.
313. Stein-Behrens, B., Mattson, M. P., Chang, I., Yeh, M., and Sapolsky, R. (1994) Stress exacerbates neuron loss and cytoskeletal pathology in the hippocampus, *J Neurosci 14*, 5373-5380.
314. Jeong, Y. H., Park, C. H., Yoo, J., Shin, K. Y., Ahn, S. M., Kim, H. S., Lee, S. H., Emson, P. C., and Suh, Y. H. (2006) Chronic stress accelerates learning and memory impairments and increases amyloid deposition in APPV717I-CT100 transgenic mice, an Alzheimer's disease model, *Faseb J 20*, 729-731.
315. Brett, R. R., and Pratt, J. A. (1990) Chronic handling modifies the anxiolytic effect of diazepam in the elevated plus-maze, *Eur J Pharmacol 178*, 135-138.
316. Esposito, P., Gheorghe, D., Kandere, K., Pang, X., Connolly, R., Jacobson, S., and Theoharides, T. C. (2001) Acute stress increases permeability of the blood-brain-barrier through activation of brain mast cells, *Brain Res 888*, 117-127.
317. Dong, H., and Csernansky, J. G. (2009) Effects of stress and stress hormones on amyloid-beta protein and plaque deposition, *J Alzheimers Dis 18*, 459-469.
318. Goodman, Y., Bruce, A. J., Cheng, B., and Mattson, M. P. (1996) Estrogens attenuate and corticosterone exacerbates excitotoxicity, oxidative injury, and amyloid beta-peptide toxicity in hippocampal neurons, *J Neurochem 66*, 1836-1844.
319. Iga, T., Awazu, S., Hanano, M., and Nogami, H. (1971) Pharmacokinetic studies of biliary excretion. IV. The relationship between the biliary excretion behavior and the elimination from plasma of azo dyes and triphenylmethane dyes in rat, *Chem Pharm Bull (Tokyo) 19*, 2609-2616.
320. Iga, T., Awazu, S., and Nogami, H. (1971) Pharmacokinetic study of biliary excretion. II. Comparison of excretion behavior in triphenylmethane dyes, *Chem Pharm Bull (Tokyo) 19*, 273-281.
321. Phillips, J. C., Mendis, D., Eason, C. T., and Gangolli, S. D. (1980) The metabolic disposition of 14C-labelled green S and Brilliant Blue FCF in the rat, mouse and guinea-pig, *Food Cosmet Toxicol 18*, 7-13.
322. Sinton, C. M., Fitch, T. E., Petty, F., and Haley, R. W. (2000) Stressful manipulations that elevate corticosterone reduce blood-brain barrier permeability to pyridostigmine in the Rat, *Toxicol Appl Pharmacol 165*, 99-105.

323. Stonestreet, B. S., Petersson, K. H., Sadowska, G. B., Pettigrew, K. D., and Patlak, C. S. (1999) Antenatal steroids decrease blood-brain barrier permeability in the ovine fetus, *Am J Physiol 276*, R283-289.
324. Wisniewski, T., and Sigurdsson, E. M. (2010) Murine models of Alzheimer's disease and their use in developing immunotherapies, *Biochimica et Biophysica Acta (BBA) - Molecular Basis of Disease 1802*, 847-859.
325. Zhou, J., Kong, H., Hua, X., Xiao, M., Ding, J., and Hu, G. (2008) Altered blood-brain barrier integrity in adult aquaporin-4 knockout mice, *Neuroreport 19*, 1-5.
326. Liu, L., Su, Y., Yang, W., Xiao, M., Gao, J., and Hu, G. (2010) Disruption of neuronal-glial-vascular units in the hippocampus of ovariectomized mice injected with D-galactose, *Neuroscience 169*, 596-608.
327. Lemkul, J. A., and Bevan, D. R. (2012) The Role of Molecular Simulations in the Development of Inhibitors of Amyloid β-Peptide Aggregation for the Treatment of Alzheimer's Disease, *ACS Chemical Neuroscience 3*, 845-856.
328. Flaherty, D. P., Walsh, S. M., Kiyota, T., Dong, Y., Ikezu, T., and Vennerstrom, J. L. (2007) Polyfluorinated Bis-styrylbenzene β-Amyloid Plaque Binding Ligands, *Journal of Medicinal Chemistry 50*, 4986-4992.
329. Maya, Y., Ono, M., Watanabe, H., Haratake, M., Saji, H., and Nakayama, M. (2008) Novel Radioiodinated Aurones as Probes for SPECT Imaging of β-Amyloid Plaques in the Brain, *Bioconjugate Chemistry 20*, 95-101.
330. Ono, M., Kung, M.-P., Hou, C., and Kung, H. F. (2002) Benzofuran derivatives as Aβ-aggregate-specific imaging agents for Alzheimer's disease, *Nuclear Medicine and Biology 29*, 633-642.
331. Ye, L., Morgenstern, J. L., Lamb, J. R., and Lockhart, A. (2006) Characterisation of the binding of amyloid imaging tracers to rodent Aβ fibrils and rodent-human Aβ co-polymers, *Biochemical and Biophysical Research Communications 347*, 669-677.
332. Zeng, F., Alagille, D., Tamagnan, G. D., Ciliax, B. J., Levey, A. I., and Goodman, M. M. (2010) Synthesis and In Vitro Evaluation of Imidazo[1,2-b]pyridazines as Ligands for β-Amyloid Plaques, *ACS Medicinal Chemistry Letters 1*, 80-84.
333. Zhuang, Z.-P., Kung, M.-P., Wilson, A., Lee, C.-W., Plössl, K., Hou, C., Holtzman, D. M., and Kung, H. F. (2002) Structure−Activity Relationship of Imidazo[1,2-a]pyridines as Ligands for Detecting β-Amyloid Plaques in the Brain, *Journal of Medicinal Chemistry 46*, 237-243.
334. Liu, Y. H., Wang, Y. R., Xiang, Y., Zhou, H. D., Giunta, B., Manucat-Tan, N. B., Tan, J., Zhou, X. F., and Wang, Y. J. (2014) Clearance of Amyloid-Beta in Alzheimer's Disease: Shifting the Action Site from Center to Periphery, *Mol Neurobiol*.
335. Deane, R., Bell, R. D., Sagare, A., and Zlokovic, B. V. (2009) Clearance of amyloid-beta peptide across the blood-brain barrier: implication for therapies in Alzheimer's disease, *CNS Neurol Disord Drug Targets 8*, 16-30.
336. Ito, S., Matsumiya, K., Ohtsuki, S., Kamiie, J., and Terasaki, T. (2013) Contributions of degradation and brain-to-blood elimination across the blood-brain barrier to cerebral clearance of human amyloid-beta peptide(1-40) in mouse brain, *J Cereb Blood Flow Metab 33*, 1770-1777.
337. Wang, Y. J., Zhou, H. D., and Zhou, X. F. (2006) Clearance of amyloid-beta in Alzheimer's disease: progress, problems and perspectives, *Drug Discov Today 11*, 931-938.

338. Ito, S., Ohtsuki, S., Kamiie, J., Nezu, Y., and Terasaki, T. (2007) Cerebral clearance of human amyloid-β peptide (1–40) across the blood–brain barrier is reduced by self-aggregation and formation of low-density lipoprotein receptor-related protein-1 ligand complexes, *Journal of Neurochemistry 103*, 2482-2490.
339. Zlokovic, B. V. (2004) Clearing amyloid through the blood-brain barrier, *J Neurochem 89*, 807-811.
340. Miners, J. S., Barua, N., Kehoe, P. G., Gill, S., and Love, S. (2011) Abeta-degrading enzymes: potential for treatment of Alzheimer disease, *J Neuropathol Exp Neurol 70*, 944-959.
341. Borzelleca, J. F., and Hallagan, J. B. (1987) Lifetime toxicity/carcinogenicity study of FD & C Red No. 3 (erythrosine) in mice, *Food and Chemical Toxicology 25*, 735-737.
342. Borzelleca, J. F., Capen, C. C., and Hallagan, J. B. (1987) Lifetime toxicity/carcinogenicity study of FD & C Red No. 3 (erythrosine) in rats, *Food and Chemical Toxicology 25*, 723-733.
343. Jennings, A. S., Schwartz, S. L., Balter, N. J., Gardner, D., and Witorsch, R. J. (1990) Effects of oral erythrosine (2′,4′,5′,7′-tetraiodofluorescein) on the pituitary-thyroid axis in rats, *Toxicology and Applied Pharmacology 103*, 549-556.
344. Tanaka, T. (2001) Reproductive and neurobehavioural toxicity study of erythrosine administered to mice in the diet, *Food and Chemical Toxicology 39*, 447-454.
345. Halpert, B., and Hanke, M. T. (1932) Some Phases Of Liver And Gall-Bladder Function: Experiments on Rabbits with Certain Organic Compounds, Particularly Dyes, *American Journal of Physiology -- Legacy Content 100*, 433-442.
346. Collins, T. F. X., and Long, E. L. (1976) Effects of chronic oral administration of erythrosine in the Mongolian gerbil, *Food and Cosmetics Toxicology 14*, 233-248.
347. Kuluz, J. W., Prado, R., He, D., Zhao, W., Dietrich, W. D., and Watson, B. (2007) New Pediatric Model of Ischemic Stroke in Infant Piglets by Photothrombosis: Acute Changes in Cerebral Blood Flow, Microvasculature, and Early Histopathology, *Stroke 38*, 1932-1937.
348. Dalal, A., and Poddar, M. K. (2009) Short-term erythrosine B-induced inhibition of the brain regional serotonergic activity suppresses motor activity (exploratory behavior) of young adult mammals, *Pharmacology Biochemistry and Behavior 92*, 574-582.
349. Zuno, A., Marcon, F., Leopardi, P., Salvatore, G., Carere, A., and Crebelli, R. (1994) An assessment of the in vivo clastogenicity of erythrosine, *Food and Chemical Toxicology 32*, 159-163.
350. Abdel Aziz, A. H., Shouman, S. A., Attia, A. S., and Saad, S. F. (1997) A Study On The Reproductive Toxicity Of Erythrosine In Male Mice, *Pharmacological Research 35*, 457-462.
351. Hiasa, Y., Ohshima, M., Kitahori, Y., Konishi, N., Shimoyama, T., Sakaguchi, Y., Hashimoto, H., Minami, S., and Kato, Y. (1988) The Promoting Effects of Food Dyes, Erythrosine (Red 3) and Rose Bengal B (Red 105), on Thyroid Tumors in Partially Thyroidectomized N-Bis(2-hydroxypropyl)- nitrosamine-treated Rats, *Cancer Science 79*, 314-319.
352. Lutty, G. A. (1978) The acute intravenous toxicity of biological stains, dyes, and other fluorescent substances, *Toxicology and Applied Pharmacology 44*, 225-249.

353. Butterworth, K. R., Gaunt, I. F., Grasso, P., and Gangolli, S. D. (1976) Acute and short-term toxicity studies on erythrosine BS in rodents, *Food and Cosmetics Toxicology 14*, 525-531.
354. Hansen, W. H., Zwickey, R. E., Brouwer, J. B., and Fitzhugh, O. G. (1973) Long-term toxicity studies of erythrosine. I. Effects in rats and dogs, *Food and Cosmetics Toxicology 11*, 527-534.
355. Vorhees, C., Butcher, R., Brunner, R., Wootten, V., and Sobotka, T. (1983) A developmental toxicity and psychotoxicity evaluation of FD and C Red Dye #3 (erythrosine) in rats, *Archives of Toxicology 53*, 253-264.
356. Walton, K., Walker, R., van de Sandt, J. J. M., Castell, J. V., Knapp, A. G. A. A., Kozianowski, G., Roberfroid, M., and Schilter, B. (1999) The application of in vitro data in the derivation of the Acceptable Daily Intake of food additives, *Food and Chemical Toxicology 37*, 1175-1197.

Appendix A: Chapter 2 (In Vitro Structure-Activity Relationship Analysis of Erythrosin B Analogs Reveals That Halogenation Generates Effective Binders and Modulators of Amyloid-Beta Monomer Aggregation and Neurotoxicity) Supplemental Information

Table A1 - Spectral interference in the MTT absorbance by the residual dyes in the plate after washing. *1st Row of Table A1 - Determination of the Dye Remaining in the Plate During the MTT Assay.* The MTT assay was carried out as described previously in the MTT methods section in Chapter 2, but with 10 μL of each dye-only control (3x concentration - no Aβ) being added to each well. The absorbance of each dye was read at the respective absorbance maximum (ERB – 540 nm, PHB – 554 nm, EOB – 520 nm, ROB – 562 nm, EOY – 530 nm, and FLN – 492 nm) both before and after the washing steps described. After subtracting the appropriate background for both readings, the post-washing absorbance was normalized to the pre-wash absorbance in order to determine the fraction of each dye remaining after washing. *2nd and 3rd Rows of Table A1 - Determination of the Spectral Interference of the Dyes During the MTT Assay*. To quantify the interference that varying fractions of residual dye remaining in the cell wells have on the final reduced form of MTT (MTT-formazan) absorbance signal, fresh media was first added to a new cell culture plate without cells. Next, 7 μL of 1 mg/mL MTT-formazan in DMSO was added to each well along with 0.01 and 0.05 fractions of each original dye amount or PBS. The absorbance of the samples was measured at 506 nm. After subtracting the background contribution of the media and DMSO, the absorbance values of the wells containing the varying dye fractions and MTT-formazan mixture were normalized to the wells with PBS/MTT-formazan to obtain the change induced in the MTT signal by the dyes left behind after washing (minimum triplicates tested).

Dye		**FLN**	**ERB**	**EOY**	**ROB**	**PHB**	**EOB**
Residual dye after washing (%)		1.3	1.8	1.0	1.6	1.0	2.5
Change in the MTT absorbance with dye (%)	**1% dye**	1.4	0.4	-1.4	3.6	1.1	2.3
	5% dye	5.1	0.4	-1.8	3.8	0.9	3.9

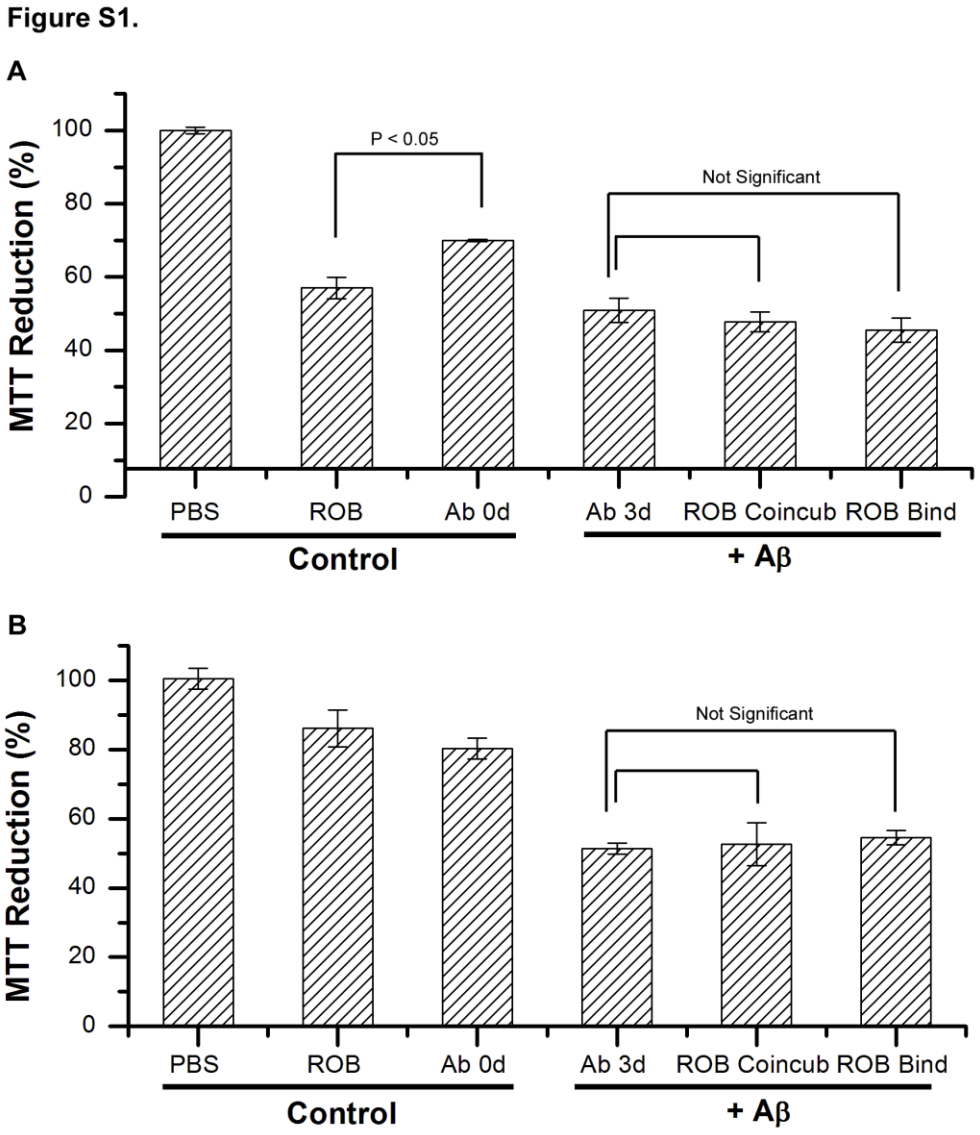

Figure A1 - MTT assay for ROB to assess viability of neuroblastoma SH-SY5Y cells. Three controls (PBS buffer, ROB, and Aβ 0 d monomer) and two Aβ aggregates formed in the absence (Aβ 3 d) or presence (ROB Coincub) of 3x ROB at 37 °C for 3 days. The Aβ and ROB concentrations used were 5 and 15 μM, respectively (A). The Aβ and ROB concentrations used were 2.5 and 7.5 μM, respectively (B). The ROB Bind sample refers to taking Aβ 3d aggregates formed in the absence of any dye and mixing them with 3x ROB immediately before addition to the cells. Values represent means ± standard deviation ($n \geq 3$). Values are normalized to the viability of cells administered with PBS buffer only. Two-sided Student's t-tests were applied to the MTT reduction data. (Not significant: $P > 0.05$).

Figure S2.

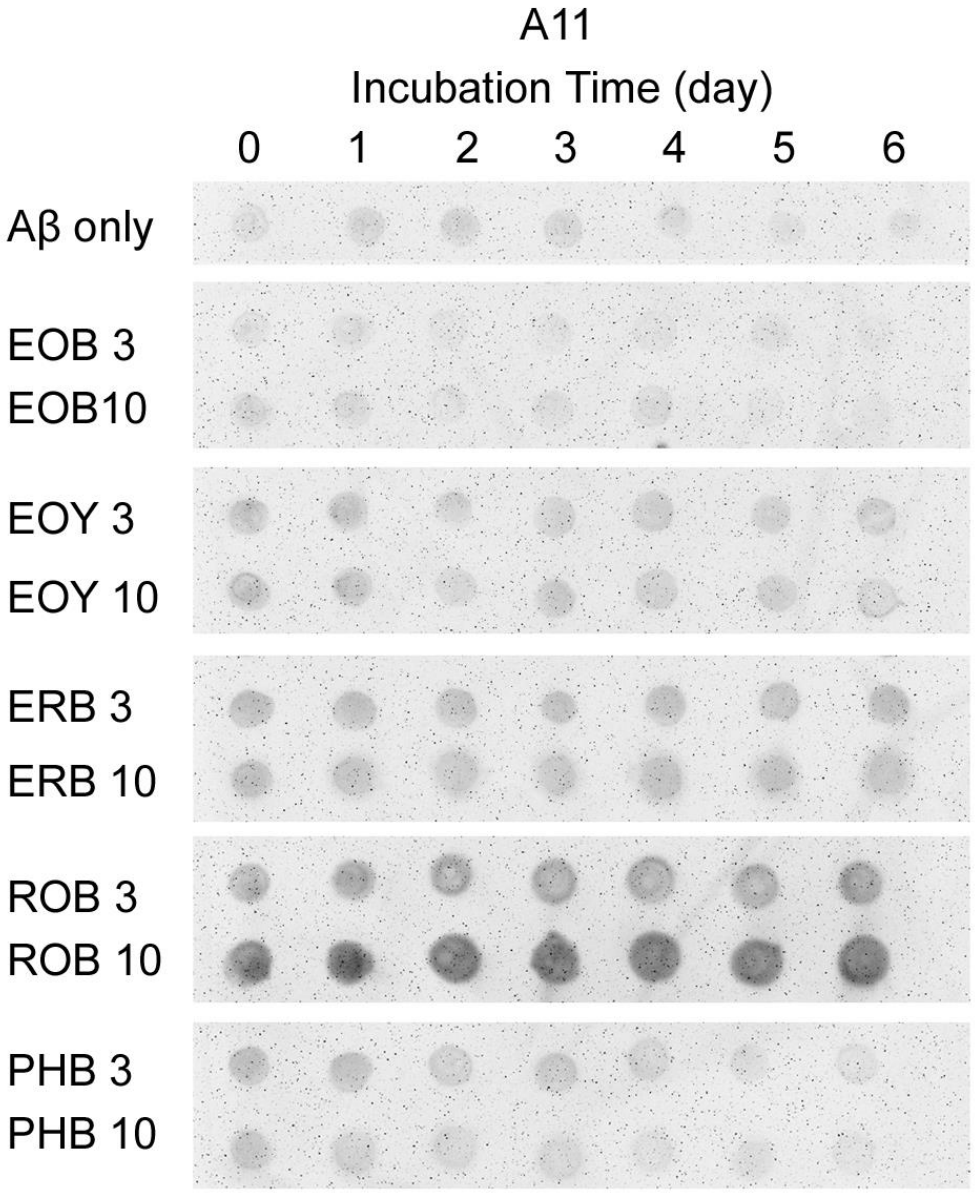

Figure A2 - Dot blot assay results using the A11 antibody. 50 μM of Aβ monomer was incubated at 37 °C in the absence (Aβ only) or presence of 3x and 10x ERB analogs (EOB, EOY, ERB, ROB, and PHB) for up to 6 days. The samples were taken on the indicated day and then all samples were spotted onto one nitrocellulose membrane. The membrane was immunostained with the A11 antibody. For clearer presentation, the sections of the membrane were cut and re-arranged.

Figure S3.

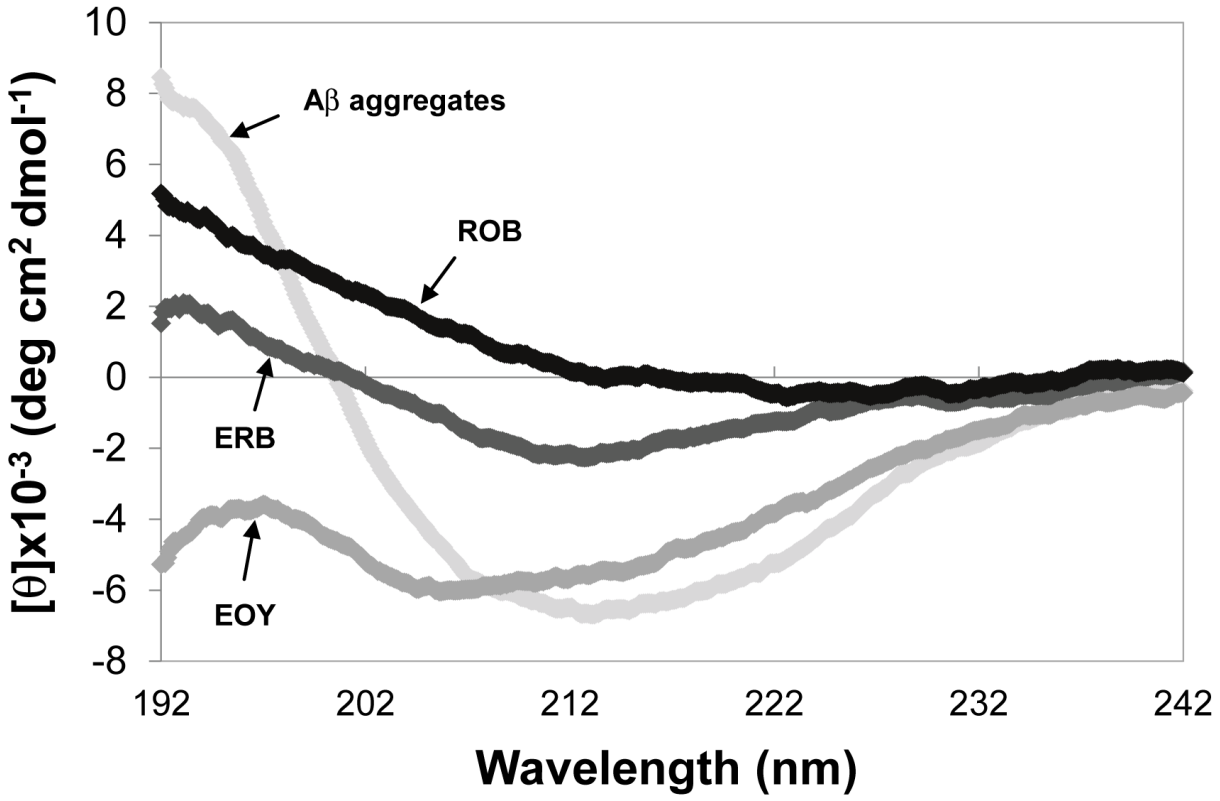

Figure A3 - CD spectra of the Aβ aggregates formed in the absence (Aβ aggregates) or presence of 3x EOY, ERB, or ROB for 9 days at 37 °C.

Figure S4.

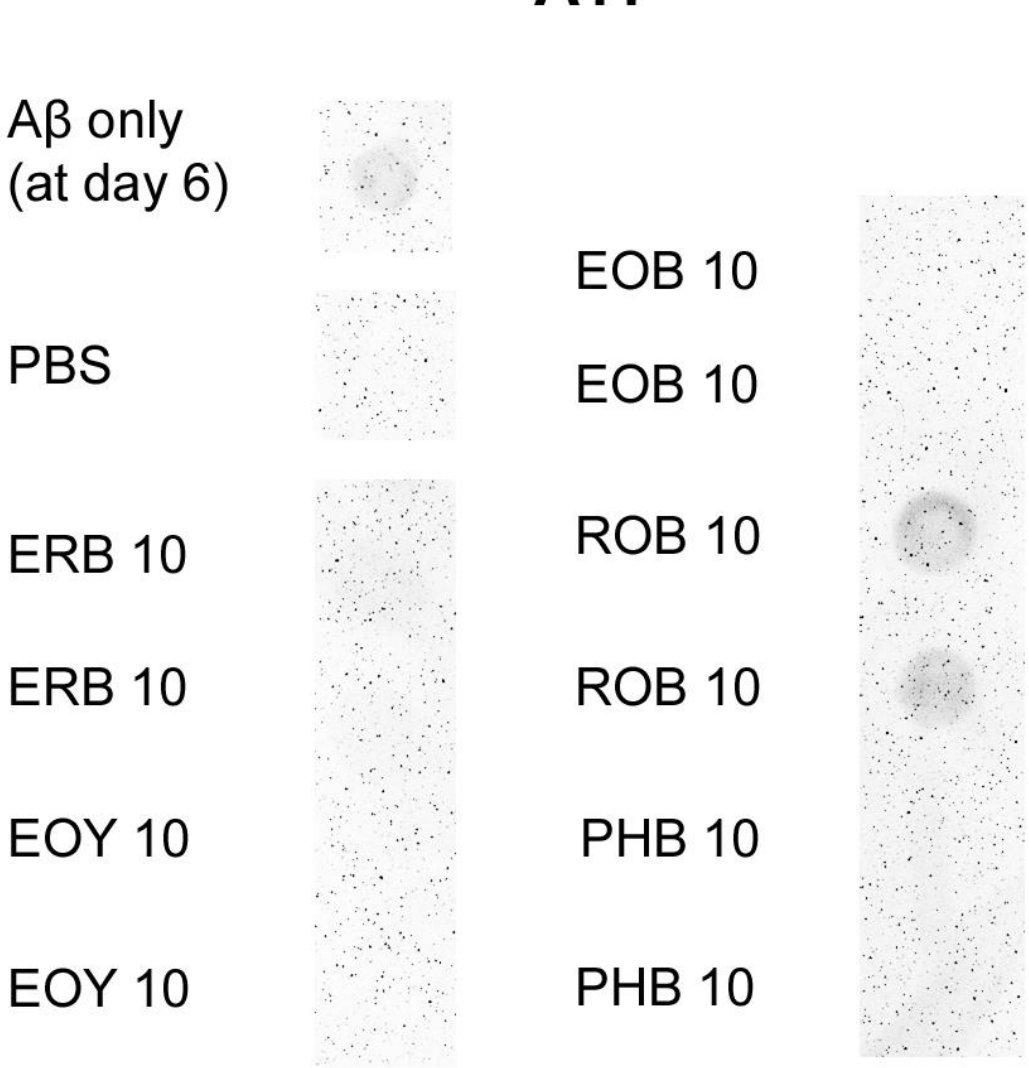

Figure A4 - Dot-blot assay results using the A11 antibody. The A11-reactive Aβ aggregates (Aβ at day 6), PBS buffer, and 10x ERB analogs were spotted into one nitrocellulose membrane. Then, the membrane was immunostained with the A11 antibody. The sections from the same membrane were cut and re-arranged.

Figure S5.

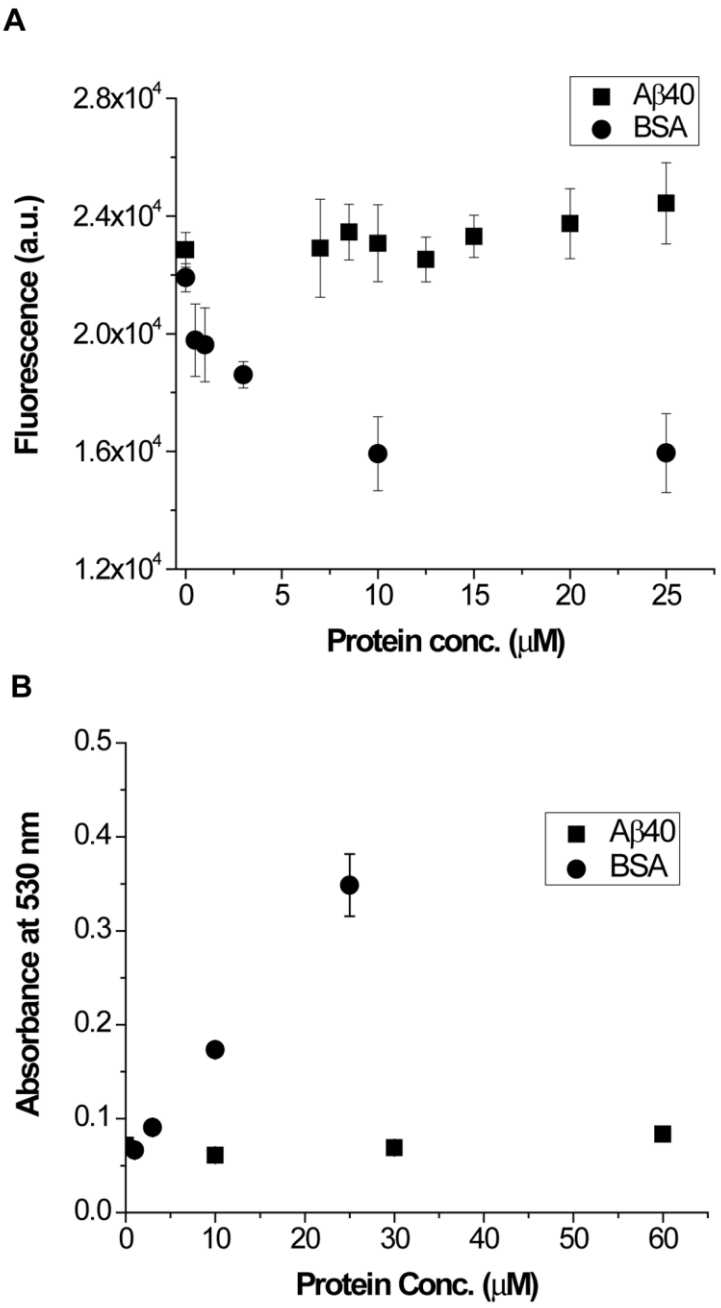

Figure A5 - Assessment of binding of FLN and EOB to Aβ40 monomers and BSA. (A) Fluorescence of FLN with varying concentrations (0 to 25 μM) of BSA and Aβ40 (excitation at 432 nm and emission at 512 nm). (B) Absorbance of EOB with varying concentrations of BSA (0 to 25 μM) and Aβ40 (0 to 60 μM).

Appendix B: Chapter 3 (Creation and Use of an In Vitro Ligand Binding Site Identification Method to Characterize Erythrosin B and Structural Analogs Ligand Binding Sites on Aβ Target Peptide Monomer) Supplemental Information

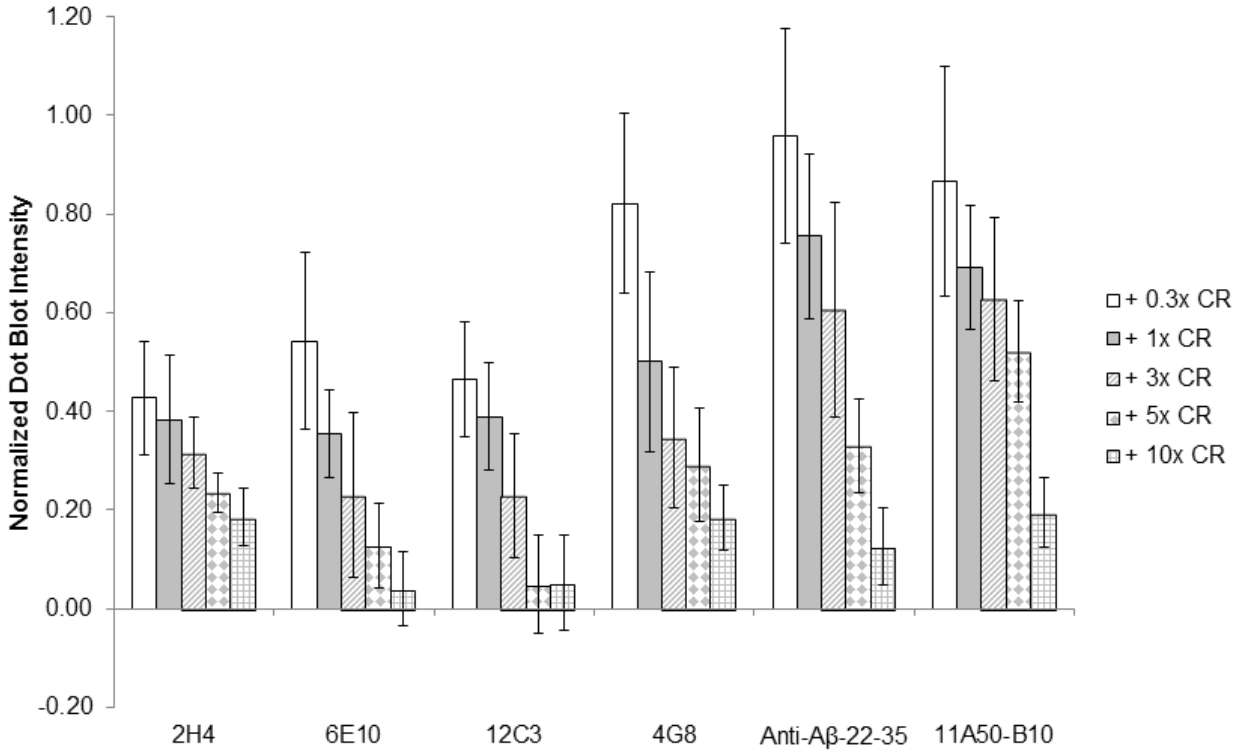

Figure B1 - Congo Red (CR) ligand binding site identification quantification and dose dependency using sequence specific antibody panel. Average dot blot intensities (quantified using Image J) of 0.3x (white bars), 1x (grey bars), 3x (diagonal marked bars), 5x (diamond marked bars), and 10x (checker marked bars) CR samples normalized to each respective Aβ40 (no CR) control sample average signal. Error bars indicate standard deviation, $n \geq 6$.

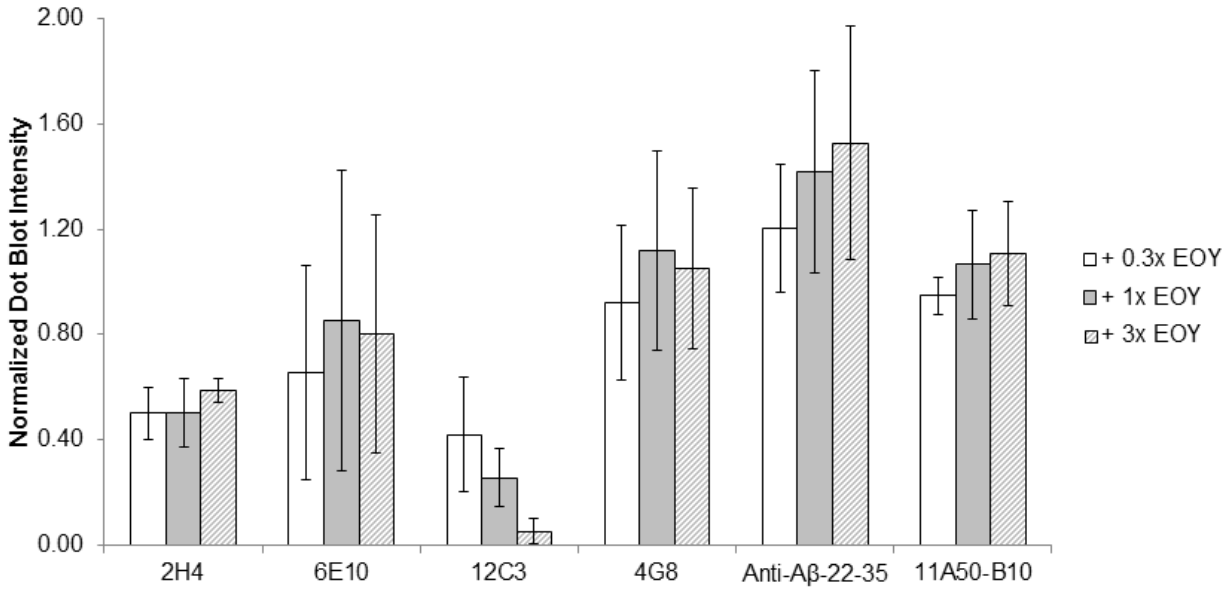

Figure B2 - Eosin Y (EOY) ligand binding site identification quantification and dose dependency using sequence specific antibody panel. Average dot blot intensities (quantified using Image J) of 0.3x (white bars), 1x (grey bars), and 3x (diagonal marked bars) EOY samples normalized to each respective Aβ40 (no EOY) control sample average signal. Error bars indicate standard deviation, $n \geq 4$.

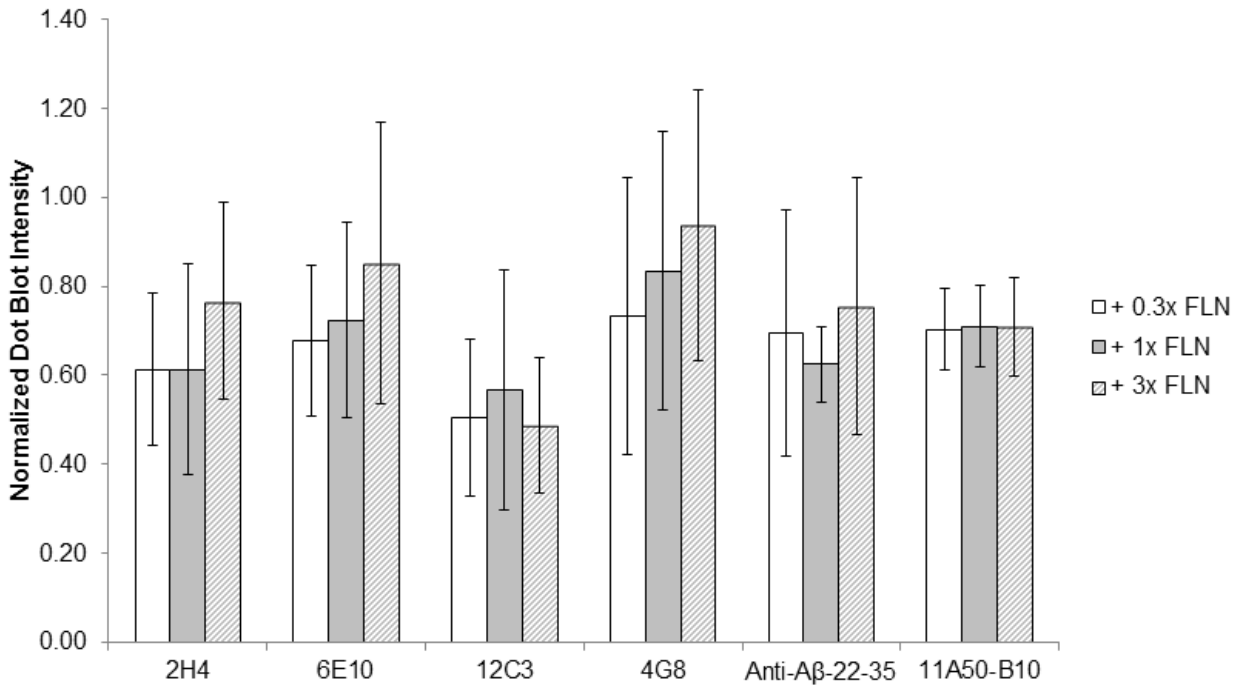

Figure B3 - Fluorescein (FLN) ligand binding site identification quantification and dose dependency using sequence specific antibody panel. Average dot blot intensities (quantified using Image J) of 0.3x (white bars), 1x (grey bars), and 3x (diagonal marked bars) FLN samples normalized to each respective Aβ40 (no FLN) control sample average signal. Error bars indicate standard deviation, $n \geq 4$.

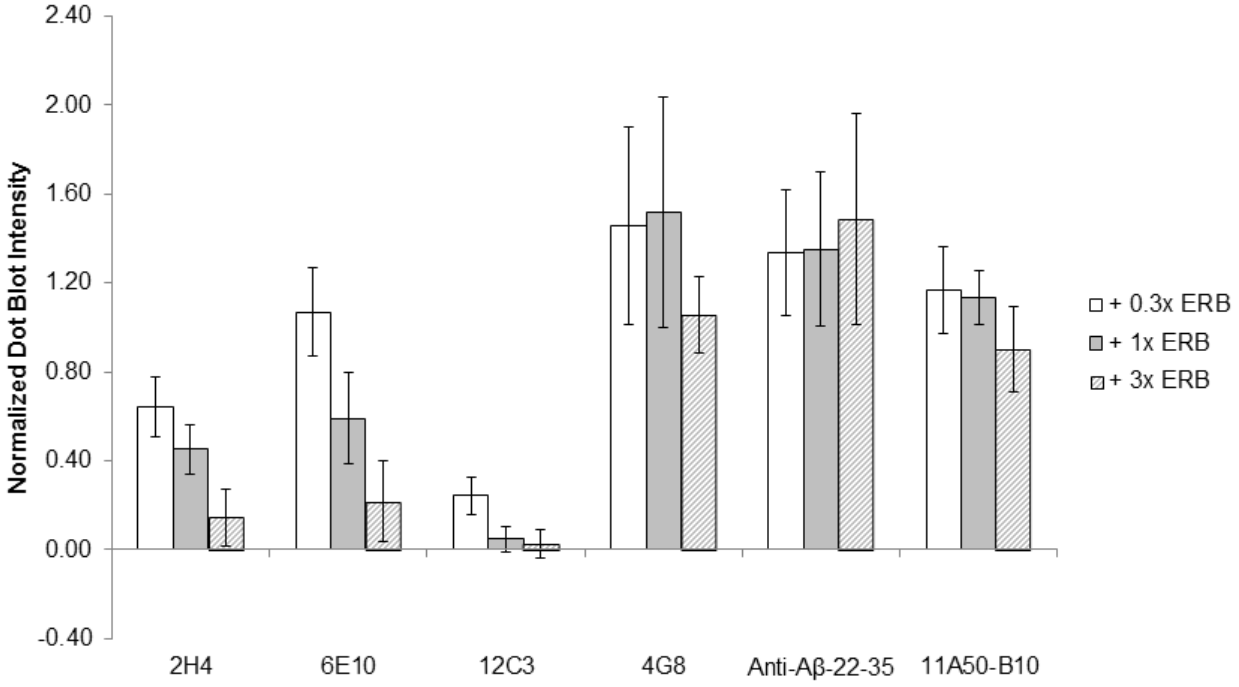

Figure B4 - Erythrosin B (ERB) ligand binding site identification quantification and dose dependency using sequence specific antibody panel. Average dot blot intensities (quantified using Image J) of 0.3x (white bars), 1x (grey bars), and 3x (diagonal marked bars) ERB samples normalized to each respective Aβ40 (no ERB) control sample average signal. Error bars indicate standard deviation, $n \geq 3$.

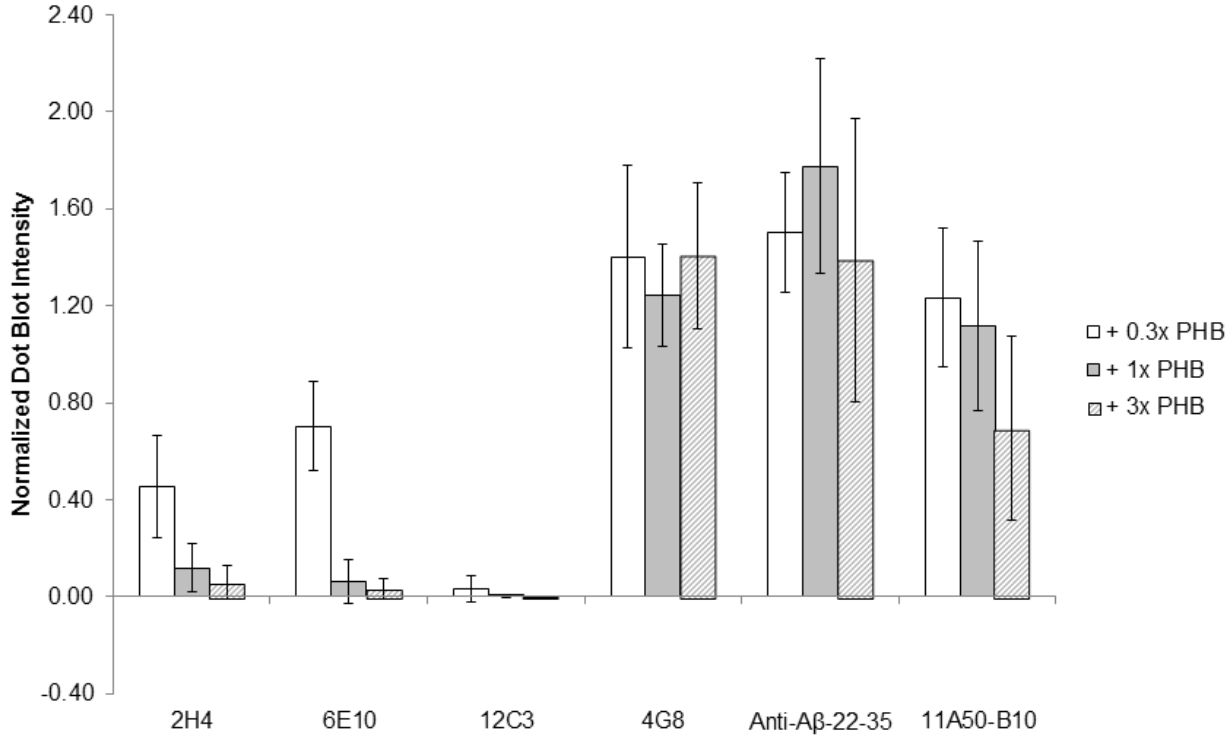

Figure B5 - Phloxine B (PHB) ligand binding site identification quantification and dose dependency using sequence specific antibody panel. Average dot blot intensities (quantified using Image J) of 0.3x (white bars), 1x (grey bars), and 3x (diagonal marked bars) PHB samples normalized to each respective Aβ40 (no PHB) control sample average signal. Error bars indicate standard deviation, $n \geq 4$.

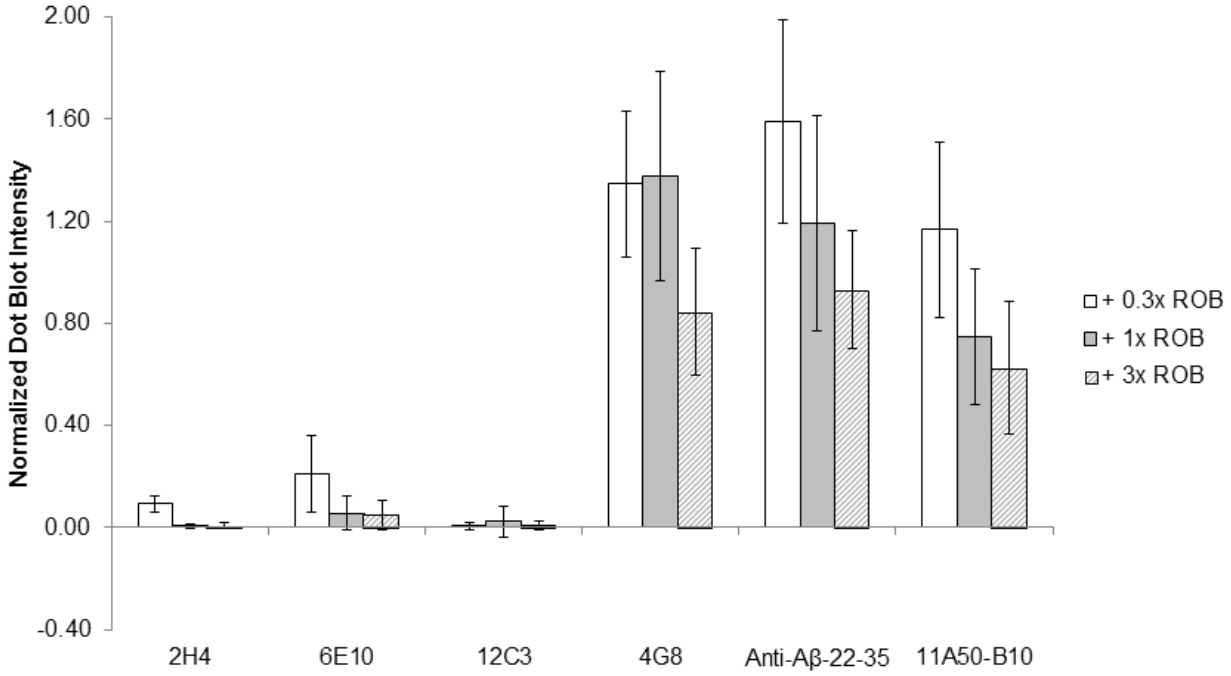

Figure B6 - Rose Bengal (ROB) ligand binding site identification quantification and dose dependency using sequence specific antibody panel. Average dot blot intensities (quantified using Image J) of 0.3x (white bars), 1x (grey bars), and 3x (diagonal marked bars) ROB samples normalized to each respective Aβ40 (no ROB) control sample average signal. Error bars indicate standard deviation, $n \geq 3$.

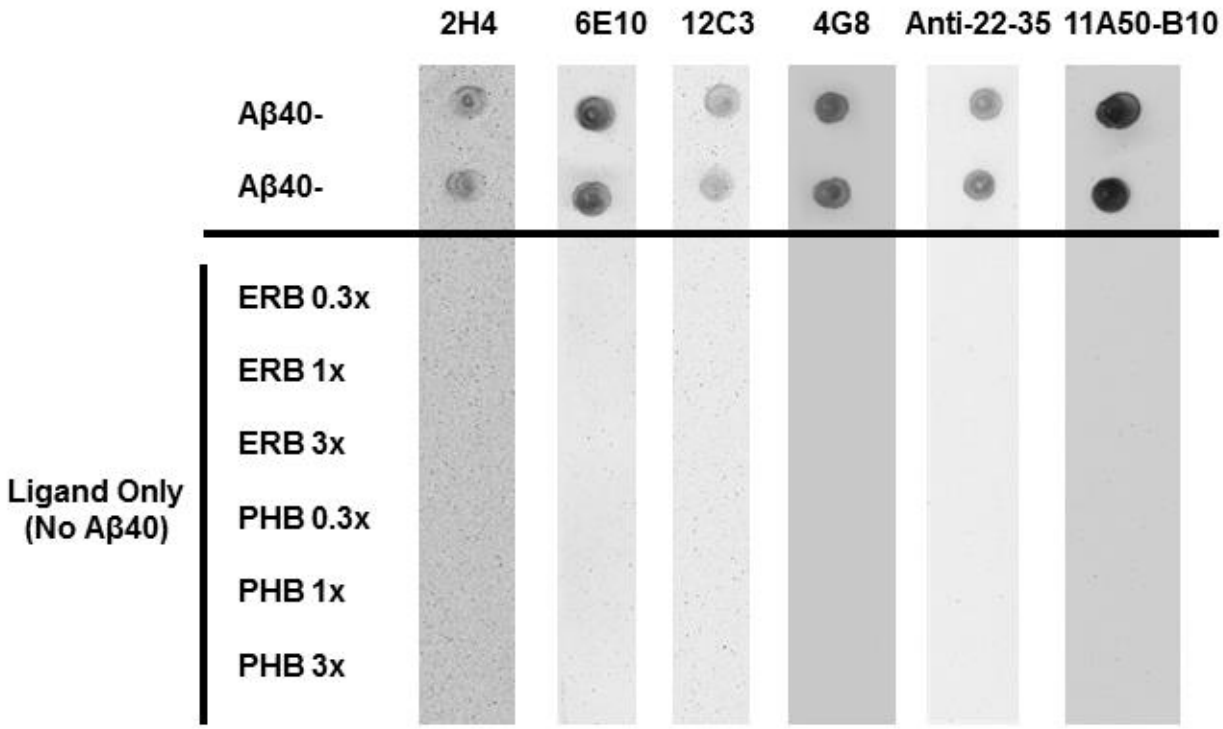

Figure B7 - Ligand-only dot blotting using sequence specific antibody panel. Dot blotting results of Aβ40 monomers mixed without ligand (Top Panel, Aβ40-) and 0.3-3x molar excess concentrations (15-150 μM) of Erythrosin B (ERB) and Phloxine B (PHB) ligand only (Bottom Panel, no 50 μM Aβ40 added) for the six sequence specific antibodies. For better ease of viewing, each antibody was developed on a separate membrane and then cut and pasted for the compiled results.

Table B1 - Decrease in fluorescence due to ligand-Aβ peptide sub-fragment binding. 20 μM of each fluorescent ligand (ERB, EOY, PHB, ROB, or FLN) was added to 0-25 μM amounts of Aβ peptide fragment, and the percent decrease in average fluorescence between the free ligand and excess peptide fragment samples was calculated. Low salt, pH 4.5 buffer was used for all samples. Values are expressed as percent decrease between average fluorescence ± each assay's standard deviation. ND (not detected) indicates that the percent decrease in fluorescence due to ligand-peptide binding was less than the assay standard deviation.

	Decrease in Fluorescence Due to Ligand-Peptide Binding				
Aβ Fragment	ERB	EOY	PHB	ROB	FLN
Aβ1-11	ND	ND	ND	ND	ND
Aβ11-22	33.1 ± 6.8%	19.0 ± 4.9%	20.2 ± 2.5%	40.6 ± 2.5%	ND
Aβ17-24	ND	ND	ND	ND	ND
Aβ33-40	ND	ND	ND	ND	ND

Appendix C: Chapter 4 (Different Fates of Alzheimer's Disease Amyloid-Beta (Aβ) Fibrils Remodeled by Biocompatible Small Molecules) Supplemental Information

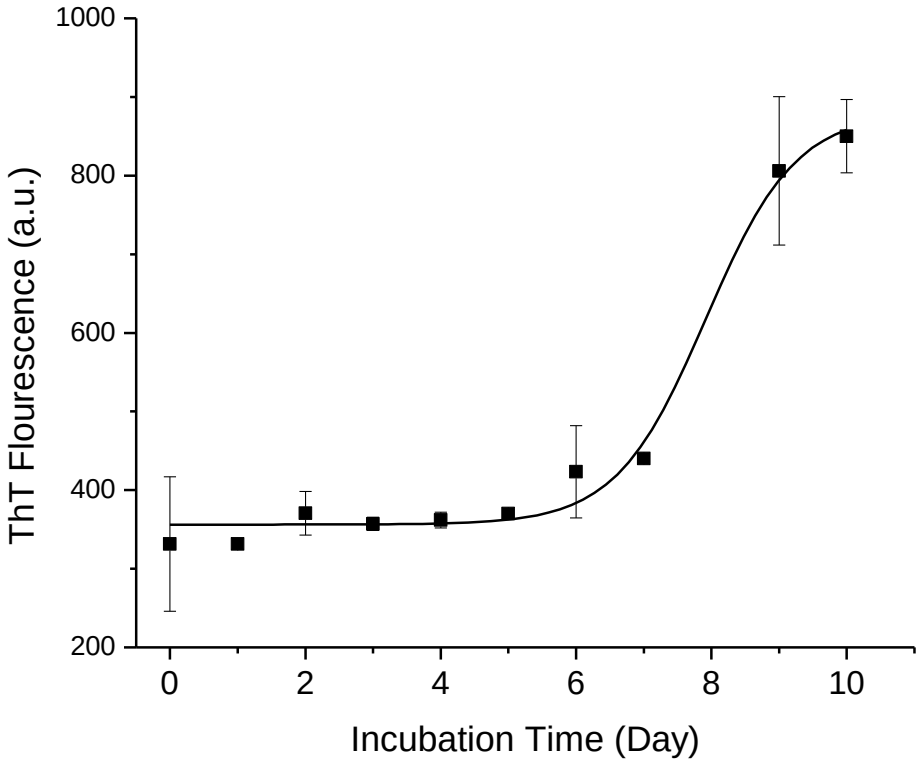

Figure C1 - ThT fluorescence monitoring during Aβ fibril formation (N ≥ 2). The data were fit into a sigmoidal curve (R2 = 0.99).

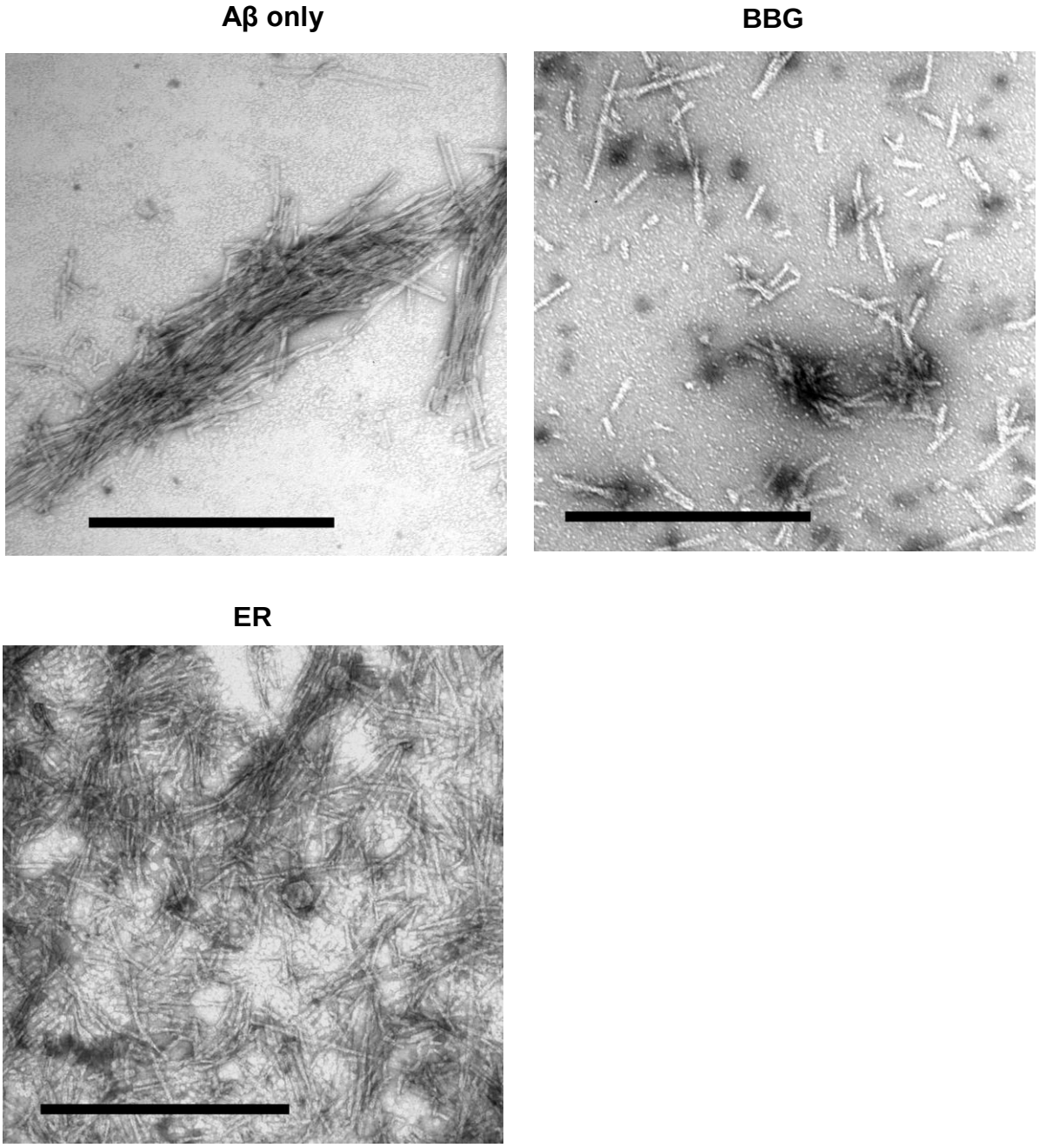

Figure C2 - Wider-frame (1 µm x1 µm panel view) TEM images of Aβ fibrils incubated in the absence (Aβ only panel) or presence of 10X BBG (BBG panel) and 10X ERB (ER panel). Scale bars are all 500 nm.

Table C1 - Measured[a] AFM length (A) and width (B) distribution[b] of Aβ fibrils incubated in the presence or absence of 10X BBG and 10X ERB for one day at 37 degrees Celsius.

A.

		Length of Aβ Aggregates (μm)									
	Sample Size	0.05	0.1	0.15	0.2	0.25	0.3	0.35	0.4	>0.4	Average (nm)
Fibrils Only	23	ND	ND	17%	13%	13%	9%	4%	9%	35%	329 ± 161
10X BBG	141	5%	58%	26%	10%	1%	ND	1%	ND	ND	96 ± 40
10X ERB	103	ND	15%	33%	35%	6%	8%	3%	1%	ND	162 ± 60

B.

		Width of Aβ Aggregates (nm)													
	Sample Size	20	25	30	35	40	45	50	55	60	65	70	75	>75	Average (nm)
Fibrils Only	98	ND	ND	ND	2%	1%	1%	7%	15%	15%	5%	7%	6%	40%	73 ± 23
10X BBG	116	ND	ND	1%	1%	3%	9%	16%	26%	10%	9%	9%	6%	10%	58 ± 14
10X ERB	116	1%	3%	20%	29%	26%	15%	5%	1%	ND	ND	ND	ND	ND	35 ± 6

[a]Measured using Gwyddion SPM analysis software.
[b] The aggregate length or width bin labels represent the maximum length or width of aggregates in each respective bin. Shown on the table are the proportions of each sample population measured possessing the respective maximum bin length or width.
ND: Not Detected

Table C2 - Secondary structure content[a] of Aβ fibrils incubated[b] in the absence or presence of MB analyzed using SP175 Reference Set.

Small molecule added[c]	α-helix	β-sheet	β-turn	Unordered
-	12.2%	36.4%	12.1%	39.3%
MB	8.4%	37.3%	12.9%	41.3%

[a] Determined by DichroWeb using CONTIN method and SP175 reference proteins

[b] Incubated at 37 °C without shaking for one day.

[c] Aβ:MB = 1:10 molar ratio

Appendix D: Chapter 5 (Triphenylmethane Food Dye Analog Crosses Blood-Brain Barrier and Rescues Neuronal Loss and Amyloid-Beta Pathologies In A Transgenic Mouse Model of Alzheimer's Disease) Supporting Information

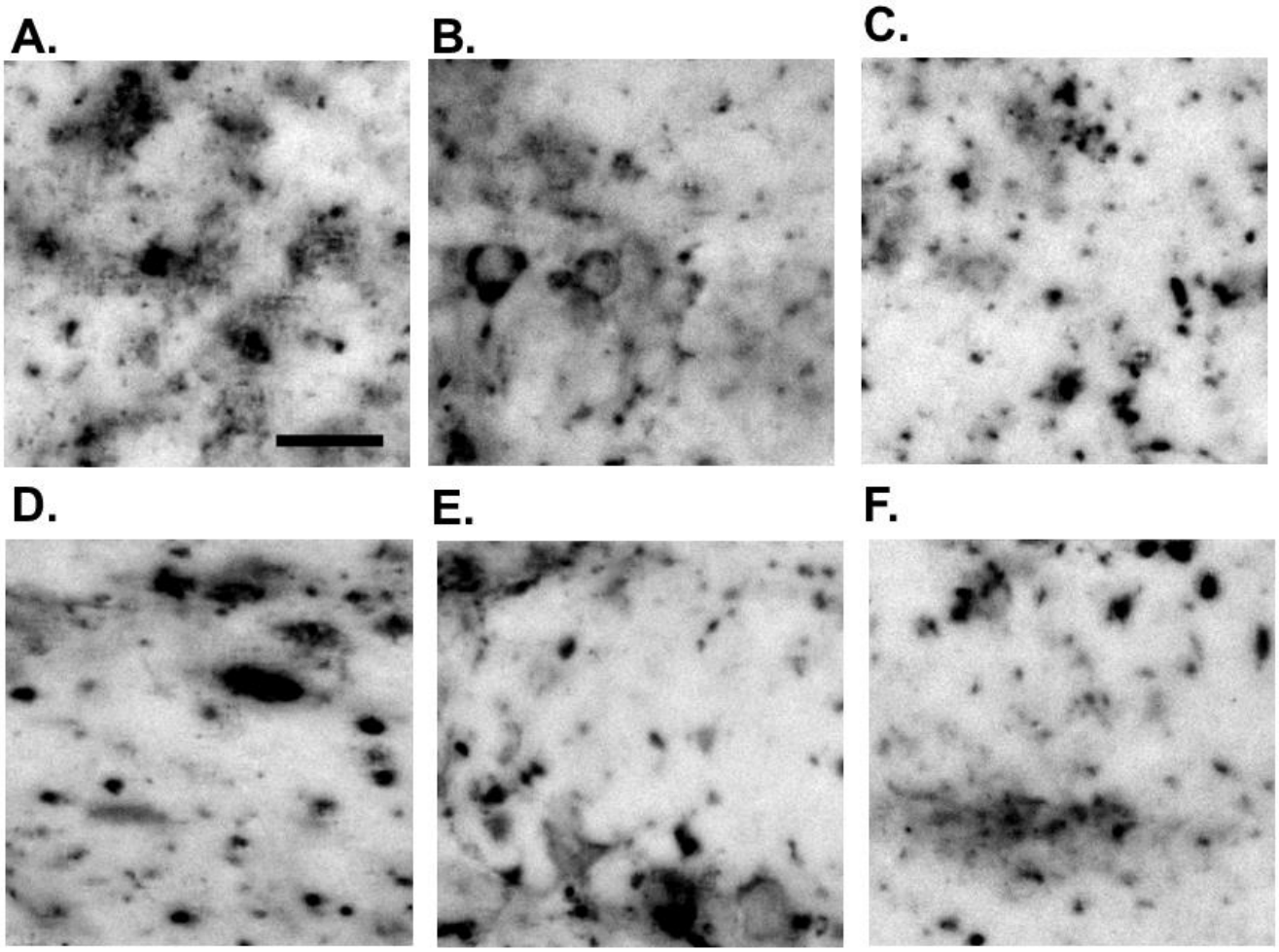

Figure D1 – Qualitative analysis of nature of M87 antibody immunohistochemical staining. Representative 20x objective light microscopy images of M87 staining in the cerebral cortex (A) and CA1 pyramidal neuron layer (B), stratum radiatum (C), lacunosum moleculare (D), top dentate gyrus granule layer (E), and bottom dentate gyrus granule layer (F) of the hippocampus for an untreated control APPSwDI/NOS2-/- mouse. Scale bar displayed = 20 μm.

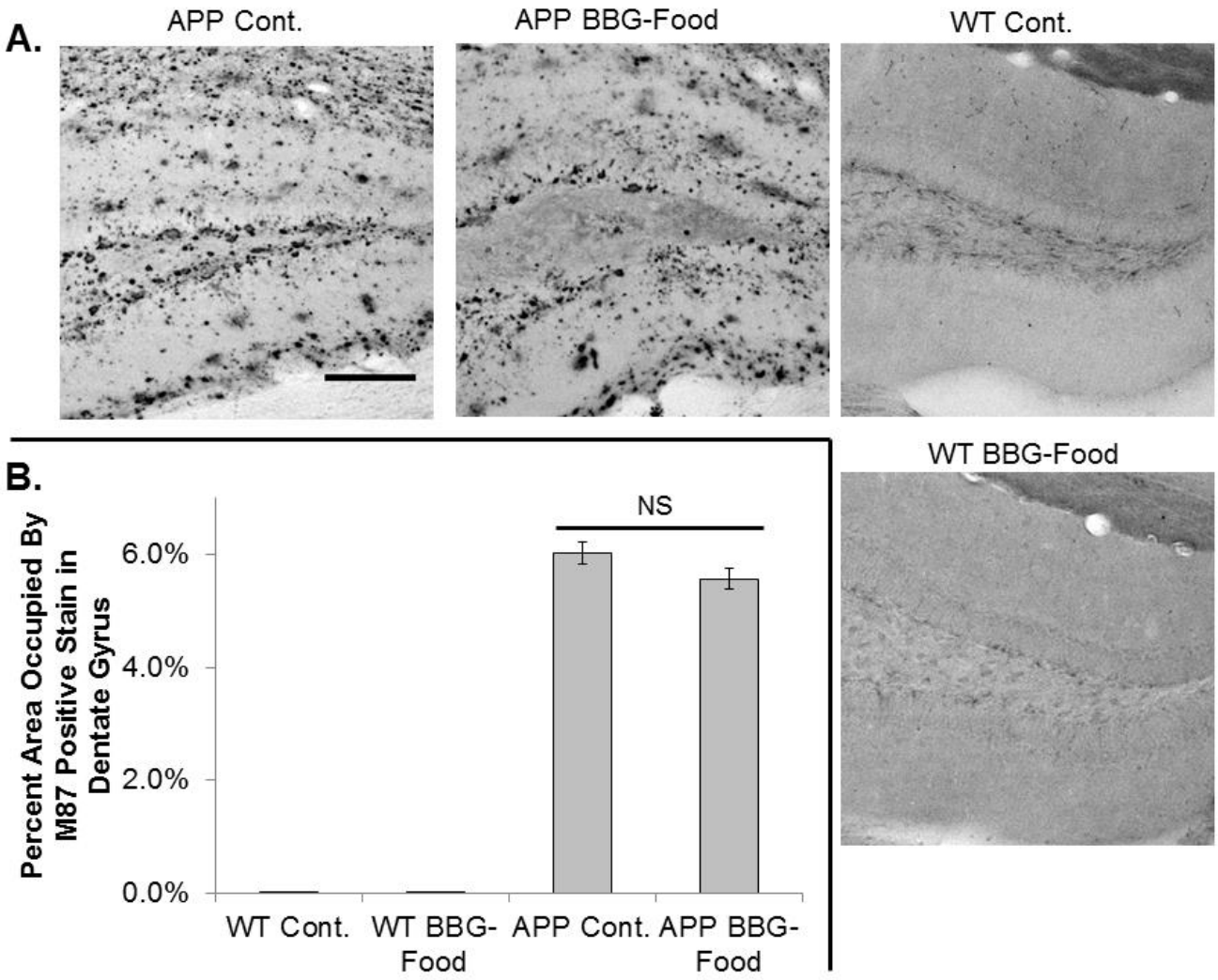

Figure D2 – M87 immunohistochemical assessment of Aβ loading in the dentate gyrus with oral Brilliant Blue G (BBG) administration. (A) Representative light microscopy images of M87 Aβ aggregation intermediate staining in the dentate gyrus region of the hippocampus. Images are displayed for untreated control (Cont.) and 3-month orally administered BBG (BBG-Food) groups of both wild type (WT) and transgenic APPSwDI/NOS2-/- (APP) mice. Scale bar displayed = 150 μm. (B) Quantification of Aβ loading expressed as the average percentage of area occupied by M87-positive stain per total area analyzed ± SEM ($n \geq 145$ replicates, 3 animals per transgenic group). NS indicates no statistically significant difference detected ($p > 0.05$ from two-sided Student's t-test).

Table D1 – Weekly weight monitoring during 3 month Brilliant Blue G (BBG) injection administration period. Percent weight change of APPSwDI/NOS2-/- (APP) and wild type (WT) untreated (Cont. Non-Inj.) and i.p injection-administered BBG (BBG-Inj.) mice. Data expressed as the overall change in each group's average weight in a respective week during 3 month BBG administration period compared to starting weight, +/- SEM (n = 4-5 mice per group).

	% Weight Change During 3 Month BBG Administration Period													
Group	**1**	**2**	**3**	**4**	**5**	**6**	**7**	**8**	**9**	**10**	**11**	**12**	**13**	**14**
APP BBG -Inj.	-2.7 ± 3.1%	-0.9 ± 3.0%	-1.8 ± 3.1%	-2.7 ± 3.7%	-2.3 ± 2.3%	-4.5 ± 1.9%	-2.3 ± 1.3%	-3.4 ± 2.2%	0.0 ± 1.9%	0.0 ± 1.9%	0.0 ± 1.9%	0.0 ± 1.9%	1.1 ± 2.2%	0.0 ± 1.9%
APP Cont. (Non -Inj.)	1.0 ± 1.5%	1.0 ± 2.2%	1.9 ± 1.0%	1.0 ± 0.0%	3.4 ± 1.4%	2.2 ± 1.2%	2.2 ± 1.2%	1.0 ± 2.0%	4.6 ± 2.3%	7.0 ± 2.3%	4.6 ± 1.2%	4.6 ± 1.2%	3.4 ± 1.4%	3.4 ± 1.4%
WT BBG -Inj.	2.2 ± 2.2%	4.5 ± 3.4%	6.7 ± 2.2%	5.6 ± 2.9%	5.6 ± 2.9%	3.4 ± 2.6%	6.7 ± 2.2%	7.9 ± 2.6%	9.0 ± 3.4%	9.0 ± 2.2%	12.4 ± 1.8%	11.2 ± 3.4%	9.0 ± 3.4%	9.0 ± 2.2%
WT Cont. (Non -Inj.)	0.9 ± 1.1%	2.7 ± 2.0%	0.9 ± 1.1%	1.8 ± 0.9%	5.4 ± 1.1%	4.5 ± 1.8%	4.5 ± 2.3%	5.4 ± 1.1%	6.3 ± 1.7%	7.1 ± 2.4%	6.3 ± 1.7%	7.1 ± 2.4%	8.0 ± 2.2%	9.8 ± 2.3%

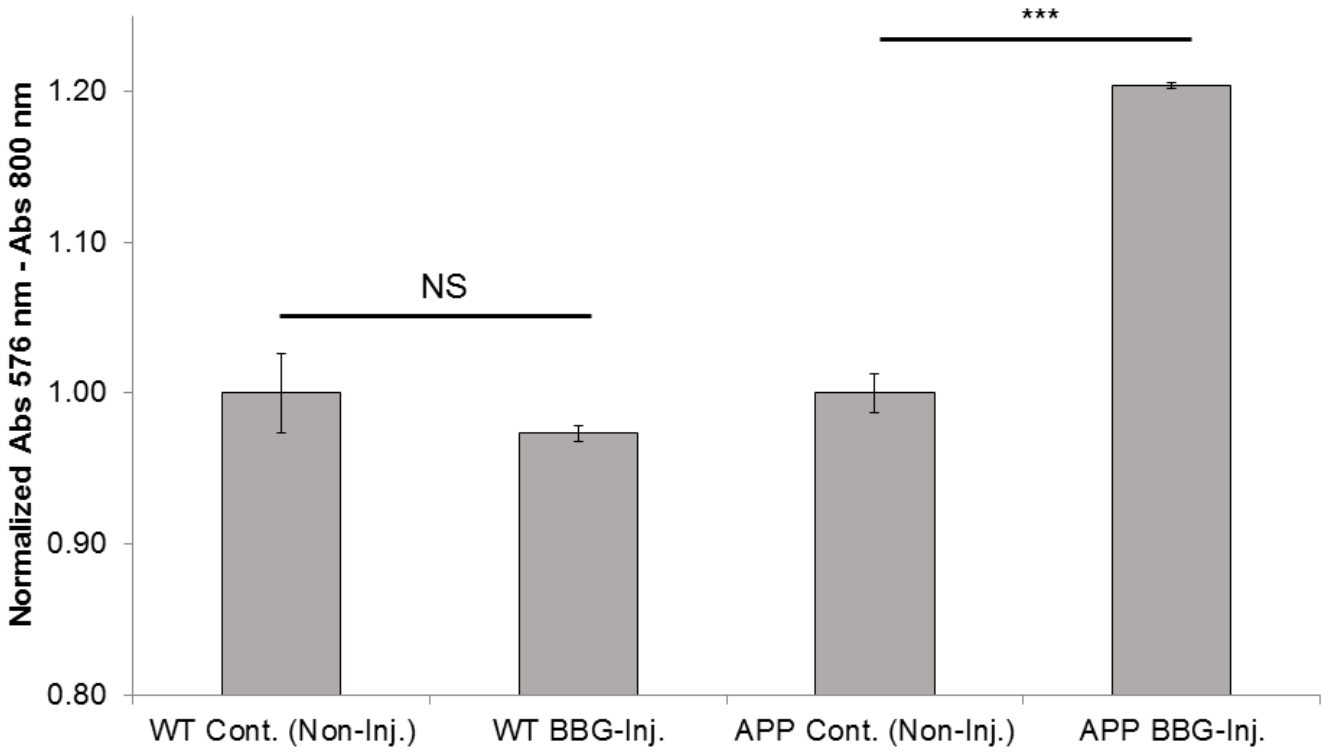

Figure D3 – Spectroscopic analysis of injection administration of Brilliant Blue G (BBG) in mouse brain tissue. Average reference subtracted normalized absorbance values of homogenized brain tissue from wild type (WT) and APPSwDI/NOS2-/- (APP) transgenic AD mice either untreated (Cont. Non-Inj.) or injected i.p. with BBG for 3 months (BBG-Inj.). Error bars indicate ± SEM ($n \geq 20$ replicates, 1-2 mice per group). NS indicates no statistically significant difference detected ($p > 0.1$ from two-sided Student's t-test). *** indicates significant difference ($p < 0.001$).

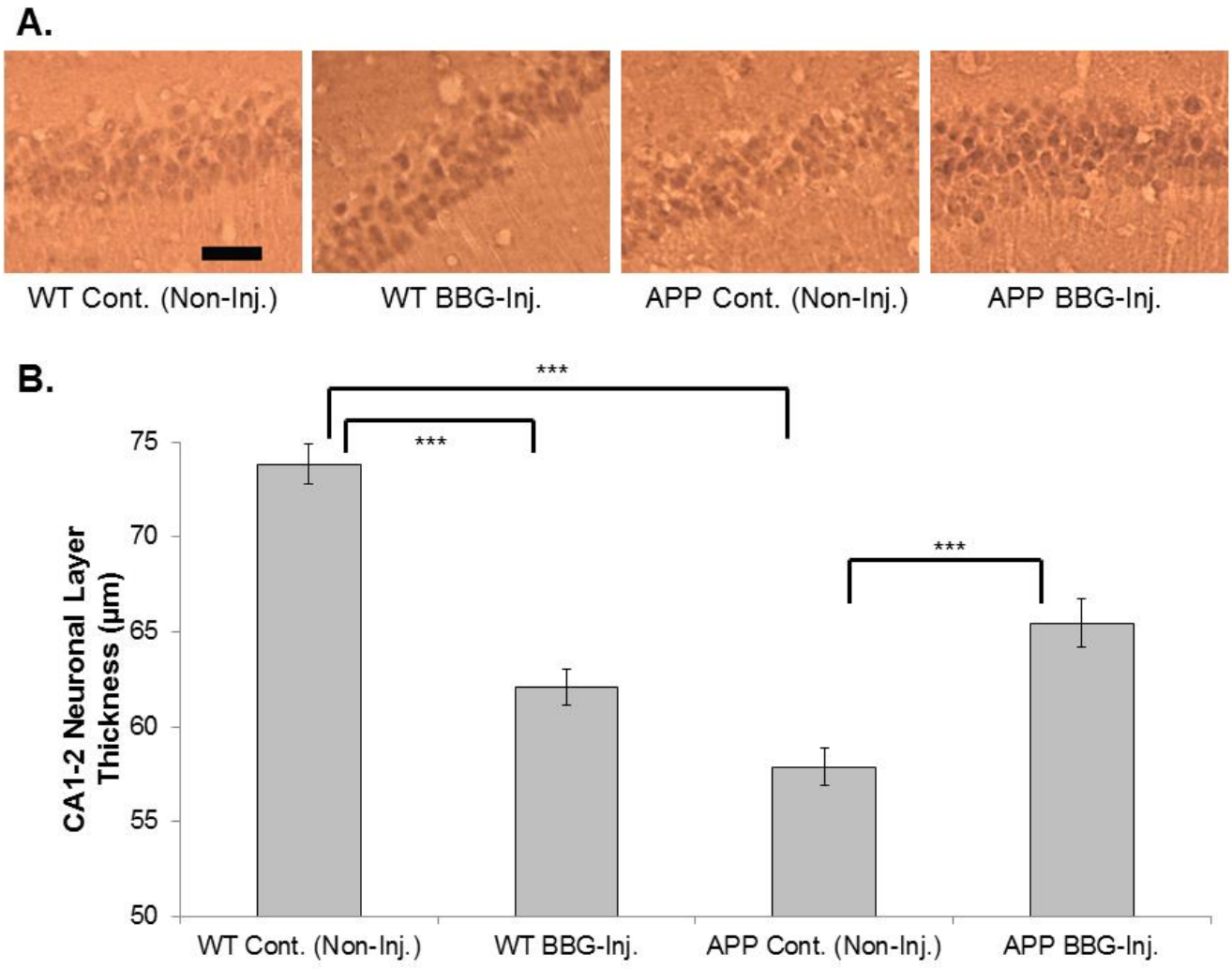

Figure D4 – NeuN immunohistochemical assessment of neuronal loss in CA1-CA2 pyramidal cell layer of hippocampus with Brilliant Blue G (BBG) injection administration. (A) Representative light microscopy images of NeuN staining in the CA1-CA2 cell layer of the hippocampus for wild type (WT) and APPSwDI/NOS2-/- (APP) mice either untreated (Control Non-Inj.) or i.p. injected for 3 months with BBG (BBG-Inj.). Scale bar displayed = 40 µm. (B) Neuronal loss quantification by measuring width/thickness of the CA1-2 neuron layer. Data expressed as average thickness ± SEM ($n \geq 410$ replicates, 3 animals per group). *** indicates significant differences detected ($p < 0.001$ from two-sided Student's t-test).

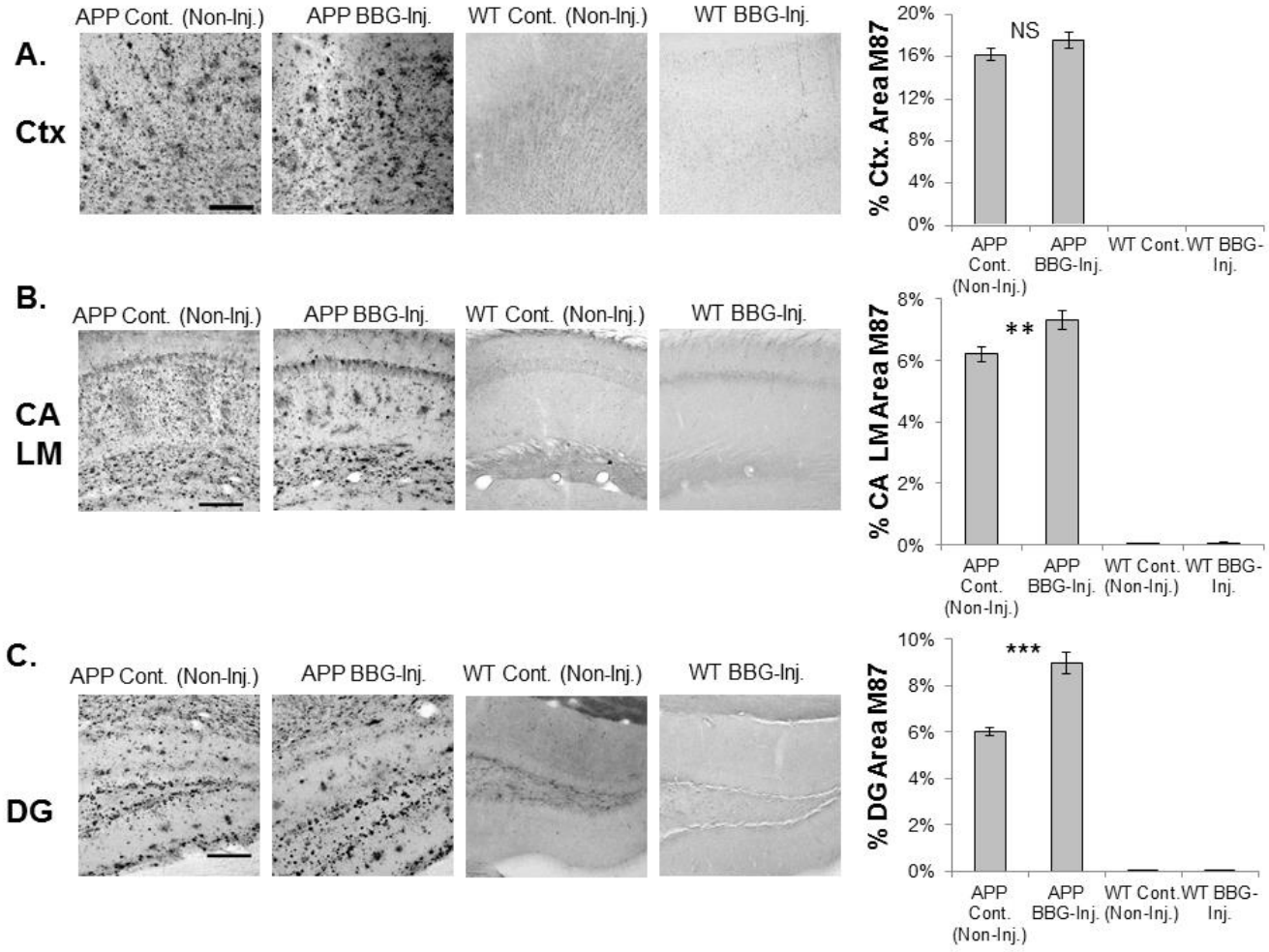

Figure D5 – M87 immunohistochemical assessment of Aβ loading in cortex and hippocampus with Brilliant Blue G (BBG) injection administration. Left panels display representative light microscopy images of M87 Aβ aggregation intermediate staining in the (A) cerebral cortex (Ctx.) and the (B) CA / lacunosum moleculare (CA LM) and (C) dentate gyrus (DG) regions of the hippocampus. Images are displayed for untreated control (Cont. Non-Inj.) and 3-month i.p. injection administered BBG (BBG-Inj.) groups of both wild type (WT) and transgenic APPSwDI/NOS2-/- (APP) mice. Scale bars displayed = 150 µm. Right panels display quantification of Aβ loading in each separate region expressed as the average percentage of area occupied by M87-positive stain per total area analyzed ± SEM ($n \geq 95$ replicates, 3 animals per transgenic group). NS indicates no statistically significant difference detected ($p > 0.1$ from two-sided Student's t-test). ** and *** indicate significant differences detected (with $p < 0.01$ and $p < 0.001$, respectively).

Supporting Information D1 - In Vivo Relationship Between Small-Molecule Modulators of Aβ Aggregation and Aβ Clearance Mechanisms

In the in vivo investigation of new Alzheimer's Disease therapeutics targeting the mechanism of Aβ aggregation modulation, it is valuable to have an understanding of how and where in the body the small molecule can exert potential effects on its Aβ target.

The therapeutic process starts when the small molecule enters the blood-stream and circulates to the brain region. At the blood-brain barrier, there exists an equilibrium between Aβ in the peripheral blood stream and that inside the central nervous system.[334] In the periphery, Aβ above the equilibrium level is quickly cleared through the liver and kidneys by lipid-associated transporters.[334] Aβ is transported in the blood-to-brain direction primarily by receptor-mediated transcytosis by the receptor for advanced glycation end products (RAGE).[335] Conversely, Aβ inside the brain is cleared in monomeric/aggregated form by enzymatic degradation[336] or in monomeric form, transported in the brain-to-blood direction by low-density lipoprotein receptor related protein-1 (LRP1).[337, 338] Inside the brain parenchyma, there exists another equilibrium between Aβ in its soluble/monomeric form and higher order aggregated forms.[339]

In regards to Aβ therapy, the brain can be thought of as two different compartments: the cerebrospinal fluid (CSF), which surrounds the brain, and the brain parenchyma, where the neurons reside. A small molecule therapeutic can enter the CSF at a rate inversely related to its size, but it is likely cleared very quickly since the CSF fluid turns over every 2 hours by being recirculated back in to the peripheral blood stream via convection bulk flow.[260] Given the quick turnover of the CSF and the fact that passage from the CSF in to the brain parenchyma is very slow and diffusion controlled,[260] the small molecule therapy is unlikely to enter the brain

parenchyma area through the CSF route. Therefore, the primary entry access point for a small molecule therapeutic to Aβ in the brain parenchyma is through the blood-brain barrier.

Once the small molecule Aβ aggregation modulator has entered the brain parenchyma, it can exert therapeutic benefit in three potential ways. First, by inhibiting aggregation from the monomeric Aβ state, the small molecule prevents the levels of aggregates which are neurotoxic. Second, by binding Aβ monomer to inhibit aggregation, the small molecule could have the side effect of shifting brain equilibrium between free/un-bound monomer and aggregated Aβ towards the monomer, allowing Aβ to be transported by LRP1.[339] The third manner relates to Aβ degradation in the brain by proteolytic enzymes, the two most widely studied being neprilysin and insulin-degrading enzyme.[337] Although all known Aβ degrading enzymes can cleave the monomeric form of the peptide, it has been reported that the formation of large fibril forms of Aβ greatly reduces the ability of the enzymes to act, likely because their proteolytic cleavage site becomes buried inside the large aggregate.[340] Thus, by preventing the formation of large fibrils, small molecule Aβ aggregation modulators can also exert therapeutic benefit by increasing the efficiency of endogenous enzymatic degradation mechanisms.

Supporting Information D2 - Metabolism, Bioavailability, and Biocompatibility of Erythrosin B (ERB)

Being a widely used FDA-approved food dye, the biological fate of ERB (FD&C Red No. 3) has been studied extensively in the literature in humans, rats, mice, pigs, dogs, gerbils, and rabbits.[37, 38, 115, 116, 207, 341-355] ERB is highly lipid soluble and so crosses the BBB.[115, 116] Despite its relatively high molecular weight (800 Da), the in vivo BBB permeability value of ERB was found to be 39 µl/min/g brain.[116] Although there exists a significant amount of disagreement in the literature about the exact no-effect dosage levels in different species, ERB is overall agreed to be a well-tolerated compound with a good biocompatibility profile. The current Acceptable Daily Intake (ADI) for ERB is only 0.1 mg/kg/day.[356] However, a two week study analyzing the effect of oral intake of ERB on thyroid function in adult human males found no adverse effects at a dosage level of up to 200 mg/day/person (corresponds to between 1.6-3.0 mg/kg/day).[207] Since this study, there has not been a motivation to study higher, more aggressive dosage regimens in humans since the estimated daily consumption of ERB is only 2 mg[207] and ERB has not been a therapeutic candidate for other diseases. In rodent studies, more aggressive dosage regimens have been attempted. Borzelleca and Hallagan fed mice ERB for two years and found no adverse effect levels of 1834 mg/kg/day for female mice and 4759 mg/kg/day for male mice.[341] Importantly, they also reported a pink discoloration of the hair, skin, and urine, a red color of the feces, and no consistent biologically significant compound-related effects on behavior, morbidity, mortality, and haematology stemming from administration of ERB. The pink coloring of the mouse extremities is a promising indicator that ERB can achieve distribution throughout the circulatory system from oral intake. Furthermore, Zuno et. al. found that i.p. dosage of 100 mg/kg/day of ERB did not result in any adverse effects and found no evidence of

genotoxicity.[349] Metabolic studies of ERB upon oral intake have revealed that 10% of the compound is absorbed in to the stomach bile, with the rest being excreted in the feces.[37] Intriguingly, the ERB recovered in the fecal matter is primarily in an undegraded state, indicating that the Fluorescein structure may still be active. No palatability issues were reported in the literature regarding oral intake of ERB.